

Designing Iridium Catalysts for Selective C-O Cleavage

By

Caleb D. Fast

Dissertation

Submitted to the Faculty of the

Graduate School of Vanderbilt University

in partial fulfillment of the requirements

for the degree of

DOCTOR OF PHILOSOPHY

In

Chemistry

October 31, 2021

Nashville, Tennessee

Approved:

Dr. Nathan D. Schley (Advisor)

Dr. Timothy P. Hanusa

Dr. Janet E. Macdonald

Dr. Paul E. Laibinis

Copyright © 2021 Caleb Daniel Fast
All Rights Reserved

Acknowledgements

I would like to begin by thanking my advisor, Dr. Nathan Schley, who accepted me into his group as a transfer student in 2018 and for his mentorship. My family and friends have been very supportive and I hope that you all know how appreciated you are. Lastly and most importantly, I want to acknowledge my wife, Kelsey Webb, for her love and support.

Table of Contents

| | |
|---|------------|
| ACKNOWLEDGMENTS..... | iii |
| LIST OF TABLES | vi |
| LIST OF FIGURES..... | vii |
| LIST OF SCHEMES..... | viii |
| LIST OF ABBREVIATIONS..... | ix |
| CHAPTER 1: Introduction to Polar Hydrosilylative Reductions via Silane Heterolysis | 1 |
| I. Scope of Dissertation..... | 1 |
| II. Reduction of Alkyl Ethers..... | 1 |
| III. Silane Heterolysis via Sigma Complexes..... | 2 |
| IV. Iridium-Catalyzed C-O Cleavage via Silane Heterolysis..... | 4 |
| V. Borane-Catalyzed C-O Cleavage via Silane Heterolysis..... | 7 |
| VI. Conclusions | 9 |
| VII. References | 9 |
| CHAPTER 2: Selectivity of Cationic Iridium Bis(phosphines) for C-O Cleavage of Carbocyclic Ethers | 16 |
| I. Introduction | 16 |
| II. Applying [CODIr(PPh₃)₂]BAR^F₄ to Six-Membered Carbocyclic Ether Cleavage | 17 |
| III. Rational Design of Iridium Bis(phosphine) Precatalysts Towards Conformational Selectivity of Cyclohexyl Methyl Ether Cleavage | 20 |
| IV. Confirming Catalyst-Controlled Selectivity in Cyclohexyl Methyl Ether Cleavage | 23 |
| V. Conclusions..... | 24 |
| CHAPTER 3: Mechanistic Studies of Iridium Bis(phosphine)-Catalyzed C-O Cleavage of Cyclohexyl Methyl Ethers | 26 |
| I. Studying the Mechanisms of Demethoxylation vs. Demethylation of Cyclohexyl Methyl Ethers | 26 |
| II. Applying S_N2 Demethylation and S_N1 Demethoxylation to Bile Acid Derivatives | 27 |
| III. Studying the Activation of Olefin-Bound Precatalyst 1a in Catalysis | 29 |
| IV. Applying Water Activation to Catalysis with 1a Generated <i>In-Situ</i> | 31 |
| V. Catalyst Speciation and Mechanism..... | 33 |
| VI. Conclusions..... | 37 |
| VII. References for Chapter 2 and Chapter 3..... | 38 |
| Appendix I. Experimental Section for Chapter 2 and Chapter 3 | 43 |
| CHAPTER 4: Light-Promoted Transfer of an Iridium Hydride in Alkyl Ether Cleavage | 173 |

| | | |
|-------------|---|------------|
| I. | Introduction | 173 |
| II. | Catalytic Reaction Optimizations | 175 |
| III. | Application of Optimized Conditions to a Broader Substrate Scope | 177 |
| IV. | Reaction Mechanism Studies..... | 181 |
| V. | Conclusions | 187 |
| VI. | References | 188 |
| VII. | Appendix for Chapter 4..... | 193 |

List of Tables

| Table | Page |
|--|------------|
| 2.1: Computed energies (kcal·mol⁻¹) for chair conformations that place the OMe group axial versus equatorial compared with experimental selectivity for ether cleavage | 20 |
| 2.2: Catalyst-controlled reduction of <i>cis</i>-3..... | 22 |
| 2.3: Catalyst-controlled reduction of <i>trans</i>-3 | 22 |
| 2.4: Catalyst-controlled reduction of 10..... | 23 |
| 2.2: Catalyst-controlled reduction of 11..... | 24 |
| 4.1: Identification of conditions for photochemical alkyl ether cleavage..... | 176 |
| 4.2: Hydrosilylative alkyl ether cleavage by 2/NaBAR^F₄..... | 178 |
| 4.3: Hydrosilylative anisole demethylation by 2/NaBAR^F₄..... | 179 |
| 4.4: Cyclohexyl methyl ether cleavage by 2/NaBAR^F₄..... | 180 |
| 4.5: Sterol methyl ether cleavage by 2/NaBAR^F₄..... | 181 |

List of Figures

| Figure | Page |
|--|------|
| 1.1: Representative schemes of heterolytic (left) and homolytic (right) bond cleavage | 2 |
| 1.2: Representative binding modes of metal sigma complexes..... | 3 |
| 1.3: Oxidative addition (left) and heterolysis (right) of metal sigma complexes..... | 3 |
| 1.4: Cationic iridium silane heterolysis catalysts | 4 |
| 1.5: Proposed mechanism for the iridium-catalyzed silylation of alkyl ethers | 5 |
| 1.6: Proposed mechanism for the iridium-catalyzed silylation of alkyl ethers with Brookhart's catalyst | 6 |
| 1.7: Lewis-acid silane activation catalyst BCF..... | 7 |
| 1.8: Proposed mechanism for the borane-catalyzed silylation of alkyl ethers with BCF.... | 8 |
| 2.1: Reported catalysts for ether silylation | 16 |
| 2.2: Demethylation versus deoxygenation of cyclohexyl methyl ethers | 19 |
| 2.3: Synthesis of bis(phosphine) precatalysts tested..... | 21 |
| 3.1: Hydroxylation pattern of cholic acids..... | 27 |
| 3.2: Isolated yields for cholic acid-derived methyl ether silylation..... | 28 |
| 3.3: Depiction of the interaction of the 7 α substituent with the <i>cis</i> -fused A-ring..... | 29 |
| 3.4: Role of trace water in precatalyst (1a) activation by NMR analysis..... | 30 |
| 3.5: Bleaching of 1a at low concentration by UV-Vis..... | 31 |
| 3.6: Proposed mechanism for iridium-catalyzed 2 $^{\circ}$ ether cleavage..... | 33 |
| 3.7: Ln/Ln plot showing 2 $^{\text{nd}}$ order rate dependence on iridium loading..... | 35 |
| 3.8: ORTEP diagrams of 22a (left) and 23a (right) shown at 50% probability | 37 |
| 4.1: Role of light in modifying metal hydricity in [Cp*IrH(bipyridine)] $^{+}$ described by the Miller group..... | 174 |
| 4.2: Iridium phenylpyridine complexes examined | 175 |
| 4.3: Proposed mechanism for catalytic ether cleavage via photochemical hydride transfer to silyloxonium ions | 182 |
| 4.4: Comparison of absorbance spectrum of 5 with the output of the commercial 34W H150 Blue LED Lamp used in this study..... | 184 |

List of Schemes

| Scheme | Page |
|--|------------|
| 1.1: Silane heterolysis via nucleophilic attack of an alkyl ether to a cationic iridium σ-silane complex..... | 4 |
| 1.2: Stepwise deoxygenation of ethers with Brookhart's catalyst | 6 |
| 1.3: Exhaustive deoxygenation of a silyl-protected glucose derivative with Brookhart's catalyst..... | 7 |
| 2.1: Demethoxylation of cyclopentyl methyl ether (CPME) catalyzed by complex 1 | 17 |
| 2.2: Reduction of CPME and cyclohexyl methyl ether catalyzed by complex 1a | 18 |
| 2.3: Reduction of <i>cis</i>-3 and <i>trans</i>-3 catalyzed by complex 1a | 18 |
| 3.1: S_N1 versus S_N2 mechanistic studies for dealkoxylation versus dealkylation selectivity | 26 |
| 3.2: Reduction of 20 on a 1.00 g scale catalyzed by 1a generated <i>in situ</i> | 32 |
| 3.3: Reduction of 21 catalyzed by 1a | 33 |
| 3.4: Resting state speciation of 1a under catalytic conditions | 34 |
| 3.5: Resting state speciation of 1f under catalytic conditions and independent synthesis | 36 |
| 4.1: Resting state analysis of 2/NaBAr^F₄ under catalytic conditions | 183 |
| 4.2: Cleavage of cyclopropyl-type substrates under catalytic conditions | 184 |
| 4.3: Reduction of a triethyloxonium ion by 5..... | 186 |
| 4.4: Reduction of acetophenone under dark and illuminated conditions | 187 |

List of Abbreviations

| | |
|--|---|
| (Et ₃ Si) ₂ O | hexamethylidisiloxane |
| [Ph ₃ C]BAr ^F ₄ | triphenylcarbenium tetrakis[3,5-bis(trifluoromethyl)phenyl]borate |
| 2° | secondary |
| BAr ^F ₃ | tris[3,5-bis(trifluoromethyl)phenyl]borate |
| BAr ^F ₄ | tetrakis[3,5-bis(trifluoromethyl)phenyl]borate |
| BCF | tris(pentafluorophenyl)borane |
| COD / cod | cyclooctadiene |
| Cp | cyclopentadiene |
| Cp* | pentamethylcyclopentadiene |
| CPME | Cyclopentyl methyl ether |
| DCM | dichloromethane |
| DI | deionized |
| DMF | Dimethylformamide |
| EtOAc | Ethyl acetate |
| Et ₃ SiH | triethylsilane |
| g | gram |
| HRMS | high resolution mass spectroscopy |
| MeI | methyl iodide |
| MeOH | methanol |
| MHz | megahertz |
| Min | minutes |
| mL | milliliter |
| mmol | millimole |
| MTBE | methyl tert-butyl ether |
| NMR | nuclear magnetic resonance |
| OAc | acetate |
| OMe | methoxy |
| Ph | phenyl |
| PhMe | toluene |
| PPh ₃ | triphenylphosphine |
| PPh ₂ Me | methyldiphenyl phosphine |
| PMe ₂ Ph | dimethylphenyl phosphine |
| PAr ^F ₃ | tris[3,5-bis(trifluoromethyl)phenyl]phosphine |
| Q-TOF | quadrupole time-of-flight |
| TBAF | tetrabutylammonium fluoride |
| ^t Bu | tert-butyl |
| TBDPS | tert-butyl diphenylsilane |
| TBDPSCI | tert-butylchlorodiphenylsilane |
| TES-OCy | triethylsilyl cyclohexyl ether |
| THF | tetrahydrofuran |
| TLC | thin layer chromatography |

Chapter 1: Introduction to Polar Hydrosilylative Reductions via Silane Heterolysis

I. Scope of Dissertation

In this dissertation, research on iridium-catalyzed C-O cleavage of ethers via hydrosilylative reductions will be thoroughly outlined. Chapter 1 details Si-H heterolysis for C-O cleavage with both transition metal and Lewis Acid catalysts. Chapter 2 outlines the use of air-stable iridium catalysts used for alkyl ether cleavage. The focus of Chapter 2 is on reactivity of six-membered carbocyclic alkyl ethers and understanding the effect of conformational bias in C-O cleavage. Additionally, the role of catalyst structure will be outlined through the use of a series of bis(phosphine)-type iridium complexes. Based on reactivity displayed in the second chapter, chapter 3 then discusses a thorough mechanistic investigation for iridium-catalyzed cleavage of alkyl ethers with cationic iridium bis(phosphine) complexes through speciation, isotope incorporation, activation, and kinetic studies. Chapter 4 details an unusual method of tailoring C-O cleavage of alkyl ethers, where blue light is used to change reactivity of a catalytic intermediate rather than using synthetic modifications in an example of a catalytic photochemical transfer from an iridium hydride in alkyl ether cleavage.

II. Reduction of Alkyl Ethers

Traditionally, ethers are utilized for their inert nature and see application largely as solvents and protecting groups.¹ By virtue of this relative inertness, C-O bond cleavage via reduction typically requires harsh conditions that lack high-selectivity, such as hydrogenolysis over heterogeneous catalysts and using strong acids at elevated temperatures.²⁻⁴ In more recent years, a more mild, selective method for C-O cleavage of alkyl ethers has been developed via C-O silylation using silanes. Hydrosilylative C-O cleavage is a mild method that operates by silane

heterolysis, followed by a reduction of an oxonium ion by a hydride source that is formed *in-situ*.⁵⁻
¹⁷ The following sections detail previous iridium and borane ether cleavage examples while following chapters will show a system with greater tunability of selectivity profiles through the use of a modular iridium bis(phosphine) system and through illumination of a catalytic intermediate with blue light.

III. Silane Heterolysis via Sigma Complexes

Hydrosilylative C-O bond cleavage of alkyl ethers occur via Si-H heterolysis. In this process, a silylium transfer to an alkyl ether from an silyl-iridium complex takes place and forms a silyloxonium ion. A heterolytic bond cleavage occurs when a 2-electron distribution to a single atom occurs (Figure 1.1).^{18,19} Heterolytic cleavage occurs regularly in organic chemistry such as elimination and substitution reactions.^{20,21} This varies from homolytic bond cleavage, which occurs through the distribution of an electron to each atom upon breaking of a bond and is very common in radical reactions (Figure 1.1).²²⁻²⁹ In the context of alkyl ether cleavage and this work, the focus will lie on using cationic iridium catalysts for the heterolysis of triethylsilane from electrophilic sigma complexes.

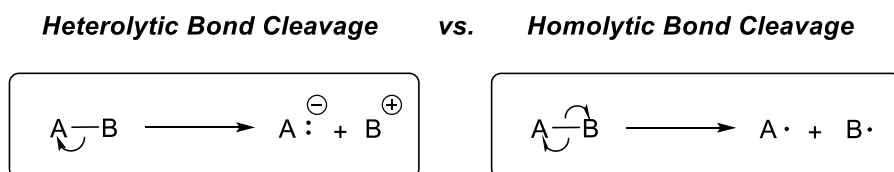


Figure 1.1: Representative schemes of heterolytic (left) and homolytic (right) bond cleavage

Transition metal sigma complexes are characterized by the binding of a sigma bond to a metal center (Figure 1.2).³⁰ Complexes of metal-bound dihydrogen (H₂) and other H-X (X = C, B, Si, Ge, and Sn) variants are the most common examples of organometallic sigma complexes.³¹⁻³⁸ When coordinated to metal centers, the ligands of sigma complexes are stabilized by donation of

electrons from the d_{π} orbitals of the metal center to the σ^* orbitals of the ligand, which is called π -backbonding.^{30,34}

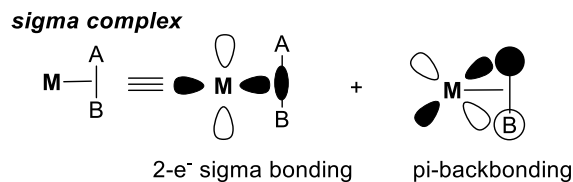


Figure 1.2: Representative binding modes of metal sigma complexes

In cases where π -backbonding is strong enough due to the electron richness of a metal center, the sigma bond of the ligand can break and form two anionic ligands on the metal center, this is termed an oxidative addition (Figure 1.3).^{30,34} In less electron-rich metal sigma complexes, such as cationic metal complexes, the relative stability of anionic ligand formation is in large part driven by ligand polarization rather than a formal oxidative addition. This reactivity makes nucleophilic abstraction of the polarized ligand component with the partial positive charge character possible (Figure 1.3). A classic example of this would be the polarization of hydrogen to make a hydride and a protonated nucleophile/base.³⁰

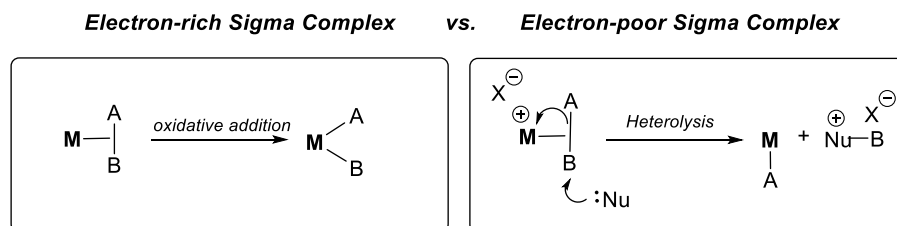
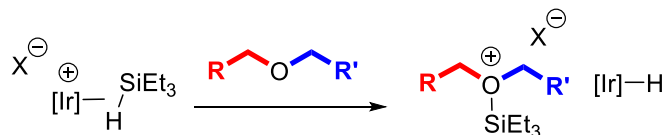


Figure 1.3: Oxidative addition (left) and heterolysis (right) of metal sigma complexes

The aforementioned heterolysis at cationic metal centers will be the mode of reactivity in focus for this dissertation. Cationic iridium complexes will be employed for heterolytic Si-H cleavage of triethyl silane, where an alkyl ether substrate serves as a Lewis-basic nucleophile attacks an electrophilic silane in a cationic iridium complex to form a neutral iridium hydride and a silyloxonium ion (Scheme 1.1).



Scheme 1.1: Silane heterolysis via nucleophilic attack of an alkyl ether to a cationic iridium σ -silane complex

IV. Iridium-catalyzed C-O Cleavage via Silane Heterolysis

A variety of cationic iridium catalysts which activate silanes and generate an electrophilic silylium ion have been reported (some examples in Figure 1.4) which operate through silane heterolysis for the reduction of carbonyl derivatives^{39–44} and alkyl halides⁴⁵, as well for alcohol dehydrosilylation.^{46–48}

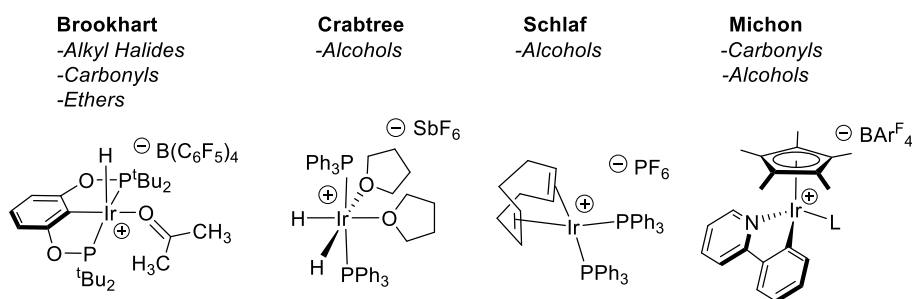


Figure 1.4: Cationic iridium silane heterolysis catalysts

The primary focus of this work lies in the field of iridium-catalyzed C-O bond cleavage of ethers with triethylsilane. The proposed mechanism by which this reduction occurs is shown in Figure 1.5; a cationic iridium precatalyst (**A**) binds with triethylsilane to form a cationic sigma silane complex (**B**), in the presence of substrate ether, silane heterolysis can occur through a silylium transfer to an alkyl ether to form the corresponding neutral iridium hydride and silyloxonium ion pair (**C**). Upon formation of the neutral iridium hydride and silyloxonium ion, a hydride transfer occurs from the neutral iridium hydride to the silyloxonium ion, which generates the C-O cleavage products of an alkane and silyl ether, respectively, and closes the catalytic cycle.¹³

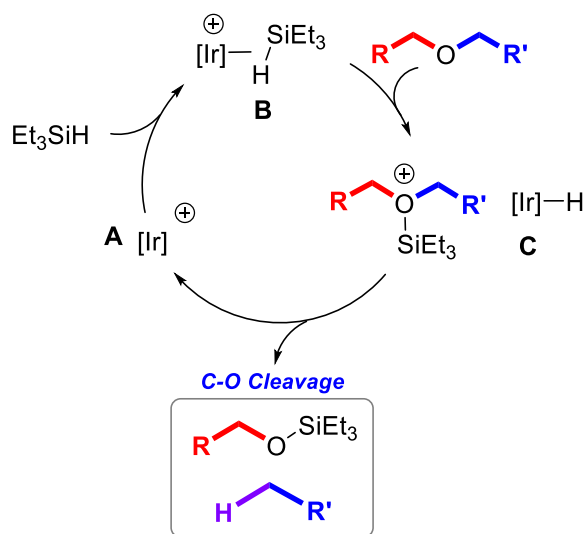


Figure 1.5: Proposed mechanism for the iridium-catalyzed silylation of alkyl ethers

Iridium-catalyzed ether cleavage via silane heterolysis was pioneered by the Brookhart group, where a POCOP-supporting cationic iridium catalyst (Figure 1.4) was developed as an ether cleavage catalyst in 2008.¹³ It was observed that in the presence of this POCOP-supported catalyst and triethylsilane, alkyl ethers could undergo C-O cleavage to produce an alkane and corresponding silyl ether. Mechanistic investigations were conducted and was shown to likely proceed via a similar mechanism (Figure 1.6) led to the proposal above where silane heterolysis occurs to generate a neutral iridium dihydride (C) which is in equilibrium with a trihydridosilyl (E) complex and reduces a silyloxonium ion (D) to give alkane and silyl ether products.

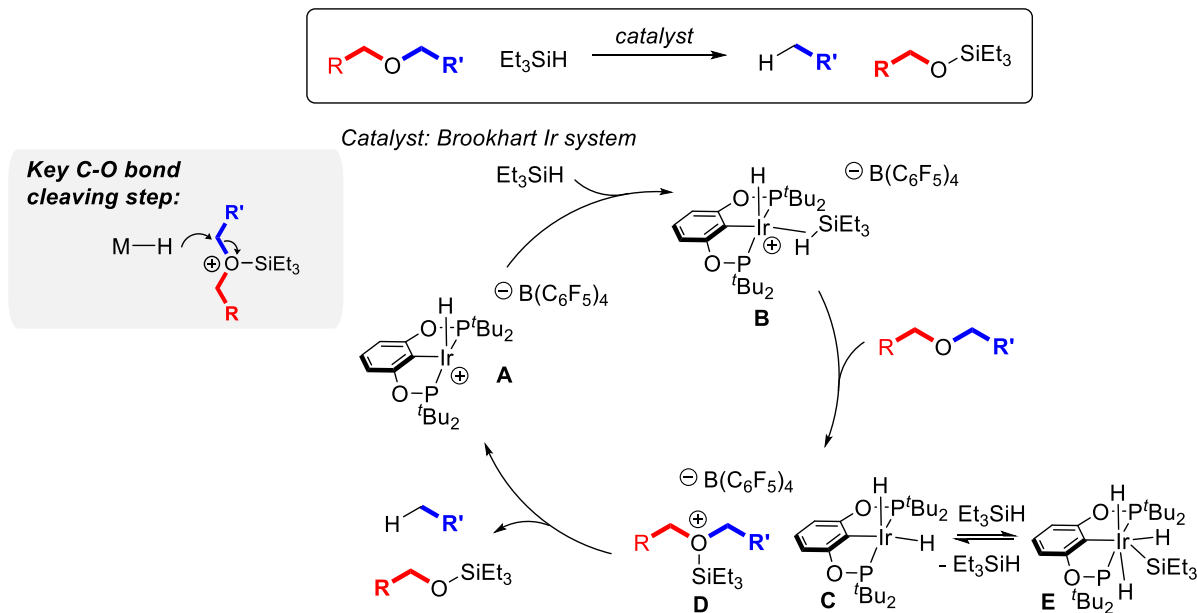
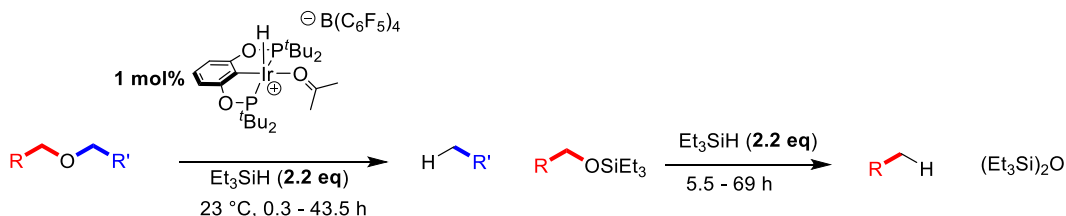


Figure 1.6: Proposed mechanism for the iridium-catalyzed silylation of alkyl ethers with Brookhart's catalyst

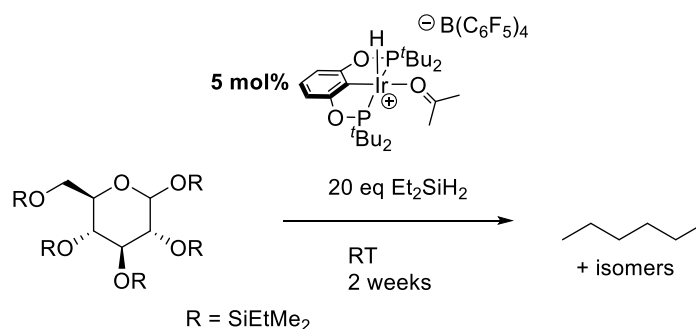
Brookhart also showed that with additional triethylsilane and extended time periods, that the silyl ethers produced upon the initial C-O cleavage step can be further reduced down to the corresponding alkane and hexaethyldisiloxane products (Scheme 1.2).



Scheme 1.2: Stepwise deoxygenation of ethers with Brookhart's catalyst

The reactivity of Brookhart's catalyst for reducing silyl ethers after the initial C-O cleavage of the alkyl ether was then adapted by the Gagné group in 2013 and applied to the reduction of more complex molecules.¹⁴ Gagné demonstrated that persilyl glucopyranose in the presence of excess diethylsilane and 5 mol% Brookhart's catalyst undergoes ring-opening of the pyranose core followed by exhaustive deoxygenation of the polysilyl ether to produce n-hexanes and isomers (Scheme 1.3) showing the ability of this system to achieve a high-degree of reduction of complex

carbohydrates, but lacks in unique selectivity profiles. Additionally, Brookhart's catalyst requires a 5-step synthesis from resorcinol.⁴⁹ More tunable scaffolds are needed for tailoring unique selectivity profiles in iridium-catalyzed ether silylation, which will be addressed in this dissertation.



Scheme 1.3: Exhaustive deoxygenation of a silyl-protected glucose derivative with Brookhart's catalyst

V. Borane-catalyzed C-O Cleavage via Silane Heterolysis

Highly Lewis-acidic triaryl borane catalysts are another common class of silane activation catalysts for a variety of transformations such as alcohol dehydrosilylation⁷, carbonyl-containing ketone and aldehyde-type reductions^{50–52}, amide deoxygenations^{53,54,54,55}, and C-O cleavage of alkyl ethers.⁷ The most commonly employed borane catalyst for the heterolysis of silanes is a tris(pentafluorophenyl)borane (BCF) shown in Figure 1.7.

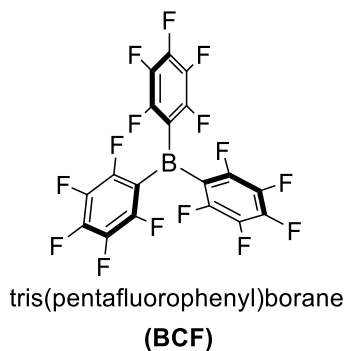


Figure 1.7: Lewis-acid silane activation catalyst BCF

In 1999, the Yamamoto group developed BCF as a C-O cleavage catalyst for alkyl ethers via silane heterolysis.^{7,56} Mechanistically, BCF operates similarly to the previously discussed cationic iridium precursors, with the main difference being the formation of an anionic borohydride as opposed forming a neutral iridium-hydride as discussed in the previous section. The proposed mechanism for BCF-catalyzed ether silylation is shown in Figure 1.8. Silane first coordinates to the borane catalyst, activating the silane followed by Si-H heterolysis via nucleophilic attack by the ethereal substrate. Upon the nucleophilic attack of the alkyl ether to the activated silane, an ion-pair composed of an anionic borohydride and a silyloxonium ion is formed. The following step is the selectivity determining C-O cleavage step where a hydride transfer from the borohydride to the silyloxonium ion produces the corresponding alkane and silyl ether product.

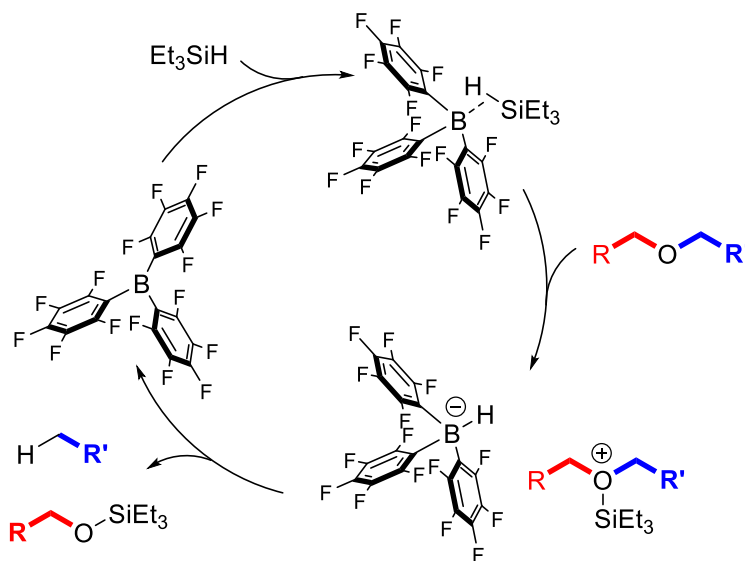


Figure 1.8: Proposed mechanism for the borane-catalyzed silylation of alkyl ethers with BCF

Similar to Brookhart's iridium system, Yamamoto also showed that with additional triethylsilane and extended time periods, the silyl ether products are further reduced to the corresponding alkane and hexaethyldisiloxane. This reactivity was later adapted by the Gagné group which applied this system to the exhaustive deoxygenation of a silyl protected glucose

derivative.⁶ Since this discovery, BCF has also been utilized by the Gagné group for a variety of ring-opening and acetal reductions of carbohydrates.^{5,8,53,57-60} As with Brookhart's catalyst, the synthesis of this catalyst is fairly difficult and therefore tailoring reactivity cannot be done readily, as BCF requires a Grignard and purification via sublimation. This makes the synthesis of new variants, specifically with unique substituents beyond the current triaryl-scaffold for the incorporation of substituents such as alkyl groups to tune the electronics and sterics of the boron center difficult.^{54,60} This furthers the need for a tunable catalyst manifold for C-O cleavage in order to produce unique selectivity profiles.

VI. Conclusion

Using both iridium and borane catalysts, a wide variety of reductions via Si-H heterolysis can be achieved and proceed through similar mechanistic pathways. This work will focus on the use of iridium catalysts, as there is more opportunity for tailoring reactivity through commercially-available phosphine and 2-phenylpyridine ligand use. Primarily, I will focus on tailoring the reactivity of the metal hydride through altering the electronic environment of the metal center with varying ligands and through illumination with blue light in order to achieve unique selectivity in hydrosilylative C-O cleavage of alkyl ethers via silane heterolysis.

VII. References

- (1) Protection for the Hydroxyl Group, Including 1,2- and 1,3-Diols. In *Greene's Protective Groups in Organic Synthesis*; John Wiley & Sons, Ltd, 2006; pp 16-366.
- (2) Furimsky, E. Catalytic Hydrodeoxygenation. *Appl. Catal. Gen.* **2000**, *199* (2), 147-190.
- (3) Burwell, R. L. The Cleavage of Ethers. *Chem. Rev.* **1954**, *54* (4), 615-685.

- (4) Ramos, R.; Tišler, Z.; Kikhtyanin, O.; Kubička, D. Towards Understanding the Hydrodeoxygenation Pathways of Furfural–Acetone Aldol Condensation Products over Supported Pt Catalysts. *Catal. Sci. Technol.* **2016**, *6* (6), 1829–1841.
- (5) Adduci, L. L.; Bender, T. A.; Dabrowski, J. A.; Gagné, M. R. Chemoselective Conversion of Biologically Sourced Polyols into Chiral Synthons. *Nat. Chem.* **2015**, *7* (7), 576–581.
- (6) Adduci, L. L.; McLaughlin, M. P.; Bender, T. A.; Becker, J. J.; Gagné, M. R. Metal-Free Deoxygenation of Carbohydrates. *Angew. Chem. Int. Ed.* **2014**, *53* (6), 1646–1649.
- (7) Gevorgyan, V.; Rubin, M.; Benson, S.; Liu, J.-X.; Yamamoto, Y. A Novel B(C₆F₅)₃-Catalyzed Reduction of Alcohols and Cleavage of Aryl and Alkyl Ethers with Hydrosilanes. *J. Org. Chem.* **2000**, *65* (19), 6179–6186.
- (8) Bender, T. A.; Dabrowski, J. A.; Zhong, H.; Gagné, M. R. Diastereoselective B(C₆F₅)₃-Catalyzed Reductive Carbocyclization of Unsaturated Carbohydrates. *Org. Lett.* **2016**, *18* (16), 4120–4123.
- (9) Delineating The Multiple Roles of B(C₆F₅)₃ in the Chemoselective Deoxygenation of Unsaturated Polyols. *ACS Catal.* **2016**, *6* (12), 8399–8403
- (10) Drosos, N.; Ozkal, E.; Morandi, B. Catalytic Selective Deoxygenation of Polyols Using the B(C₆F₅)₃/Silane System. *Synlett* **2016**, *27* (12), 1760–1764.
- (11) Drosos, N.; Morandi, B. Boron-Catalyzed Regioselective Deoxygenation of Terminal 1,2-Diols to 2-Alkanols Enabled by the Strategic Formation of a Cyclic Siloxane Intermediate. *Angew. Chem. Int. Ed.* **2015**, *54* (30), 8814–8818.
- (12) Monsigny, L.; Feghali, E.; Berthet, J.-C.; Cantat, T. Efficient Reductive Depolymerization of Hardwood and Softwood Lignins with Brookhart’s Iridium(III) Catalyst and Hydrosilanes. *Green Chem.* **2018**, *20* (9), 1981–1986.
- (13) Yang, J.; White, P. S.; Brookhart, M. Scope and Mechanism of the Iridium-Catalyzed Cleavage of Alkyl Ethers with Triethylsilane. *J. Am. Chem. Soc.* **2008**, *130* (51), 17509–17518.
- (14) McLaughlin, M. P.; Adduci, L. L.; Becker, J. J.; Gagné, M. R. Iridium-Catalyzed Hydrosilylative Reduction of Glucose to Hexane(s). *J. Am. Chem. Soc.* **2013**, *135* (4), 1225–1227.

- (15) Jones, C. A. H.; Schley, N. D. Selective Alkyl Ether Cleavage by Cationic Bis(Phosphine)Iridium Complexes. *Org. Biomol. Chem.* **2018**, *17*, 1744-1748.
- (16) Jones, C. A. H.; Schley, N. D. Selective Demethylation of O-Aryl Glycosides by Iridium-Catalyzed Hydrosilylation. *Chem. Commun.* **2021**, *57*, 5935-5956.
- (17) Fast, C. D.; Jones, C. A. H.; Schley, N. D. Selectivity and Mechanism of Iridium-Catalyzed Cyclohexyl Methyl Ether Cleavage. *ACS Catal.* **2020**, *10* (11), 6450–6456.
- (18) Franz, A. K. Organic Chemistry. By David R. Klein. *Angew. Chem. Int. Ed.* **2012**, *51* (43), 10701–10702.
- (19) Armentrout, P. B.; Simons, J. Understanding heterolytic bond cleavage. *J. Am. Chem. Soc.* **1992**, *114* (22), 8627-8663.
- (20) Kim, D. W.; Song, C. E.; Chi, Y. D. Significantly Enhanced Reactivities of the Nucleophilic Substitution Reactions in Ionic Liquid. *J. Org. Chem.* **2003**, *68* (11), 4281-4285.
- (21) Griffin, R. J.; Henderson, A.; Curtin, N. J.; Echaliier, A.; Endicott, J. A.; Hardcastle, I. R.; Newell, D. R.; Noble, M. E. M.; Wang, L.-Z.; Golding, B. T. Searching for Cyclin-Dependent Kinase Inhibitors Using a New Variant of the Cope Elimination. *J. Am. Chem. Soc.* **2006**, *128* (18), 6012–6013.
- (22) Slocum, G. H.; Schuster, G. B. Photochemistry of Naphthylmethyl Halides. Direct and Sensitized Paths to Homolytic and Heterolytic Carbon-Halogen Bond Cleavage. *J. Org. Chem.* **1984**, *49* (12), 2177–2185.
- (23) Nishina, Y.; Ohtani, B.; Kiushima, K. Bromination of Hydrocarbons with CBr₄, Initiated by Light-Emitting Diode Irradiation. *Beilstein J. Org. Chem.* **2013**, *9*, 1663-1667.
- (24) Fokin, A. A.; Schreiner, P. R. Selective Alkane Transformations via Radicals and Radical Cations: Insights into the Activation Step from Experiment and Theory. *Chem. Rev.* **2002**, *102* (5), 1551-1594.
- (25) Sinditskii, V. P.; Kolesov, V. I.; Egorshv, V. Yu.; Patrikeev, D. I.; Dorofeeva, O. V. Thermochemistry of Cyclic Acetone Peroxides. *Thermochim. Acta* **2014**, *585*, 10–15.

- (26) Swain, C. G.; Stockmayer, W. H.; Clarke, J. T. Effect of Structure on the Rate of Spontaneous Thermal Decomposition of Substituted Benzoyl Peroxides. *J. Am. Chem. Soc.* **1950**, *72* (12), 5426–5434.
- (27) March's Advanced Organic Chemistry: Reactions, Mechanisms, and Structure, 6th Ed By Michael B. Smith *J. Am. Chem. Soc.* **2007**, *129* (16), 5296–5296.
- (28) González-Esguevillas, M.; Miró, J.; Jeffrey, J. L.; MacMillan, D. W. C. Photoredox-Catalyzed Deoxyfluorination of Activated Alcohols with Selectfluor®. *Tetrahedron* **2019**, *75* (32), 4222–4227.
- (29) Nicewicz, D. A.; Romero, N. A. Organic Photoredox Catalysis. *Chem. Rev.* **2016**, *116* (17), 10075–10166.
- (30) Crabtree, R. H. Transition Metal Complexation of σ Bonds. *Angew. Chem. Int. Ed. Engl.* **1993**, *32* (6), 789–805.
- (31) Corey, J. Y. Reactions of Hydrosilanes with Transition Metal Complexes. *Chem. Rev.* **2016**, *116* (19), 11291–11435.
- (32) Brookhart, M.; Green, M. L. H.; Parkin, G. Agostic Interactions in Transition Metal Compounds. *Proc. Natl. Acad. Sci.* **2007**, *104* (17), 6908–6914.
- (33) Eleazer, B. J.; Smith, M. D.; Popov, A. A.; Peryshkov, D. V. Rapid Reversible Borane to Boryl Hydride Exchange by Metal Shuttling on the Carborane Cluster Surface. *Chem. Sci.* **2017**, *8* (8), 5399–5407.
- (34) Crabtree, R. H. Dihydrogen Complexation. *Chem. Rev.* **2016**, *116* (15), 8750–8769.
- (35) Esteruelas, M. A.; López, A. M.; Oliván, M. Polyhydrides of Platinum Group Metals: Nonclassical Interactions and σ -Bond Activation Reactions. *Chem. Rev.* **2016**, *116* (15), 8770–8847.
- (36) Matthews, S. L.; Pons, V.; Heinekey, D. M. Silane Complexes of Electrophilic Metal Centers. *Inorg. Chem.* **2006**, *45* (16), 6453–6459.
- (37) Zyder, M.; Kochel, A.; Handzlik, J.; Szymańska-Buzar, T. Photochemical Reaction of $\text{Mo}(\text{CO})_6$ with Et_2GeH_2 : NMR and DFT Studies of Reaction Products; Crystal Structure of a Novel Complex $[\{\text{Mo}(\mu\text{-H}_2\text{-H-GeEt}_2)(\text{CO})_4\}_2]$. *Organometallics* **2009**, *28* (20), 5857–5865.

- (38) Handzlik, J.; Kochel, A.; Szymańska-Buzar, T. H–Ge Bond Activation by Tungsten Carbonyls: An Experimental and Theoretical Study. *Polyhedron* **2012**, *31* (1), 622–631.
- (39) Park, S.; Brookhart, M. Hydrosilylation of Carbonyl-Containing Substrates Catalyzed by an Electrophilic H1-Silane Iridium(III) Complex. *Organometallics* **2010**, *29* (22), 6057–6064.
- (40) Metsänen, T. T.; Hrobárik, P.; Klare, H. F. T.; Kaupp, M.; Oestreich, M. Insight into the Mechanism of Carbonyl Hydrosilylation Catalyzed by Brookhart's Cationic Iridium(III) Pincer Complex. *J. Am. Chem. Soc.* **2014**, *136* (19), 6912–6915.
- (41) Corre, Y.; Rysak, V.; Trivelli, X.; Agbossou-Niedercorn, F.; Michon, C. A Versatile Iridium(III) Metallacycle Catalyst for the Effective Hydrosilylation of Carbonyl and Carboxylic Acid Derivatives. *Eur. J. Org. Chem.* **2017**, *2017* (32), 4820–4826.
- (42) Corre, Y.; Rysak, V.; Nagyházi, M.; Kalocsai, D.; Trivelli, X.; Djukic, J. -P.; Agbossou-Niedercorn, F.; Michon, C. One-Pot Controlled Reduction of Conjugated Amides by Sequential Double Hydrosilylation Catalyzed by an Iridium(III) Metallacycle. *Eur. J. Org. Chem.* **2020**, *2020* (39), 6212–6220.
- (43) Park, S.; Brookhart, M. Development and Mechanistic Investigation of a Highly Efficient Iridium(V) Silyl Complex for the Reduction of Tertiary Amides to Amines. *J. Am. Chem. Soc.* **2012**, *134* (1), 640–653.
- (44) Park, S.; Bézier, D.; Brookhart, M. An Efficient Iridium Catalyst for Reduction of Carbon Dioxide to Methane with Trialkylsilanes. *J. Am. Chem. Soc.* **2012**, *134* (28), 11404–11407.
- (45) Yang, J.; Brookhart, M. Iridium-Catalyzed Reduction of Alkyl Halides by Triethylsilane. *J. Am. Chem. Soc.* **2007**, *129* (42), 12656–12657.
- (46) Luo, X. L.; Crabtree, R. H. Homogeneous catalysis of silane alcoholysis via nucleophilic attack by the alcohol on an Ir(η -2-HSiR₃) intermediate catalyzed by [IrH₂S₂(PPh₃)₂]SbF₆ (S = solvent). *J. Am. Chem. Soc.* **1989**, *111* (7), 2527-2535.
- (47) Chung, M.-K.; Schlaf, M. Regioselectively Trisilylated Hexopyranosides through Homogeneously Catalyzed Silane Alcoholysis. *J. Am. Chem. Soc.* **2005**, *127* (51), 18085–18092.

- (48) Hamdaoui, M.; Ney, M.; Sarda, V.; Karmazin, L.; Bailly, C.; Sieffert, N.; Dohm, S.; Hansen, A.; Grimme, S.; Djukic, J.-P., Evidence of a Donor–Acceptor (Ir–H)→SiR₃ Interaction in a Trapped Ir(III) Silane Catalytic Intermediate. *Organometallics* **2016**, *35*, 2207–2223.
- (49) Göttker-Schnetmann, I.; White, P.; Brookhart, M. Iridium Bis(Phosphinite) p-XPCP Pincer Complexes: Highly Active Catalysts for the Transfer Dehydrogenation of Alkanes. *J. Am. Chem. Soc.* **2004**, *126* (6), 1804–1811.
- (50) Gevorgyan, V.; Rubin, M.; Liu, J.-X.; Yamamoto, Y. A Direct Reduction of Aliphatic Aldehyde, Acyl Chloride, Ester, and Carboxylic Functions into a Methyl Group. *J. Org. Chem.* **2001**, *66* (5), 1672–1675.
- (51) Bach, P.; Albright, A.; Laali, K. K. Influence of Lewis Acid and Solvent in the Hydrosilylation of Aldehydes and Ketones with Et₃SiH; Tris(Pentafluorophenyl)Borane B(C₆F₅)₃ versus Metal Triflates [M(OTf)₃; M = Sc, Bi, Ga, and Al] – Mechanistic Implications. *Eur. J. Org. Chem.* **2009**, *2009* (12), 1961–1966.
- (52) Seo, Y.; Gudz, A.; Lowe, J. M.; Gagné, M. R. Selective Deoxygenation of Gibberellic Acid with Fluoroarylborane Catalysts. *Tetrahedron* **2019**, *75* (49), 130712.
- (53) Bender, T. A.; Payne, P. R.; Gagné, M. R. Late-Stage Chemoselective Functional-Group Manipulation of Bioactive Natural Products with Super-Electrophilic Silylium Ions. *Nat. Chem.* **2018**, *10* (1), 85–90.
- (54) Peruzzi, M. T.; Mei, Q. Q.; Lee, S. J.; Gagné, M. R. Chemoselective Amide Reductions by Heteroleptic Fluoroaryl Boron Lewis Acids. *Chem. Commun.* **2018**, *54* (46), 5855–5858.
- (55) Peruzzi, M. T.; Gallou, F.; Lee, S. J.; Gagné, M. R. Site Selective Amide Reduction of Cyclosporine A Enables Diverse Derivation of an Important Cyclic Peptide. *Org. Lett.* **2019**, *21* (9), 3451–3455.
- (56) Lowe, J. M.; Bowers, B. E.; Seo, Y.; Gagné, M. R. Modulating Electrostatic Interactions in Ion Pair Intermediates To Alter Site Selectivity in the C–O Deoxygenation of Sugars. *Angew. Chem. Int. Ed.* **2020**, *59* (39), 17297–17300.

- (57) Seo, Y.; Lowe, J. M.; Gagné, M. R. Controlling Sugar Deoxygenation Products from Biomass by Choice of Fluoroarylborane Catalyst. *ACS Catal.* **2019**, *9* (8), 6648–6652.
- (58) Hein, N. M.; Seo, Y.; Lee, S. J.; Gagné, M. R. Harnessing the Reactivity of Poly(Methylhydrosiloxane) for the Reduction and Cyclization of Biomass to High-Value Products. *Green Chem.* **2019**, *21* (10), 2662–2669.
- (59) Seo, Y.; Gagné, M. R. Positional Selectivity in the Hydrosilylative Partial Deoxygenation of Disaccharides by Boron Catalysts. *ACS Catal.* **2018**, *8* (1), 81–85.
- (60) Gudz, A.; Payne, P. R.; Gagné, M. R. Phosphines as Silylium Ion Carriers for Controlled C–O Deoxygenation: Catalyst Speciation and Turnover Mechanisms. *Organometallics* **2017**, *36* (20), 4047–4053.

Chapter 2: Selectivity of Cationic Iridium Bis(phosphines) for C-O Cleavage of Carbocyclic

Ethers*

*Fast, C. D.; Jones, C. A. H.; Schley, N. D. Selectivity and Mechanism of Iridium-Catalyzed Cyclohexyl Methyl Ether Cleavage. *ACS Catal.* **2020**, *10* (11), 6450–6456.

Copyright 2020 American Chemical Society

I. Introduction

Nature provides complex, stereochemically-rich organic feedstocks in oxygenated molecules including lignins and carbohydrates. The efficient utilization of such materials as valuable organic building blocks relies on the availability of selective methods for their reduction. Traditional methods for the cleavage of C–O bonds in biomass rely on direct hydrogenolysis over heterogeneous catalysts, which lack design features necessary for selective processes.^{1,2} The conversion of alcohol derivatives to a leaving group followed by reduction in a second step offers enhanced opportunities for selectivity in complex substrates.^{3–9} However in recent years, a more-direct catalytic approach has emerged allowing alkyl- and silyl ether cleavage via reduction of a silyloxonium ion generated in situ.^{10–12}

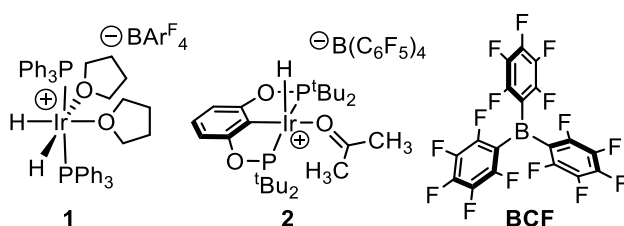
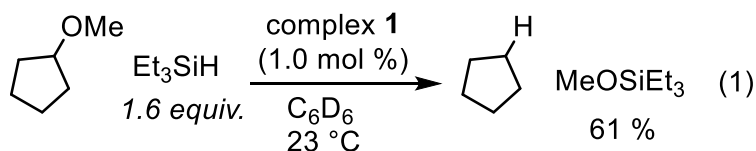


Figure 2.1 Reported catalysts for ether silylation.^{10,12,13}

The reductive cleavage of ether-derived silyloxonium ions requires a catalyst capable of effecting hydrosilane heterolysis. Yamamoto reported that the electron deficient triaryl borane tris(pentafluorophenyl)borane (**BCF**) catalyzes the deoxygenation of alcohols with silanes via initial dehydrosilylation to the silyl ether and showed that this system also cleaves

dialkylethers.^{10,11} (Figure 2.1). Gagné has applied this catalyst to both the partial and complete deoxygenation of carbohydrate substrates.^{14–16} Work by Brookhart showed that a cationic pincer-supported iridium complex (**2**) operates by a similar mechanism,¹² however attempts by Gagné to apply this system in complex polyether substrates provided products resulting from unselective C-O cleavage.^{14,17} In recent work Caleb Jones has shown that a simple cationic bis(phosphine)iridium dihydride complex (**1**) is capable of effecting the selective cleavage of alkyl ethers with silane.¹³ Crucially, the resulting silyl ethers are stable with respect to further reduction, unlike in the Brookhart system.



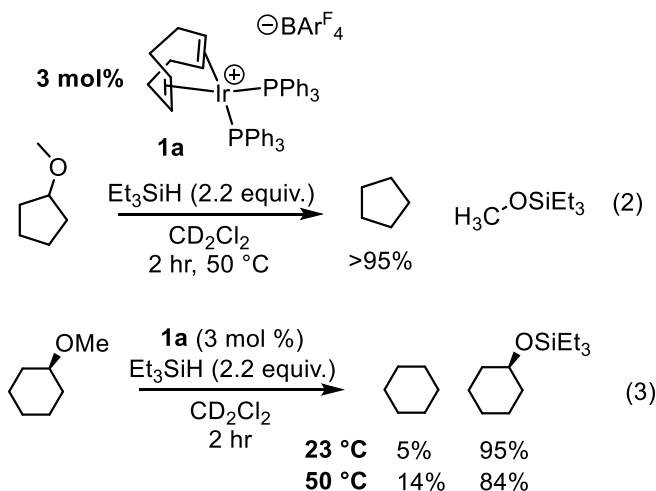
Scheme 2.1: Demethoxylation of cyclopentyl methyl ether (CPME) catalyzed by complex **1**.

Furthermore, in our previous study of the preliminary reactivity of complex **1**, Caleb Jones discovered that cyclopentyl methyl ether (CPME) underwent selective demethoxylation at the secondary position to give cyclopentane (eqn. 1).¹³ This observation contrasts with the selectivity observed from tris(pentafluorophenyl)borane which gives preferential cleavage at the methyl position.^{10,18} As secondary alcohols and ethers are common functional groups in biologically-relevant compounds including carbohydrates, I was encouraged to develop a catalytic system capable of the direct demethoxylation of secondary methyl ethers.

II. Applying [codIr(PPh₃)₂]BAR^F₄ to Six-Membered Carbocyclic Ether Cleavage

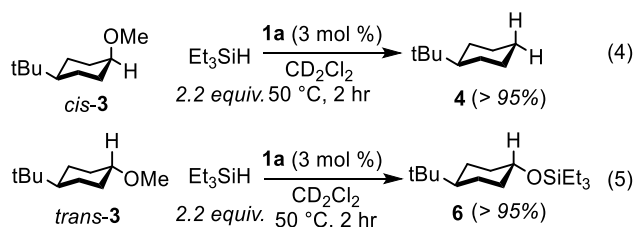
Previous efforts from the Schley group identified that in a single example, the iridium complex **1** could effect the selective cleavage of CPME at the secondary position in preference to demethylation (eqn. 1).¹³ Complex **1** is synthesized by hydrogenation of the air-stable 1,5-

cyclooctadiene complex **1a** in THF solvent, but this step has been found to be unnecessary, as complex **1a** serves as a comparably competent precatalyst to **1** (eqn 2). Surprisingly, the homologated substrate cyclohexyl methyl ether does not show the same preference, giving triethylsiloxycyclohexane as the major product (95:5 TES-OCy:CyH) (eqn. 3).



Scheme 2.2: Reduction of CPME and cyclohexyl methyl ether catalyzed by complex **1a**

The difference in selectivity for cleavage of cyclohexyl and cyclopentyl methyl ethers provided an impetus to examine the factors that influence the selectivity of iridium-catalyzed 2° methyl ether cleavage in detail. The conformationally-biased pair of substrates *cis*- and *trans*-(tert-butyl)-4-methoxycyclohexane were prepared (*cis*-**3** and *trans*-**3** respectively). By virtue of the 1,3-diaxial interactions with the tertiary butyl group, these substrates adopt conformations that place the methoxy substituent axial and equatorial in the *cis* and *trans* isomers respectively.^{19,20}



Scheme 2.3: Reduction of *cis*-**3** (top) and *trans*-**3** (bottom) catalyzed by complex **1a**

Under catalytic conditions, we observe that *cis*-**3** is cleaved to **4** and that *trans*-**3** is selectively demethylated to give silyl ether **6** (eqns. 4 and 5). These observations appear to argue for the importance of substrate conformation in hydrosilylative ether cleavage by **1a**.

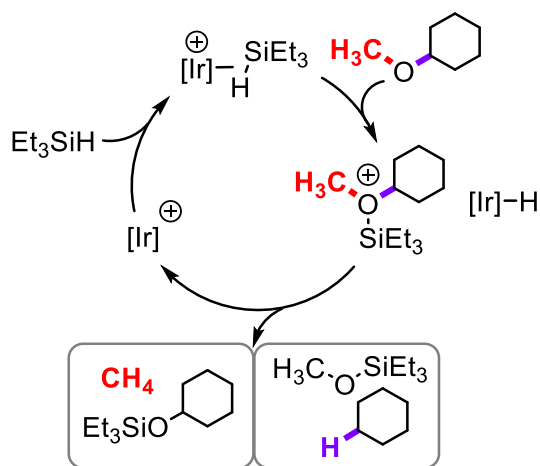


Figure 2.2. Demethylation versus deoxygenation of cyclohexyl methyl ethers

The selectivity obtained for *cis*- and *trans*-**3** can be interpreted in the context of the simplified proposed mechanism given in Figure 2.2. Based on mechanistic work on related catalysts, the cationic catalyst promotes silane heterolysis via formal transfer of a silylium ion-equivalent to the ether.^{12,13} The selectivity-determining step is proposed to be attack by a neutral iridium hydride on the incipient silyloxonium ion.^{12,13} The important reactivity difference between *cis*-**3** and *trans*-**3** should stem from different reactivity of the silyloxonium ions formed *in situ*. A computational approach was used to determine the relative energies of the chair conformations of triethylsilyloxonium ions in Table 1.1. The experimentally-determined yields of demethylation versus 2° cleavage track well with the computed difference in energies, confirming that substrates with a strong energetic preference for a conformation that places the silyloxonium ion group ($\Delta E_{ax-eq} > \sim 5$ Kcal) in the equatorial position undergo preferential demethylation by **1a**.

| Ether | Silyloxonium | $E_{ax-E_{eq}}$ | Yield A | Yield B |
|---------|--------------|-----------------|---------|---------|
| cis-3 | | -0.6 | - | >95 |
| trans-7 | | 3.1 | 32 | 68 |
| cis-8 | | 3.2 | 31 | 69 |
| CyOMe | | 4.9 | 84 | 14 |
| trans-8 | | 8.3 | >95 | - |
| cis-7 | | 10.7 | >95 | - |
| trans-3 | | 11.3 | >95 | - |

Table 2.1. Computed energies ($\text{kcal}\cdot\text{mol}^{-1}$) for chair conformations that place the OMe group axial versus equatorial compared with experimental selectivity for ether cleavage.

III. Rational Design of Iridium Bis(phosphine) Precatalysts Towards Conformational Selectivity of Cyclohexyl Methyl Ether Cleavage

Our observations on the determinants of selectivity in cyclohexyl methyl ether cleavage inspired the synthesis of an array of catalyst variants in the hopes of finding derivatives that could override the intrinsic substrate biases demonstrated in Table 2.1. The six complexes examined are given in Figure 2.3. **1a-1c** differ by variation of the phosphine substituents from PPh_3 to PMePh_2 to PMe_2Ph (**1a**, **1b** and **1c**) which decrease the steric demand of the catalyst while increasing the electron-richness of the metal center. The phosphine substituents in complexes **1d-1f** are varied from meta-xylyl to 3-methyl-5-trifluoromethyl to 3,5-bis(trifluoromethyl) (**1d**, **1e** and **1f**). This

second set represents an attempt to prepare an isosteric set of catalysts that would give intermediates with progressively decreasing hydride nucleophilicity.

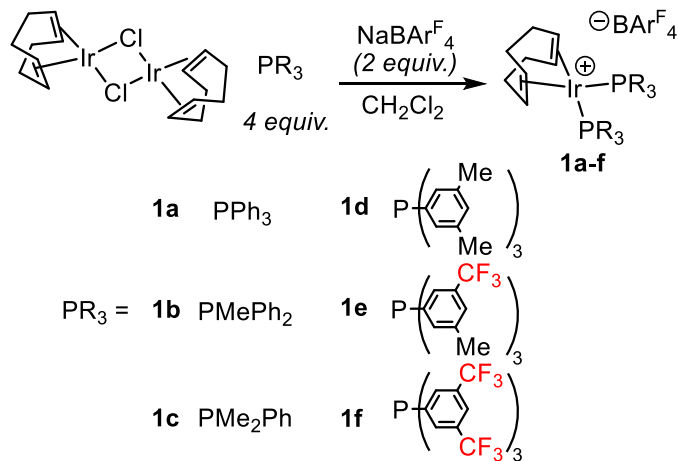
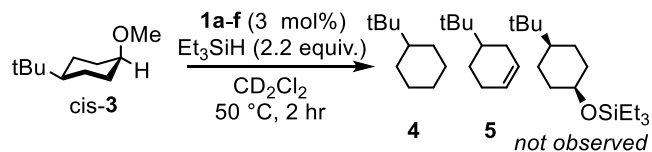


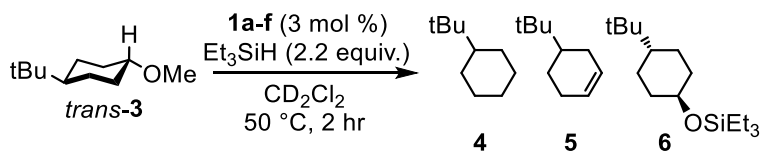
Figure 2.3. Synthesis of bis(phosphine) precatalysts tested

When the suite of catalysts **1a-f** were examined with *cis*-**3**, all six gave the product of 2° C-O bond cleavage **4** (Table 2.2). The same selectivity is not observed with the borane catalyst BCF which gives largely the product of elimination **5**. In contrast, the equatorially-predisposed methyl ether substrate *trans*-**3** shows varying selectivity across the selection of catalysts tested (Table 2.3). In cases where triphenylphosphine catalyst **1a** was highly selective for demethylation, the electron-deficient catalysts **1e** and **1f** promote selective demethoxylation. Considering the quasi-isosteric set of catalysts **1d**, **1e**, and **1f**, the replacement of one of the two methyl groups on the xylyl substituent (**1d**) by trifluoromethyl (**1e**) is sufficient to flip the observed selectivity. Additionally, when the substrates shown in Table 2.1 are examined with the electron-deficient precatalyst **1e**, products of 2° C-O cleavage are obtained in all cases (Figure S63).



| Entry | Catalyst | Yield of 4 | Yield of 5 |
|-------|-----------|-------------------|-------------------|
| 1 | 1a | > 95% | - |
| 2 | 1b | > 95% | - |
| 3 | 1c | 95% | 3% |
| 4 | 1d | > 95% | - |
| 5 | 1e | > 95% | - |
| 6 | 1f | 91% | 9% |

Table 2.2. Catalyst-controlled reduction of *cis*-**3**.

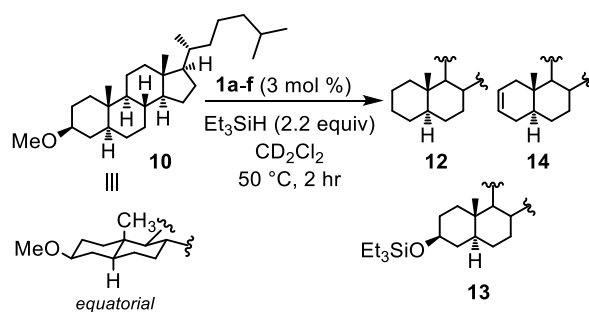


| Entry | Catalyst | Yield of 4 | Yield of 5 | Yield of 6 |
|-------|-----------|-------------------|-------------------|-------------------|
| 1 | 1a | - | - | > 95% |
| 2 | 1b | 45% | - | 54% |
| 3 | 1c | 58% | 12% | 28% |
| 4 | 1d | - | - | >95% |
| 5 | 1e | 95% | 4% | - |
| 6 | 1f | 92% | - | - |

Table 2.3. Catalyst-controlled reduction of *trans*-**3**.

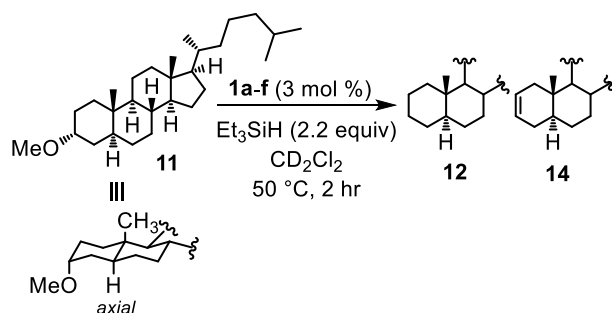
IV. Confirming Catalyst-Controlled Selectivity in Cyclohexyl Methyl Ether Cleavage

Another direct comparison of catalysts **1a-f** can be made using the *trans* decalin-based substrates **10** and **11**. These substrates cannot undergo a ring flip and thus their product distributions should directly telegraph the relative reactivity of **1a-f** for both an axial and equatorial case. The selectivity trends for complexes **1a-f** established with substrates *cis*-**3** and *trans*-**3** appear to hold for both the **10** and its axial epimer **11**. (Tables 2.4 and 2.5).



| Entry | Catalyst | Yield of 12 | Yield of 14 | Yield of 13 |
|-------|-----------|--------------------|--------------------|--------------------|
| 1 | 1a | - | - | > 95% |
| 2 | 1b | 22% | 6% | 72% |
| 3 | 1c | 47% | 19% | 34% |
| 4 | 1d | - | - | >95% |
| 5 | 1e | 91% | 9% | - |
| 6 | 1f | 64% | 36% | - |

Table 2.4. Catalyst-controlled reduction of **10**.



| Entry | Catalyst | Yield of 12 | Yield of 14 |
|-------|-----------|--------------------|--------------------|
| 1 | 1a | > 95% | - |
| 2 | 1b | 95% | 5% |
| 3 | 1c | 89% | 11% |
| 4 | 1d | > 95% | - |
| 5 | 1e | 92% | 8% |
| 6 | 1f | 96% | 4% |

Table 2.5. Catalyst-controlled reduction of **11**.

Thus, we have found that the experimental selectivity for unsymmetrical cyclohexyl methyl ether cleavage with **1a** depends strongly on the axial or equatorial disposition of the incipient silyloxonium ion, while less electron-rich catalyst variants prefer 2° C–O cleavage in all cases tested.

V. Conclusions

In summary, we have demonstrated that cationic bis(phosphine)iridium complexes function as tunable and selective catalysts for the cleavage of C–O bonds in cyclohexyl methyl ethers. For the parent bis(triphenylphosphine) precatalyst **1a** the selectivity for demethylation versus 2° C–O cleavage is determined primarily by the axial or equatorial disposition of the silyloxonium substituent in the intermediate ion. This selectivity can be overridden by the use of less electron-

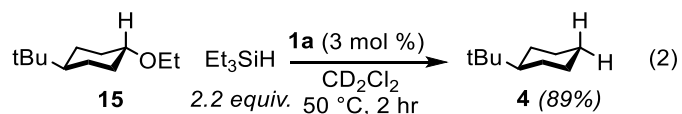
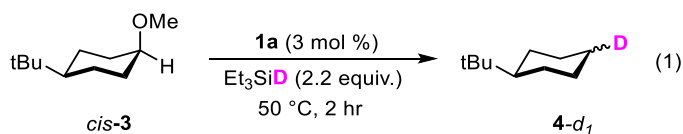
rich precatalysts **1e** and **1f** such that both axial and equatorial groups undergo cleavage at the 2° position. These findings are confirmed in trans-decalin substrates.

Chapter 3. Mechanistic Studies of Iridium Bis(phosphine)-Catalyzed C-O Cleavage of Cyclohexyl Methyl Ethers

I. Studying the Mechanism of Demethoxylation vs. Demethylation of Cyclohexyl Methyl Ethers

This chapter will focus on understanding the previously observed reactivity trends in iridium bis(phosphine)-catalyzed cyclohexyl methyl ether silylation as well as reactivity towards more complex sterol-derived substrates.

The selectivity for methyl versus 2° C-O cleavage observed in chapter 2 is likely dictated by the relative rates of S_N1 cleavage of the silyloxonium versus S_N2 cleavage of the methyl group. The apparent preference for S_N1 reactivity at substrates with significant axial silyloxonium populations can be rationalized on the basis of the known increased rate of solvolysis of axial cyclohexane substituents relative to their equatorial isomers.^{19,21} In the case of **1a**, evidence for S_N1 substitution has been obtained through the cleavage of *cis*-**3** using Et₃SiD, which gives a near-1:1 mixture of *cis* and *trans* **4-d₁** (eqn. 1). Evidence for an S_N2 mechanism for demethylation has been obtained by the reduction of **15**, which undergoes selective deethoxylation. (eqn. 2) This outcome is expected given the much lower rate of S_N2 reactions of ethyl groups versus methyl groups.



Scheme 3.1. S_N1 (top) versus S_N2 (bottom) mechanistic studies for dealkoxylation versus dealkylation selectivity.

II. Applying S_N2 Demethylation and S_N1 Demethoxylation to Bile Acid Derivatives

Our success in developing selective catalysts for equatorial cyclohexyl methyl ether C-O cleavage encouraged the examination of more-complex substrates derived of cholic acid (Figure 3.1).⁵ Cholic acid and its derivatives are synthesized in the liver from cholesterol²² and play an important role in cholesterol homeostasis²³ and lipid metabolism.²⁴ In particular, they function as signaling molecules for nuclear receptors²⁵ with unnatural variants occasionally possessing desirable target selectivity.^{26,27}

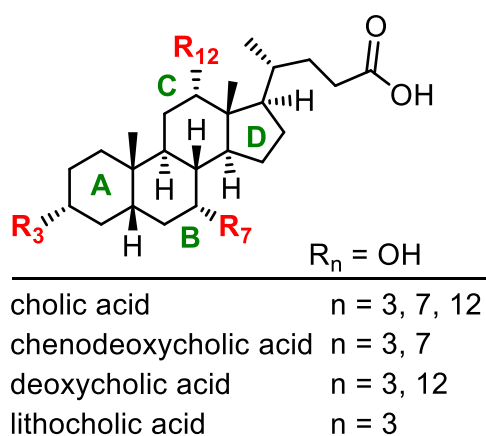


Figure 3.1. Hydroxylation pattern of cholic acids.

The sites of hydroxylation, their stereochemistry, and the degree of polyhydroxylation are species-dependent, with the parent cholic acid being hydroxylated on the α face at the 3, 7, and 12 positions on the A, B and C rings respectively (Figure 3.1). Their biological relevance has inspired studies of the relative reactivity of each site of hydroxylation. Deoxycholic acid has been previously prepared by B-ring deoxygenation via selective oxidation of the 7 α -hydroxyl to the mono ketone^{28,29} followed by Wolff-Kishner reduction.³⁰ A similar strategy has been used to deoxygenate the C ring of 6,12-dihydroxy-cholanoic acid.³¹ For the unprotected triols, the A-ring

hydroxyl is considered to be the least reactive site with respect to oxidation by chromic oxide.³²

34

When methyl ether substrates **16-19** were subjected to optimized catalytic conditions using complex **1a** as a catalyst we observed in all cases selective reaction at the 3 α -methoxy substituent of the A ring. (Figure 3.2) This observation is particularly noteworthy given the number of potential positions for reduction in cholanol derivative **19**.

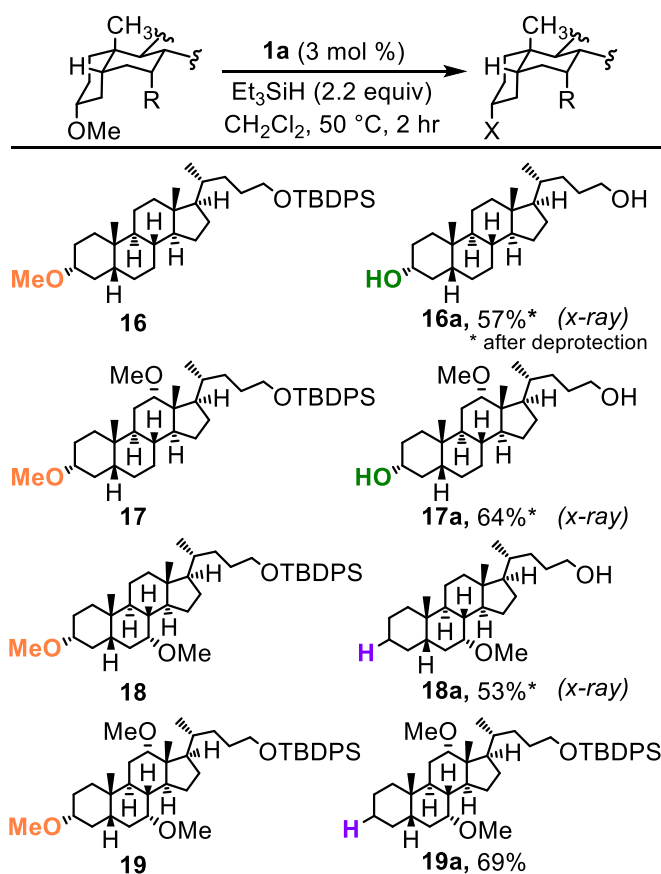


Figure 3.2. Isolated yields for cholanic acid-derived methyl ether silylation. Single crystal X-ray data for **16a**, **17**, **17a**, and **18a** is provided as supplemental information.

While all four cholanol derivatives **16-19** undergo selective reaction at the 3 α -substituent on the A ring, the fate of this methyl ether appears to be dictated by substitution on the neighboring B ring. For both the protected lithocholanol and deoxycholanol derivatives **16** and **17**, the 3 α -methoxy group undergoes demethylation – an outcome consistent with the selectivity expected for

an equatorial methyl ether with **1a** as the catalyst. With the same catalyst however, chenodeoxycholanol **18** and cholanol **19** undergo 2° cleavage of the 3 α -methoxy substituent. When examining the four cholanol substrates together it appears that the presence or absence of the 7 α -methoxy substituent on the B ring controls the fate of the 3 α -methoxy group under our silylation conditions with **1a**.

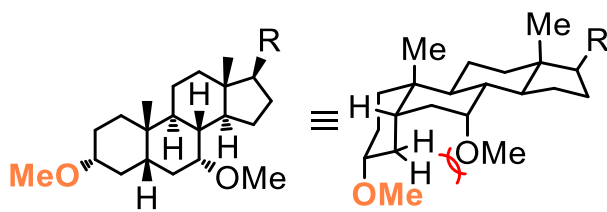


Figure 3.3. Depiction of the interaction of the 7 α substituent with the *cis*-fused A-ring

A depiction of the *cis*-fusion of the A and B rings of cholic acids is shown in Figure 3.3. The 7 α group is spatially located to participate in a pseudo syn-pentane interaction with the C4 methylene of the A ring. This steric interaction likely destabilizes the chair conformation of the A-ring relative to the twist-boat. Since the ionization of cyclohexane substituents is believed to proceed through the twist-boat and not directly from the chair in many cases^{21,35,36} our hypothesis is that differential destabilization of the chair by the 7 α -OMe group in **18** and **19** increases the rate of S_N1 substitution of the 3 α -silyloxonium intermediate and thus promotes deoxygenation.

III. Studying the Activation of Olefin-Bound Precatalyst **1a** in Catalysis

Although the 1,5-cyclooctadiene complex **1a** serves as an equally competent catalyst to the corresponding dihydride cation complex **1** (Figure 2.1) used in our previous study,¹³ the two possess different reactivity profiles at short reaction times when reactions were set up in an inert atmosphere glove box with dried reagents. In particular, the distinctive red color of the precursor complex **1a** ($\lambda_{\text{max}} = 588 \text{ nm}$) was found to persist for up to 30 minutes after mixing, during which

time no reaction product is formed (Figure 3.4, orange). In contrast, catalysis with the dihydride cation **1** initiates rapidly. Analysis of product mixtures resulting from catalysis by **1a** show no products of 1,5-cyclooctadiene hydrosilylation. Instead, the only organic product resulting from the diene ligand of the precatalyst is cyclooctane, which we estimate by NMR is formed in sufficient quantity to account for the entire balance of the 1,5-cyclooctadiene ligand in the precatalyst. Activation of **1a** by formation of cyclooctane would require dihydrogen or an equivalent reagent, which we postulated could arise via dehydrosilylation of trace water, protic impurities, or silanols on the surface of the glass reaction vessel.

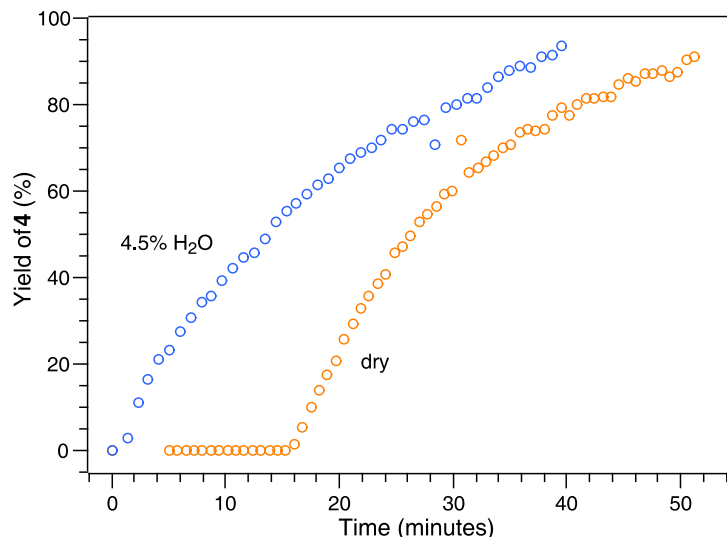


Figure 3.4. Role of trace water in precatalyst (**1a**) activation by NMR analysis.

The hypothesis that added or adventitious water serves as an H₂ source via reaction with silane can be confirmed by ¹H NMR analysis of a catalytic reaction containing 4.5 mol % H₂O. (Figure 3.4, blue) At the point of onset of catalysis a signal corresponding to dissolved H₂ (ca. 1.3 mol %) is observed at 4.62 ppm in the catalytic reaction conducted in the presence of water, while the H₂ signal is absent in reactions conducted under anhydrous conditions. When the activation of **1a** is observed by UV-Vis under more dilute conditions (1.2 mM Ir vs 6.0 mM Ir used in catalytic reactions and Figure 3.5) a ca. 2 minute induction period is seen even in moist solvent, however

the addition of either 0.10 equivalents of the dihydride **1** or bubbling H_2 leads to near-instantaneous bleaching of **1a** and activation (Figure 3.5).

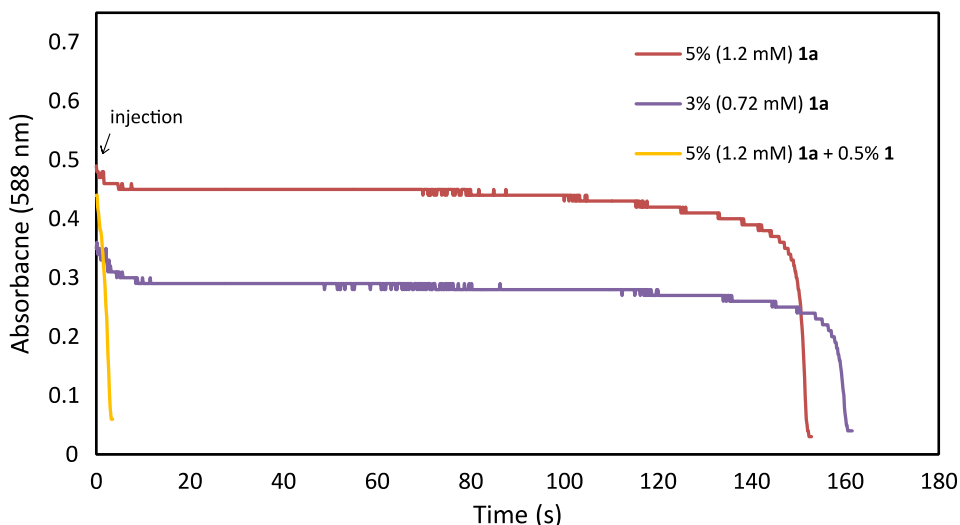
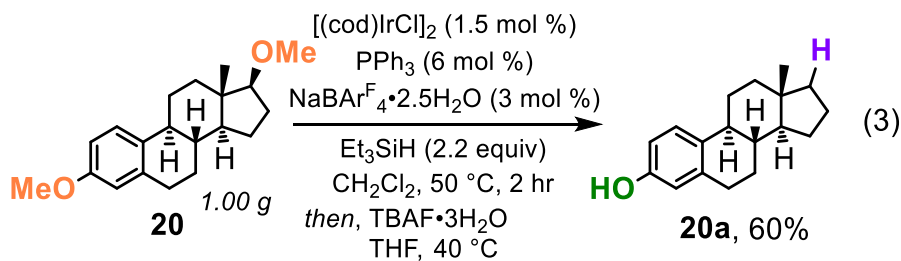


Figure 3.5. Bleaching of **1a** at low concentration by UV-Vis. Role of added **1** shown (yellow). *Note:* Bleaching is near instantaneous under typical reaction conditions (6.0 mM Ir, non-dry solvent)

In total, these experiments argue that initiation of catalysis by **1a** is aided by dihydrogen generated by catalytic dehydrosilylation of trace moisture in the reagents and reaction solvents ($H_2O + 2HSiEt_3 \rightarrow H_2 + O(SiEt_3)_2$). The observed induction period can be explained by assuming that diene precursor **1a** is a substantially inferior catalyst for this dehydrosilylation reaction versus activated species like **1**, leading to apparent autocatalytic behavior in the activation kinetics. In fact, a different salt of **1** has been reported as an efficient dehydrosilylation catalyst.³⁷ Conveniently, the water content of reagent-grade dichloromethane that has not been dried over alumina or molecular sieves appears to be sufficient for rapid catalyst activation under our optimized conditions. When dry solvent is readily available, the deliberate addition of 1.5 to 3 molar equivalents of water relative to catalyst serves the same purpose without apparent decrease in reaction yield.

IV. Applying Water Activation to Catalysis with **1a** Generated *In-Situ*.

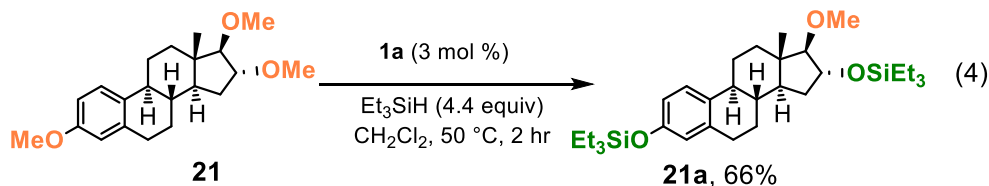
Upon discovering that this bis(phosphine) system is not only tolerant of trace water, but that catalytic onset is actually enhanced in its presence, we sought to further test the robustness of this system by generating catalyst **1a** in-situ, in air, using entirely commercially-available reagents. The previously discussed water-promoted catalyst activation is important in the context of this reaction because upon air/moisture exposure, NaBAR^F₄ is hygroscopic and takes on ~2.5 molar equivalents of water. A previous report showed that mixtures of NaBAR^F₄ and [(cod)IrCl]₂ were inactive for ether silylation on their own,¹⁷ however we speculated that the addition of triphenylphosphine would allow for direct synthesis of complex **1a** *in situ*.



Scheme 3.2. Reduction of **20** on a 1.00 g scale catalyzed by **1a** generated *in situ*.

Prior to setup of the catalytic reaction, solid samples of [(cod)IrCl]₂, NaBAR^F₄, and triphenyl phosphine were left open to the air for 24 h. On small scales (0.040 mmol) the catalyst generated in situ gave comparable outcomes for the demethoxylation and demethylation of *cis*-**3** and *trans*-**3** respectively. The reduction of 1.00 gram of dimethylestradiol (**20**) could also be accomplished in air using catalyst generated *in situ*. Under these conditions dimethylestradiol undergoes both demethylation of the anisole functional group and demethoxylation of the D ring to give 17-deoxyestradiol (**20a**) in 60% isolated yield after deprotection (eqn. 3). It is interesting to note that although deoxygenation of the 17 β -OMe group in **20** is observed, this group occupies a pseudo-equatorial position by virtue of the C/D ring fusion.³⁸ As further evidence for the

important role of local conformation, trimethylestriol (**21**) (differing from **20** by addition of a methoxy substituent at C16) is not reduced at C17 under our conditions (eqn. 4).



Scheme 3.3. Reduction of **21** catalyzed by **1a**.

V. Catalyst Speciation and Mechanism

A complete proposed mechanism for ether cleavage by bis(phosphine) iridium catalysts is given in Figure 3.6 and is based on work by Brookhart and our own previous study.^{12,13} A cationic σ -silane compound (**A**) is believed to transfer an equivalent of triethylsilylium ion to substrate ether to give a silyloxonium ion (**D**) and a neutral metal hydride (**B/C**). Since silyloxonium ions undergo silylium exchange with ethers,¹² the selectivity-determining step should be hydride delivery to the silyloxonium ion (**D**).

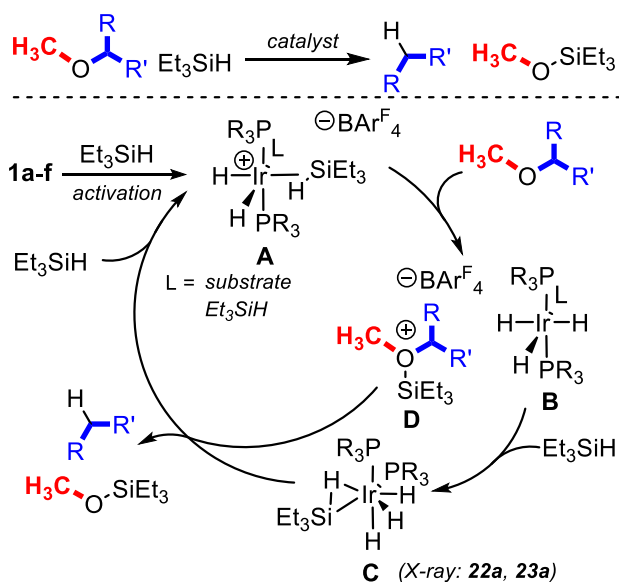
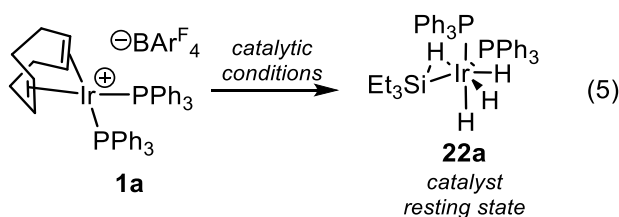


Figure 3.6. Proposed mechanism for iridium-catalyzed 2° ether cleavage.

In our previous report we showed that complex **1** operates by a mechanism analogous to the Brookhart system, with a neutral tetrahydridosilyl species $[(\text{PPh}_3)_2\text{IrH}_4\text{SiEt}_3]$ (**22a**) serving as both the catalyst resting state (**D**) and plausible hydride source in silyloxonium cleavage.¹³ Although we previously characterized this species by NMR spectroscopy, after independent synthesis from $(\text{PPh}_3)_2\text{IrH}_5$,³⁹ the lack of structural data led us to propose a *trans* arrangement of the two triphenylphosphine ligands to account for the single resonance observed by ³¹P NMR spectroscopy.¹³ We now find that under our optimized conditions for ether silylation, the precatalyst **1a** gives the same catalyst resting state (**C/22a**) (eqn. 5) (Figures S4 and S5).



Scheme 3.4. Resting state speciation of **1a** under catalytic conditions

The observation that complex **22a** serves as the catalyst resting state when **1a** is the precatalyst implies that the turnover-limiting step is the reaction of **C** with silyloxonium ion **D**. As **D** is formed in the same silane heterolysis step that leads to **C**, the concentration of **D** should be equal to that of **B** (not observed) + **C**. Thus, a bimolecular turnover-limiting step between **C** and **D** is expected to give a rate law with 2nd order dependence on the iridium concentration. Indeed, kinetic analyses of the cleavage of *trans*-**3** by **1a** are consistent with a 2nd order dependence on iridium loading (Figure 3.7). With 2 mol % **1a**, the reduction of *trans*-**3** takes 5 minutes to reach 40% yield and only 60 seconds to reach the same point when the **1a** loading is doubled to 4 mol %. Direct NMR evidence for a free silyloxonium ion (**D**) during catalysis is complicated by rapid exchange with substrate ether, however, Brookhart has been able to characterize a relevant silyloxonium ion under related conditions.¹²

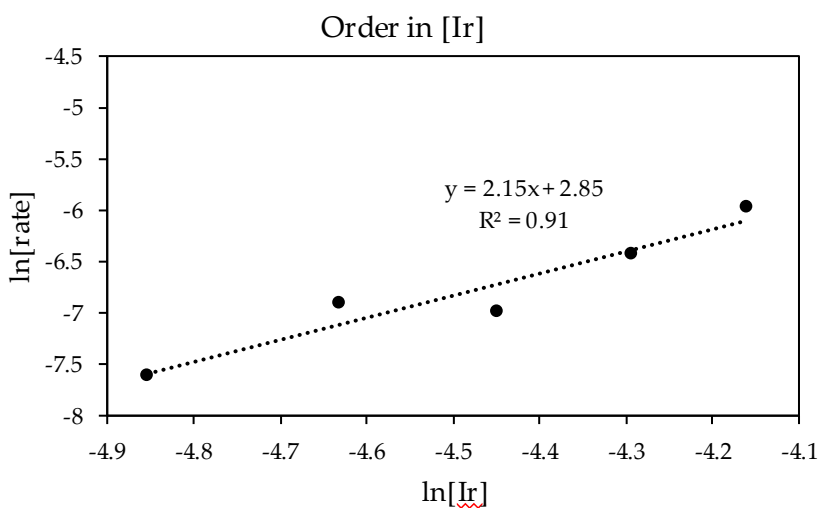
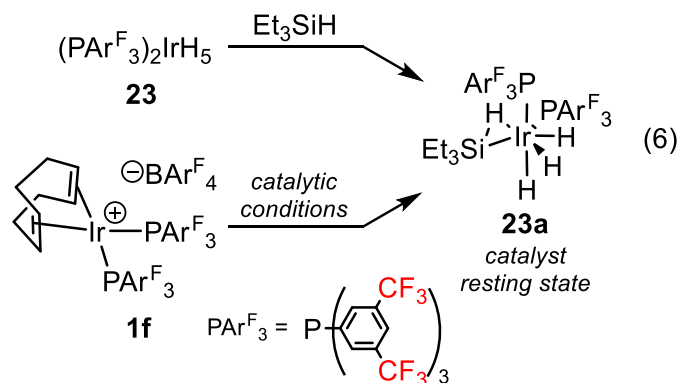


Figure 3.7. Ln/Ln plot showing 2nd order rate dependence on iridium loading.

Furthermore, we have been successful in obtaining single-crystal samples of the resting state species **C/22a** suitable for X-ray crystallography. Our X-ray crystallographic analysis demonstrates that the two phosphine ligands occupy *cis* sites in the solid state, with one being *trans* to the silyl ligand. (Figure 3.8, left) The high quality of the structural data has allowed us to locate and refine the four metal hydride atom positions. (See Appendix I. for additional details) This analysis shows that one of the hydride ligands occupies a bridging position between the iridium ion and the silyl ligand. By using the refined, restrained hydrogen atom positions as initial coordinates for a DFT calculation, we find that this results in calculated bond lengths of 1.70 Å and 1.80 Å for the Ir-H and H-Si bonds respectively. The latter represents a significantly elongated Si-H bonding contact but does not rule out some non-classical, σ -silane character.⁴⁰



Scheme 3.5. Resting state speciation of **1f** under catalytic conditions and independent synthesis.

At present it is unknown whether the solid-state structure of **22a** aligns with its structure in solution. The single ^{31}P NMR resonance observed in solution suggests a structure with higher symmetry, however rapid silane dissociation or other exchange processes could also be responsible for the higher apparent symmetry of the ^{31}P NMR signal. The characterization of the catalyst resting state when **1a** is used as a precatalyst inspired us to pursue a similar study on the less electron-releasing phosphine variants that gave rise to distinct selectivity profiles in C-O bond cleavage of cyclo-hexyl methyl ethers (*vide supra*). Like **1a**, the tris(3,5-bis(trifluoromethyl)phenyl)phosphine-ligated complex **1f** also gives a single resonance by ^{31}P NMR spectroscopy during catalysis (Figure S6). Independent preparation of the tetrahydridosilyl compound **23a** from **23** (eqn. 6) allows us to confirm that **23a** is the catalyst resting state when **1f** is used as a precatalyst. Characterization of **23a** by single-crystal X-ray diffraction confirms that **22a** and **23a** share a similar solid-state geometry (Figure 3.8). Thus, we can conclude that the changes in selectivity on moving from complex **1a** to **1f** stem from differences in reactivity of comparable catalytic intermediates rather than a switch in overall catalyst structure resulting from modification of the phosphine ligands.

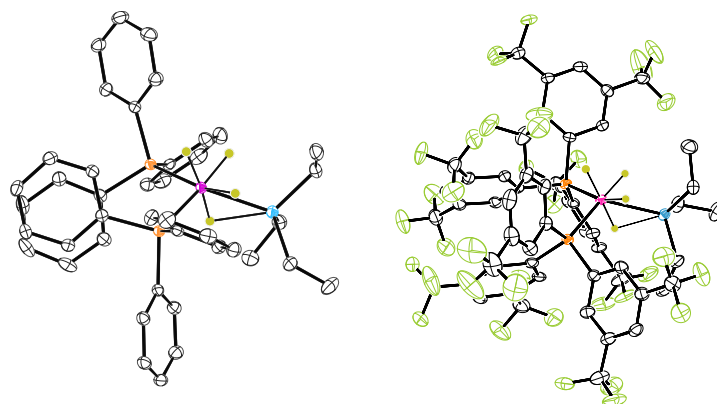


Figure 3.8. ORTEP dia grams of **22a** (left) and **23a** (right) shown at 50% probability.

The apparent structural similarity of **22a** and **23a** extends to their DFT-optimized hydrogen positions. The Si–H bond distance in **23a** is calculated to be identical to that in **22a** (1.82 Å versus 1.80 Å). Given the less electron-releasing ligands in **23a**, we had expected to see a contraction of the Si–H bond distance resulting from reduced backdonation into the Si–H σ^* . The lack of such an observation is telling given that the potential energy surface for elongation of the Si–H bond in σ -silane complexes is known to be shallow.⁴¹ Accordingly, **22a** and **23a** appear to have comparable degrees of σ -silane character, despite representing two extremes of a highly-tunable hydride equivalent for silyloxonium-ion reduction.

VI. Conclusions

In summary we have demonstrated mechanistic details of cationic bis(phosphine)iridium complexes catalyzing the cleavage of C–O bonds in cyclohexyl methyl ethers. The outcome of a deuterium incorporation experiment is consistent with 2° alkyl ether cleavage occurring via an S_N1 -type substitution reaction of the silyloxonium intermediate, while the relative reactivity of an ethoxy derivative is a hallmark of an S_N2 process for demethylation.

This class of catalysts has been extended to cholic acid derivatives bearing a *cis* fusion at the **A** and **B** rings. In these cases, the 3 α -OMe group undergoes reduction in preference to other

positions, with the selectivity for demethoxylation versus demethylation being controlled by the presence or absence of a 7α -OMe substituent respectively. Studies of the structure of the catalyst resting state demonstrate that both the PPh_3 and 3,5 tris(bis(trifluoromethyl)phenyl)phosphine variants of the catalyst adopt a comparable tetrahydridosilyliridium structure with similar degrees of σ -Si-H character. The significant change in ligand electronics is able to switch the selectivity profile of the resulting catalysts without major perturbation of the resting-state structure, presumably by modulation of the hydride nucleophilicity.

Finally, we find that catalysis by this class of cationic bis(phosphine) complexes is remarkably robust. The catalysts can be generated from commercially-available materials directly in air and is activated by trace water in solution. In total, we find that cationic bis(phosphine)iridium complexes are operationally simple and tunable catalysts for the selective reduction of 2° methyl ethers. Our groups ongoing efforts aim to extend the scope of suitable substrates for selective deoxygenation from sterols to complex carbohydrate-derived polyethers, and have recently been shown as selective C3-demethylation catalysts for *o*-cresol-type carbohydrates.⁴²

VII. References for Chapter 2 and Chapter 3

- (1) Hydrogenation and Hydrogenolysis of Ethers | Journal of the American Chemical Society.
- (2) Zaheer, M.; Kempe, R. Catalytic Hydrogenolysis of Aryl Ethers: A Key Step in Lignin Valorization to Valuable Chemicals. *ACS Catal.* **2015**, *5* (3), 1675–1684.
- (3) Hartwig, W. Modern Methods for the Radical Deoxygenation of Alcohols. *Tetrahedron* **1983**, *39* (16), 2609–2645.
- (4) König, B.; Hermann, J. M. Reductive Deoxygenation of Alcohols: Catalytic Methods Beyond Barton–McCombie Deoxygenation. *Euro. J. Org. Chem.* **2013**, *31*, 7017–7027.

- (5) Dai, X.-J.; Li, C.-J. En Route to a Practical Primary Alcohol Deoxygenation. *J. Am. Chem. Soc.* **2016**, *138* (16), 5433–5440.
- (6) Bauer, J. O.; Chakraborty, S.; Milstein, D. Manganese-Catalyzed Direct Deoxygenation of Primary Alcohols. *ACS Catal.* **2017**, *7* (7), 4462–4466.
- (7) Yang, S.; Tang, W.; Yang, Z.; Xu, J. Iridium-Catalyzed Highly Efficient and Site-Selective Deoxygenation of Alcohols. *ACS Catal.* **2018**, *8* (10), 9320–9326.
- (8) Barton, D. H. R.; McCombie, S. W. A New Method for the Deoxygenation of Secondary Alcohols. *J. Chem. Soc. Perkin I* **1975**, No. 16, 1574–1585.
- (9) Burwell, R. L. The Cleavage of Ethers. *Chem. Rev.* **1954**, *54* (4), 615–685.
- (10) Gevorgyan, V.; Liu, J.-X.; Rubin, M.; Benson, S.; Yamamoto, Y. A Novel Reduction of Alcohols and Ethers with a HSiEt₃catalytic B(C₆F₅)₃ System. *Tetrahedron Lett.* **1999**, *40* (50), 8919–8922.
- (11) Gevorgyan, V.; Rubin, M.; Benson, S.; Liu, J.-X.; Yamamoto, Y. A Novel B(C₆F₅)₃-Catalyzed Reduction of Alcohols and Cleavage of Aryl and Alkyl Ethers with Hydrosilanes. *J. Org. Chem.* **2000**, *65* (19), 6179–6186.
- (12) Yang, J.; White, P. S.; Brookhart, M. Scope and Mechanism of the Iridium-Catalyzed Cleavage of Alkyl Ethers with Triethylsilane. *J. Am. Chem. Soc.* **2008**, *130* (51), 17509–17518.
- (13) Jones, C. A. H.; Schley, N. D. Selective Alkyl Ether Cleavage by Cationic Bis(Phosphine)Iridium Complexes. *Org. Biomol. Chem.* **2018**.
- (14) Adduci, L. L.; McLaughlin, M. P.; Bender, T. A.; Becker, J. J.; Gagné, M. R. Metal-Free Deoxygenation of Carbohydrates. *Angew. Chem. Int. Ed.* **2014**, *53* (6), 1646–1649.

- (15) Hein, N. M.; Seo, Y.; Lee, S. J.; Gagné, M. R. Harnessing the Reactivity of Poly(Methylhydrosiloxane) for the Reduction and Cyclization of Biomass to High-Value Products. *Green Chem.* **2019**, *21* (10), 2662–2669.
- (16) Seo, Y.; Lowe, J. M.; Gagné, M. R. Controlling Sugar Deoxygenation Products from Biomass by Choice of Fluoroarylborane Catalyst. *ACS Catal.* **2019**, *9* (8), 6648–6652.
- (17) McLaughlin, M. P.; Adduci, L. L.; Becker, J. J.; Gagné, M. R. Iridium-Catalyzed Hydrosilylative Reduction of Glucose to Hexane(s). *J. Am. Chem. Soc.* **2013**, *135* (4), 1225–1227.
- (18) Yang, J.; Brookhart, M. Iridium-Catalyzed Reduction of Alkyl Halides by Triethylsilane. *J. Am. Chem. Soc.* **2007**, *129* (42), 12656–12657.
- (19) Winstein, S.; Holness, N. J. Neighboring Carbon and Hydrogen. XIX. t-Butylcyclohexyl Derivatives. Quantitative Conformational Analysis. *J. Am. Chem. Soc.* **1955**, *77* (21), 5562–5578.
- (20) Buchanan, G. W.; Ross, D. A.; Stothers, J. B. A New Approach to Conformational Analysis. Carbon-13 Nuclear Magnetic Resonance. *J. Am. Chem. Soc.* **1996**, *88* (18), 4301-4302.
- (21) Nordlander, J. E.; Blank, J. M.; Jindal, S. P. Solvolysis Rates of 4,4-Dimethylcyclohexyl Tosylate. Evidence on Conformational Reactivities. *Tetrahedron Lett.* **1969**, *10* (40), 3477–3479.
- (22) Bloch, K. The Biological Conversion of Cholesterol to Pregnanediol. *J. Biol. Chem.* **1945**, *157* (2), 661–666.
- (23) Russell, D. W.; Setchell, D. R. Bile acid biosynthesis. *Biochemistry* **1992**, *31* (20), 4737-4749
- (24) Qi, Y.; Jiang, C.; Cheng, J.; Krausz, K. W.; Li, T.; Ferrell, J. M.; Gonzalez, F. J.; Chiang, J. Y. L. Bile Acid Signaling in Lipid Metabolism: Metabolomic and Lipidomic Analysis of

- Lipid and Bile Acid Markers Linked to Anti-Obesity and Anti-Diabetes in Mice. *Biochim. Biophys. Acta* **2015**, *1851* (1), 19–29.
- (25) Li, T.; Chiang, J. Y. L. Nuclear Receptors in Bile Acid Metabolism. *Drug Metab. Rev.* **2013**, *45* (1), 145–155.
- (26) Festa, C.; Renga, B.; D'Amore, C.; Sepe, V.; Finamore, C.; De Marino, S.; Carino, A.; Cipriani, S.; Monti, M. C.; Zampella, A.; Fiorucci, S. Exploitation of Cholane Scaffold for the Discovery of Potent and Selective Farnesoid X Receptor (FXR) and G-Protein Coupled Bile Acid Receptor 1 (GP-BAR1) Ligands. *J. Med. Chem.* **2014**, *57* (20), 8477–8495.
- (27) Yu, D. D.; Sousa, K. M.; Mattern, D. L.; Wagner, J.; Fu, X.; Vaidehi, N.; Forman, B. M.; Huang, W. Stereoselective Synthesis, Biological Evaluation, and Modeling of Novel Bile Acid-Derived G-Protein Coupled Bile Acid Receptor 1 (GP-BAR1, TGR5) Agonists. *Bioorg. Med. Chem.* **2015**, *23* (7), 1613–1628.
- (28) Gallagher, T. F.; Long, W. P. PARTIAL OXIDATION OF CHOLIC ACID. *J. Biol. Chem.* **1943**, *147* (1), 131–134.
- (29) Fieser, L. F.; Rajagopalan, Srinivasa. Selective Oxidation with N-Bromosuccinimide. I. Cholic Acid. *J. Am. Chem. Soc.* **1949**, *71* (12), 3935–3938.
- (30) Hoehn, W. M.; Linsk, J. 3,12-Dihydroxy-7-Ketocholanic Acid¹. *J. Am. Chem. Soc.* **1945**, *67* (2), 312–314.
- (31) Sonders, R.C.; Elliot, W. H. Bile acids. XXVI. Metabolism of 12 α -hydroxycholanoic acid-24-14C in the rat. *Biochemistry*, **1969**, *8* (1), 405-413.
- (32) Fieser, L. F.; Rajagopalan, S. Oxidation of Steroids. III. Selective Oxidations and Acylations in the Bile Acid Series¹ | *J. Am. Chem. Soc.* **1950**, *72* (12), 5530-5536.

- (33) Bergström, S.; D. Haslewood, G. A. 122. Substituted KetochoLANic Acids. *J. Chem. Soc. Resumed* **1939**, 0 (0), 540–541.
- (34) Kuwada, S.; Morimoto, S. Über Die Partielle Oxydation Des Cholsäuremethylesters. (Untersuchungen Über Sterine, XXVI). *Bull. Chem. Soc. Jpn.* **1942**, 17 (3), 147–152.
- (35) Evaluation of the Relative Importance of Charge-Dipole Interactions and Steric Strain Acceleration in Conformationally Mobile Systems. *J. Am. Chem. Soc.* **1964**, 86 (6), 1161-1166.
- (36) Jr. S. V. J.; Jewett, J. G. Nonchair Transition State Conformation in trans-4-t-Butylcyclohexyl Brosylate Solvolysis. *J. Am. Chem. Soc.* **1965**, 87 (6), 1383-1384.
- (37) Luo, X. L.; Crabtree, R. H. Homogeneous catalysis of silane alcoholysis via nucleophilic attack by the alcohol on an Ir(η -2-HSiR₃) intermediate catalyzed by [IrH₂S₂(PPh₃)₂]SbF₆ (S = solvent). *J. Am. Chem. Soc.* **1989**, 111 (7), 2527-2535.
- (38) Barton, H. R. The Conformation of the Steroid Nucleus. *Experientia* **1950**, 6 (8), 316–320.
- (39) Loza, M.; Faller, J. W.; Crabtree, R. H. Seven-Coordinate Iridium(V) Polyhydrides with Chelating Bis(silyl) Ligands. *Inorg. Chem.* **1995**, 34 (11), 2937-2941.
- (40) *Advances in Organometallic Chemistry*; Academic Press, 1971.
- (41) Recent Advances in Nonclassical Interligand Si-H Interactions - Vanderbilt University.
- (42) Jones, C. A. H.; Schley, N. D. Selective Demethylation of O-Aryl Glycosides by Iridium-Catalyzed Hydrosilylation. *Chem. Commun.* **2021**, 57, 5935-5956.

Appendix I. Experimental Section for Chapter 2 and Chapter 3

Supporting Information

I. General Information

General Considerations. Syntheses and manipulations with organometallic reagents were carried out using standard vacuum, Schlenk, cannula, or glovebox techniques under N₂ unless otherwise specified. All catalytic transformations and organic syntheses were conducted in air, unless otherwise specified. Tetrahydrofuran, dichloromethane, toluene, pentane, and diethyl ether were degassed with argon and dried over activated alumina using a solvent purification system. The following chemicals were purchased from chemical vendors and used as received: IrCl₃·H₂O, triphenylphosphine, tris(3,5-xylyl)phosphine, methyldiphenylphosphine, dimethylphenylphosphine, and hydrogen.

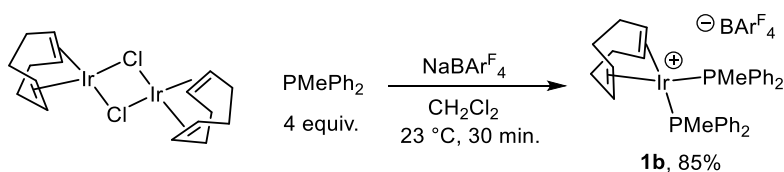
Spectroscopy. ¹H, ²H, ¹³C, ³¹P, and ¹⁹F NMR spectra were recorded on Bruker NMR spectrometers at ambient temperatures unless otherwise noted. ¹H and ¹³C chemical shifts are referenced to residual solvent signals, ³¹P chemical shifts are referenced to an external H₃PO₄ standard, and ¹⁹F chemical shifts are referenced to an external C₆F₆ standard. ¹³C assignments were made with assistance of 2D methods.

Elemental Analysis. Elemental analyses of complexes (**1b-f**, **22a**, **23**, and **23a**) are of the bulk samples for which yields are reported. No additional purification operations are carried out prior to packaging for analysis, but samples are dried under vacuum for *ca.* 2 days to remove residual or co-crystallized solvent. Elemental analyses were performed at the University of Rochester CENTC Elemental Analysis Facility or by Midwest Microlab.

Synthesis and Characterization

Bis(1,5-cyclooctadiene)diiridium(I) dichloride $[(\text{cod})\text{IrCl}]_2$,¹ sodium tetrakis[3,5-bis(trifluoromethyl)phenyl]borate ($\text{NaBAR}^{\text{F}_4}$), $[(\text{cod})\text{Ir}(\text{PPh}_3)_2]\text{BAR}^{\text{F}_4}$ (**1a**),² and $[\text{H}_4(\text{Et}_3\text{Si})\text{Ir}(\text{PPh}_3)_2]$ (**20a**)³ were prepared by published procedures.

Substrate precursors. Estriol, cholic acid, 5α -cholestan- 3β -ol, deoxycholic acid, and chenodeoxycholic acid were purchased from commercial sources and used as supplied. Estradiol was purchased from a commercial source and dried under vacuum for 24 h.



Preparation of $[(\text{cod})\text{Ir}(\text{PMePh}_2)_2]\text{BAR}^{\text{F}_4}$ (1b**).** A 20 mL glass vial was charged with a stir bar, bis(1,5-cyclooctadiene)diiridium(I) dichloride (0.1001 g, 0.149 mmol), methyl diphenyl phosphine (0.1190 g, 111 μL , 0.597 mmol, 4.01 equiv.), and sodium tetrakis[3,5-bis(trifluoromethyl)phenyl]borate (0.2649 g, 0.299 mmol, 2.01 equiv.) and 4.0 mL of dry dichloromethane. The resulting solution was allowed to stir for 30 minutes and was then diluted with 10 mL of dry diethyl ether and allowed to stir for an additional hour. At this point the precipitate was filtered off using a 0.45 μm PTFE syringe filter. The resulting filtrate was evaporated to dryness under vacuum to give a red foam. The foam was crushed with a spatula and the residue was treated with a 5 mL portion of dry pentane which was then evaporated. This operation was repeated once to give a dry, bright red solid. The red solid was suspended in 3 mL pentane and filtered. The residue was washed with two, 3 mL portions of pentane to give the product as a red solid after drying under vacuum. Yield: 0.3962 g (85%). Crystals suitable for X-

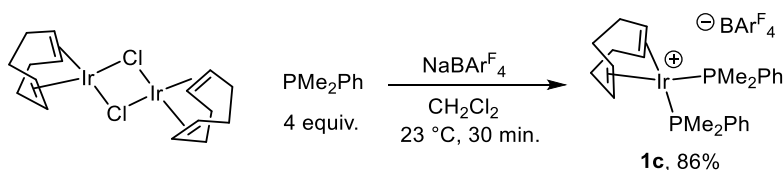
ray diffraction were obtained by layering dry pentane on a saturated ether solution of **1b** at 23 °C.

Elemental Analysis for C₆₆H₅₀BF₂₄IrP₂: C, 50.68; H, 3.22. Found: C, 50.64; H, 3.13.

¹H NMR (400 MHz, 23 °C, CD₂Cl₂): δ 1.70 (d, J = 7.43 Hz, 6H), 2.08 (m, 4H), 2.22 (m, 4H), 4.23 (br, 4H), 7.45 – 7.56 (m, 20H) 7.56 (s, 4H), 7.73 (s, 8H).

³¹P{¹H} NMR (162 MHz, 23 °C, CD₂Cl₂): δ 2.6 (s).

¹³C{¹H} NMR (100 MHz, 23 °C, CD₂Cl₂): δ 14.3 (m), 30.9, 87.1 (t, J = 5.6 Hz), 117.4 (m), 124.5 (q, J = 272.5), 128.8 (qq, J = 31.5 Hz, J = 3.0 Hz), 129.0 (t, J = 4.9 Hz), 130.8 (m), 131.7, 132.7 (t, J = 5.5 Hz), 134.7, 161.7 (q, J = 49.9 Hz).



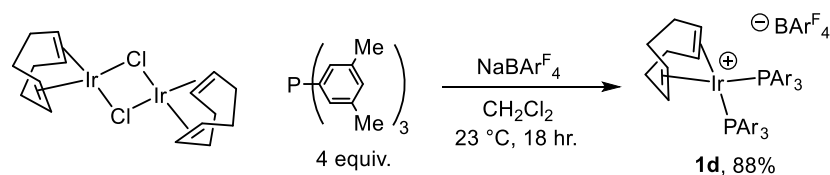
Preparation of [(cod)Ir(PMe₂Ph)₂]⁺BARF₄⁻ (1c**).** A 20 mL glass vial was charged with a stir bar, bis(1,5-cyclooctadiene)diiridium(I) dichloride (0.1003 g, 0.149 mmol), dimethylphenylphosphine (0.0824 g, 84.9 μL, 0.597 mmol, 4.01 equiv.), and sodium tetrakis[3,5-bis(trifluoromethyl)phenyl]borate (0.2649 g, 0.299 mmol, 2.01 equiv.) and 4.0 mL of dry dichloromethane. The resulting solution was allowed to stir for 30 minutes and was then diluted with 10 mL of dry diethyl ether and allowed to stir for an additional hour. At this point the precipitate was filtered off using a 0.45 μm PTFE syringe filter. The resulting filtrate was evaporated to dryness under vacuum to give a red foam. The foam was crushed with a spatula and the residue was treated with a 5 mL portion of dry pentane which was then evaporated. This operation was repeated once to give a dry, bright red solid. The red solid was suspended in 3 mL pentane and filtered. The residue was washed with three, 3 mL portions of pentane to give the product as a red solid after drying under vacuum. Yield: 0.3680 g (86%). Crystals suitable for X-

ray diffraction were obtained by slow diffusion of a dilute solution of **1c** in ether into pentane at 35 °C. Elemental Analysis for C₅₆H₄₆BF₂₄IrP₂: C, 46.71; H, 3.22. Found: C, 46.33; H, 3.04.

¹H NMR (400 MHz, 23 °C, CD₂Cl₂): δ 1.47 (d, J= 8.5 Hz, 12H), 2.18 – 2.38 (m, 8H), 4.67 (bs, 4H), 7.42 – 7.54 (m, 10H), 7.56 (s, 4H), 7.72 (s, 8H).

³¹P{¹H} NMR (162 MHz, 23 °C, CD₂Cl₂): δ -11.2 (s).

¹³C{¹H} NMR (100 MHz, 23 °C, CD₂Cl₂): δ 13.4 (m), 31.2, 85.5 (t, J = 5.6 Hz), 117.4 (m), 124.5 (q, J = 272.8), 128.8 (qq, J = 31.6 Hz, J = 3.1 Hz), 129.2 (t, J = 5.3 Hz), 131.4 (t, J = 5.8 Hz), 131.6, 133.4 (m), 134.7, 161.7 (q, J = 49.8 Hz).



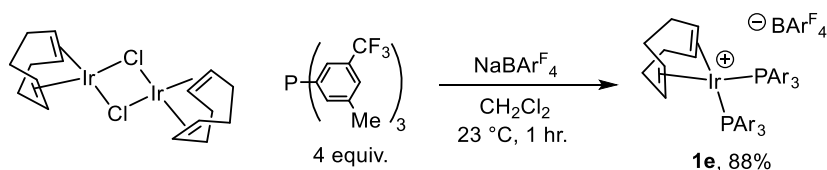
Preparation of [(cod)Ir(P(3,5-xilyl)₃)₂]⁺BARF₄⁻ (1d**).** A 20 mL glass vial was charged with a stir bar, bis(1,5-cyclooctadiene)diiridium(I) dichloride (0.100 g, 0.149 mmol), tris(3,5-xilyl)phosphine (0.2109 g, 0.611 mmol, 4.1 equiv.), and sodium tetrakis[3,5-bis(trifluoromethyl)phenyl]borate (0.2649 g, 0.310 mmol, 2.1 equiv.) and 3.0 mL of dry dichloromethane. The resulting solution was allowed to stir for 18 h followed by filtration using a 0.45 μm PTFE syringe filter. The filter was washed with three 2 mL portions of dichloromethane and the combined filtrate was evaporated to dryness under vacuum to give a red foam. The foam was crushed with a spatula and the residue was treated with a 5 mL portion of dry pentane which was then evaporated. This operation was repeated once to give a dry, bright red solid. The red solid was suspended in 3 mL pentane and filtered. The residue was washed with three, 3 mL portions of pentane to give the product as a red solid after drying under vacuum. Yield: 0.4818 g (88%). Crystals suitable for X-ray diffraction were obtained by layering pentane on a saturated solution

of **1d** at 23 °C. Elemental Analysis for $C_{88}H_{78}BF_{24}IrP_2$: C, 56.93; H, 4.24. Found: C, 57.06; H, 4.03

1H NMR (400 MHz, 23 °C, CD_2Cl_2): δ 1.90 (m, 4H), 2.16 (s, 36H), 2.24 - 2.31 (m, 4H), 4.13 (s, 4H), 6.94 (d, $J = 10.1$ Hz, 12H), 7.04 (s, 6H), 7.56 (s, 4H), 7.73 (s, 8H).

$^{31}P\{^1H\}$ NMR (162 MHz, 23 °C, CD_2Cl_2): δ 18.8 (s).

$^{13}C\{^1H\}$ NMR (100 MHz, 23 °C, CD_2Cl_2): δ 20.2, 31.1, 85.9 (t, $J = 5.5$ Hz), 117.37 (m), 124.5 (q, $J = 272.4$), 128.79 (qq, $J = 31.4$ Hz, $J = 3.1$ Hz), 129.9 (m), 132.0 (t, $J = 5.4$ Hz), 132.57, 134.7, 132.0 (t, $J = 5.5$ Hz), 161.7 (q, $J = 49.8$ Hz).



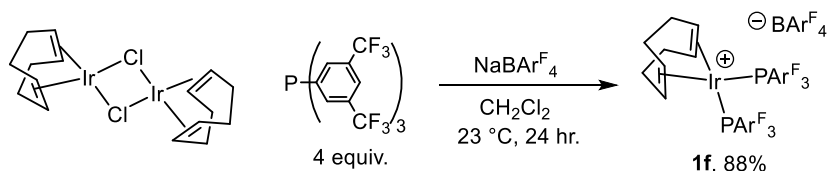
Preparation of $[(cod)Ir(P(3,5-CF_3CH_3C_6H_3)_2)BARF_4]$ (1e**).** A 20 mL glass vial was charged with a stir bar, bis(1,5-cyclooctadiene)diiridium(I) dichloride (0.100 g, 0.149 mmol), tris(3-methyl-5-(trifluoromethyl)phenyl)phosphine (**20**) (0.6038 g, 1.19 mmol, 4.05 equiv.), and sodium tetrakis[3,5-bis(trifluoromethyl)phenyl]borate (0.5198 g, 0.587 mmol, 2.0 equiv.) and 6.0 mL of dry dichloromethane. The resulting solution was allowed to stir for 30 minutes and was then diluted with 10 mL of dry diethyl ether and allowed to stir for an additional 30 minutes. At this point the precipitate was filtered off using a 0.45 μm PTFE syringe filter. The filter was washed with three 2 mL portions of dichloromethane and the combined filtrate was evaporated to dryness under vacuum to give a red foam. The foam was crushed with a spatula and was then triturated with three successive 20 mL portions of dry pentane. After the pentane was decanted the residue was dried under vacuum to give the product as a dark red solid. Yield: 0.4818 g (88%). Crystals suitable for X-ray diffraction were obtained by layering pentane on a saturated solution of **1e** in diethyl ether at 23 °C. Elemental Analysis for $C_{88}H_{60}BF_{42}IrP_2$: C, 48.48; H, 2.77. Found: C, 48.27; H, 2.49.

^1H NMR (400 MHz, 23 °C, CD_2Cl_2): δ 2.11 (m, 4H), 2.28 (s, 18H), 2.32 – 2.39 (m, 4H), 4.31 (s, 4H), 7.17 (d, 6H, $J = 9.5$), 7.48 – 7.56 (m, 10H), 7.60 (br, 6H), 7.71 (s, 8H)

$^{31}\text{P}\{^1\text{H}\}$ NMR (162 MHz, 23 °C, CD_2Cl_2): δ 20.2 (s).

$^{19}\text{F}\{^1\text{H}\}$ NMR (471 MHz, 23 °C, CD_2Cl_2): δ -61.9 (s), -61.2 (s)

$^{13}\text{C}\{^1\text{H}\}$ NMR (151 MHz, 23 °C, CD_2Cl_2): δ 20.9, 31.0, 91.3 (t, $^1J_{\text{CP}} = 5.1$ Hz), 117.4 (m), 123.2 (q, $J = 273.1$), 124.6 (q, $J = 272.6$), 127.8, 128.9 (qq, $J = 30.7$ Hz, $J = 2.3$ Hz), 129.6 (m), 129.9, 131.5 (qt, $J = 32.9$ Hz, $J = 5.6$ Hz), 134.8, 137.2, 140.9 (t, $J = 4.7$), 161.7 (q, $^1J_{\text{CB}} = 49.8$)



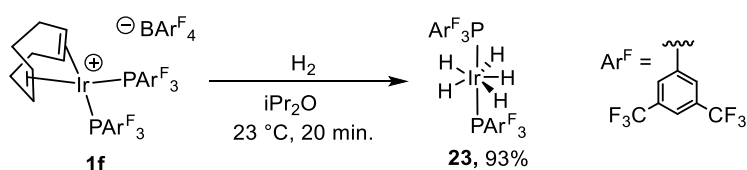
Preparation of [(cod)Ir(P(3,5-(CF₃)₂C₆H₃)₂)₂]BARF₄·CH₂Cl₂ (1f**).** A 20 mL glass vial was charged with bis(1,5-cyclooctadiene)diiridium(I) dichloride (0.1002 g, 0.149 mmol), tris(3,5-bis(trifluoromethyl)phenyl)phosphine (0.4490 g, 0.670 mmol, 4.5 equiv.), and sodium tetrakis[3,5-bis(trifluoromethyl)phenyl]borate (0.2770 g, 0.670 mmol, 2.1 equiv.) and 8.0 mL of dry dichloromethane. The unstirred solution was shaken once and allowed to stand at room temperature for 24 h. At this point large, bright-red crystals and a finely-divided colorless solid presumed to be NaCl had separated from the solution. The remaining solvent was decanted and discarded. The red crystals were separated from the colorless solid by washing with four 4 mL portions of dry diethyl ether. This was effectively accomplished by swirling the vial to suspend the white solid and carefully decanting the suspension. The red crystals were dried under vacuum to give the solid product as the dichloromethane solvate. Yield: 0.7211 g (88%). Crystals suitable for X-ray diffraction were obtained from the synthetic procedure above. Elemental Analysis for C₈₈H₄₂BF₆₀IrP₂·CH₂Cl₂: C, 41.29; H, 1.71. Found: C, 41.49; H, 1.53.

^1H NMR (600 MHz, 23 °C, C_6F_6 with CD_2Cl_2 standard): δ 0.88 (br, 4H), 1.29 (m, 4H), 2.22 (m, 4H), 2.51 (m, 4H), 4.80 (br, 4H), 7.47 (s, 4H), 7.82 (s, 8H), 8.22 (d, $J = 8.3$ Hz, 12H), 8.42 (s, 6H).

^{31}P NMR (202 MHz, 23 °C, C_6F_6 with C_6D_6 standard): δ 20.3 (s)

^{19}F NMR (471 MHz, 23 °C, $\text{C}_6\text{H}_4\text{F}_2$ with C_6D_6 standard): δ -63.0 (s), -61.4 (s)

$^{13}\text{C}\{^1\text{H}\}$ NMR (151 MHz, 23 °C, C_6F_6 with a CD_2Cl_2 standard): δ 30.6, 96.9 (bt, $J = 4.1$ Hz), 116.7, 121.9 (q, $J = 272.8$ Hz), 124.4, (q, $J = 272.1$ Hz), 127.6, 128.8, (q, $J = 30.8$ Hz), 130.2 (apparent d, $J = 52.9$ Hz), 133.2, 134.5 (qt, $J = 35.2$ Hz, $J = 4.9$ Hz), 134.8, 137.9 (m), 161.9 (q, $J = 49.8$ Hz)



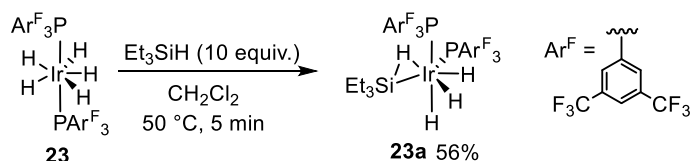
Preparation of $(\text{P}(3,5\text{-(CF}_3)_2\text{C}_6\text{H}_3)_2\text{IrH}_5$ (23**):** In an inert atmosphere glovebox a 20 mL scintillation vial was charged with a stir bar, $[(\text{cod})\text{Ir}(\text{P}(3,5\text{-(CF}_3)_2\text{C}_6\text{H}_3)_2\text{BAr}^{\text{F}}_4 \cdot \text{CH}_2\text{Cl}_2$ (**1f**) (0.2530 g, 0.0977 mmol), and dry iPr_2O (6.0 mL). The vial was brought out of the glovebox and was sparged with hydrogen at 23 °C while stirring vigorously for 20 minutes, giving an off-white precipitate. The vial was brought back into the glovebox and the solid was filtered off and washed successively with dry iPr_2O (3 x 1.00 mL), diethyl ether (2 x 1.00 mL), and pentane (2 x 1.00 mL). The resulting residue was dried under vacuum for 24 h to give the product as an off-white solid. Yield: 0.1400 g (93%). Crystals suitable for X-ray diffraction were grown directly from the reaction mixture. Elemental analysis for $\text{C}_{48}\text{H}_{23}\text{F}_{36}\text{IrP}_2$: C, 37.49; H, 1.51. Found: C, 37.36; H, 1.39.

^1H NMR (400 MHz, 23 °C, C_6F_6 with C_6D_6 standard): δ -8.44 (t, $J = 13.9$ Hz, 5H), 7.95 (s, 6H), 8.22 (t, $J = 5.2$ Hz, 12H)

$^{31}\text{P}\{^1\text{H}\}$ NMR (162 MHz, 23 °C, CD_2Cl_2): δ 20.4 (s)

$^{19}\text{F}\{^1\text{H}\}$ NMR (471 MHz, 23 °C, CD_2Cl_2): δ -62.0 (s)

$^{13}\text{C}\{^1\text{H}\}$ NMR (151 MHz, 23 °C, CD_2Cl_2): δ 122.6 (q, $J = 273.2$ Hz), 125.8, 132.3 (qt, $J = 12.8$ Hz, $J = 5.1$ Hz), 133.5, 137.0 (t, $J = 28.6$ Hz)



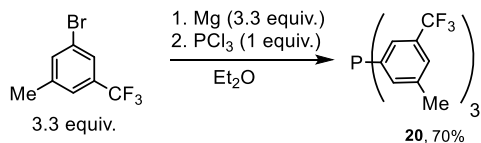
Preparation of (P(3,5-(CF₃)₂C₆H₃)₂IrH₄(SiEt₃)) (23a): Under an inert glovebox atmosphere, a 4 mL glass vial was charged with **18** (0.1001 g, 0.0650 mmol), and 2.0 mL of dry dichloromethane. Triethylsilane (0.65 mmol, 0.10 mL, 10 equiv.) was added to the suspension of **23**. The reaction vessel was brought out of glovebox and heated at 50 °C for 5 minutes to give a homogeneous yellow solution. The vial was brought back into the glovebox and the solvent was removed under vacuum. The resulting residue was extracted with pentane (1 x 1.00 mL) which was separated, filtered, and evaporated to yield the product **23a** as a pale-yellow powder. Yield: 0.0602 g (56%). Crystals suitable for X-ray diffraction were obtained directly from a concentrated toluene solution at 23 °C. Elemental analysis for C₅₄H₃₇F₃₆IrP₂Si: C, 39.26; H, 2.26. Found: C, 39.64; H, 2.37

^1H NMR (400 MHz, 23 °C, CD_2Cl_2): δ -10.82 (t, $J = 11.6$ Hz, 4H), 0.47 (bq, $J = 6.8$ Hz, 6H), 0.66 (t, $J = 7.6$ Hz, 9H) 7.81 (bd, $J = 8.4$ Hz, 12H), 7.94 (s, 6H)

$^{31}\text{P}\{^1\text{H}\}$ NMR (162 MHz, 23 °C, CD_2Cl_2): δ 21.0 (s)

$^{19}\text{F}\{^1\text{H}\}$ NMR (471 MHz, 23 °C, CD_2Cl_2): δ -62.1 (s)

$^{13}\text{C}\{^1\text{H}\}$ NMR (125 MHz, 23 °C, CD_2Cl_2): δ 7.8, 14.3, 122.3 (q, $J = 277.0$), 125.4, 132.2 (qt, $J = 34.4$ Hz, $J = 8.7$ Hz), 132.9, 136.4 (apparent d, $J = 46.7$ Hz)



Preparation of tris(3-methyl-5-(trifluoromethyl)phenyl)phosphine (24): A dry 100 mL Schlenk flask was charged with magnesium turnings (0.2330 g, 9.59 mmol, 3.3 equiv.), 35 mL dry, degassed Et₂O, and a single crystal of I₂. The suspension was stirred under nitrogen until the iodine color had bleached. At this point 3-trifluoromethyl-5-methylbromobenzene (2.292 g, 9.59 mmol, 3.3 equiv.) was added. At this point, Grignard initiation was effected by the addition of 3 drops of a 1.2 M diisobutylaluminum hydride solution which led to an exothermic reaction and rapid magnesium consumption. After 2 h at reflux the solution was cooled to room temperature and PCl₃ (0.25 mL, 2.9 mmol, 1 equiv.) was added dropwise over 10 minutes with stirring. After stirring 16 h at room temperature the suspension was filtered quickly in air. The filtrate was diluted to 60 mL total volume with Et₂O, a portion of silica was added, and the suspension evaporated to dryness. The silica-adsorbed mixture was dry-loaded onto a silica gel column and was purified by silica gel chromatography (5% EtOAc in hexanes). The fractions containing the pure phosphine were quickly combined and evaporated to minimize time in air. The resulting oil was moved into an inert atmosphere glove box to give the product as a yellow oil that crystallized on standing overnight. Yield: 1.0171 g (70%). Crystals suitable for X-ray diffraction were obtained from the bulk sample after spontaneous crystallization of the neat oil.

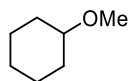
¹H NMR (400 MHz, 23 °C, CD₂Cl₂): δ 2.39 (s, 9H), 7.35 (d, J = 7.6 Hz, 3H), 7.43 (d, J = 7.6 Hz, 3H), 7.50 (s, 3H)

³¹P{¹H} NMR (162 MHz, 23 °C, CD₂Cl₂): δ -3.3 (s)

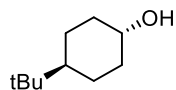
$^{13}\text{C}\{^1\text{H}\}$ NMR (151 MHz, 23 °C, CD_2Cl_2): δ 20.9, 124.1 (q, $J = 272.5$ Hz), 126.8 (q, $J = 3.4$ Hz), 127.3 (dq, $J = 22.4$ Hz, $J = 4.7$ Hz), 130.9 (qd, $J = 31.7$ Hz, $J = 7.8$ Hz), 137.2 (d, $J = 13.8$ Hz), 137.6 (d, $J = 18.9$ Hz), 139.8 (d, $J = 6.5$ Hz)

LRMS (ESI) m/z $[\text{M}+\text{H}]^+$ calcd for $\text{C}_{24}\text{H}_{18}\text{F}_9\text{P}^+$ 509.10, found 509.08

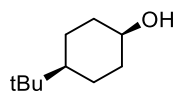
Substrate syntheses



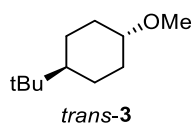
Methoxycyclohexane: This compound was prepared by a reported method.⁴



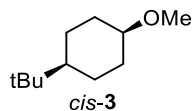
Trans-4-(tert-butyl)cyclohexan-1-ol: This compound was prepared by a reported method.⁵



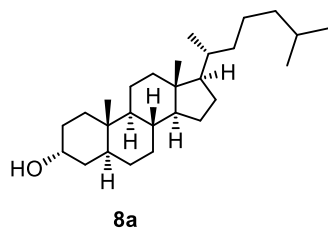
Cis-4-(tert-butyl)cyclohexan-1-ol: This compound was prepared by a reported method.⁵



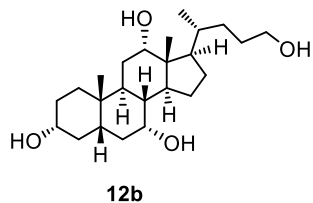
Trans-1-(tert-butyl)-4-methoxycyclohexane (*trans-3*): This compound was prepared by a reported method.⁶



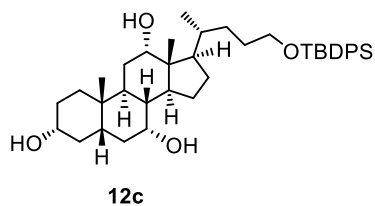
Cis-1-(tert-butyl)-4-methoxycyclohexane (*cis-3*): This compound was prepared by a reported method.⁶



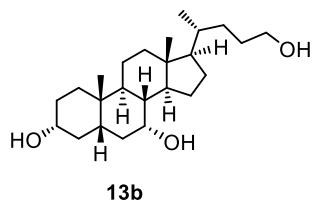
5 α -cholestan-3 α -ol (11a): This compound was prepared by a reported method.⁷



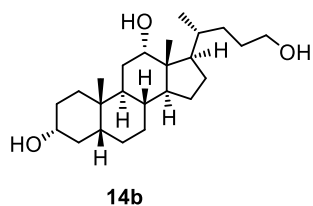
3 α ,7 α ,12 α ,24-tetrahydroxycholesterol (19b): This compound was prepared by a reported method at 23 °C.⁸



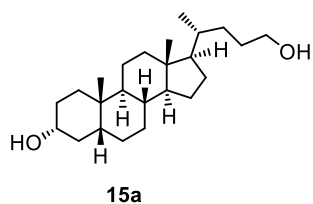
3 α ,7 α ,12 α -trihydroxy-24-*t*-butyldiphenylsilyloxycholesterol (19c): This compound was prepared by a reported method.⁹



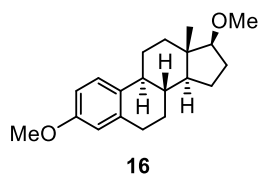
3 α ,7 α ,24-trihydroxycholesterol (18b): This compound was prepared by a reported method.¹⁰



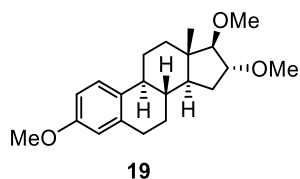
3 α ,12 α ,24-trihydroxycholesterol (17b): This compound was prepared by a reported method at 23 °C.⁸



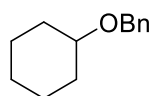
3 α ,24-dihydroxycholane (11b): This compound was prepared by a reported method.¹¹ It is also obtained as a product of catalytic demethylation of **16** after deprotection (below).



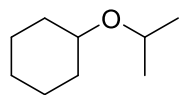
17 β -dimethylestradiol (20): This compound was prepared by a reported method with DMF used as solvent rather than THF.¹² Crystals suitable for X-ray diffraction were obtained upon purification.



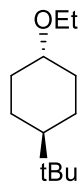
16 α ,17 β -trimethylestriol (21): This compound was prepared by a reported method.¹³



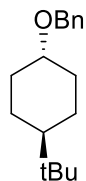
Benzyloxycyclohexane : This compound was synthesized by a reported method.¹⁴



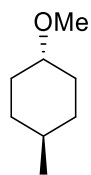
Isopropoxycyclohexane: This compound was synthesized by a reported method.¹⁵



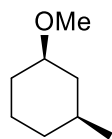
Trans-1-(tert-butyl)-4-ethoxycyclohexane (15): This known compound¹ was prepared using the same method as *trans-3*.¹⁶



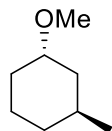
Trans-1-(tert-butyl)-4-benzyloxycyclohexane: This known compound was prepared according to a reported method.¹⁷



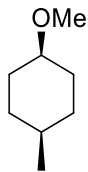
Trans-1-methoxy-4-methylcyclohexane (*trans-8*): This known compound¹⁸ was prepared using the same method as *trans-3*.



cis-1-methoxy-3-methylcyclohexane (*cis-7*): This known compound¹⁹ was prepared using the same method as *trans-3*.

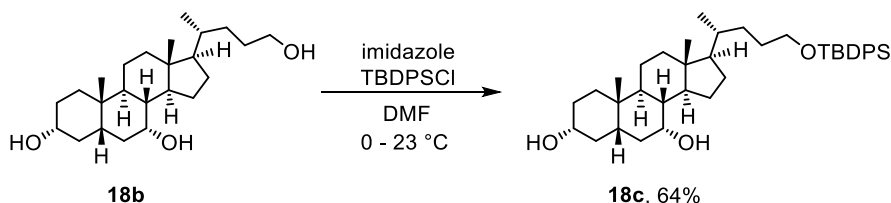


trans-1-methoxy-3-methylcyclohexane (*trans-7*): This known compound²⁰ was prepared using the same method as *trans-3*.



***cis*-1-methoxy-4-methylcyclohexane (cis-8):** This known compound²¹ was prepared using the same method as *trans*-3.

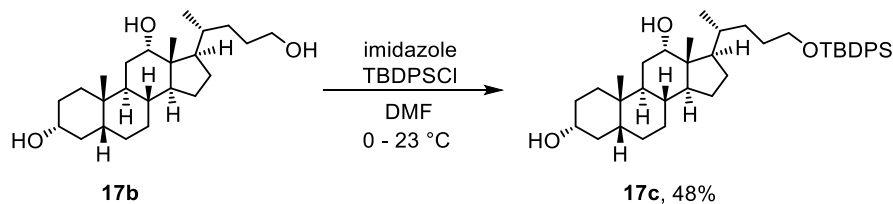
Representative procedure for the TBDPS protection of cholic acid derivatives



24-tert-butylidiphenylsilyloxy-3 α ,7 α -dihydroxycholane (18c): A flame-dried Schlenk flask under N₂ was charged with 3 α ,7 α ,24-trihydroxycholane (**18b**) (7.52 g, 19.9 mmol) in 15.0 mL of dry DMF and cooled to 0 °C. The flask was then charged with imidazole (2.70 g, 39.7 mmol) and was allowed to stir until homogeneous. To the Schlenk flask was added tert-butylchlorodiphenylsilane (TBDPSCl) dropwise (21.35 mmol, 5.7 mL). The reaction was allowed to stir for 16 h at 0 °C and allowed to warm to room temperature. The residue was purified on silica gel (5% EtOAc/Hexanes – 100 % EtOAc) to yield a white solid. Yield: 7.90 g (64%)

¹H NMR (500 MHz, 23 °C, CDCl₃): δ 0.65 (s, 3H), 0.90 – 0.91 (m, 6H), 0.94 – 1.01 (m, 1H), 1.05 (s, 9H), 1.12 – 1.73 (m, 21H), 1.80 – 1.85 (m, 3H), 1.96 – 2.00 (m, 2H), 2.22 (q, J = 11.4 Hz, 1H), 3.46 (m, 1H), 3.63 (t, J = 6.0 Hz, 2H), 3.85 (q, J = 2.7 Hz, 1H), 7.36 – 7.43 (m, 6H), 7.67 – 7.68 (m, 4H)

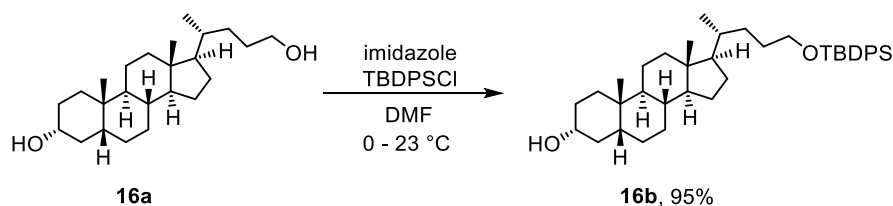
¹³C{¹H} NMR (151 MHz, 23 °C, CDCl₃): δ 11.7, 18.6, 19.1, 20.5, 22.7, 23.7, 26.8, 28.1, 29.0, 30.6, 31.8, 32.8, 34.5, 35.0, 35.3, 35.4, 39.4, 39.6, 39.8, 41.4, 42.6, 50.4, 55.9, 64.4, 68.5, 71.9, 127.5, 129.4, 134.1, 135.5



24-tert-butylidiphenylsilyloxy-3 α ,12 α -dihydroxycholeane (17c): This compound was prepared using the general procedure for the TBDPS protection of cholic acid derivatives above using 3 α ,12 α ,24-trihydroxycholeane (**17b**) (6.59 g, 17.3 mmol). The residue was purified on silica gel using 5% EtOAc/Hexanes then 80% EtOAc/Hexanes as the eluent to yield a white solid. Yield: 5.03 g (48%)

^1H NMR (500 MHz CDCl_3) δ 0.67 (s, 3H), 0.91 (s, 3H), 0.94 (d, $J = 6.7$ Hz, 3H), 0.98 – 1.01 (m, 1H), 1.05 (s, 9H), 1.10 – 1.30 (m, 4H), 1.32– 1.48 (m, 8 H), 1.48 – 1.55 (m, 5H), 1.57 – 1.70 (m, 5H), 1.73 – 1.86 (m, 5H), 3.56-3.65 (t overlapping m, $J = 6.2$ Hz, 3H), 3.99 (br, 1H), 7.36 – 7.43 (m, 6H), 7.68 (d, $J = 6.6$ Hz, 4H)

$^{13}\text{C}\{^1\text{H}\}$ NMR (126 MHz CDCl_3) δ 12.7, 17.7, 19.1, 23.1, 23.6, 26.1, 26.8, 27.1, 27.4, 28.5, 29.1, 30.5, 31.8, 33.6, 34.0, 35.1, 35.2, 36.0, 36.4, 42.0, 46.4, 47.6, 48.2, 64.4, 71.8, 73.2, 127.5, 129.4, 134.1, 135.5

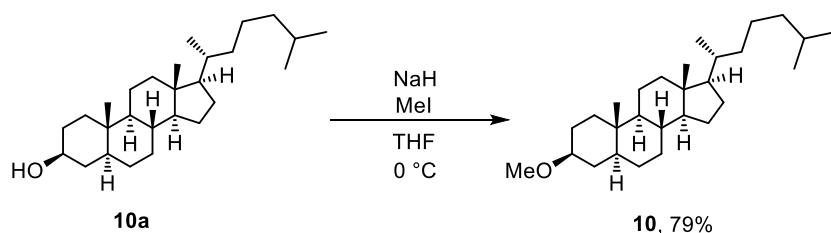


24-tert-butylidiphenylsilyloxy-3 α -hydroxycholeane (16b): This compound was prepared using the general procedure for the TBDPS protection of cholic acid derivatives above using 3 α ,24-dihydroxycholeane (**16a**) (9.38 g, 25.9 mmol). The sample was used without further purification. For characterization purposes, the residue was recrystallized in EtOAc/Pentanes at 40 °C. Yield: 14.79 g (95%)

^1H NMR (400 MHz, 23 °C, CDCl_3): δ 0.63 (s, 3H), 0.88 (d, $J = 6.5$ Hz, 3H), 0.92 (s, 3H), 1.04 (s, 12H), 1.07–1.49 (m, 18H), 1.54–1.85 (m, 7H), 1.96 (d, $J = 12$ Hz, 1H), 3.63 (t, $J = 6.4$ Hz, 3H), 7.35–7.42 (m, 6H), 7.66–7.68 (m, 4H)

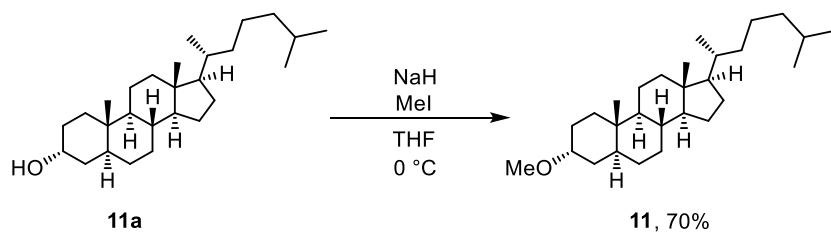
$^{13}\text{C}\{^1\text{H}\}$ NMR (101 MHz, 23 °C, CDCl_3): δ 12.0, 18.6, 19.2, 20.8, 23.4, 24.2, 26.4, 26.8, 27.2, 28.2, 29.1, 30.5, 31.9, 34.5, 35.3, 35.4, 35.8, 36.4, 40.2, 40.4, 42.1, 42.6, 56.2, 56.5, 64.5, 71.8, 127.5, 129.4, 134.1, 134.2, 135.5.

Representative procedure (A) for the synthesis of methyl ether substrates:



3 β -methoxy-5 α -cholestane (10): A flame-dried 250 mL two-necked Schlenk flask was charged with NaH (0.3300g, 12.90 mmol, 2 equiv.) in an inert atmosphere glove box. The vessel was then brought outside of the box and attached to a Schlenk line and an oil bubbler and a flow of N_2 applied. Dry THF (60 mL) was loaded into the flask to make an NaH suspension which was cooled to 0 °C. 5 α -cholestan-3 β -ol (**10a**) (2.51g, 6.43 mmol) was dissolved in dry THF (20 mL) and added dropwise over the course of 1 hour and allowed to stir at 0 °C for 1 hour. Maintaining a 0 °C reaction temperature, MeI (1.8308 g, 12.90 mmol, 2 equivalents, 0.80 mL) was added dropwise over the course of 1 hour. The reaction was slowly quenched with saturated aqueous NH_4Cl and was diluted with water until all solid was dissolved (~ 50 mL). The aqueous solution was extracted with EtOAc (3 x 150 mL) and washed with DI H_2O (2 x 100 mL) and brine (3 x 100 mL). The resulting organic layer was dried over Na_2SO_4 and filtered. The solution was concentrated under vacuum and the residue was purified on silica gel using 15% EtOAc/Hexanes as eluent to give a

white solid as the product. Yield: 1.9440 g (79%). The ^1H NMR shifts match previously reported values.²²

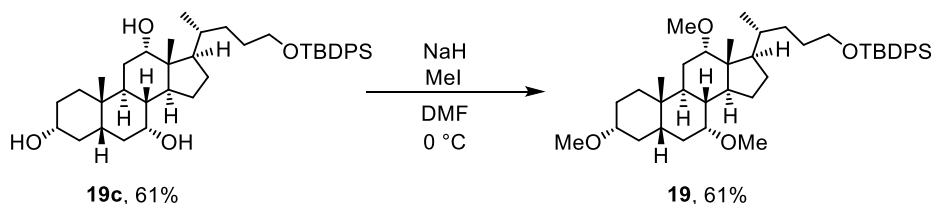


3 α -methoxy-5 α -cholestane (11): This compound was prepared according to general procedure (A) for the preparation of methyl ether substrates using 0.8501 g of **11a**. The extracted organic layer was concentrated under vacuum and the residue was sonicated in acetonitrile (10 mL) to yield a white solid, which was filtered and washed with acetonitrile (2 x 5 mL) and dried under vacuum. Yield: 0.6137 g (70%). This is a previously reported molecule.²³

^1H NMR (400 MHz, 23 °C, CDCl_3): δ 0.65 (s, 3H), 0.79 (s, 3H), 0.87 (d, $J = 6.1$ Hz, 6H), 0.90 (d, $J = 6.4$ Hz, 3H), 0.95 – 1.04 (m, 3H), 1.04 – 1.27 (m, 11H), 1.27 – 1.59 (m, 13H), 1.63 (bd, $J = 10.9$, 1H), 1.79 (bd, $J = 13.5$ Hz, 2H), 1.96 (bd, $J = 11.9$ Hz, 1H), 3.30 (s, 3H), 3.43 (br, 1H)

$^{13}\text{C}\{^1\text{H}\}$ NMR (101 MHz, 23 °C, CDCl_3): δ 11.3, 12.0, 18.6, 20.7, 22.5, 22.7, 23.7, 24.1, 25.1, 27.9, 28.2, 28.6, 31.9, 32.5, 32.7, 35.4, 35.7, 35.8, 36.1, 39.4, 39.5, 40.0, 42.5, 54.2, 55.6, 56.1, 56.5, 75.6

Representative procedure (B) for the synthesis of methyl ether substrates:



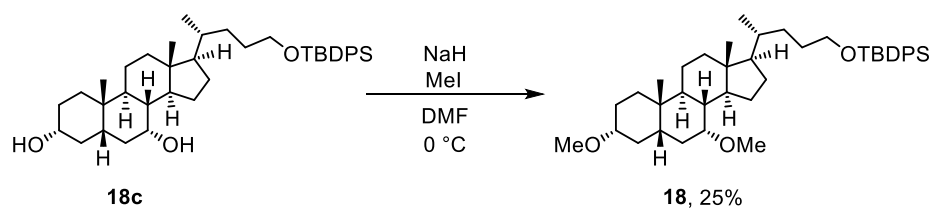
3 α ,7 α ,12 α -trimethoxy-24-tert-butyl diphenylsilyloxycholeane (19): A flame-dried 250 mL two-necked Schlenk flask was charged with NaH (3.7218 g, 155.1 mmol, 10 equiv.) in an inert

atmosphere glove box. The vessel was then brought outside of the box and attached to a Schlenk line and an oil bubbler and a flow of N₂ applied. Dry DMF (30.0 mL) was loaded into the flask to make an NaH suspension which was cooled to 0 °C. 3 α ,7 α ,12 α -trihydroxy-24-*t*-butyldiphenylsiloxycholane (**19c**) (6.3200 g, 9.98 mmol) was dissolved in 15 mL of dry DMF and added dropwise to the NaH suspension at 0 °C over the course of 30 minutes and allowed to stir for 2 h. The temperature was held at 0 °C and MeI (22.0 g, 155 mmol, 9.7 mL) was added slowly over the course of 2 h and allowed to stir for 18 h and warm to room temperature. The reaction was slowly quenched with saturated aqueous NH₄Cl and was diluted with water until all solid was dissolved (~ 50 mL). The aqueous solution was extracted with EtOAc (3 x 150 mL) and washed with deionized water (2 x 100 mL) and brine (3 x 100 mL). The resulting organic layer was dried over Na₂SO₄ and filtered. The crude oil was purified on silica gel (15% EtOAc/Hexanes) to give a white solid. Yield: 4.12 g (61%)

¹H NMR (400 MHz, 23 °C, CDCl₃): δ 0.66 (s, 3H), 0.90 – 0.92 (overlapping s,d, 6H), 0.94 – 1.01 (m, 1H), 1.06 (s, 9H), 1.16 – 1.87 (m, 19H), 1.93 (q, J = 9.7 Hz, 1H), 2.04 – 2.16 (m, 2H), 2.22 (q, J = 12.6 Hz, 1H), 3.01 (m, 1H), 3.16 (bq, J = 2.7 Hz, 1H), 3.23 (s, 3H), 3.28 (s, 3H), 3.35 (s, 3H), 3.38 (bt, J = 2.3 Hz, 1H), 3.64 (t, J = 6.3 Hz, 2H), 7.35 – 7.45 (m, 6H), 7.69 (dd, J = 6.2 Hz, J = 1.6 Hz, 4H)

¹³C{¹H} NMR (101 MHz, 23 °C, CDCl₃): δ 12.4, 17.7, 19.1, 21.9, 22.8, 23.1, 26.7, 26.8, 27.4, 27.7, 27.9, 29.1, 31.8, 34.4, 34.9, 35.2*, 39.6, 41.9, 42.6, 46.0, 46.5, 55.3, 55.6, 55.8, 64.5, 76.9, 80.7, 82.0, 127.5, 129.4, 134.1, 134.2, 135.5

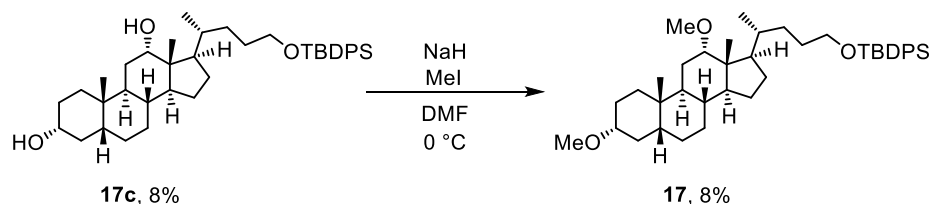
*HSQC experiments are consistent with this resonance being an overlapping methylene and methine.



3 α ,7 α -dimethoxy-24-tert-butylidiphenylsilyloxycholane (18): This compound was prepared according the general procedure (B) for the preparation of methyl ether substrates using 24-tert-butylidiphenylsilyloxy-3 α ,7 α -dihydroxycholane (**18c**) (7.90 g, 12.8 mmol). The solution was concentrated under vacuum and the residue was purified on silica gel using hexanes and then 5% EtOAc/Hexanes as the eluent to yield a white solid. Yield 2.10 g (25%).

^1H NMR (400 MHz, 23 °C, CDCl_3): δ 0.63 (s, 3H), 0.88 – 0.91 (s overlapping d, 6H), 0.95 – 1.01 (m, 1H), 1.06 (s, 9H), 1.15 – 1.31 (m, 6H), 1.31 – 1.58 (m, 10H), 1.63 – 1.67 (m, 1H), 1.68 – 1.87 (m, 6H), 1.93 (dt, $J = 11.8$ Hz, $J = 3.1$ Hz, 1H), 2.17 (q, $J = 12.5$ Hz, 1H), 2.97 – 3.05 (m, 1H), 3.18 (bq, $J = 2.3$ Hz, 1H), 3.24 (s, 3H), 3.34 (s, 3H), 3.63 (t, $J = 6.5$ Hz, 2H), 7.36 – 7.44 (m, 6H), 7.67 – 7.69 (m, 4H)

$^{13}\text{C}\{^1\text{H}\}$ NMR (126 MHz, 23 °C, CDCl_3): δ 11.6, 18.6, 19.1, 20.8, 22.9, 23.6, 26.6, 26.8, 27.9, 28.1, 29.0, 31.8, 33.6, 34.6, 35.2, 35.3, 35.4, 39.4, 39.5, 41.9, 42.3, 50.1, 55.3, 55.8, 55.8, 64.5, 77.3, 80.6, 127.5, 129.4, 134.1, 135.5

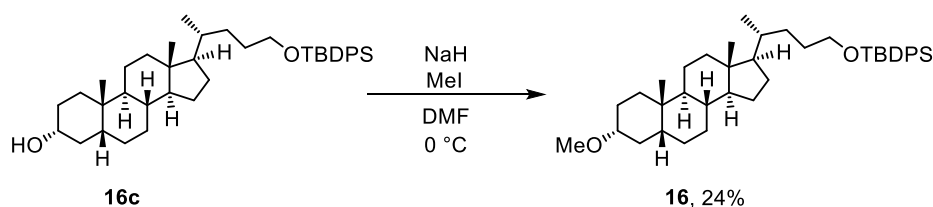


3 α ,12 α -dimethoxy-24-tert-butylidiphenylsilyloxycholane (17): This compound was prepared according the general procedure (B) for the preparation of methyl ether substrates using 24-tert-butylidiphenylsilyloxy-3 α ,12 α -dihydroxycholane (**17c**) (15.00 g, 24.3 mmol). The solution was concentrated under vacuum and the residue was purified on silica gel using 100% hexanes to 10%

EtOAc/Hexanes as eluent to yield an off-white oil. Yield: 1.22 g (8%). Crystals suitable for X-ray crystallography were obtained from a concentrated solution in dichloromethane at 23 °C.

^1H NMR (600 MHz CDCl_3) δ 0.65 (s, 3H), 0.88 (d, $J = 6.6$ Hz, 3H), 0.92 (s, 3H), 0.94 – 1.01 (m, 2H), 1.05 (s, 9H), 1.11 – 1.52 (m, 13H), 1.56 – 1.69 (m, 3H), 1.71 – 1.89 (m, 8H), 3.15 (septet, $J = 4.4$ Hz, 1H), 3.26 (s, 3H), 3.34 (s, 3H), 3.39 (bs, 1H), 3.63 (t, $J = 6.3$ Hz, 2H), 7.36 – 7.43 (m, 6H), 7.68 (d, $J = 6.6$ Hz, 4H)

$^{13}\text{C}\{^1\text{H}\}$ NMR (126 MHz CDCl_3) δ 12.7, 17.7, 19.1, 21.9, 23.2, 23.6, 26.1, 26.7, 26.8, 27.3, 27.4, 29.1, 31.8, 32.5, 33.5, 34.4, 35.2, 35.3, 36.0, 42.0, 46.2, 46.7, 48.8, 55.4, 55.6, 64.5, 80.4, 82.3, 127.5, 129.4, 134.1, 135.5.



3 α -methoxy-24-tert-butylidiphenylsilyloxycholane (16): This compound was prepared according the general procedure (B) for the preparation of methyl ether substrates using 24-tert-butylidiphenylsilyloxy-3 α -hydroxycholane (16c) (14.79 g, 24.61 mmol). The solution was concentrated under vacuum and the residue was purified on silica using 1% EtOAc/Hexanes then 10% EtOAc/Hexanes as eluent to yield a viscous oil. Yield: 3.61 g (24%)

^1H NMR (400 MHz, 23 °C, CDCl_3): δ 0.63 (s, 3H), 0.86–0.90 (m, 4H), 0.92–0.93 (m, 3H), 0.95–0.98 (m, 1H), 1.01–1.08 (m, 13H), 1.10–1.46 (m, 14H), 1.60–1.85 (m, 7H), 1.95 (dt, 1H) 3.16 (m, 1H), 3.35 (s, 3H), 3.63 (t, $J = 6.2$ Hz, 2H), 7.35–7.42 (m, 6H), 7.66–7.69 (m, 4H)

$^{13}\text{C}\{^1\text{H}\}$ NMR (126 MHz, 23 °C, CDCl_3): δ 12.0, 18.6, 19.1, 20.7, 23.4, 24.2, 26.4, 26.7, 26.8, 27.3, 28.2, 29.1, 31.8, 32.7, 34.8, 35.2, 35.4, 35.8, 40.1, 40.3, 42.0, 42.6, 55.5, 56.1, 56.4, 64.4, 80.4, 127.5, 129.4, 134.1, 135.5

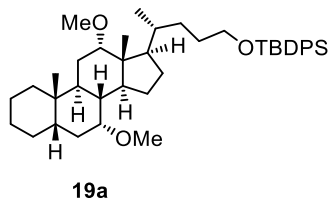
General Procedure (A) for Catalytic Ether Deoxygenation/Silylation:

In air, a 20 mL scintillation vial was charged with a stir bar, the solid precatalyst [(cod)Ir(PPh₃)₂]BAr^F₄ (**1a**) (0.0201 g, 0.03 equiv., 0.0120 mmol), dichloromethane (2.0 mL), and Et₃SiH (0.1023 g, 0.880 mmol, 2.2 equiv., 0.14 mL) and was allowed to stir vigorously until the reaction mixture changes from a red color to a pale yellow, indicating the catalyst is activated (10 – 30 seconds). Substrate ether (0.400 mmol, 1.0 equiv.) was then added to the reaction mixture and was allowed to stir at 50 °C for 2 h. The reaction mixture was removed from heat and the solvent was removed under vacuum. The residue was dissolved in dichloromethane and purified on silica gel. The resulting residue was redissolved in THF (2.0 mL) and NBu₄F·3H₂O (0.6300 g, 2.00 mmol, 5 equiv.) was added and the mixture was allowed to stir at 40 °C overnight. The resulting reaction mixture was quenched with saturated aqueous NH₄Cl. The organic layer was extracted twice with EtOAc and dried with anhydrous Na₂SO₄, filtered, and concentrated under vacuum. The respective residue was purified on silica gel.

General Procedure (B) for Catalytic Ether Deoxygenation/Silylation:

In air, a 20 mL scintillation vial was charged with a stir bar, the solid precatalyst [(cod)Ir(PPh₃)₂]BAr^F₄ (**1a**) (0.0201 g, 0.03 equiv., 0.0120 mmol), dichloromethane (2.0 mL), and Et₃SiH (0.2046 g, 1.76 mmol, 4.4 equiv., 0.28 mL) and was allowed to stir vigorously until the reaction mixture changes from a red color to a pale yellow, indicating the catalyst is activated (10 – 30 seconds). Substrate ether (0.4000 mmol, 1.0 equiv.) was then added to the reaction mixture and was allowed to stir at 50 °C for 2 h. The reaction mixture was removed from heat and the solvent was removed under vacuum. The residue was dissolved in dichloromethane and purified on silica gel. The resulting residue was redissolved in THF (2.0 mL) and NBu₄F·3H₂O (0.6300 g, 2.00 mmol, 5 equiv.) was added and the mixture was allowed to stir at 40 °C overnight. The

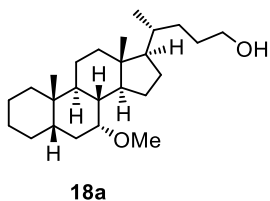
resulting reaction mixture was quenched with saturated aqueous NH_4Cl . The organic layer was extracted twice with EtOAc and dried with anhydrous Na_2SO_4 , filtered, and concentrated under vacuum. The respective residue was purified on silica gel.



7 α ,12 α -dimethoxy-24-tert-butyldiphenylsilyloxycholane (19a): This compound was synthesized according to general catalytic procedure (A) for catalytic ether silylations from **19** (0.2700 g, 0.40 mmol) with no deprotection step. The residue was purified on silica gel using 0.5% to 2% EtOAc in hexanes to yield the product as an off-white residue. Yield: 0.1732 g (69%).

^1H NMR (400 MHz, 23 °C, CDCl_3): δ 0.66 (s, 3H), 0.91 (s and d overlapped, 6H), 0.35 – 1.01 (m, 2H), 1.06 (s, 9H), 1.15 – 1.22 (m, 2H), 1.23 – 1.40 (m, 8H), 1.42 – 1.57 (m, 5H), 1.69 – 1.88 (m, 5H), 1.94 (q, $J = 9.8$ Hz, 1H), 2.03 – 2.25 (m, 3H), 3.15 (bq, $J = 2.8$ Hz, 1H), 3.23 (s, 3H), 3.29 (s, 3H), 3.38 (t, $J = 2.5$ Hz, 1H), 3.64 (t, $J = 6.4$ Hz, 2H), 7.35 – 7.45 (m, 6H), 7.67 – 7.71 (m, 4H)

$^{13}\text{C}\{^1\text{H}\}$ NMR (151 MHz, 23 °C, CDCl_3): δ 11.5, 16.8, 18.2, 20.4, 21.0, 22.2, 22.6, 25.9, 26.4, 26.7, 26.9, 27.1, 27.9, 28.1, 30.9, 34.27, 34.3, 36.6, 38.6, 41.9, 42.7, 45.1, 45.6, 54.7, 54.8, 63.5, 76.4, 81.2, 126.5, 128.4, 132.2, 134.6

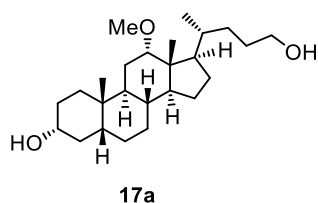


24-hydroxy-7 α -methoxycholane (18a): This compound was synthesized according to general catalytic procedure (A) for catalytic ether silylations from **18** (0.2580 g, 0.40 mmol). The residue obtained prior to deprotection was purified on silica gel using 10% to 25% EtOAc in hexanes.

After the deprotection, the residue was purified on silica gel using 5% to 10% to 25% EtOAc in hexanes to give the product as a white solid. Yield: 0.0805 g (53%). Crystals suitable for X-ray diffraction were obtained from a concentrated solution in dichloromethane at 0 °C.

^1H NMR (600 MHz, 23 °C, CDCl_3) δ 0.64 (s, 3H), 0.90 (s, 3H), 0.92 (d, $J = 6.5$ Hz, 3H), 1.02 – 1.09 (m, 3H), 1.14 – 1.35 (m, 9H), 1.37 – 1.54 (m, 8H), 1.61 – 1.66 (m, 3H), 1.73 – 1.87 (m, 4H), 1.89 – 1.94 (m, 1H), 2.09 (qd, $J = 13.4$ Hz, $J = 3.8$ Hz, 1H), 3.17 (bq, $J = 2.1$ Hz, 1H), 3.24 (s, 3H), 3.61 (m, 2H)

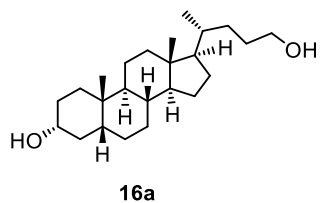
$^{13}\text{C}\{^1\text{H}\}$ NMR (100 MHz, CDCl_3) δ 11.6, 18.6, 20.8, 21.4, 23.6, 23.7, 27.6, 28.1, 28.2, 29.0, 29.3, 31.8, 33.9, 35.8, 35.7, 37.5, 39.3, 39.6, 42.4, 43.6, 50.3, 55.7, 55.9, 63.5, 77.8



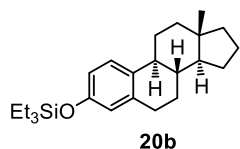
3 α ,24-dihydroxy-12 α -methoxycholeane (17a): This compound was synthesized according to general catalytic procedure (B) for catalytic ether silylations from **17** (0.2581 g, 0.40 mmol). The initial residue was purified on silica gel using 0.1% to 10% EtOAc in hexanes. After the deprotection, the residue was purified on silica gel using 5% MeOH/ CH_2Cl_2 as the eluent to yield a colorless oil. Yield: 0.1009 g (64%). Crystals suitable for X-ray diffraction were obtained from a concentrated solution in acetonitrile at 0 °C.

^1H NMR (600 MHz, 23 °C, CDCl_3): δ 0.60 (s, 3H), 0.84 (s, 3H), 0.86 (d, $J = 6.6$ Hz, 3H), 0.91 – 1.07 (m, 4H), 1.11 – 1.19 (m, 3H), 1.26 – 1.44 (m, 8H), 1.48 (bt, $J = 8.6$ Hz, 2H), 1.55 – 1.64 (m, 2H), 1.65 – 1.76 (m, 6H), 1.80 (q, $J = 9.6$ Hz, 3H), 3.21 (s, 3H), 3.34 (t, $J = 2.8$ Hz, 1H), 3.53 (apparent td overlapping m, $J = 6.4$ Hz, $J = 2.4$ Hz, 3H)

$^{13}\text{C}\{^1\text{H}\}$ NMR (151 MHz, 23 °C, CDCl_3): δ 11.7, 16.7, 21.0, 22.2, 22.7, 25.1, 26.1, 26.6, 28.4, 29.4, 30.8, 32.6, 33.1, 34.3, 34.4, 35.0, 35.4, 41.1, 45.3, 45.8, 48.0, 54.7, 62.5, 70.8, 81.5



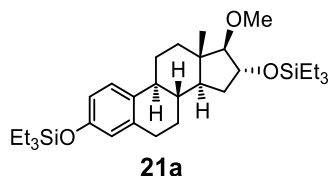
3 α ,24-dihydroxycholeane (16a): This compound was synthesized from **16** (0.2516 g, 0.40 mmol) according to general catalytic procedure (A) for catalytic ether silylations. The initial residue was purified on silica gel using 10% to 50% EtOAc in hexanes. After the deprotection, the residue was purified on silica gel using 5% to 10% to 25% EtOAc/Hexanes to yield a white solid. Yield: 0.0856 g (58%). Crystals suitable for X-ray crystallography were grown from a saturated solution in acetonitrile at 23 °C. NMR shifts match that of the previously reported values.¹¹



3-triethylsiloxy-1,3,5(10)-estratriene (20b): This compound was synthesized according to general catalytic procedure (B) for catalytic ether silylations from **20** (0.1202 g, 0.40 mmol) with no deprotection step. The residue was purified on silica gel using 0.5% to 2% EtOAc in hexanes as eluent, followed by a reverse phase C18 column using 5% to 20% MeCN in MeOH on a Biotage SP1 Flash Chromatography System to yield a colorless oil. Yield: 0.1100 g (74%)

^1H NMR (400 MHz, 23 °C, CDCl_3): δ 0.74 (q overlapping m, $J = 6.1$ Hz, 7H), 1.00 (t overlapping m, $J = 7.9$ Hz, 11H), 1.15 (qd, $J = 12.6$ Hz, $J = 4.5$ Hz, 1H), 1.34 – 1.45 (m, 2H), 1.64 (s, 3H), 1.94 – 2.03 (m, 2H), 2.08 – 2.17 (m, 1H), 2.19 – 2.34 (m, 3H), 2.35 – 2.49 (m, 2H), 2.66 (dq, $J = 14.3$ Hz, $J = 2.9$ Hz, 1H), 2.73 – 2.81 (m, 2H), 6.56 (bd, $J = 2.6$ Hz, 1H), 6.63 (dd, $J = 8.6$ Hz, $J = 3.7$ Hz, 1H), 7.16 (d, $J = 8.5$ Hz, 1H)

$^{13}\text{C}\{^1\text{H}\}$ NMR (151 MHz, 23 °C, CDCl_3): δ 5.0, 6.7, 13.5, 25.8, 27.7, 27.74, 30.3, 31.4, 37.2, 42.3, 48.9, 52.6, 117.1, 119.7, 127.0, 128.5, 132.8, 136.0, 138.4, 153.1



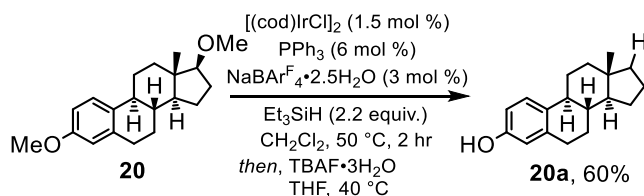
3,16-bis(triethylsiloxy)-17-methoxy-1,3,5(10)-estratriene (21a): This compound was synthesized according to general catalytic procedure (B) from trimethylestriol (21) (0.1322 g, 0.40 mmol) for catalytic ether silylations with no deprotection step. Yield: 0.1410 g (66%)

^1H NMR (400 MHz, 23 °C, CDCl_3): δ 0.63 (q, $J = 7.9$ Hz, 6H), 0.73 (q, $J = 7.9$ Hz, 6H), 0.79 (s, 3H), 0.99 (q, $J = 8.5$, 18H), 1.24 – 1.42 (m, 3H), 1.45 – 1.53 (m, 2H), 1.57 – 1.66 (m, 2H), 1.73 – 1.85 (m, 1H), 2.17 – 2.28 (m, 2H), 2.78 (m, 2H), 3.21 (d, $J = 5.2$ Hz, 1H), 3.48 (s, 3H), 4.12 (m, 1H), 6.56 (d, $J = 2.4$ Hz, 1H), 6.62 (dd, $J = 8.3$ Hz, $J = 3.3$ Hz, 1H), 7.10 (d, $J = 8.5$ Hz, 1H)

$^{13}\text{C}\{^1\text{H}\}$ NMR (151 MHz, 23 °C, CDCl_3): δ 4.8, 5.0, 6.7, 6.8, 12.7, 26.0, 27.2, 29.6, 34.8, 38.2*, 43.7, 43.8, 47.9, 59.1, 77.7, 99.5, 117.0, 119.8, 125.9, 132.9, 137.8, 153.3

*HSQC indicates that the singlet at δ 38.2 is an overlapping CH_2 and CH signal.

General Procedure (C) for Catalytic Ether Deoxygenation/Silylation on Large Scale with Catalyst Generated *in situ*:



17-Deoxyestradiol (19a): In air, a 20 mL scintillation vial was charged with $[(\text{cod})\text{IrCl}]_2$ (0.0335 g, 0.0499 mmol, 1.5 mol %), PPh_3 (0.0522 g, 0.199 mmol, 6 mol %), $\text{NaBARF}_4 \cdot 2.5 \text{H}_2\text{O}$ (0.0929

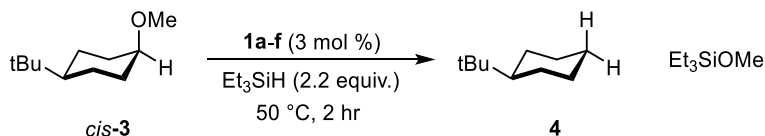
g, 0.0995 mmol, 3 mol %) and dichloromethane (17.0 mL). The solution was mixed on a vortexer for *ca.* 30 seconds and allowed to stand for 15 minutes at 23 °C. At this point a fine colorless precipitate had formed which was separated using a 0.45 μm PTFE syringe filter to transfer the filtrate into a 100 mL round-bottom flask. A stir bar was added followed by Et₃SiH (2.3 mL, 14.65 mmol, 4.4 equiv.). This mixture was stirred at 23 °C for *ca.* 2 minutes until activation was observed by a color change from red to a pale yellow and the evolution of gas. Substrate ether **20** (1.0002 g, 3.33 mmol, 1 equiv.) was added to the reaction flask which was then equipped with a reflux condenser vented by a needle through a septum at the top. The resulting reaction mixture was stirred at 50 °C for 2 h before being removed from the heat and concentrated under vacuum to give a residue. This residue was partially purified by elution through a plug of silica gel using 20% to 40% EtOAc in hexanes as the eluent. The crude mixture was evaporated to dryness and was then taken up in 10 mL of THF and transferred to a 250 mL round-bottom flask containing a stir bar. NBu₄F·3H₂O (5.25 g, 16.7 mmol, 5 equiv.) was added to the solution and the mixture was heated at 40 °C for 16h. The resulting mixture was removed from heat and the solvent evaporated under vacuum. The residue was extracted with 2 mL dichloromethane and this mixture was purified by column chromatography using 10% to 40% EtOAc in hexanes as eluent to give the product as a white solid. Yield: 0.5152 g (60%). Spectroscopic data for this compound has been previously reported.²⁴

¹H NMR (400 MHz, 23 °C, CDCl₃): δ 0.94 – 1.02 (m, 2H), 1.14 (qd, J = 12.6 Hz, J = 4.2 Hz, 1H), 1.25 (br, 1H), 1.34 – 1.42 (m, 2H), 1.63 (s, 3H), 1.92 – 2.01 (m, 2H), 2.12 (qd, J = 8.4 Hz, J = 2.3 Hz, 1H), 2.20 – 2.33 (m, 3H), 2.39 (bt, J = 11.4 Hz, 1H), 2.45 (dp, J = 12.6 Hz, J = 2.5 Hz, 1H), 2.66 (dq, J = 14.3 Hz, J = 2.1 Hz, 1H), 2.73 – 2.82 (m, 2H), 4.49 (s, 1H), 6.54 (d, J = 2.7 Hz, 1H), 6.63 (dd, J = 8.5 Hz, J = 2.7 Hz, 1H), 7.19 (d, J = 8.5 Hz, 1H)

II. Small Scale Reactions

General Procedure (A) for Small Scale Catalytic Reactions for Ether

Deoxygenation/Silylation:

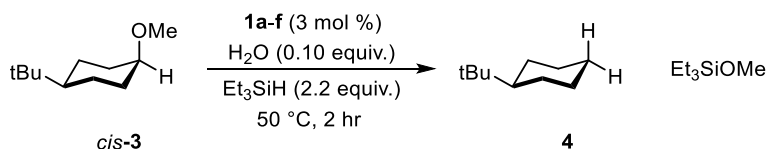


In air,* a 4 mL vial was charged with 0.15 mL of an 8.0 mM stock solution of $[(\text{cod})\text{Ir}(\text{PR}_3)_2]\text{BAr}^{\text{F}}_4$ (**1a-e**) (0.0012 mmol) in CD_2Cl_2 followed by the addition of triethylsilane (0.0102 g, 0.0875 mmol, 14.0 μL , 2.2 equiv.) the resulting mixture was mixed for approximately 30 seconds. The substrate ether (0.03927 mmol) was then added, and the vessel heated at 50 °C for 2 h. After cooling, the solution was diluted with 0.50 mL CD_2Cl_2 and transferred to an NMR tube; yields were calculated using an internal standard of mesitylene (0.0065 g, 0.036 mmol, 5.0 μL).

* Owing to the poor solubility of **1f**, stock solutions were not used for this precatalyst. Instead **1f** was weighed out in an inert atmosphere glove box.

General Procedure (B) for NMR-Scale Catalytic Reactions for Ether

Deoxygenation/Silylation with H_2O as an additive:

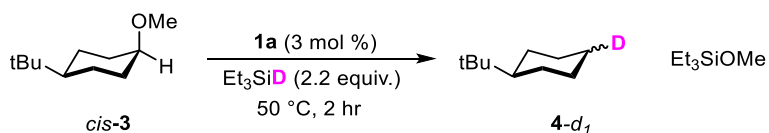


In air,* a 4 mL vial was charged with 0.15 mL of an 8.0 mM stock solution of $[(\text{cod})\text{Ir}(\text{PR}_3)_2]\text{BAr}^{\text{F}}_4$ (**1a-e**) (0.0012 mmol) in CD_2Cl_2 doped with 0.35 $\mu\text{L}/\text{mL}$ of H_2O (71.5 μg , 0.0040 mmol). Triethylsilane (0.0102 g, 0.0875 mmol, 14.0 μL , 2.2 equiv.) was added and the mixture stirred for approximately 30 seconds. The substrate ether (0.0397 mmol) was then added, and the mixture was heated at 50 °C for 2 h. After cooling, the solution was diluted with 0.50 mL CD_2Cl_2 and

transferred to an NMR tube; yields were calculated using an internal standard of mesitylene (0.0065 g, 0.036 mmol, 5.0 μ L).

* Owing to the poor solubility of **1f**, stock solutions were not used for this precatalyst. Instead **1f** was weighed out in an inert atmosphere glove box and 0.20 mL of a 0.35 μ L/mL stock solution of water in CD_2Cl_2 was added through the septum cap of the vial.

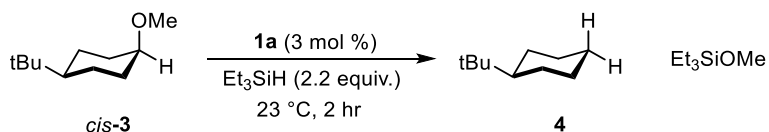
Procedure for NMR-Scale Ether Deoxygenation/Silylation using Et_3SiD



In an inert atmosphere glovebox, a 4 mL vial was charged with 0.20 mL of a 10 mg/mL solution of $[(\text{cod})\text{Ir}(\text{PPh}_3)_2]\text{BAR}^{\text{F}_4}$ (**1a**) (0.0012 mmol) in CH_2Cl_2 followed by the addition of Et_3SiD (0.0102 g, 0.0875 mmol, 14.0 μ L, 2.2 equiv.) the resulting mixture was stirred for approximately 30 seconds. At this point substrate ether *cis*-**3** was added (0.0397 mmol, 7.8 μ L) and the mixture heated at 50 $^\circ\text{C}$ for 2 h. The crude mixture was transferred to a 3 mm NMR tube and analyzed by ^2H NMR spectroscopy. The products *cis*- and *trans*-tert-butyl(4- ^2H) cyclohexane (**4-d₁**) were identified by reference to reported chemical shifts.²⁵

General Procedure for NMR-Scale Kinetic Experiments for Ether

Deoxygenation/Silylation:



In air, a septum-capped NMR tube was charged with $[(\text{cod})\text{Ir}(\text{PPh}_3)_2]\text{BAR}^{\text{F}_4}$ (**1a**) (0.0100 g, 0.00597 mmol, 3 mol%) in 0.4 mL CD_2Cl_2 . Mesitylene (0.0065 g, 0.0359 mmol, 5.0 μ L) was

added to the NMR tube as an internal standard and the solution was mixed. This was followed by the addition of triethylsilane (0.438 mmol, 69.9 μ L, 2.2 equiv.) and substrate ether *cis*-**3** (39.2 μ L, 0.199 mmol, 1 equiv.). Immediately after mixing the sample was placed in an NMR spectrometer and the reaction progress was monitored by ^1H NMR spectroscopy every 22 seconds.

“Wet” variant. In the representative “wet” experiment no precautions were taken to exclude trace water. The water content of the 0.4 mL aliquot of CD_2Cl_2 used was estimated by ^1H NMR to be 0.0093 mmol (*ca.* 4.5 mol%).

“Dry” variant. In the representative dry experiment, the following precautions were taken to exclude trace water: The catalyst and reagent solutions were stored over activated 4 \AA molecular sieves for *ca.* 2 days prior to use and were handled only in an inert atmosphere glove box. The NMR tube was oven dried, then silylated by treatment with a hexane solution of chlorotrimethylsilane. After drying under vacuum overnight the tube was handled only under inert atmosphere.

Catalyst Activation Studies

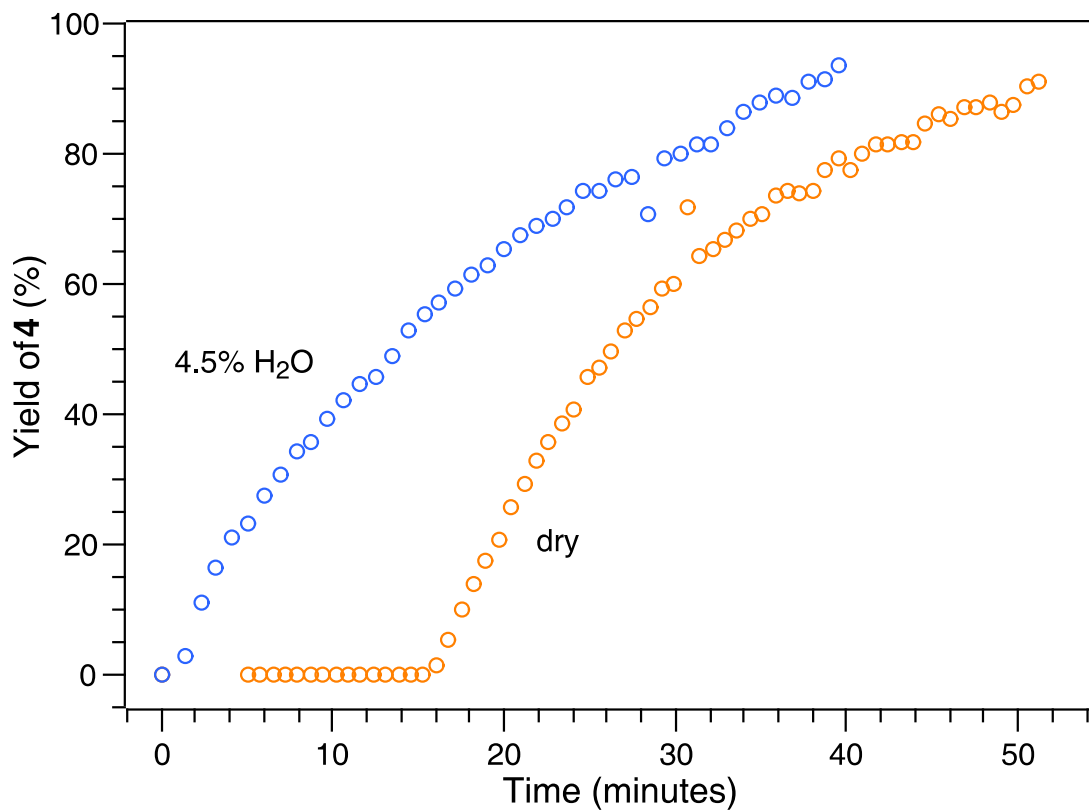


Figure S1. Role of trace water in precatalyst (**1a**) activation by NMR analysis.

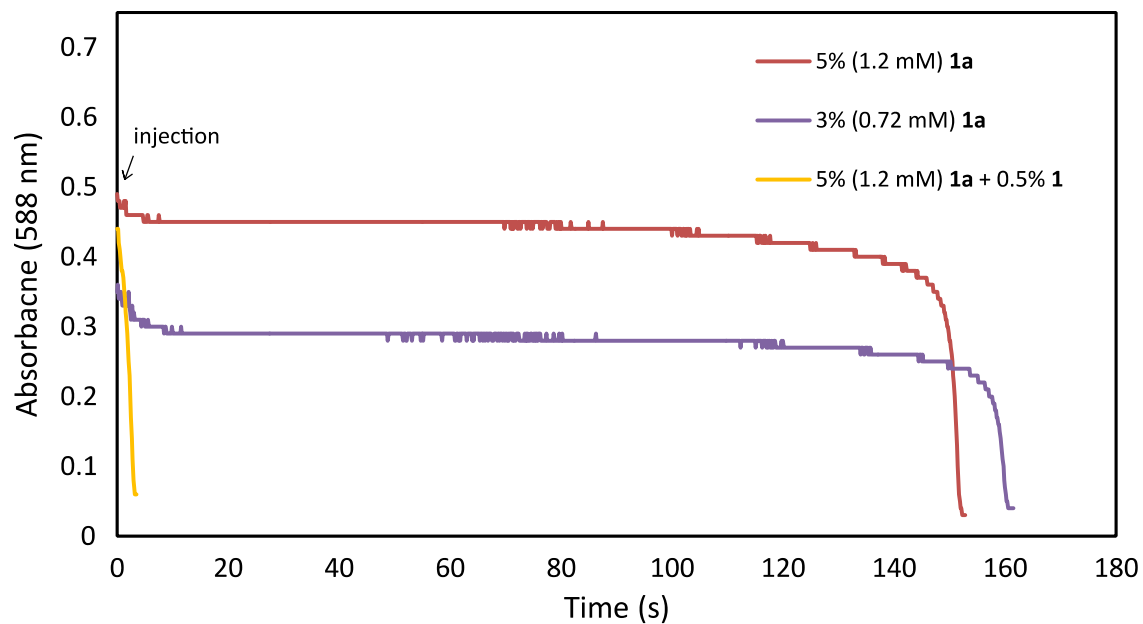


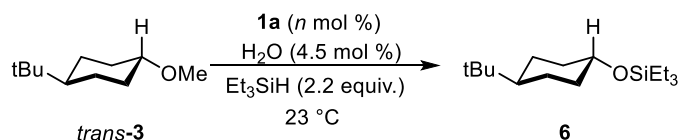
Figure S2. Bleaching of **1a** at low concentration by UV-Vis. Role of added **1** shown (yellow). *Note:* Bleaching is near instantaneous under typical reaction conditions (6.0 mM Ir, non-dry solvent)

Procedure for Monitoring **1a** Activation by UV-Vis (Figure S2).

Standard variant - Figure S2 (red). In air, a 1.0 cm cuvette was charged with 2.0 mL of a 1.2 mM stock solution of [(cod)Ir(PPh₃)₂]BAR^F₄ (**1a**) (0.0024 mmol) in dichloromethane and a stir bar. The cuvette was placed in an Ocean Optics UV-Vis cuvette holder in transmission mode mounted atop a stir plate. The solution was stirred vigorously while 21.5 μL of a solution of *cis-3* (0.0236 M, 0.0477 mmol) and Et₃SiH (0.0519 M, 0.105 mmol) was added. The consumption of **1a** was monitored by observation of the bleaching of a band centered at 558 nm.

Activated variant – Figure S2 (yellow). In air, a 1.0 cm cuvette was charged with 2.0 mL of a 1.19 mM stock solution of [(cod)Ir(PPh₃)₂]BAR^F₄ (**1a**) (0.0024 mmol), 0.8 μL of a 0.579 M solution of **1** (0.000048 mmol) in dichloromethane and a stir bar. The cuvette was placed in an Ocean Optics UV-Vis cuvette holder in transmission mode mounted atop a stir plate. The solution was stirred vigorously while 21.5 μL of a solution of *cis-3* (0.0236 M, 0.0477 mmol) and Et₃SiH (0.0519 M, 0.105 mmol) was added. The consumption of **1a** was monitored by observation of the bleaching of a band centered at 558 nm.

Determination of Rate Dependence on Catalyst Loading:



Kinetic experiments aimed at determining the rate dependence on catalyst loading for the reduction of *trans-3* were conducted according to the “Wet” variant of the general procedure for NMR-scale kinetic experiments above. Experiments were conducted at **1a** loadings of 2.0%, 2.5%, 3.0%, 3.5% and 4.0%.

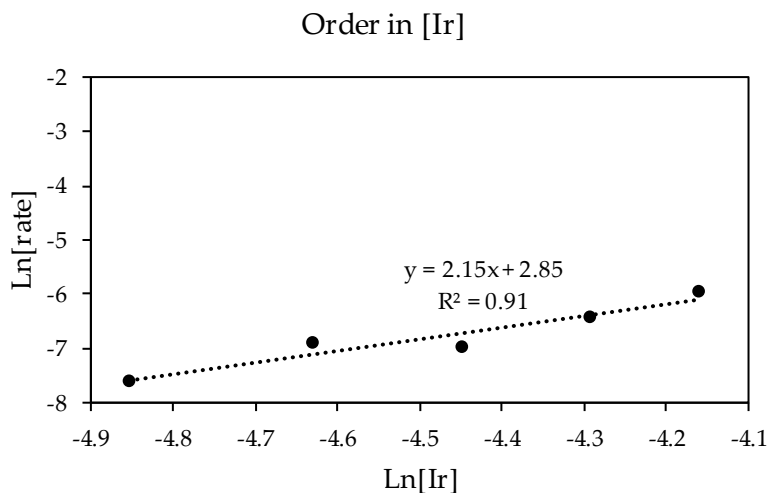


Figure S3. Ln/Ln plot showing 2nd order rate dependence on iridium loading.

Determination of Catalyst Resting state by $^{31}\text{P}\{^1\text{H}\}$ NMR:

The identity of the major phosphorus-containing species in solution was examined according to the following procedure. In air, a septum-capped NMR tube was charged with **1**, **1a** or **1f** (0.00597 mmol, 3 mol%) and 0.4 mL CD_2Cl_2 . This was followed by the addition of triethylsilane (0.438 mmol, 69.9 μL , 2.2 equiv.) and substrate ether *cis*-**3** (39.2 μL , 0.199 mmol, 1 equiv.). Immediately upon mixing the distinctive red color of the precatalyst bleached. The sample was placed in an NMR spectrometer and the reaction was analyzed by $^{31}\text{P}\{^1\text{H}\}$ NMR. In all cases a single species was observed, whose chemical shift corresponded to **22a** in the case of **1** and **1a** and **23a** in the case of catalysis with **1f**.

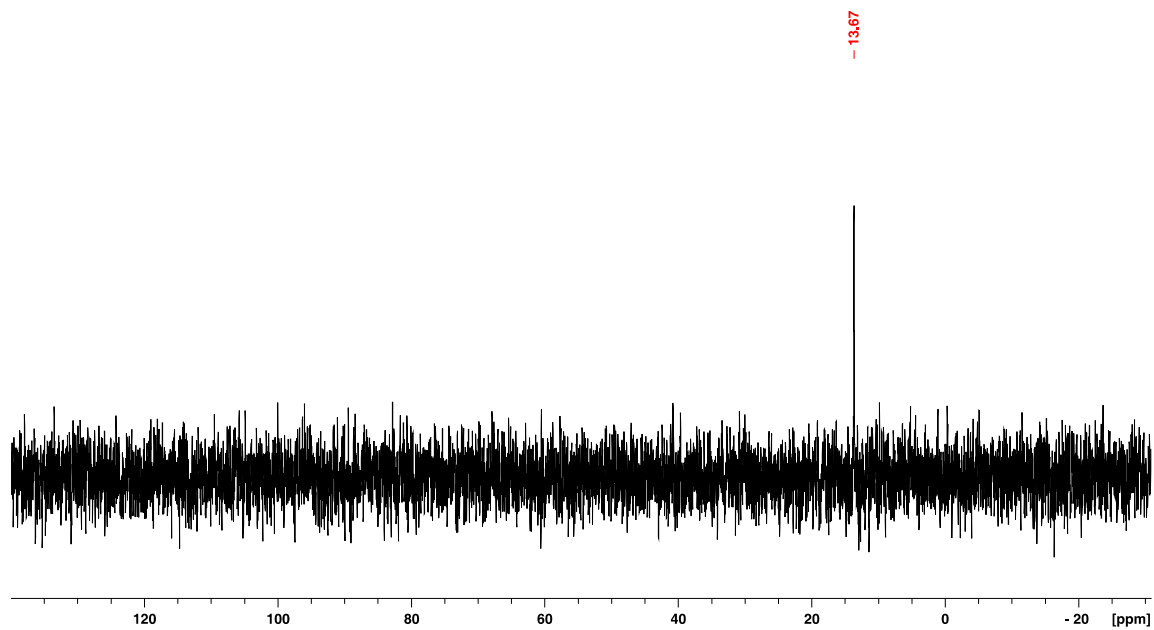


Figure S4. $^{31}\text{P}\{^1\text{H}\}$ NMR of catalytic reaction using **1** as precatalyst (CD_2Cl_2 , 23 °C)

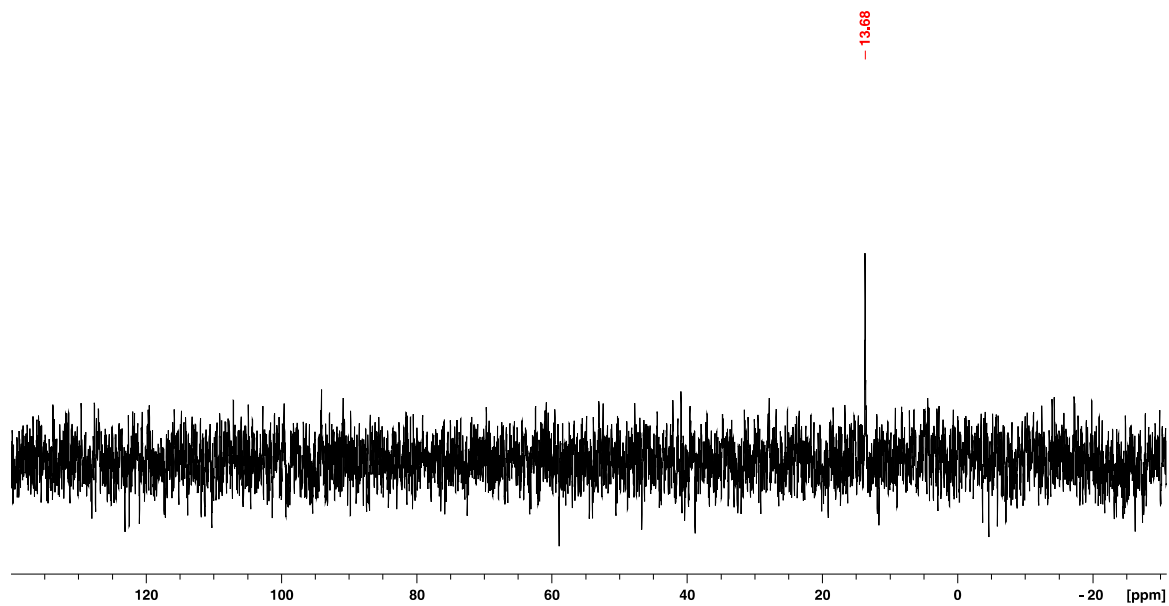


Figure S5. $^{31}\text{P}\{^1\text{H}\}$ NMR of catalytic reaction using **1a** as precatalyst (CD_2Cl_2 , 23 °C)

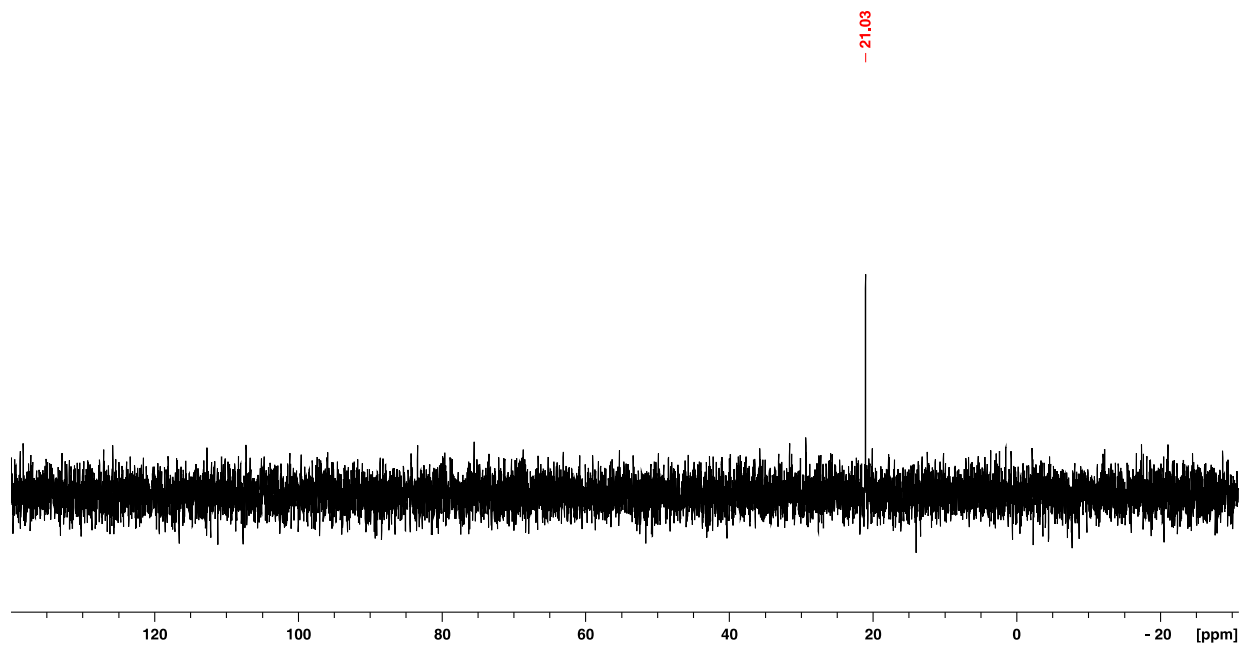


Figure S6. $^{31}\text{P}\{^1\text{H}\}$ NMR of catalytic reaction using **1f** as precatalyst (CD_2Cl_2 , 23 °C)

IV. NMR Spectra

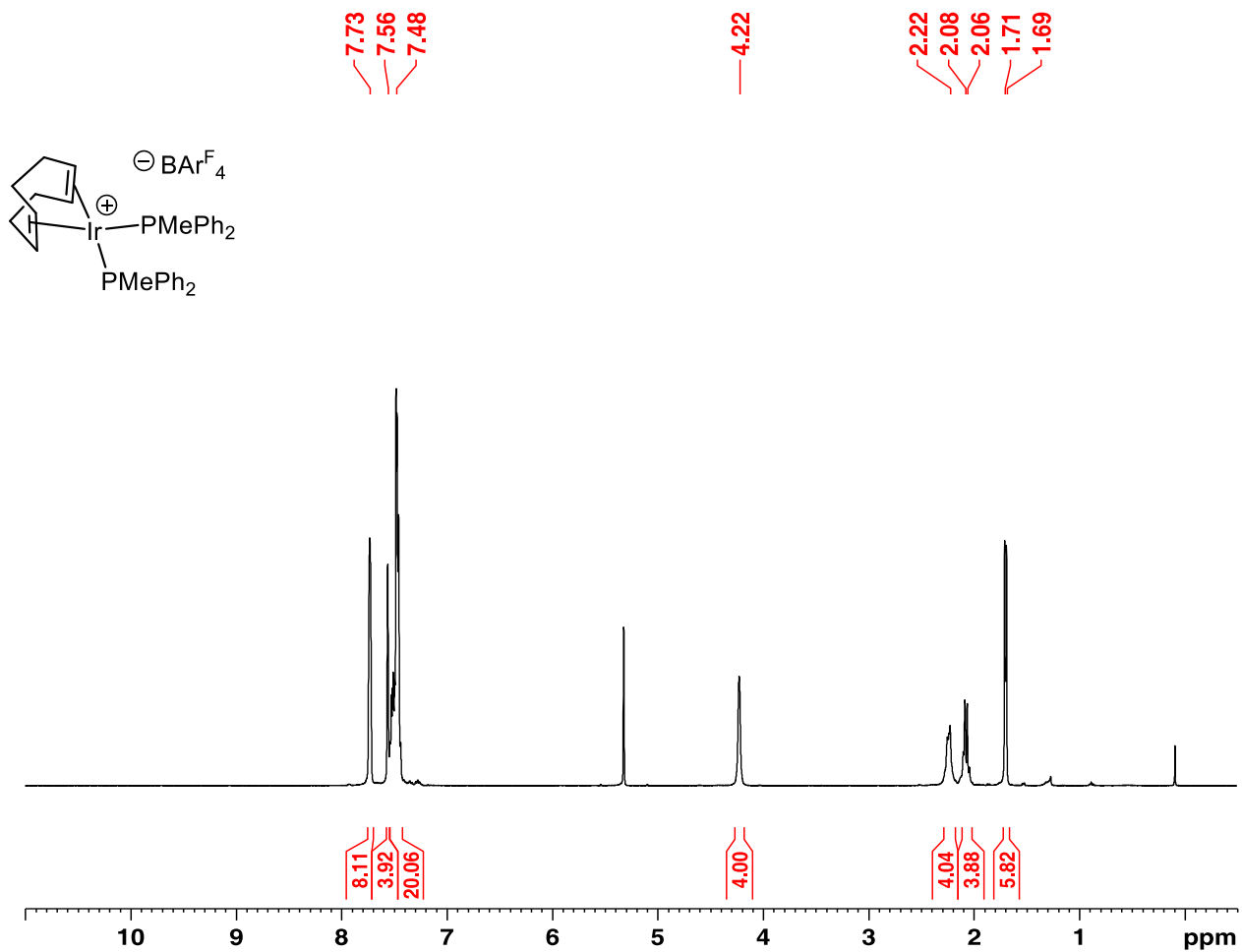


Figure S7. ^1H NMR of $[(\text{cod})\text{Ir}(\text{PMePh}_2)_2]\text{BARF}_4$ (**1b**) (CD₂Cl₂, 23 °C)

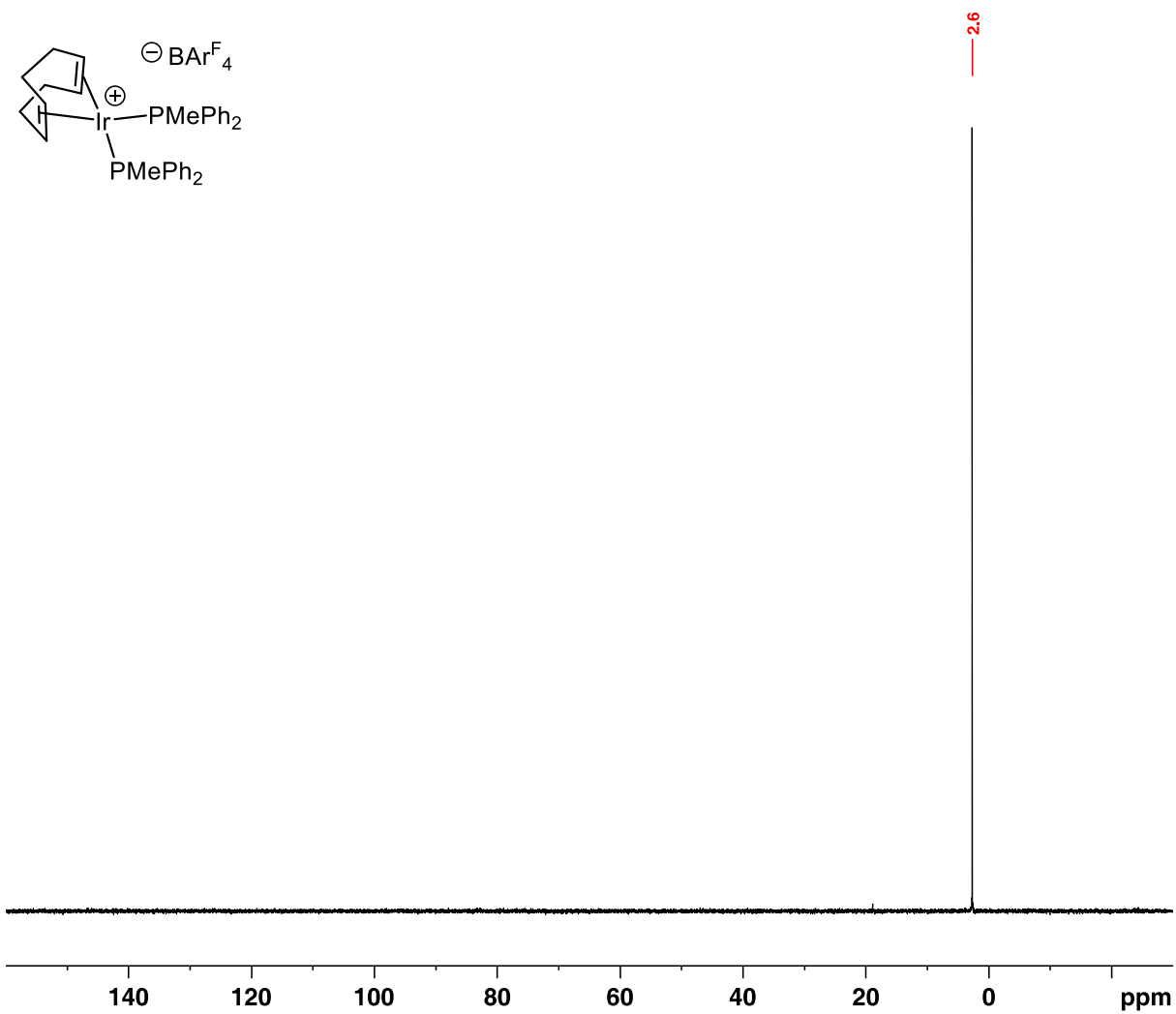


Figure S8. $^{31}\text{P}\{^1\text{H}\}$ NMR of $[(\text{cod})\text{Ir}(\text{PMePh}_2)_2]\text{BARF}_4$ (**1b**) (CD_2Cl_2 , 23 °C)

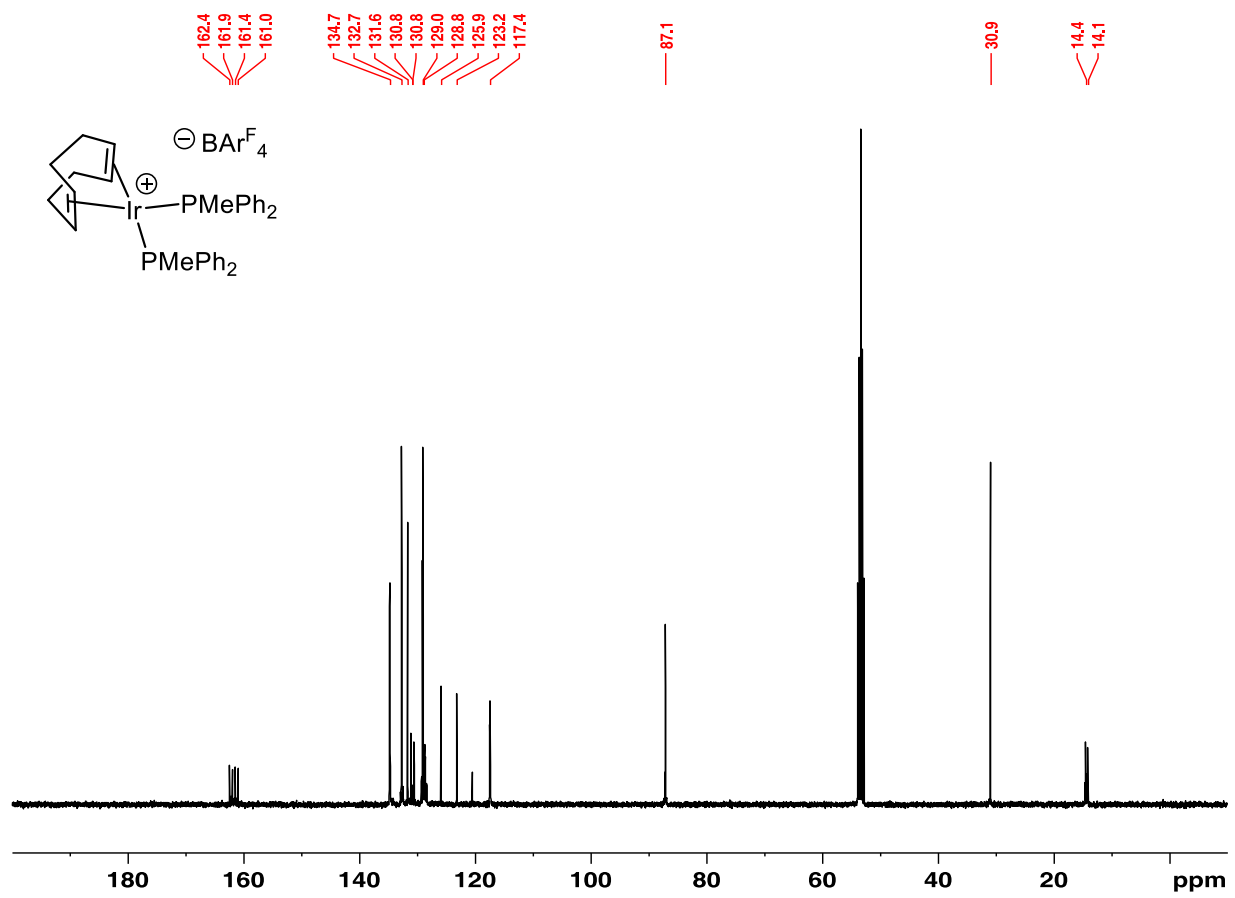


Figure S9. $^{13}\text{C}\{^1\text{H}\}$ NMR of $[(\text{cod})\text{Ir}(\text{PMePh}_2)_2]\text{BARF}_4$ (**1b**) (CD_2Cl_2 , $23\text{ }^\circ\text{C}$)

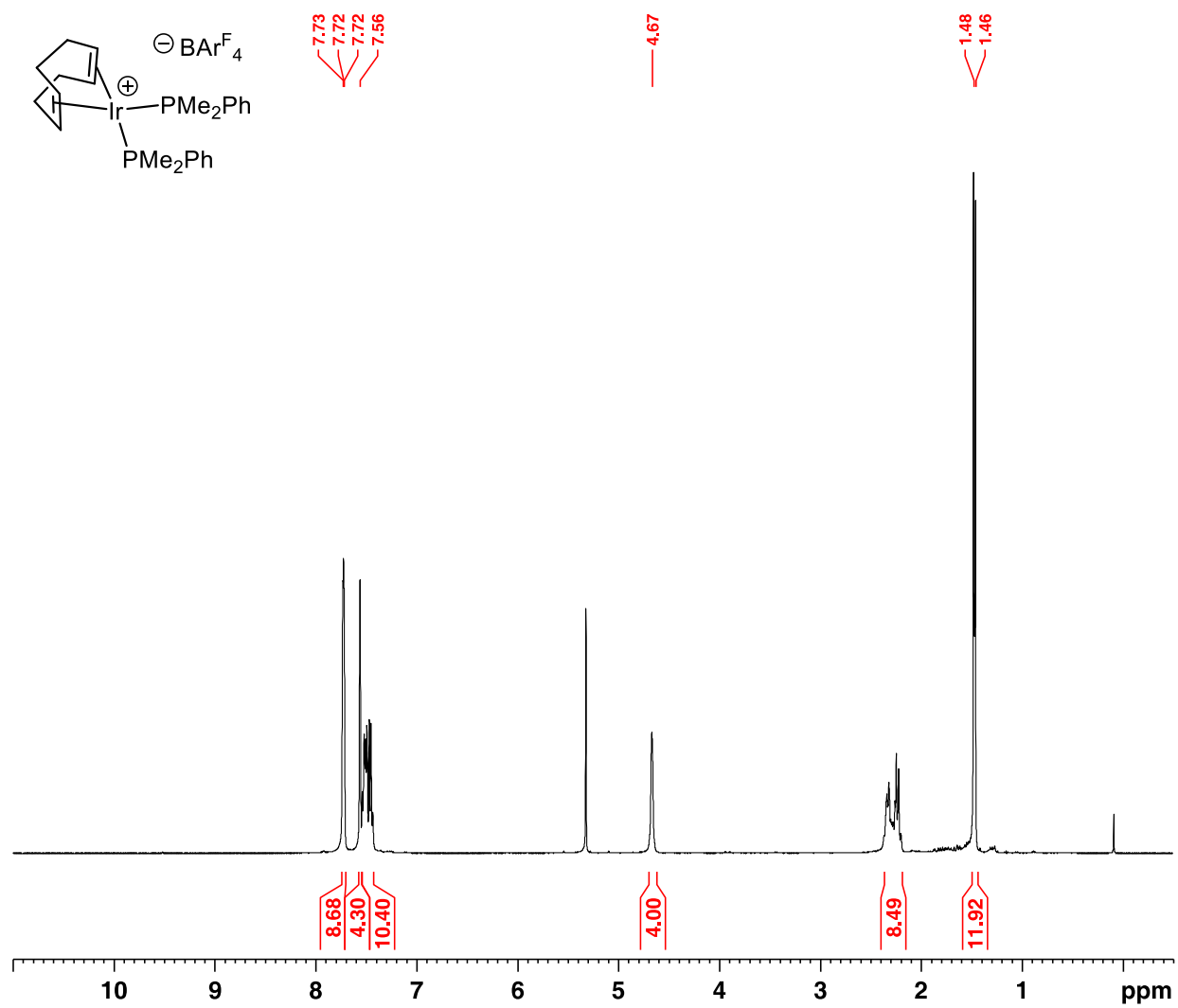


Figure S10. 1H NMR of $[(cod)Ir(PMe_2Ph)_2]BARF_4$ (**1c**) (CD_2Cl_2 , 23 °C)

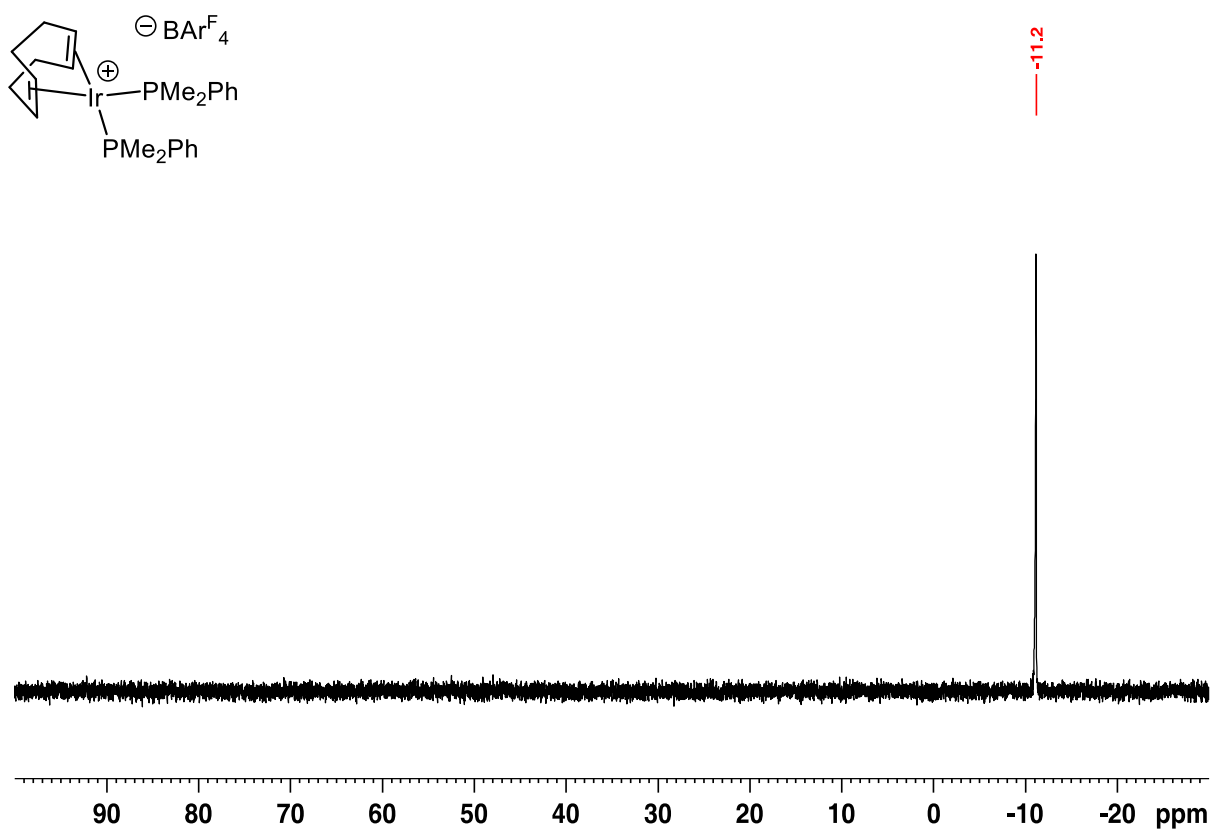


Figure S11. $^{31}\text{P}\{^1\text{H}\}$ NMR of $[(\text{cod})\text{Ir}(\text{PMe}_2\text{Ph})_2]\text{BARF}_4$ (**1c**) (CD_2Cl_2 , 23 °C)

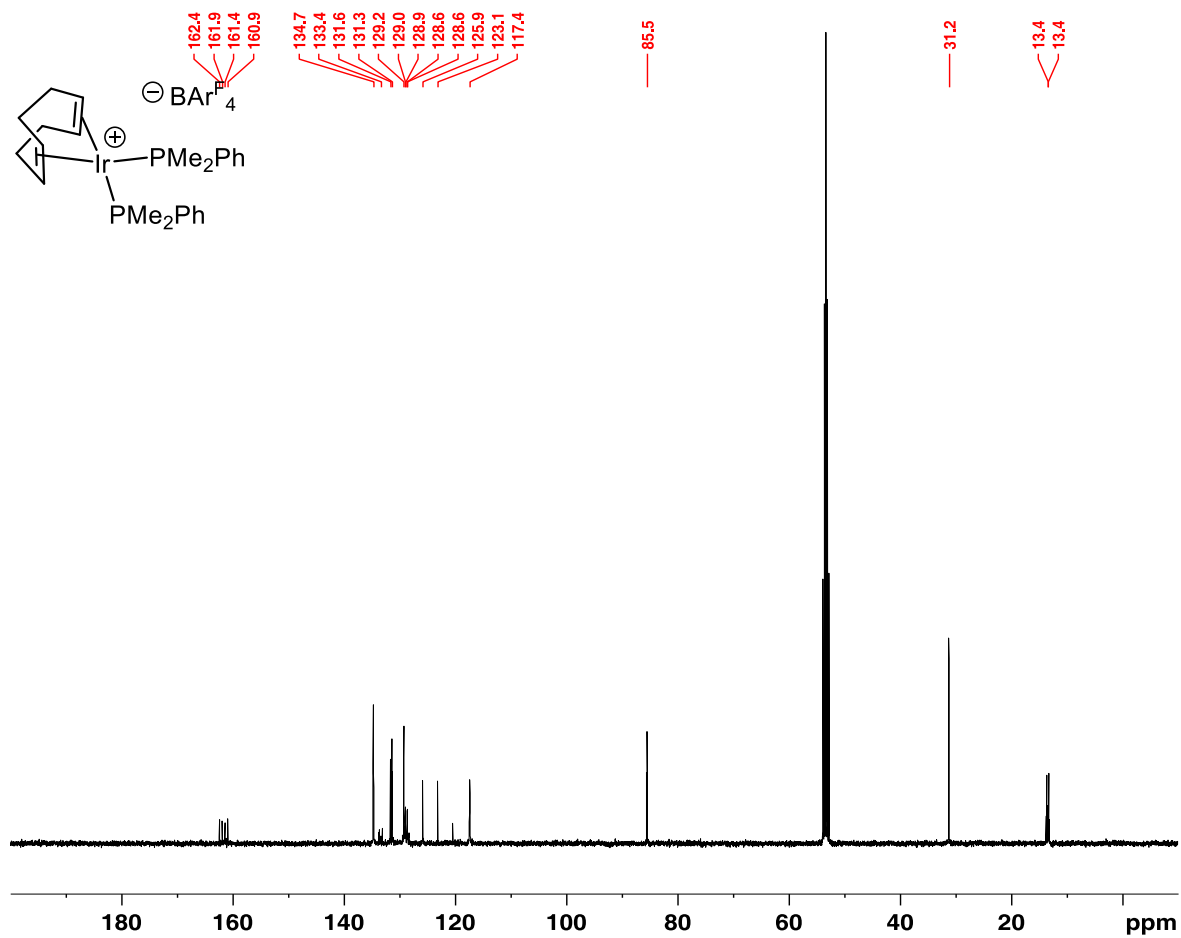


Figure S12. $^{13}\text{C}\{^1\text{H}\}$ NMR of $[(\text{cod})\text{Ir}(\text{PMe}_2\text{Ph})_2]\text{BARF}_4$ (**1c**) (CD_2Cl_2 , 23 °C)

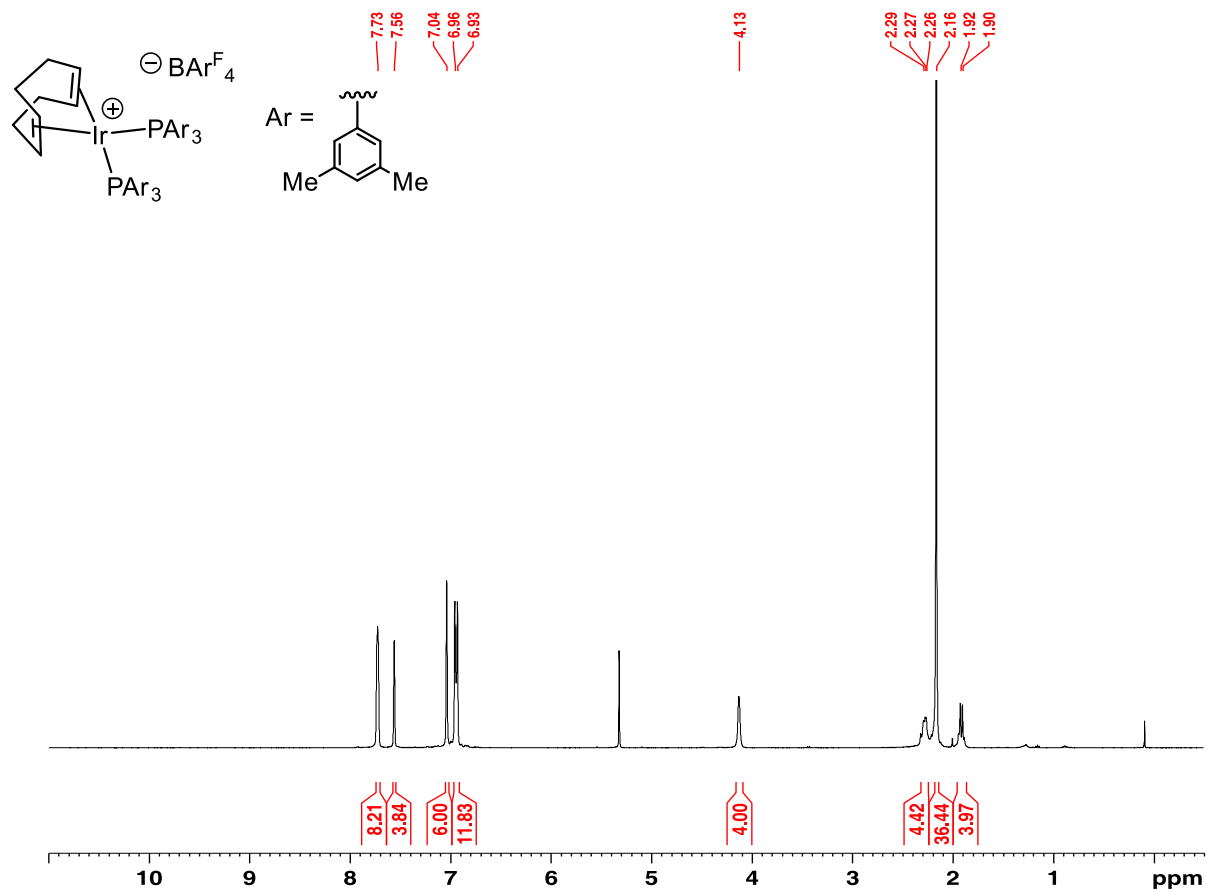


Figure S13. ^1H NMR of $[(\text{cod})\text{Ir}(\text{P}(3,5\text{-xylyl})_3)_2]\text{BARF}_4$ (**1d**) (CD_2Cl_2 , 23 °C)

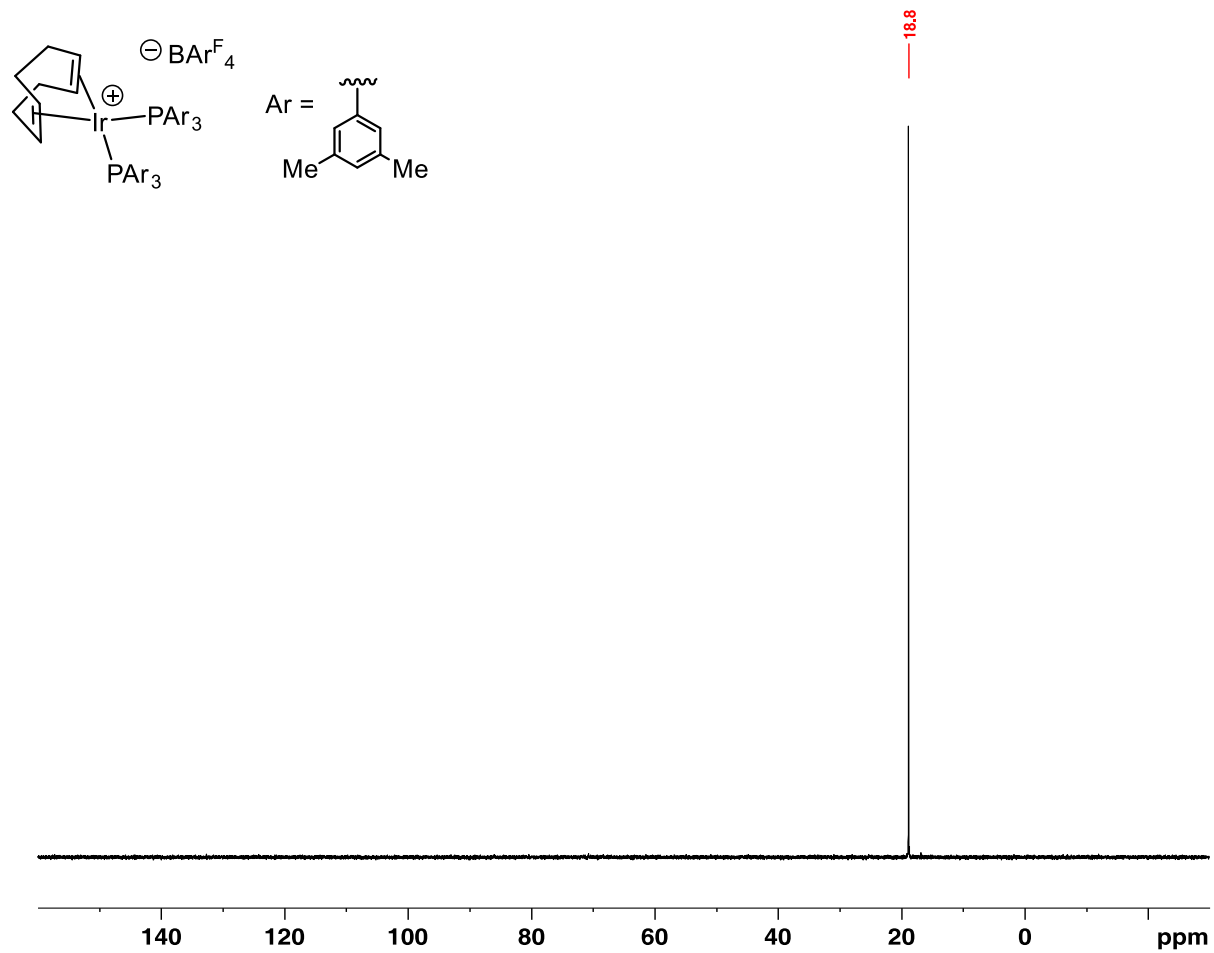


Figure S14. $^{31}P\{^1H\}$ NMR of $[(cod)Ir(P(3,5-xlylyl)_3)_2]BARF_4$ (**1d**) (CD_2Cl_2 , 23 °C)

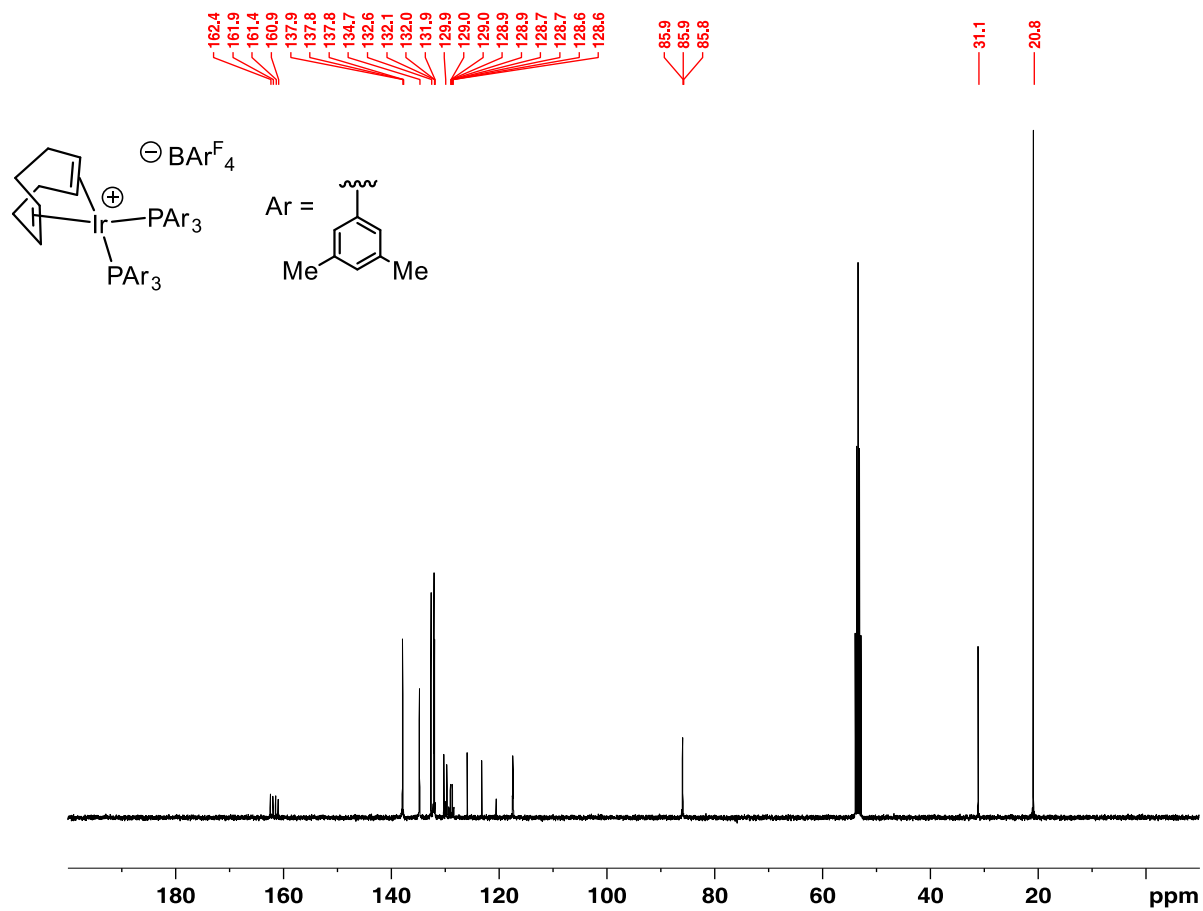


Figure S15. $^{13}\text{C}\{^1\text{H}\}$ NMR of $[(\text{cod})\text{Ir}(\text{P}(3,5\text{-xylyl})_3)_2]\text{BARF}_4$ (**1d**) (CD_2Cl_2 , $23\text{ }^\circ\text{C}$)

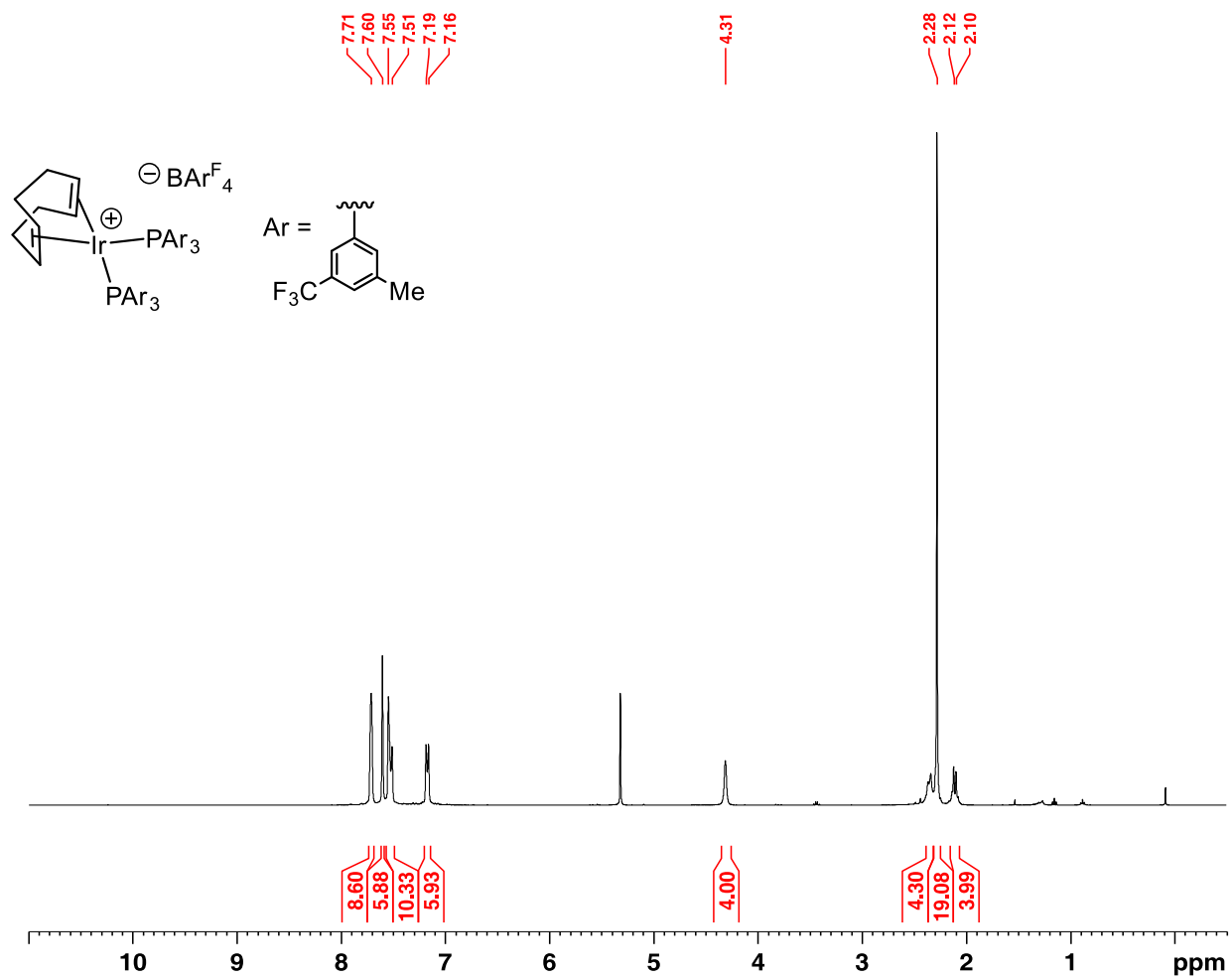


Figure S16. ^1H NMR of $[(\text{cod})\text{Ir}(\text{P}(3,5\text{-CF}_3\text{CH}_3\text{C}_6\text{H}_3)_3)_2]\text{BARF}_4$ (**1e**) (CD_2Cl_2 , 23 °C)

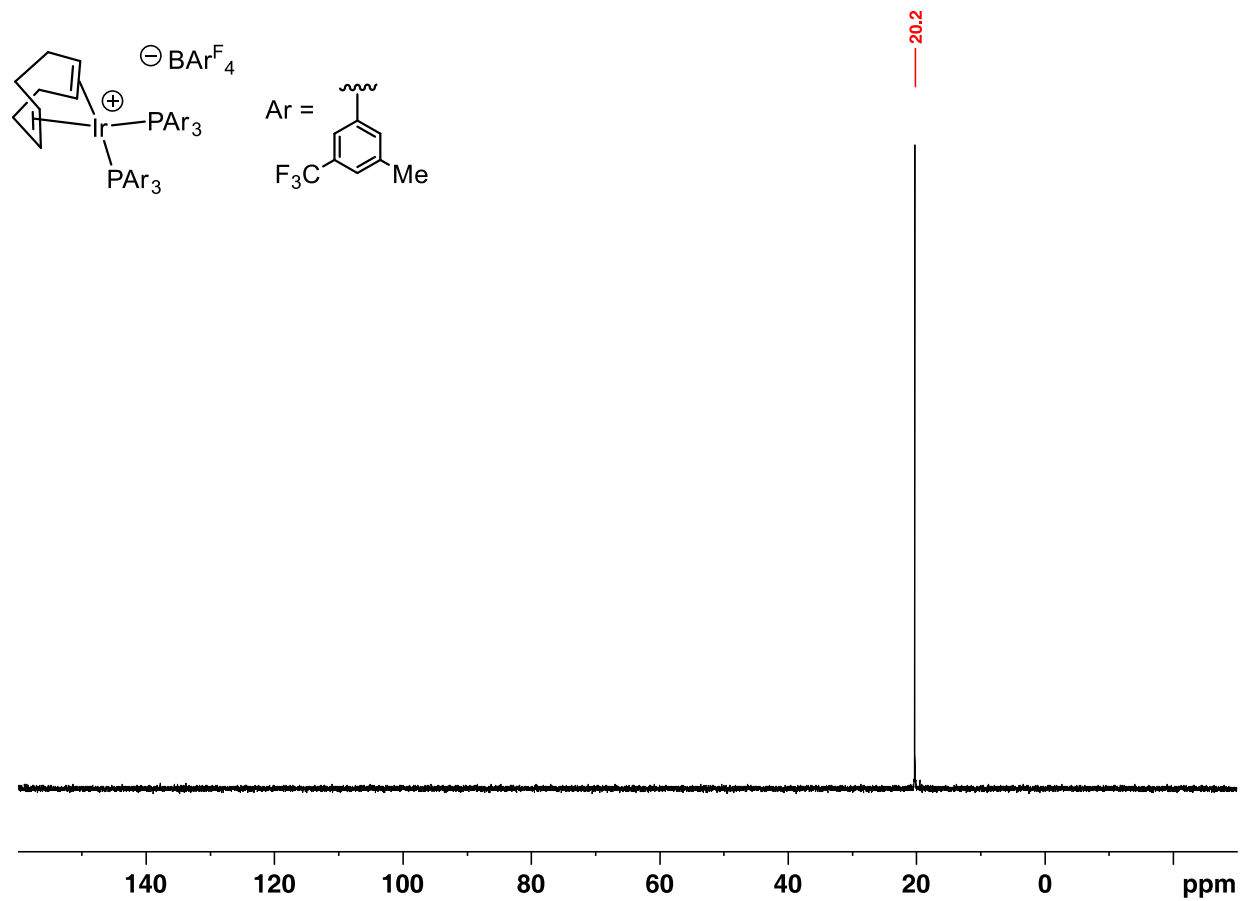


Figure S17. $^{31}\text{P}\{^1\text{H}\}$ NMR of $[(\text{cod})\text{Ir}(\text{P}(3,5\text{-CF}_3\text{CH}_3\text{C}_6\text{H}_3)_2)_2]\text{BArF}_4$ (**1e**) (CD_2Cl_2 , 23 °C)

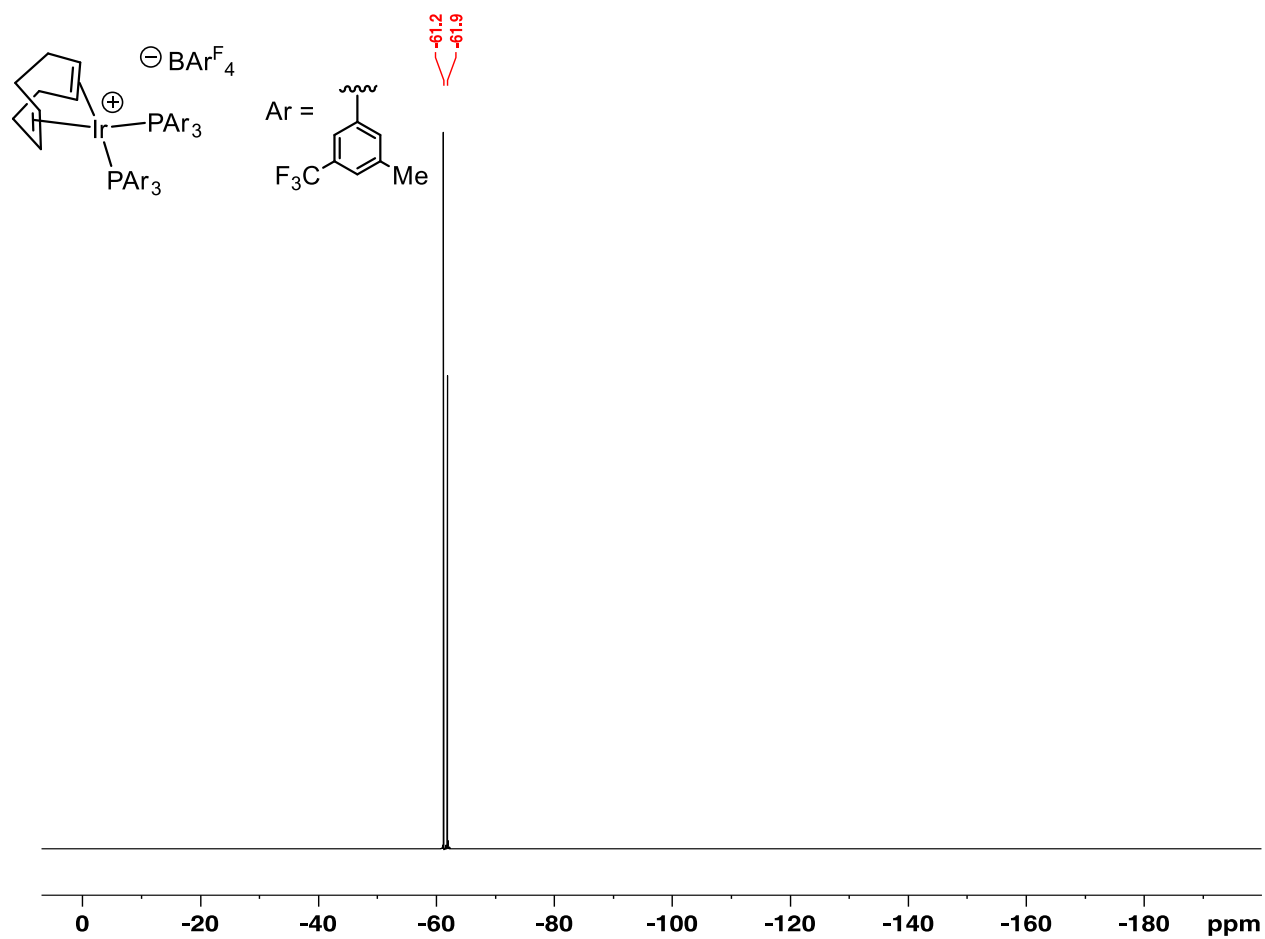


Figure S18. $^{19}\text{F}\{^1\text{H}\}$ NMR of $[(\text{cod})\text{Ir}(\text{P}(3,5\text{-CF}_3\text{CH}_3\text{C}_6\text{H}_3)_2)_2]\text{BArF}_4$ (**1e**) (CD_2Cl_2 , 23 °C)

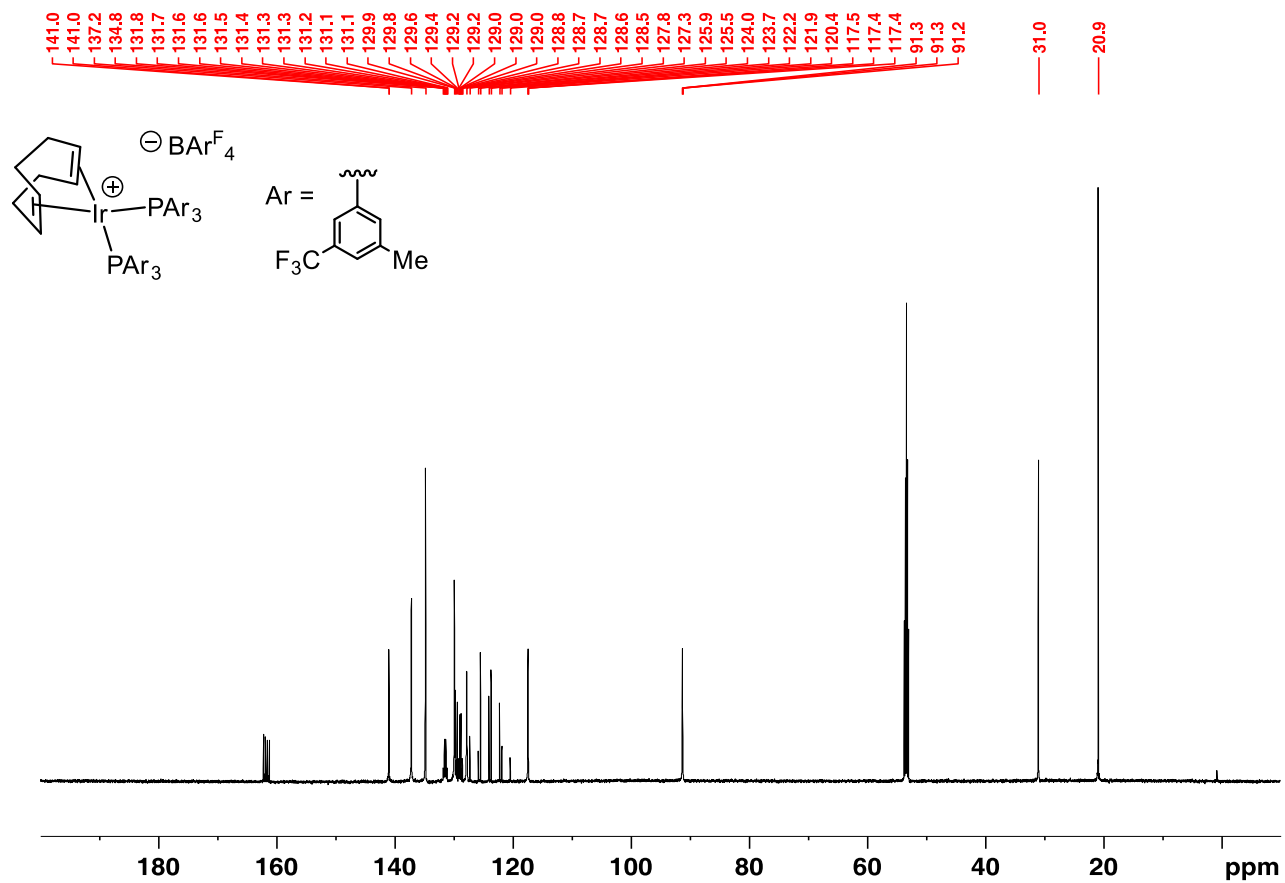


Figure S19. $^{13}C\{^1H\}$ NMR of $[(cod)Ir(P(3,5-CF_3CH_3C_6H_3)_3)_2]BARF_4$ (**1e**) (CD_2Cl_2 , 23 °C)

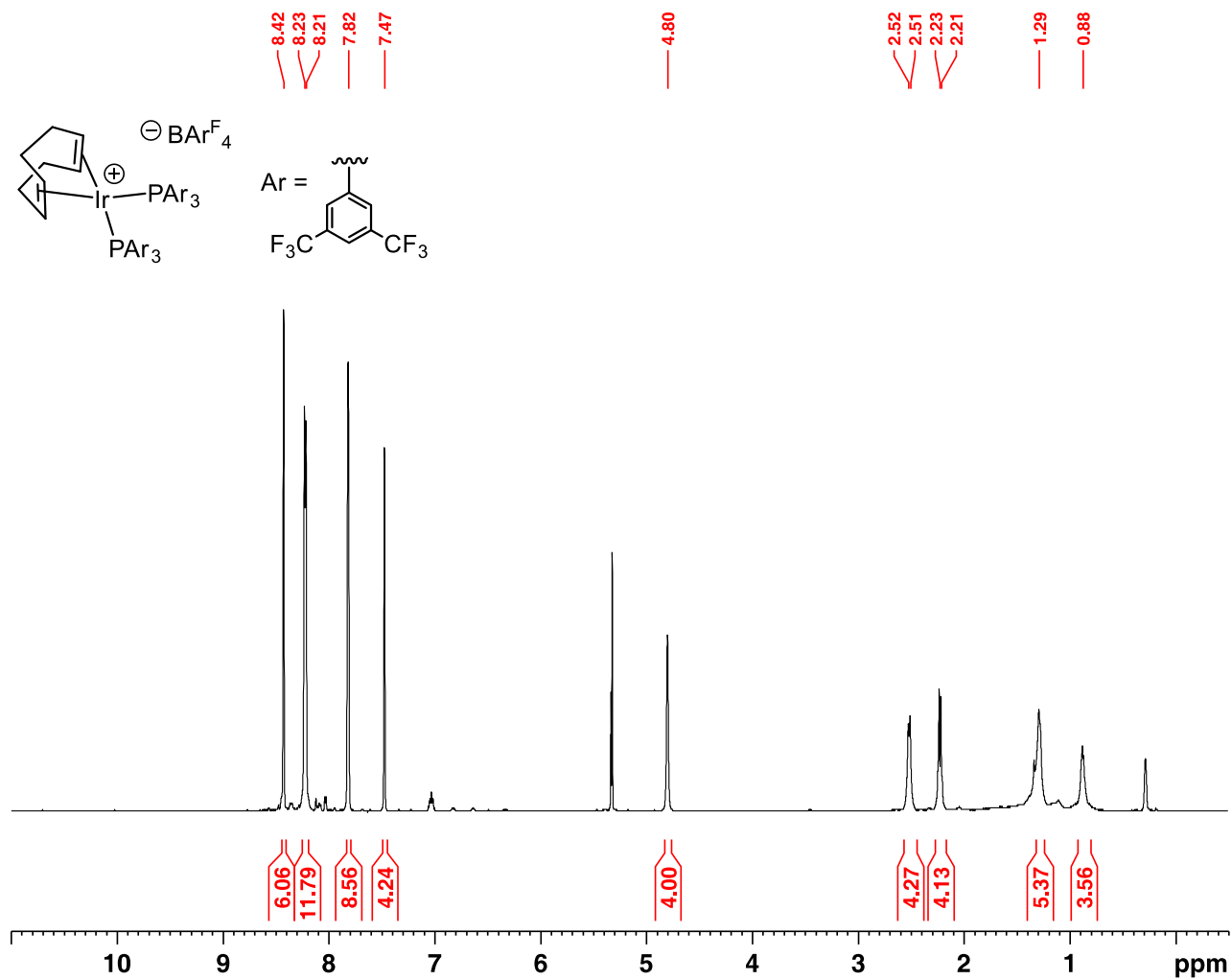


Figure S20. ^1H NMR of $[(\text{cod})\text{Ir}(\text{P}(3,5\text{-}(\text{CF}_3)_2\text{C}_6\text{H}_3)_2)_2]\text{BARF}_4$ (**1f**) ($\text{C}_6\text{F}_6/\text{CD}_2\text{Cl}_2$, 23 °C)

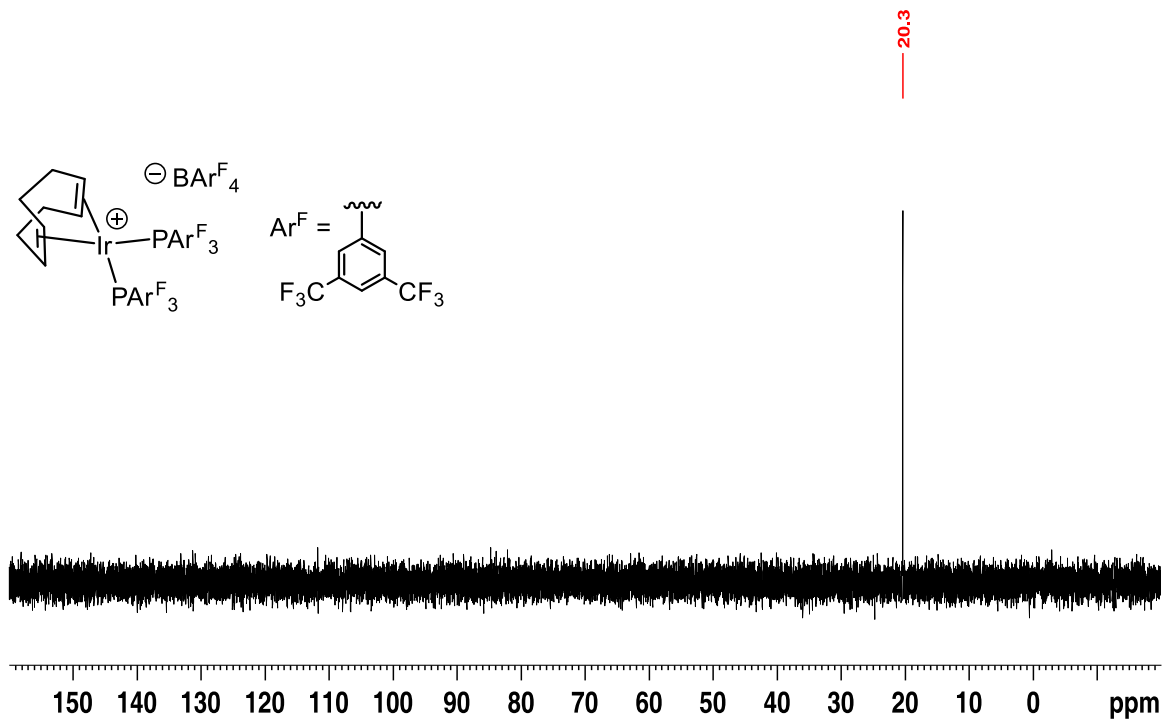


Figure S21. $^{31}\text{P}\{^1\text{H}\}$ NMR of $[(\text{cod})\text{Ir}(\text{P}(3,5\text{-(CF}_3)_2\text{C}_6\text{H}_3)_2)_2]\text{BARF}_4$ (**1f**) ($\text{C}_6\text{F}_6/\text{CD}_2\text{Cl}_2$, 23 °C)

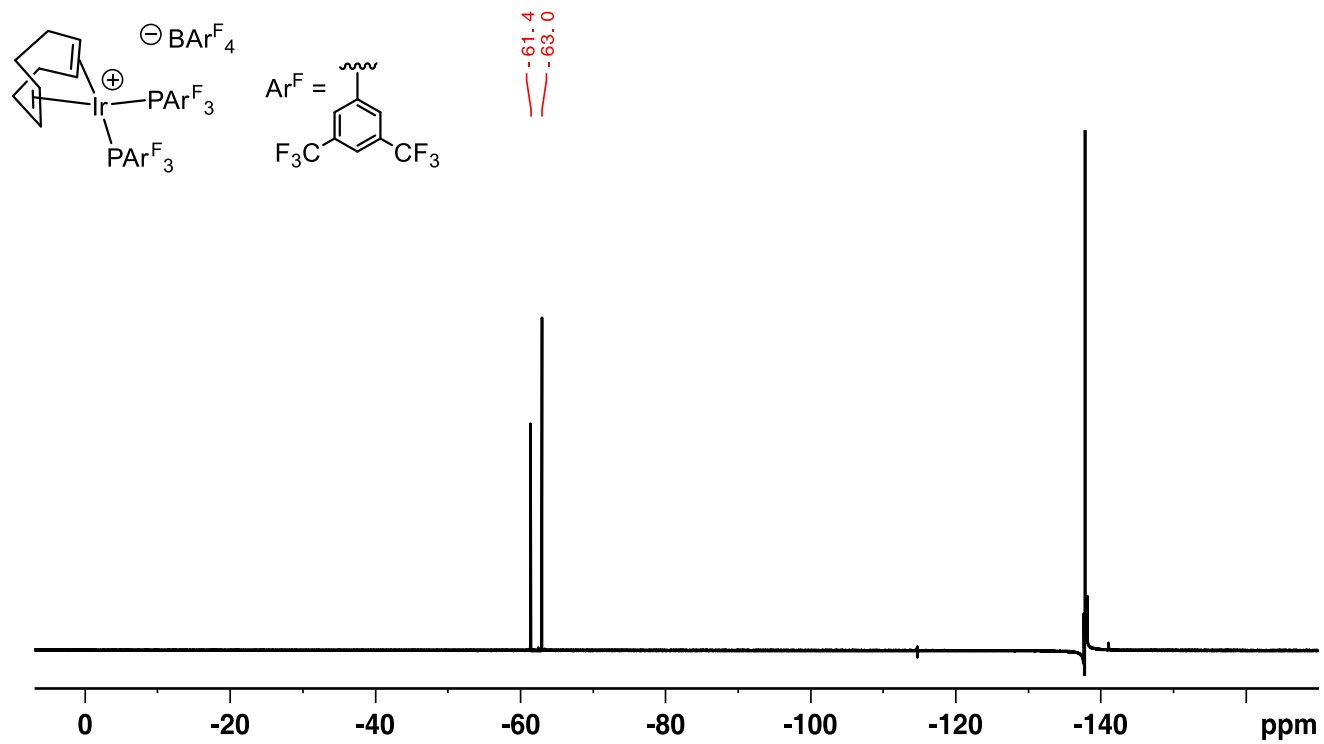


Figure S22. $^{19}\text{F}\{^1\text{H}\}$ NMR of $[(\text{cod})\text{Ir}(\text{P}(3,5\text{-(CF}_3)_2\text{C}_6\text{H}_3)_3)_2]\text{BArF}_4$ (**1f**) (*o*- $\text{C}_6\text{H}_4\text{F}_2/\text{C}_6\text{D}_6$, 23 °C)

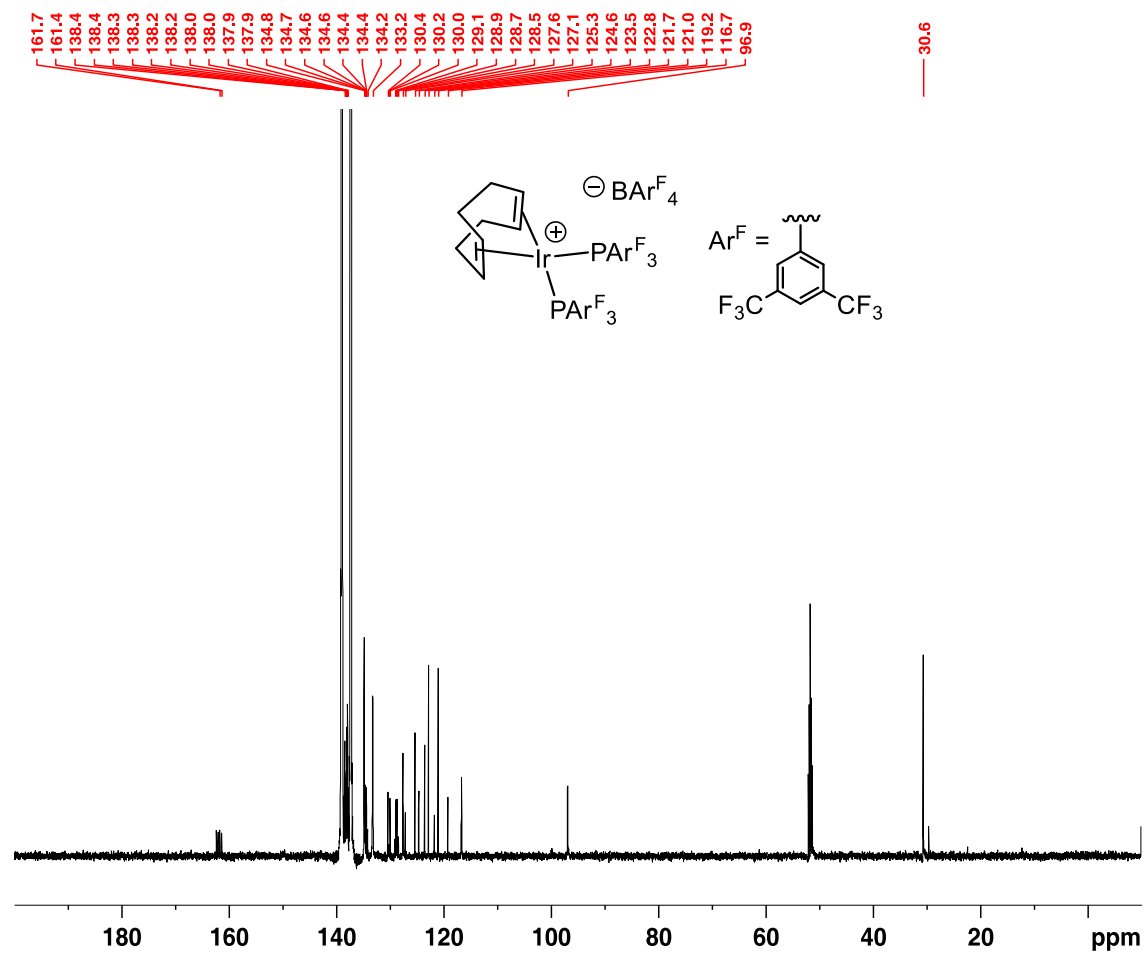


Figure S23. $^{31}\text{P}\{^1\text{H}\}$ NMR of $[(\text{cod})\text{Ir}(\text{P}(3,5\text{-}(\text{CF}_3)_2\text{C}_6\text{H}_3)_2)_2]\text{BAR}^{\text{F}}_4$ (**1f**) ($\text{C}_6\text{F}_6/\text{CD}_2\text{Cl}_2$, 23 °C)

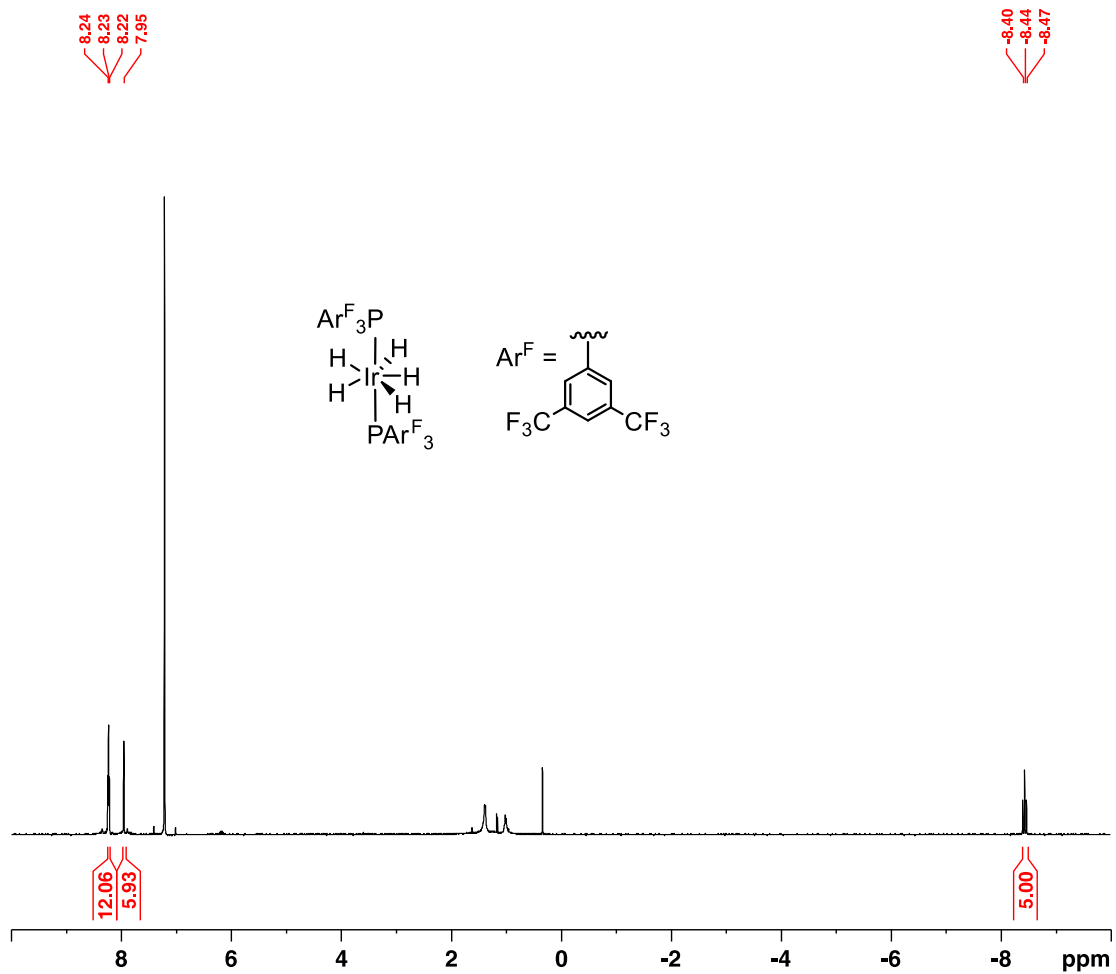


Figure S24. 1H NMR of $(P(3,5-(CF_3)_2C_6H_3)_2)_2IrH_5$ (**23**) (CD₂Cl₂, 23 °C)

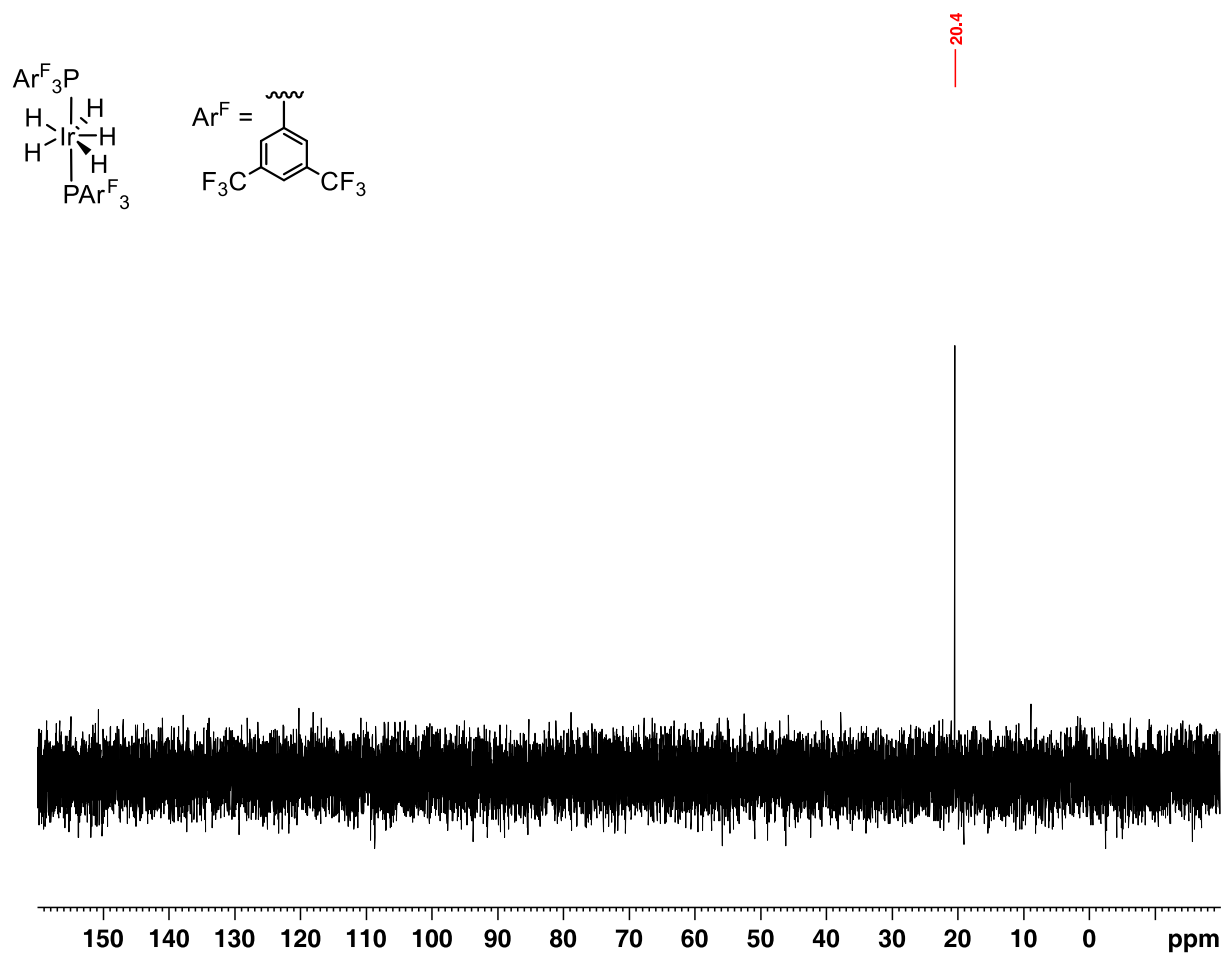


Figure S25. $^{31}\text{P}\{^1\text{H}\}$ NMR of $(\text{P}(3,5\text{-(CF}_3)_2\text{C}_6\text{H}_3)_2)_2\text{IrH}_5$ (**23**) (CD_2Cl_2 , 23 °C)

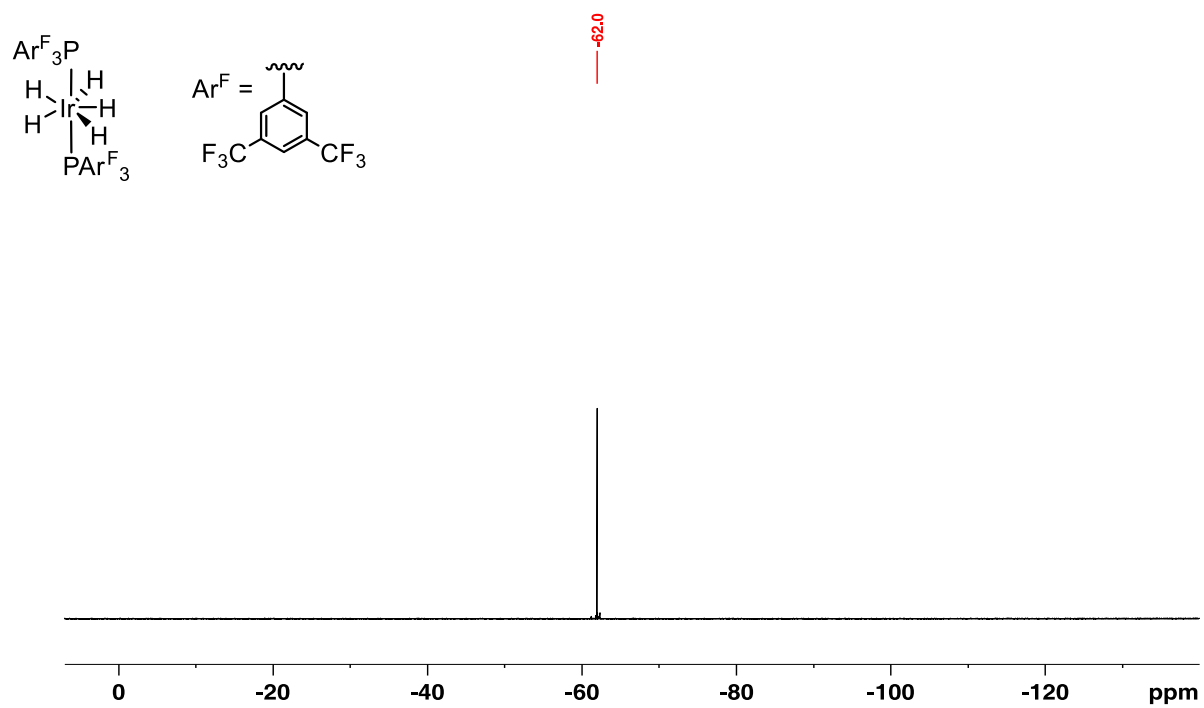


Figure S26. $^{19}F\{^1H\}$ NMR of $(P(3,5-(CF_3)_2C_6H_3)_2)IrH_5$ (**23**) (CD_2Cl_2 , 23 °C)

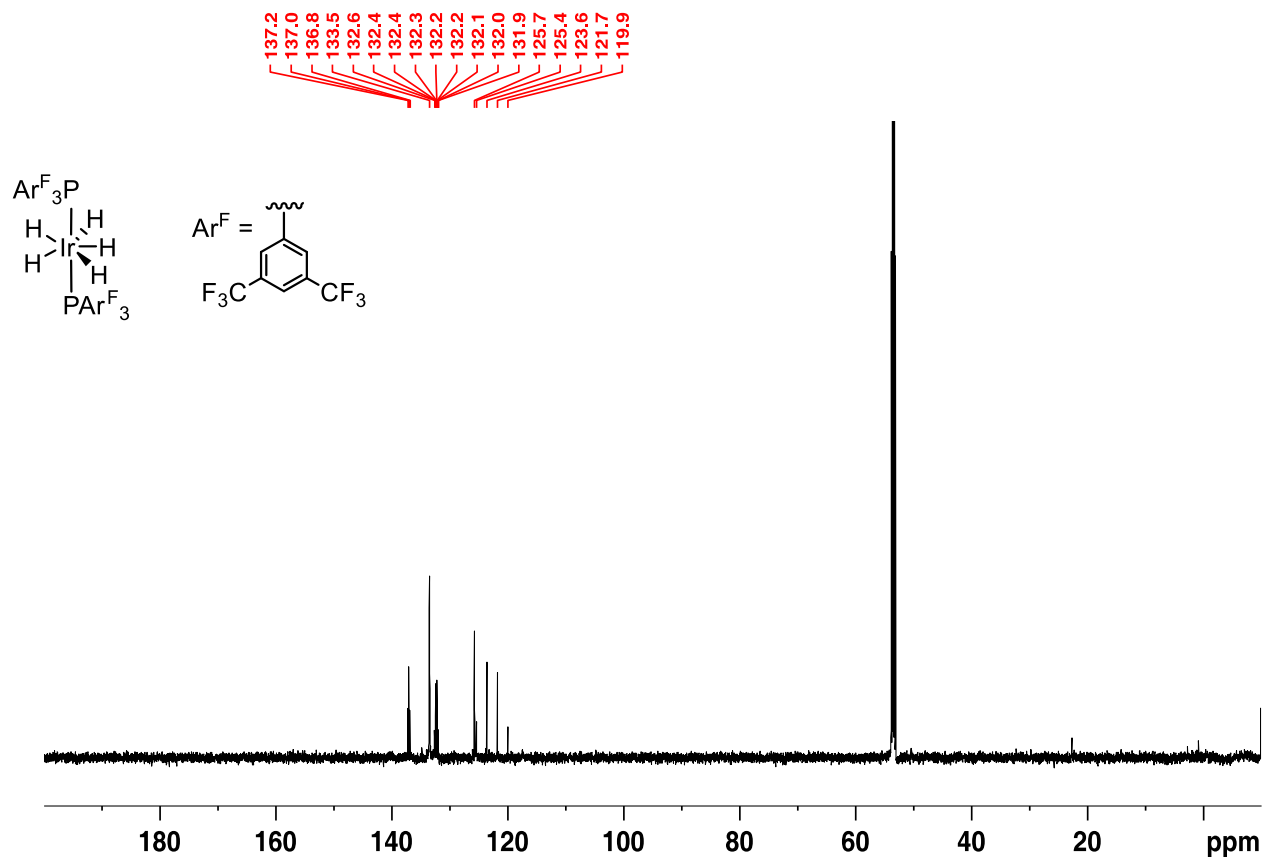


Figure S27. **Figure S22:** $^{13}\text{C}\{^1\text{H}\}$ NMR of $(\text{P}(3,5\text{-(CF}_3)_2\text{C}_6\text{H}_3)_3)_2\text{IrH}_5$ (**23**) (CD_2Cl_2 , 23 °C)

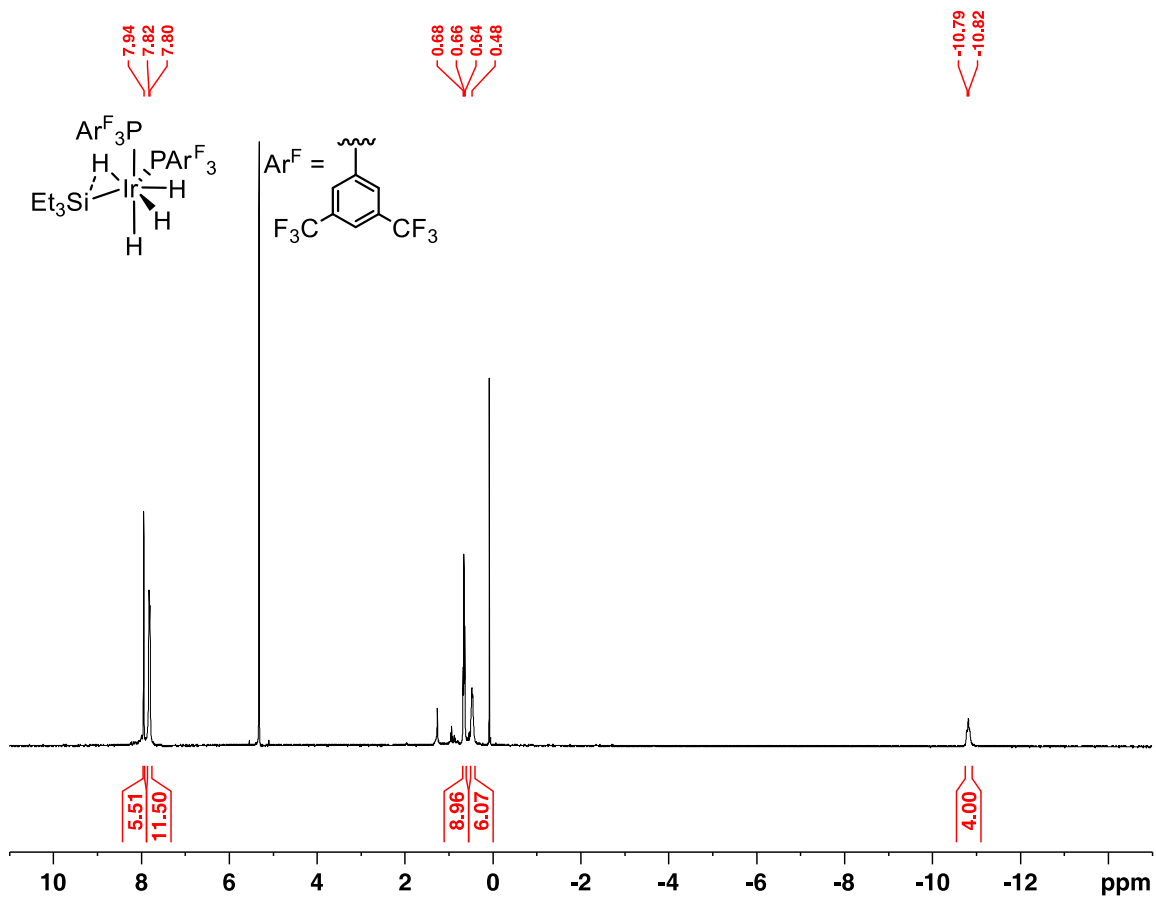


Figure S28. ^1H NMR of $(\text{P}(3,5\text{-(CF}_3)_2\text{C}_6\text{H}_3)_3)_2\text{IrH}_4(\text{SiEt}_3)$ (**23a**) (CD_2Cl_2 , $23\text{ }^\circ\text{C}$)

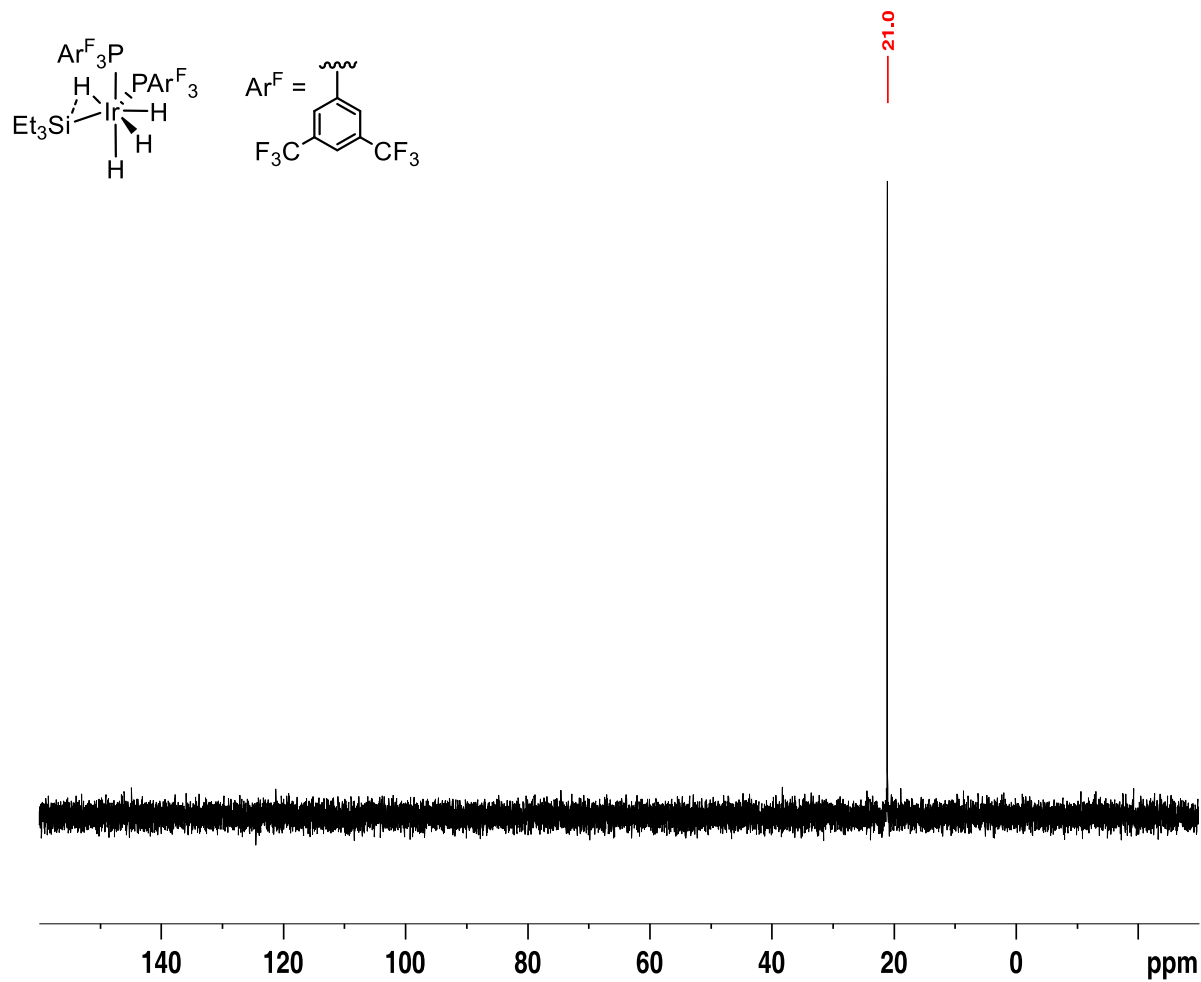


Figure S29. $^{31}P\{^1H\}$ NMR of $(P(3,5-(CF_3)_2C_6H_3)_2)IrH_4(SiEt_3)$ (**23a**) (CD_2Cl_2 , 23 °C)

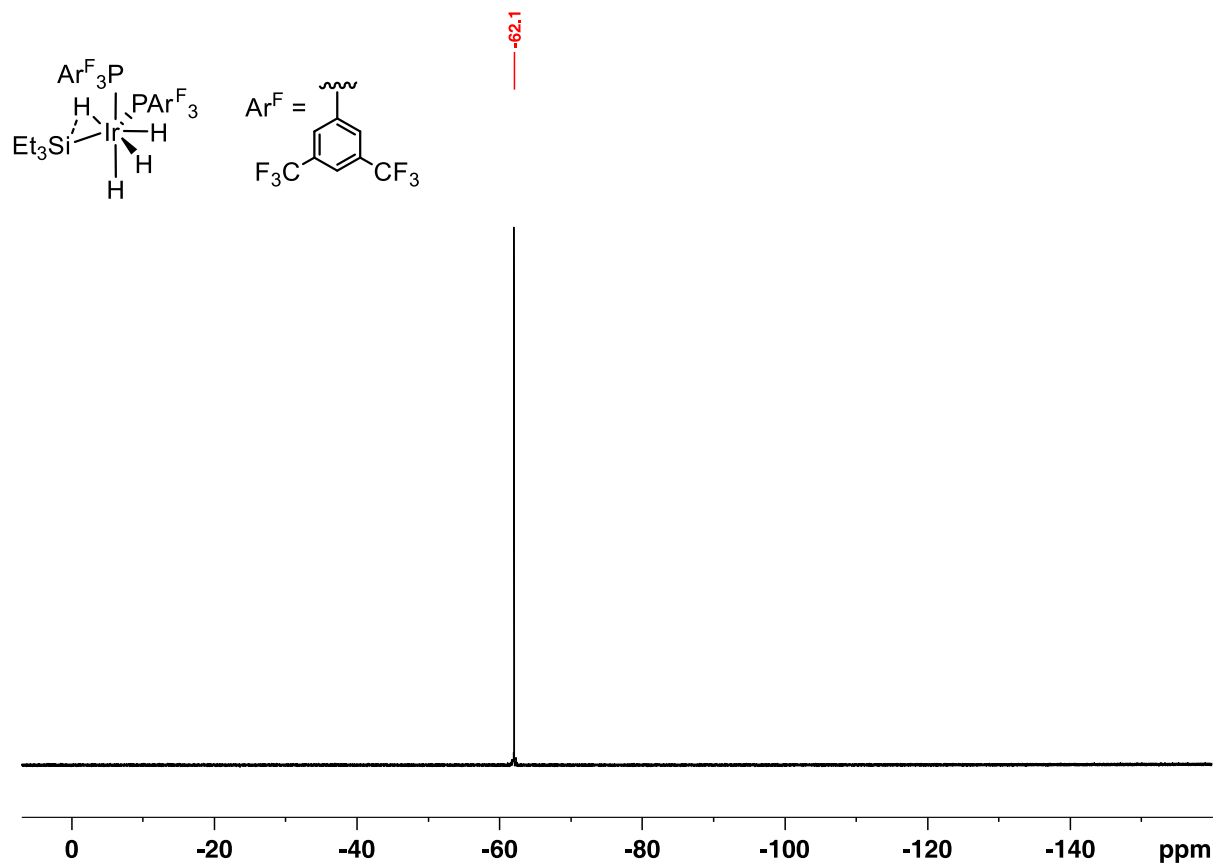


Figure S30. $^{19}\text{F}\{^1\text{H}\}$ NMR of $(\text{P}(3,5\text{-(CF}_3)_2\text{C}_6\text{H}_3)_3)_2\text{IrH}_4(\text{SiEt}_3)$ (**23a**) (CD_2Cl_2 , 23 °C)

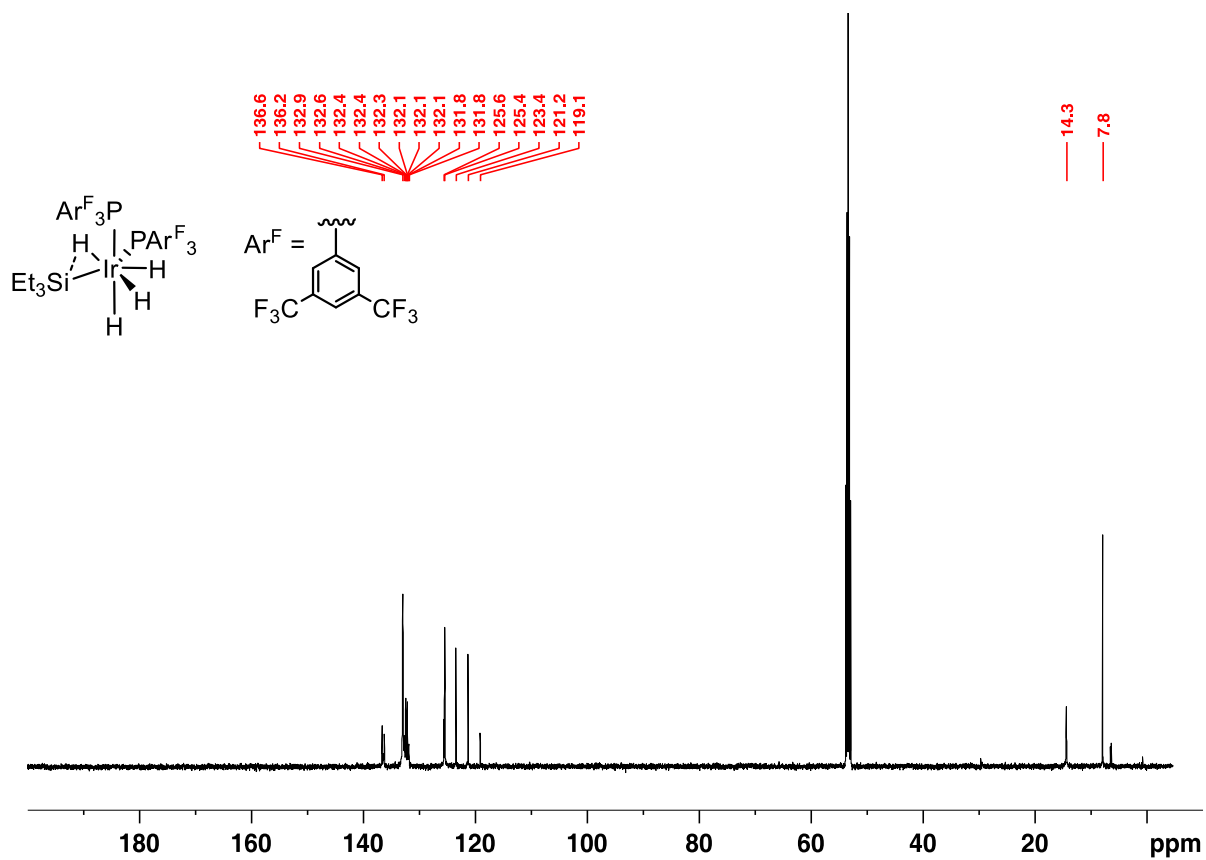


Figure S31. $^{13}C\{^1H\}$ NMR of $(P(3,5-(CF_3)_2C_6H_3)_2IrH_4(SiEt_3))$ (**23a**) (CD_2Cl_2 , 23 °C)

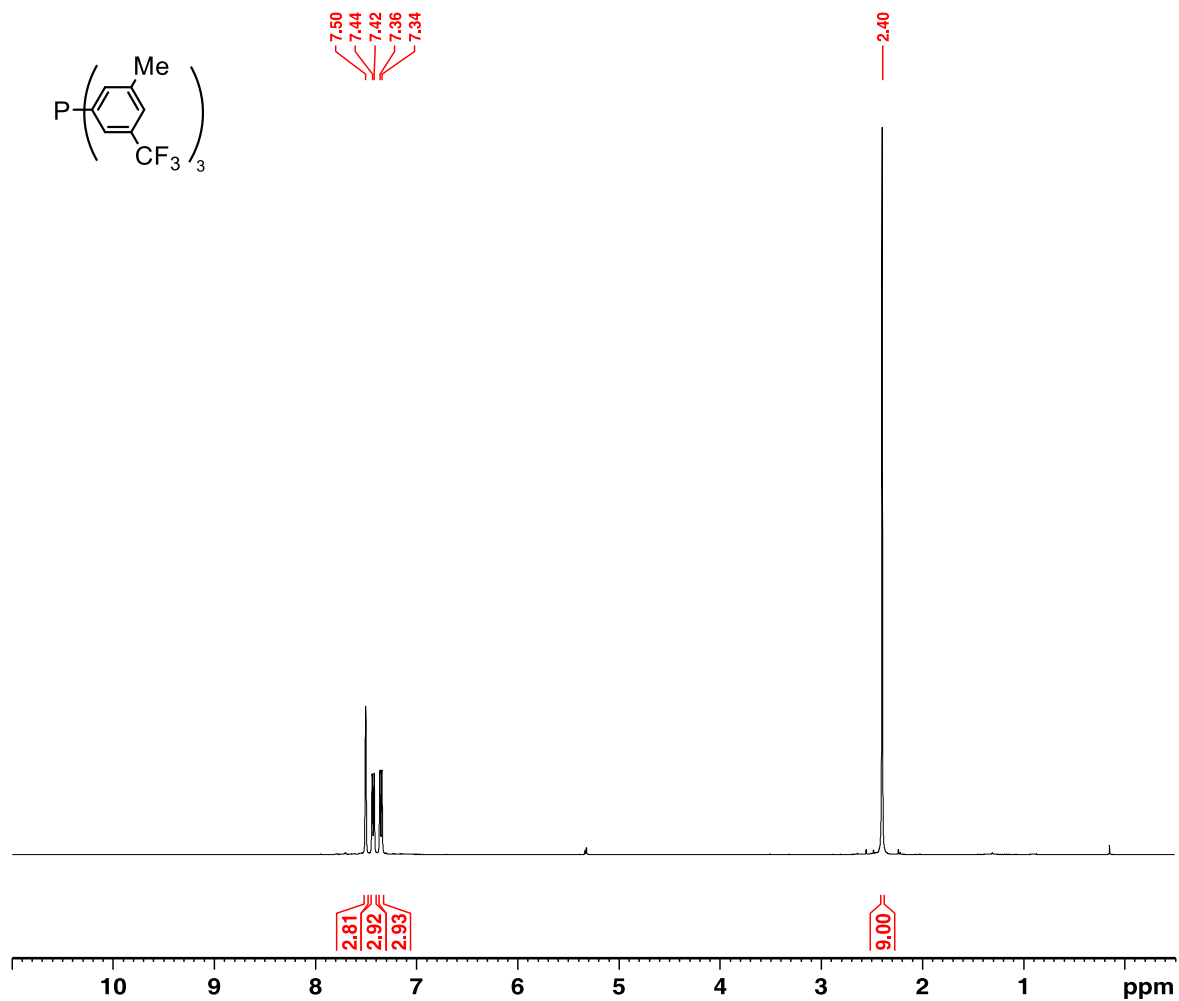


Figure S32. ¹H NMR of tris(3-methyl-5-(trifluoromethyl)phenyl)phosphine (**24**) (CD₂Cl₂, 23 °C)

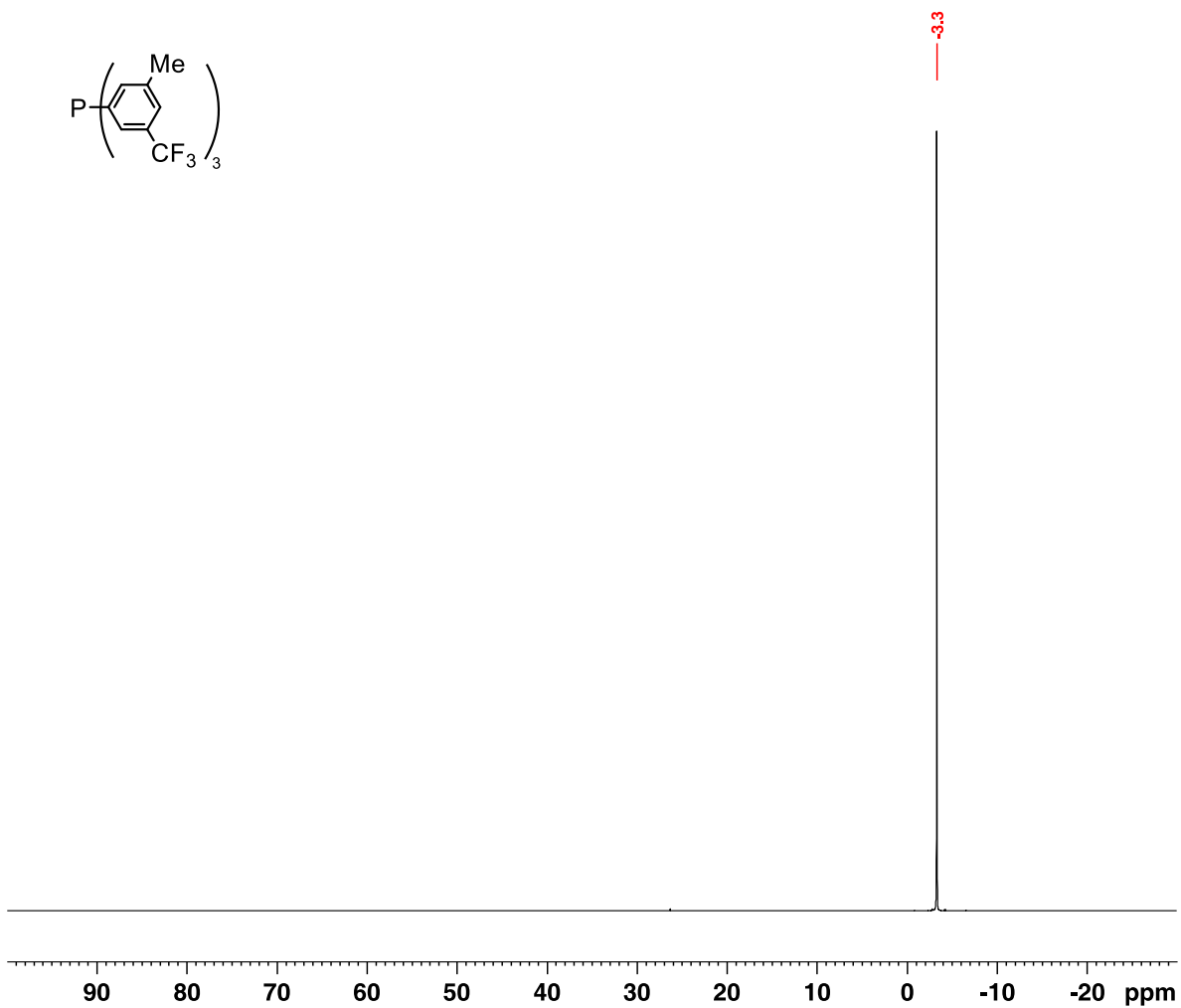


Figure S33. $^{31}\text{P}\{^1\text{H}\}$ NMR of tris(3-methyl-5-(trifluoromethyl)phenyl)phosphine (**24**)
(CD₂Cl₂, 23 °C)

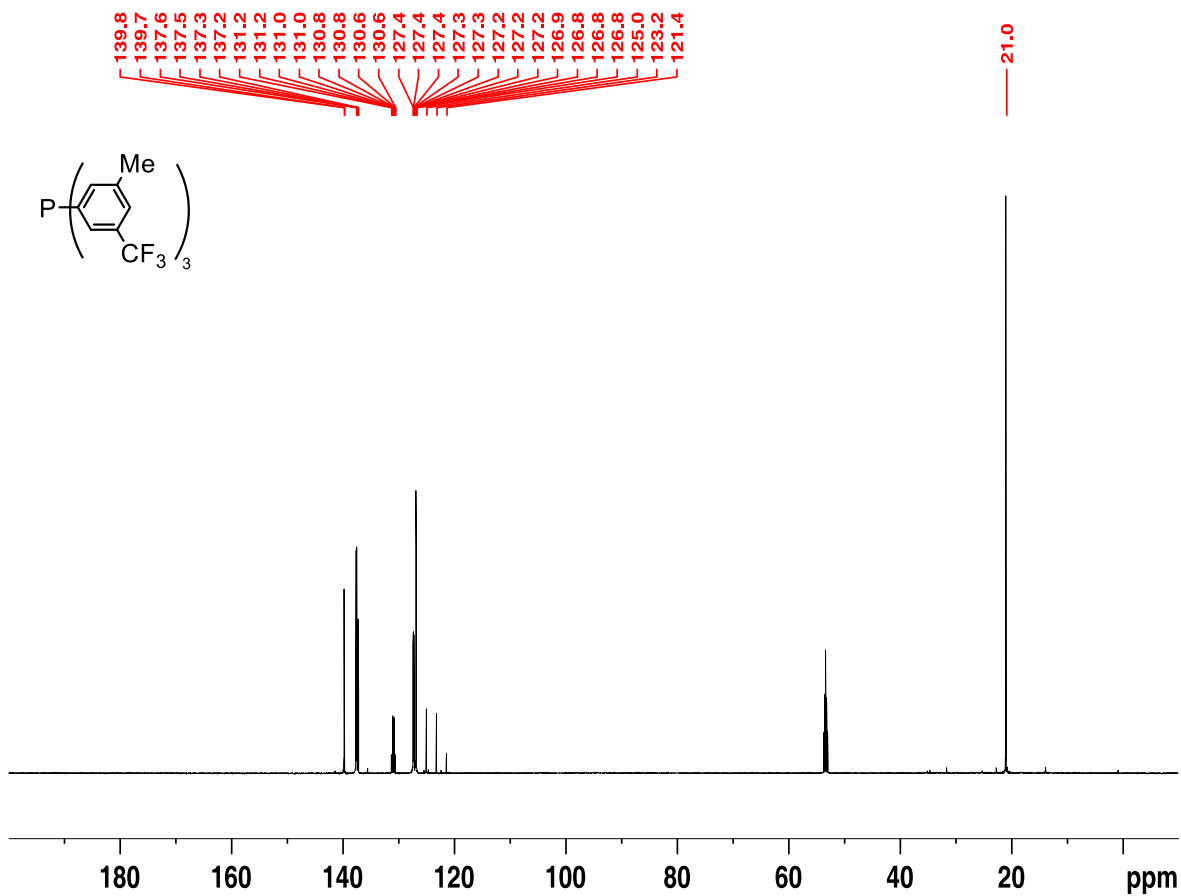


Figure S34. $^{13}\text{C}\{^1\text{H}\}$ NMR of tris(3-methyl-5-(trifluoromethyl)phenyl)phosphine (**24**) (CD_2Cl_2 , 23 °C)

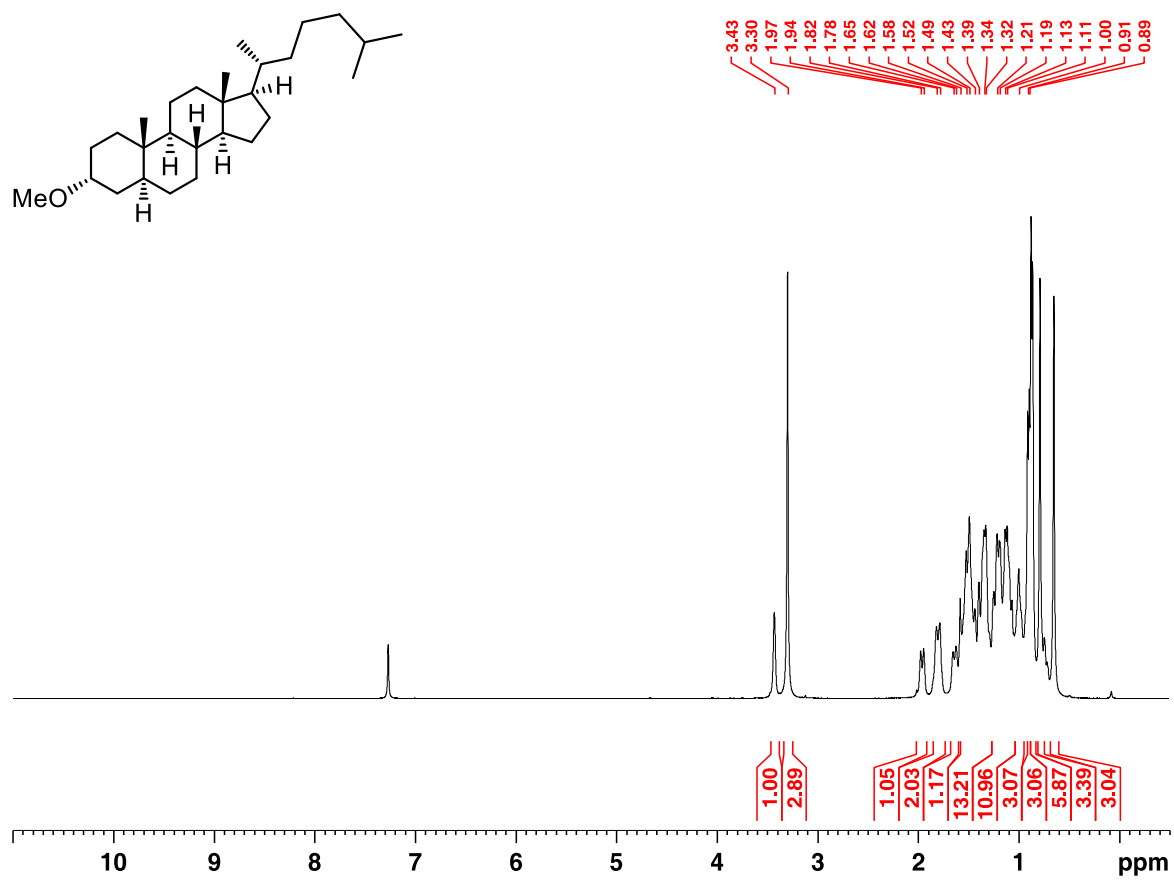


Figure S35. ^1H NMR of 3 α -methoxy-5 α -cholestane (**11**) (CDCl_3 , 23 $^\circ\text{C}$)

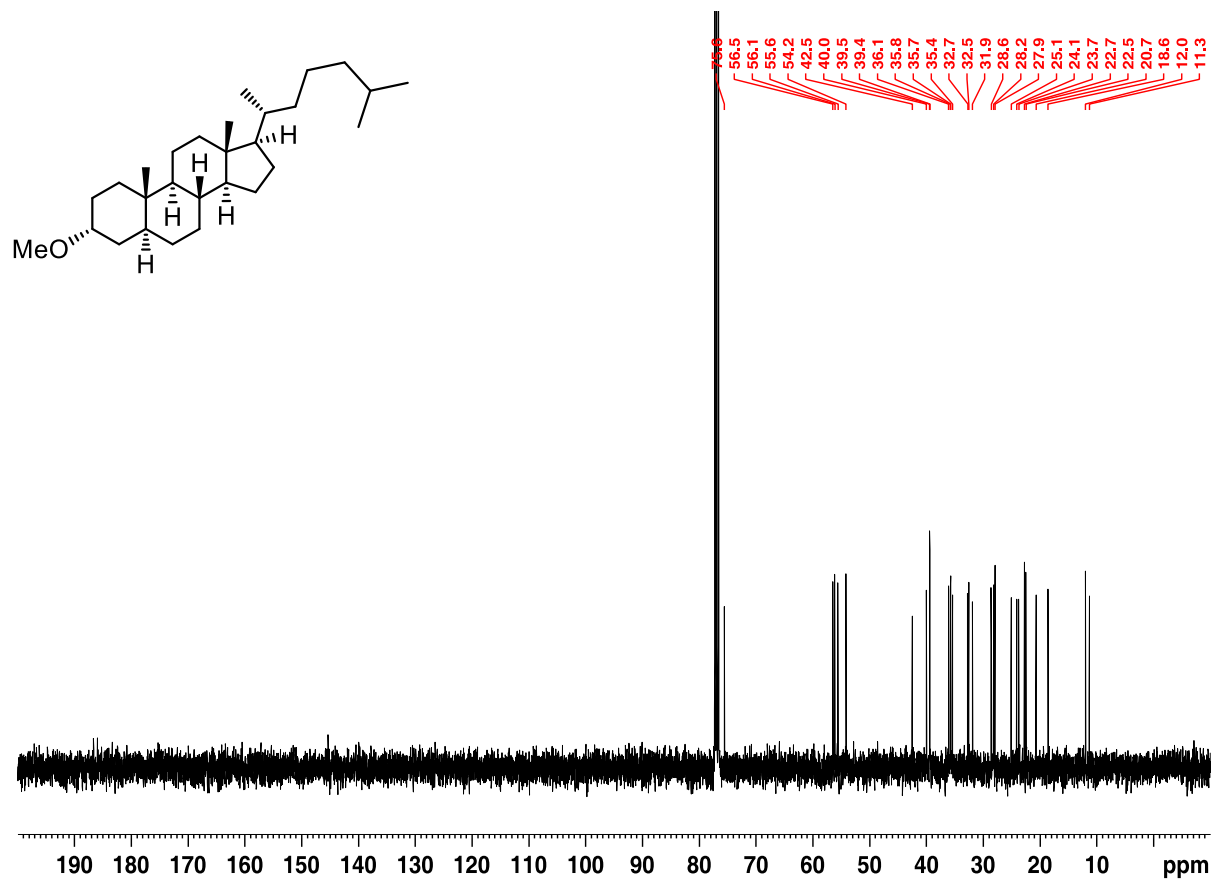


Figure S36. $^{13}\text{C}\{^1\text{H}\}$ NMR of 3 α -methoxy-5 α -cholestane (**11**) (CDCl_3 , 23 $^\circ\text{C}$)

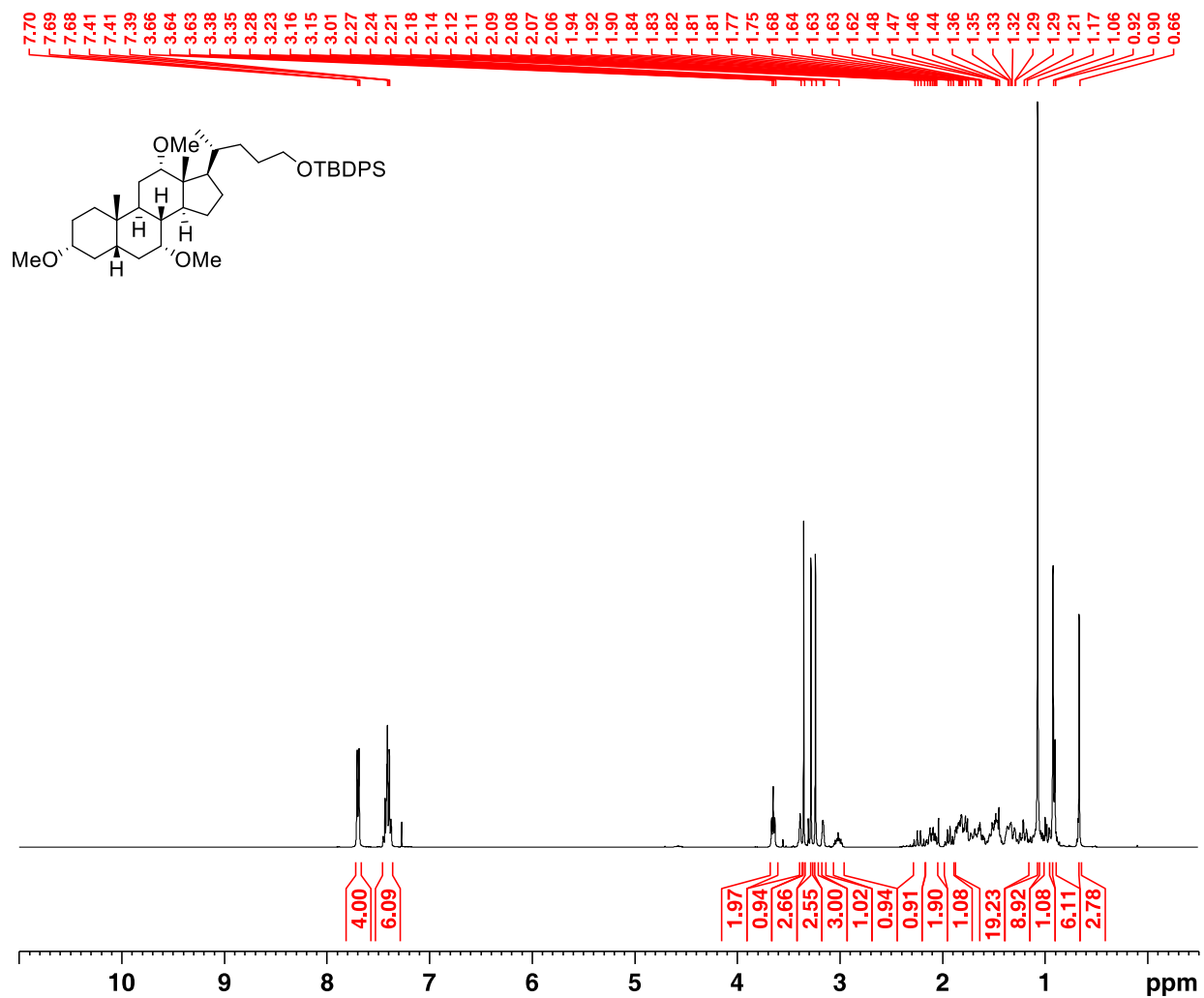


Figure S37. ^1H NMR of 3 α ,7 α ,12 α ,,-trimethoxy-24-tert-butyldiphenylsilyloxycholane (19) (CDCl₃, 23 °C)

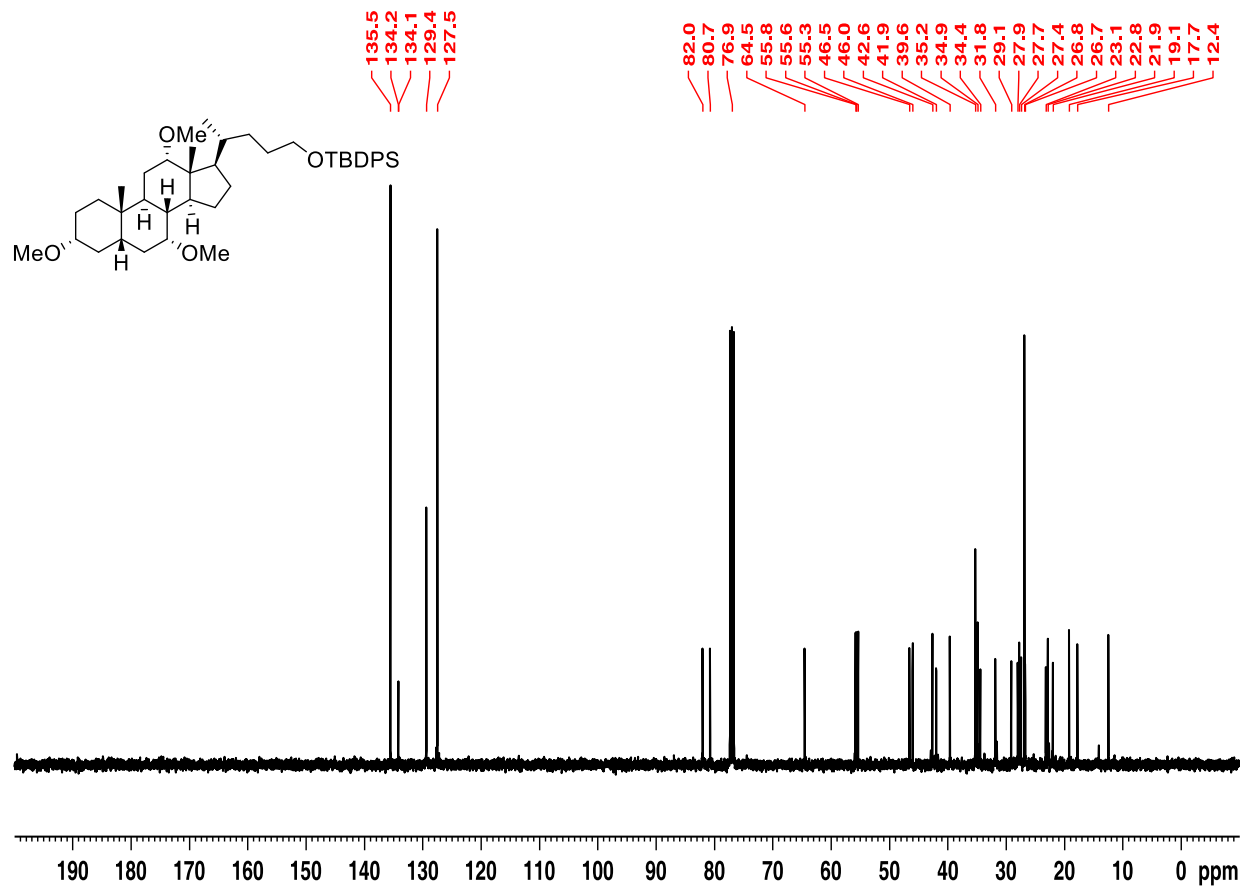


Figure S38. $^{13}\text{C}\{^1\text{H}\}$ NMR of $3\alpha,7\alpha,12\alpha$ -trimethoxy-24-tert-butyl diphenylsilyloxycholeane (**19**) (CDCl_3 , $23\text{ }^\circ\text{C}$)

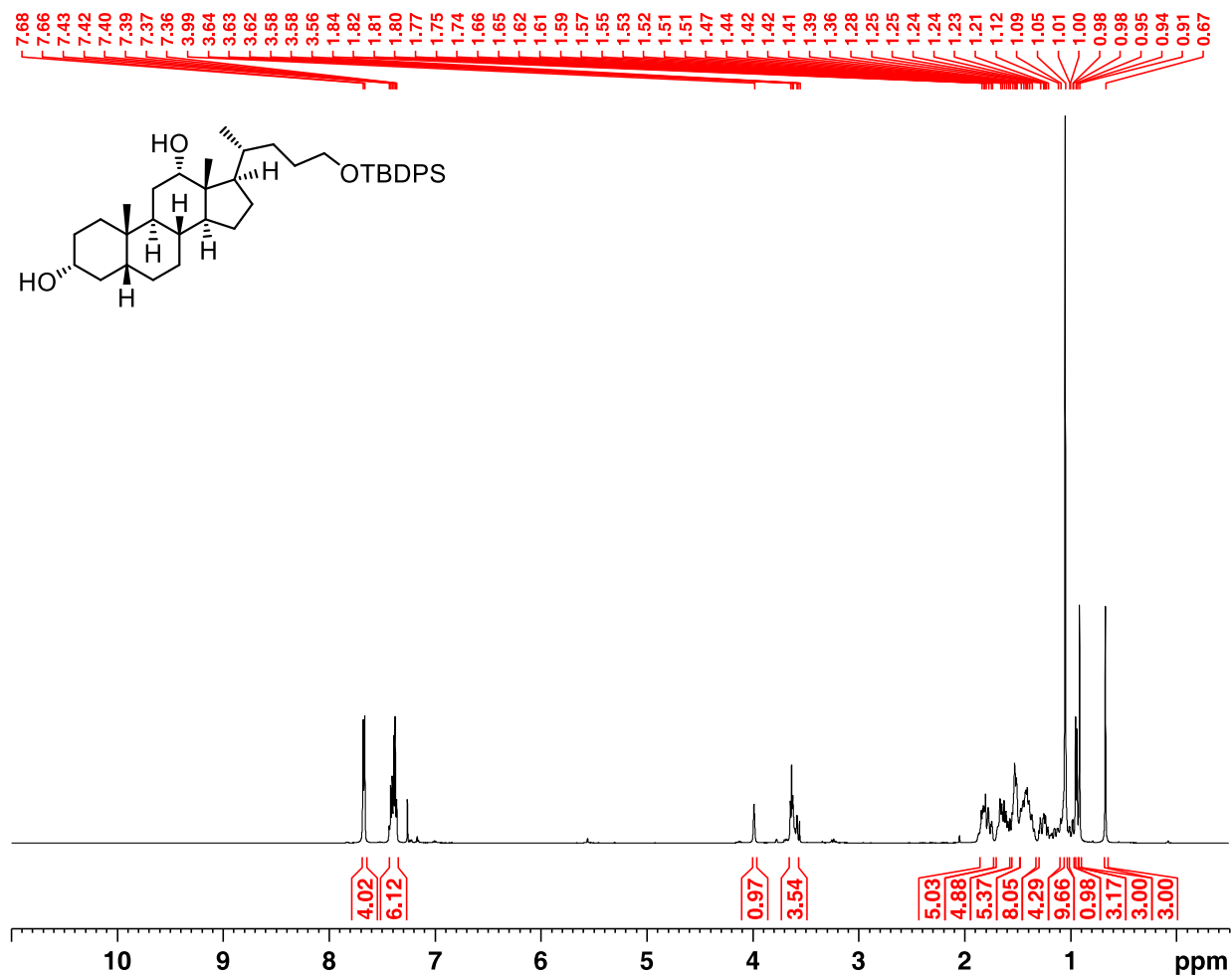


Figure S39. ¹H NMR of 24-tert-butylidiphenylsilyloxy-3 α ,12 α -dihydroxycholeane (**17c**) (CDCl₃, 23 °C)

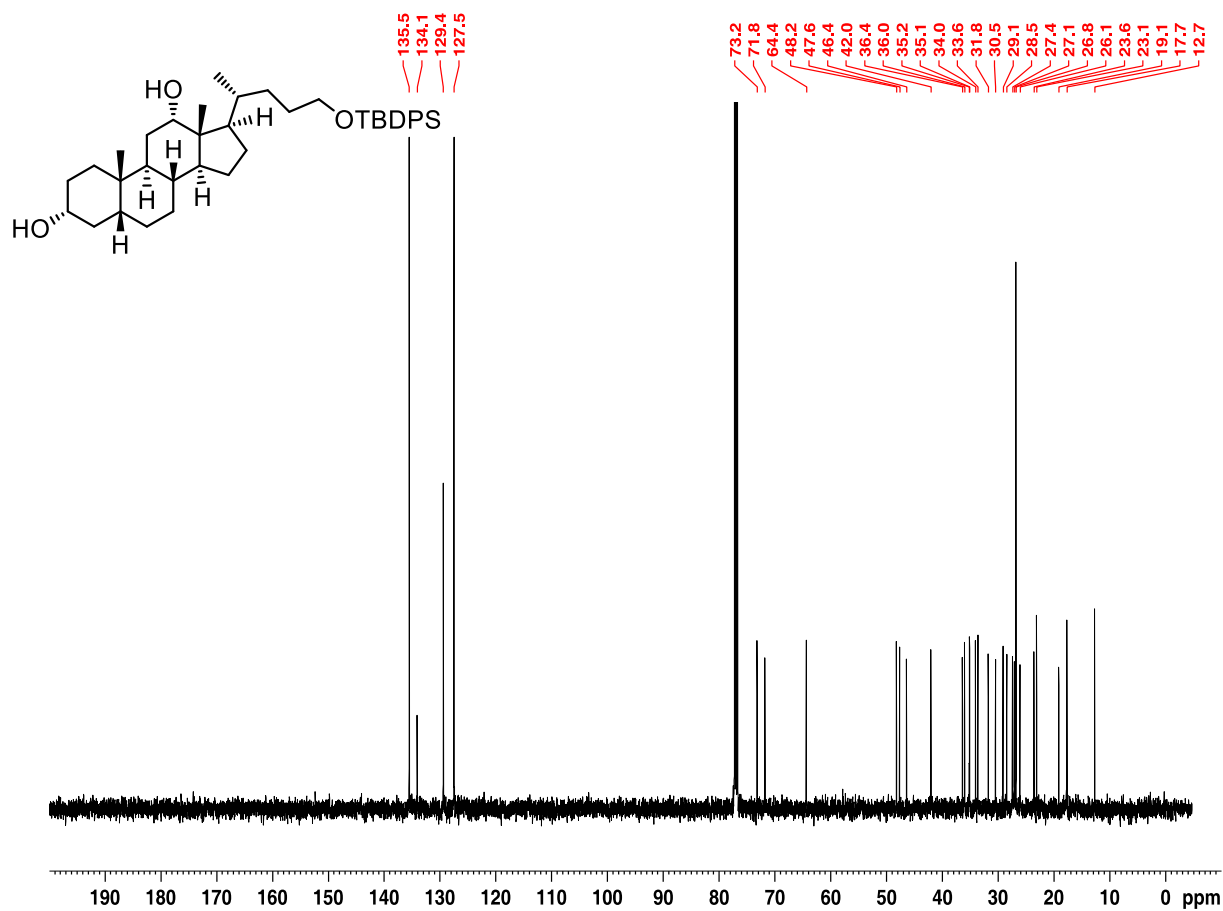


Figure S40. $^{13}\text{C}\{^1\text{H}\}$ NMR of 24-tert-butylidiphenylsilyloxy-3 α ,12 α -dihydroxycholeane (17c) (CDCl_3 , 23 $^\circ\text{C}$)

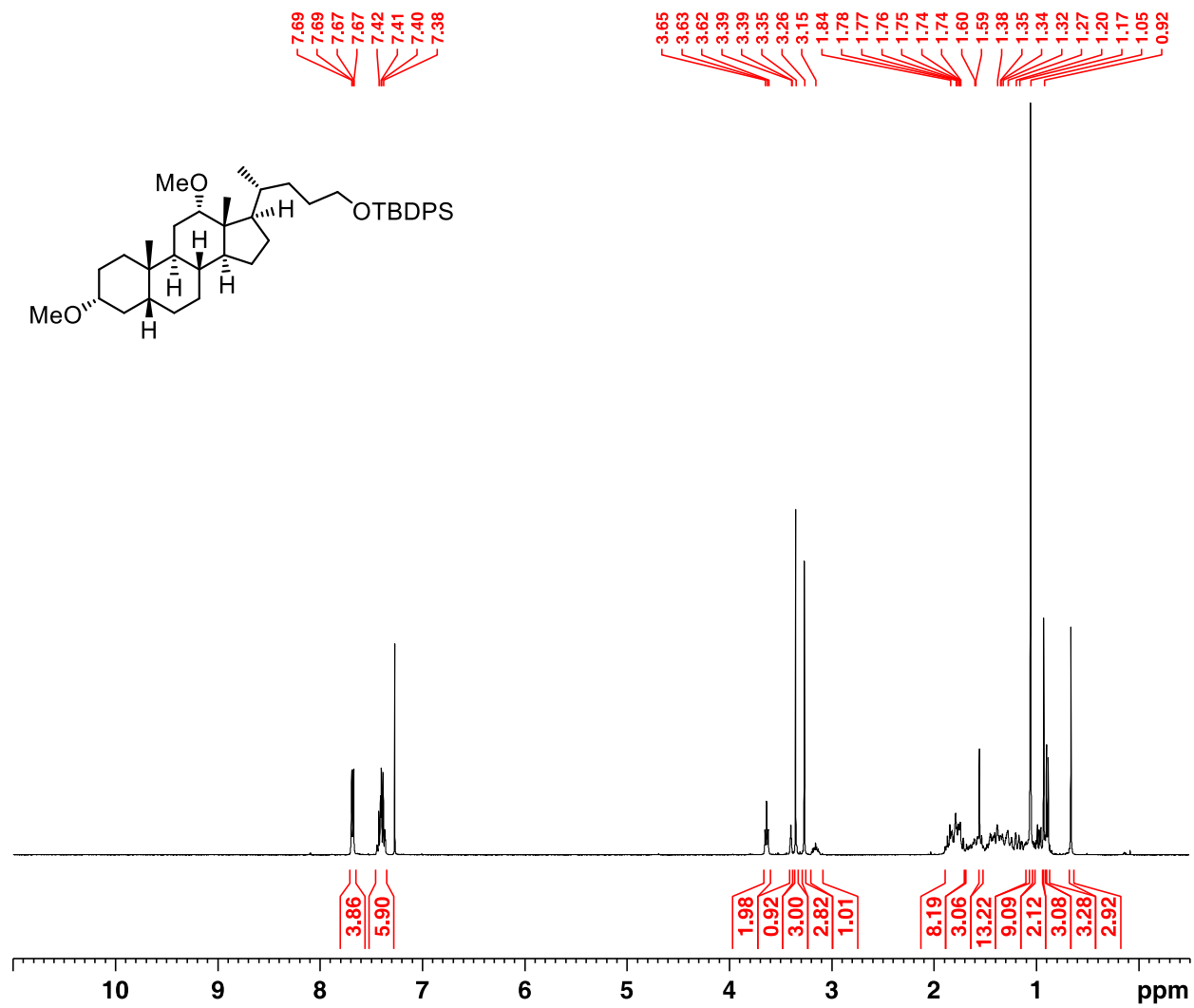


Figure S41. ^1H NMR of 3 α ,12 α -dimethoxy-24-tert-butyldiphenylsilyloxycholeane (**17**) (CDCl₃, 23 °C)

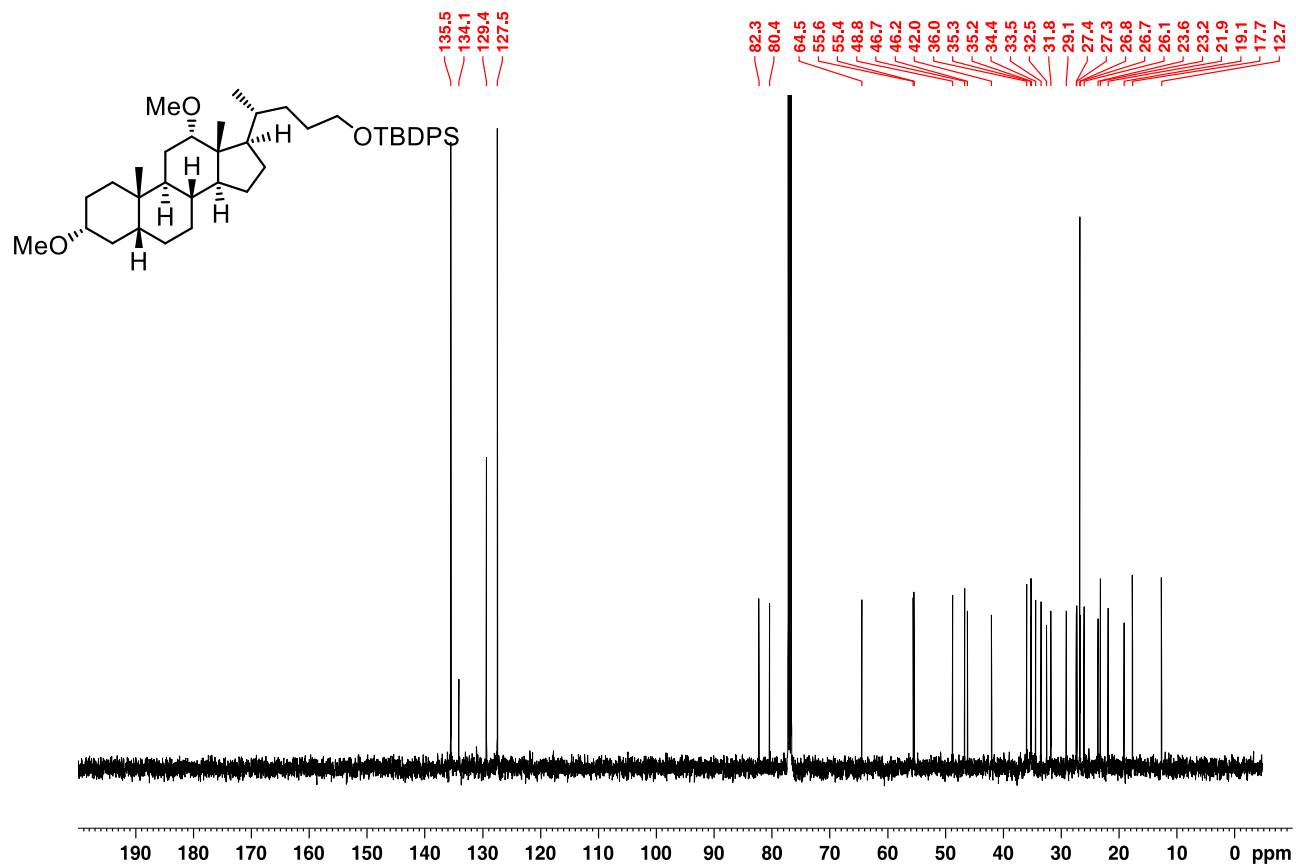


Figure S42. $^{13}\text{C}\{^1\text{H}\}$ NMR of 3 α ,12 α -dimethoxy-24-tert-butylidiphenylsilyloxycholeane (**17**) (CDCl_3 , 23 °C)

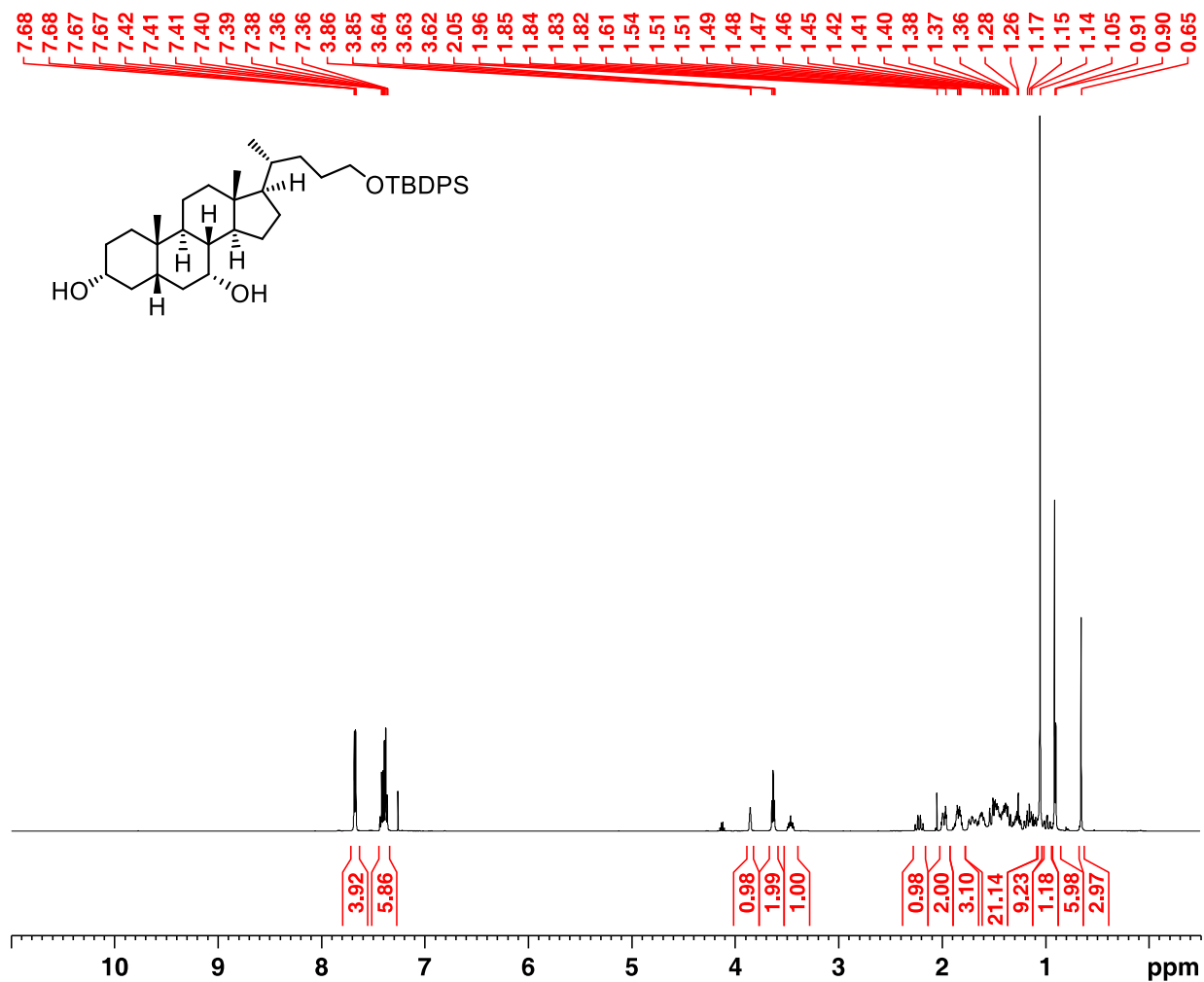


Figure S43. ¹H NMR of 24-tert-butylidiphenylsilyloxy-3 α ,7 α -dihydroxycholane (**18c**) (CDCl₃, 23 °C)

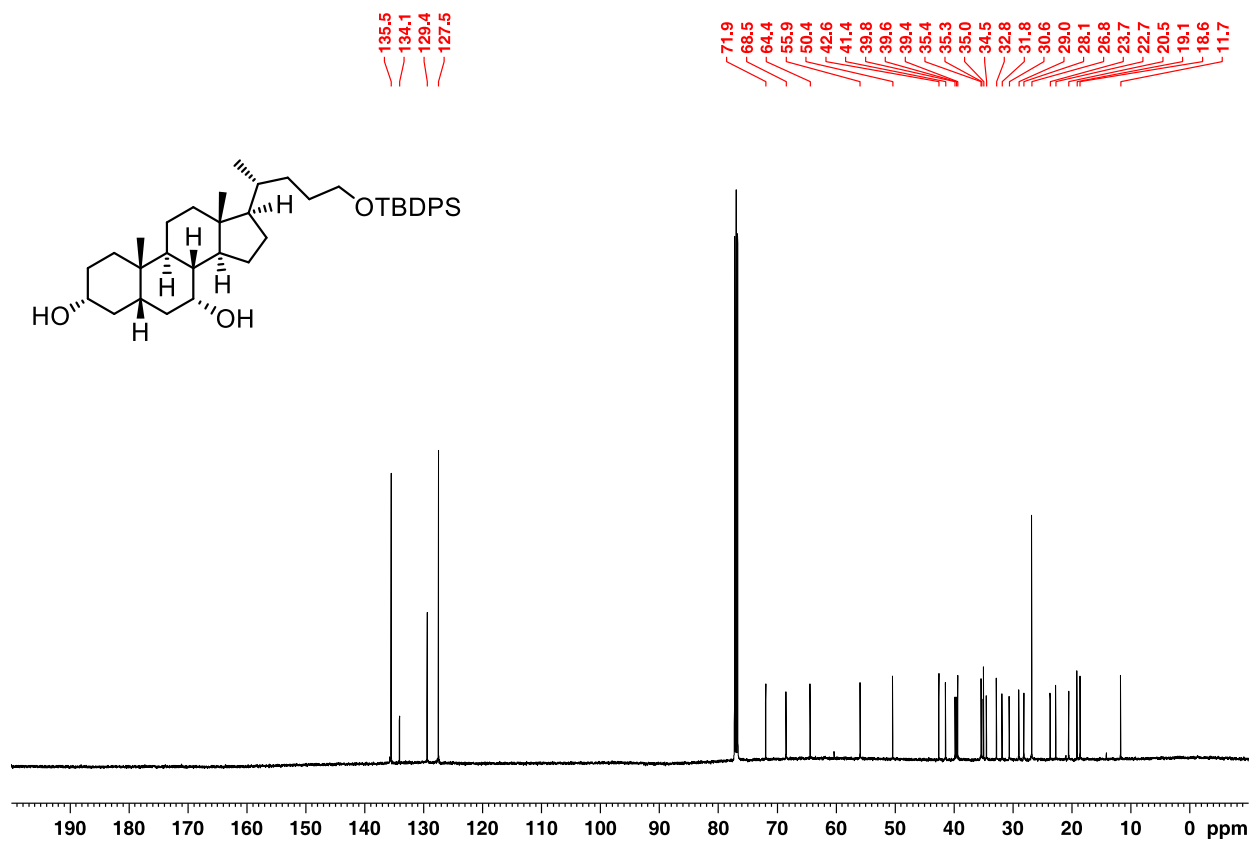


Figure S44. $^{13}\text{C}\{^1\text{H}\}$ NMR of 24-tert-butylidiphenylsilyloxy-3 α ,7 α -dihydroxycholeane (18c) (CDCl₃, 23 °C)

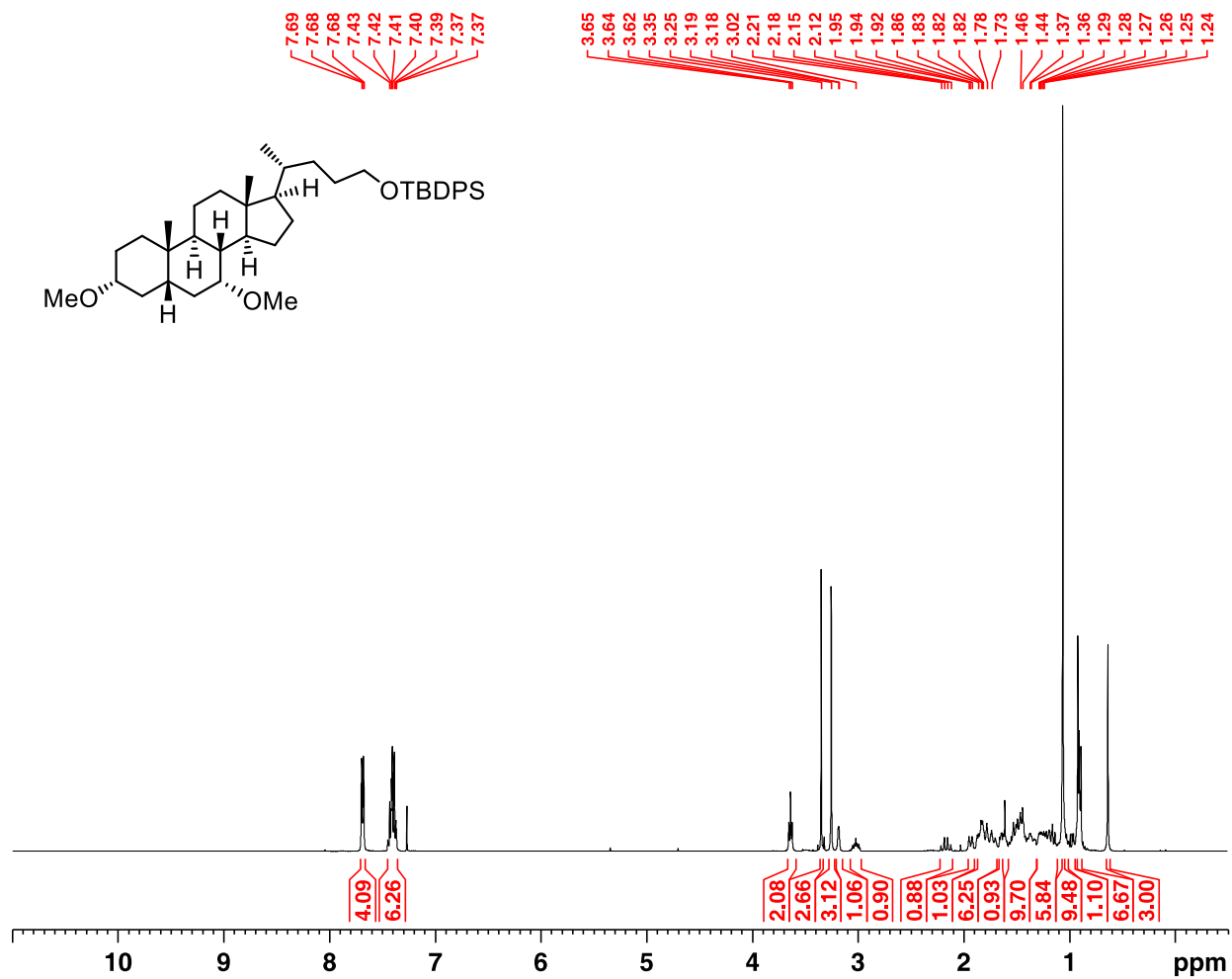


Figure S45. ¹H NMR of 3 α ,7 α -dimethoxy-24-tert-butylidiphenylsilyloxycholeane (**18**) (CDCl₃, 23 °C)

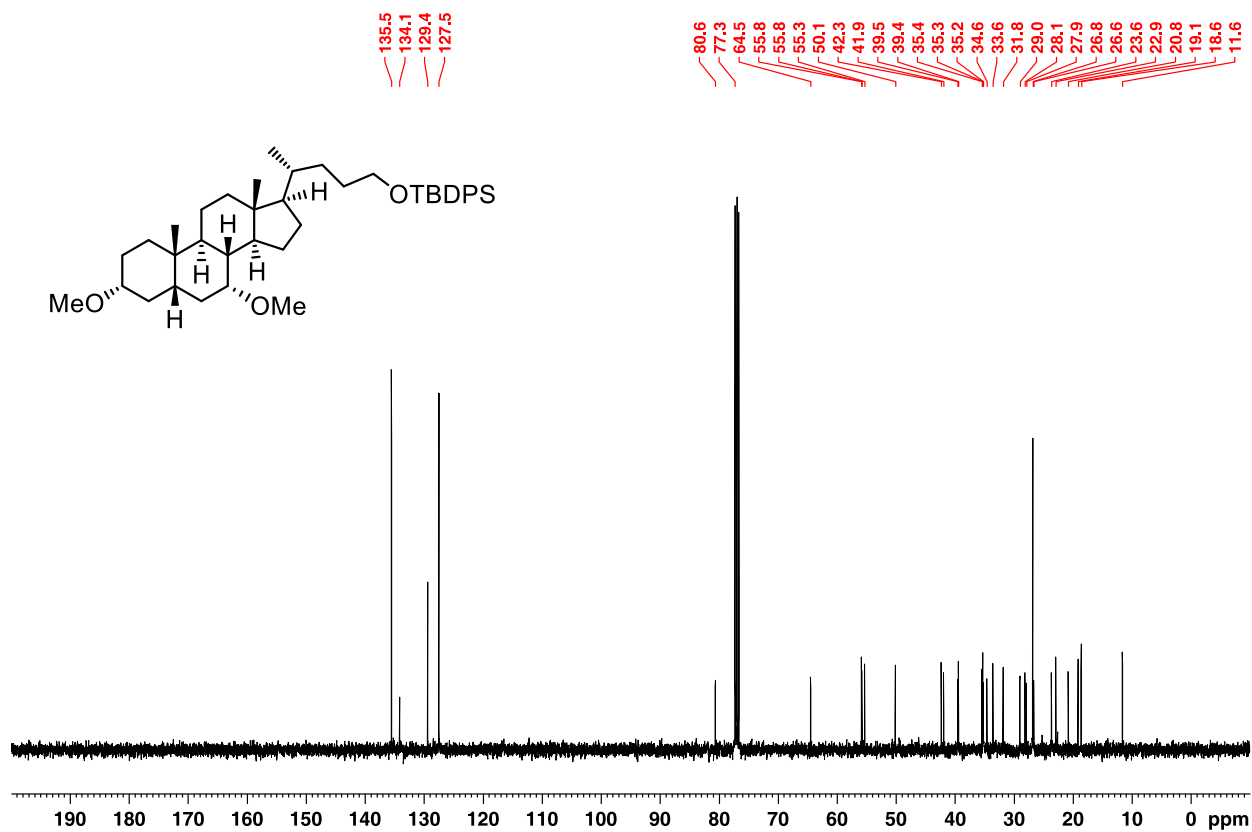


Figure S46. $^{13}\text{C}\{^1\text{H}\}$ NMR of 3 α ,7 α -dimethoxy-24-tert-butylidiphenylsilyloxycholeane (18) (CDCl₃, 23 °C)

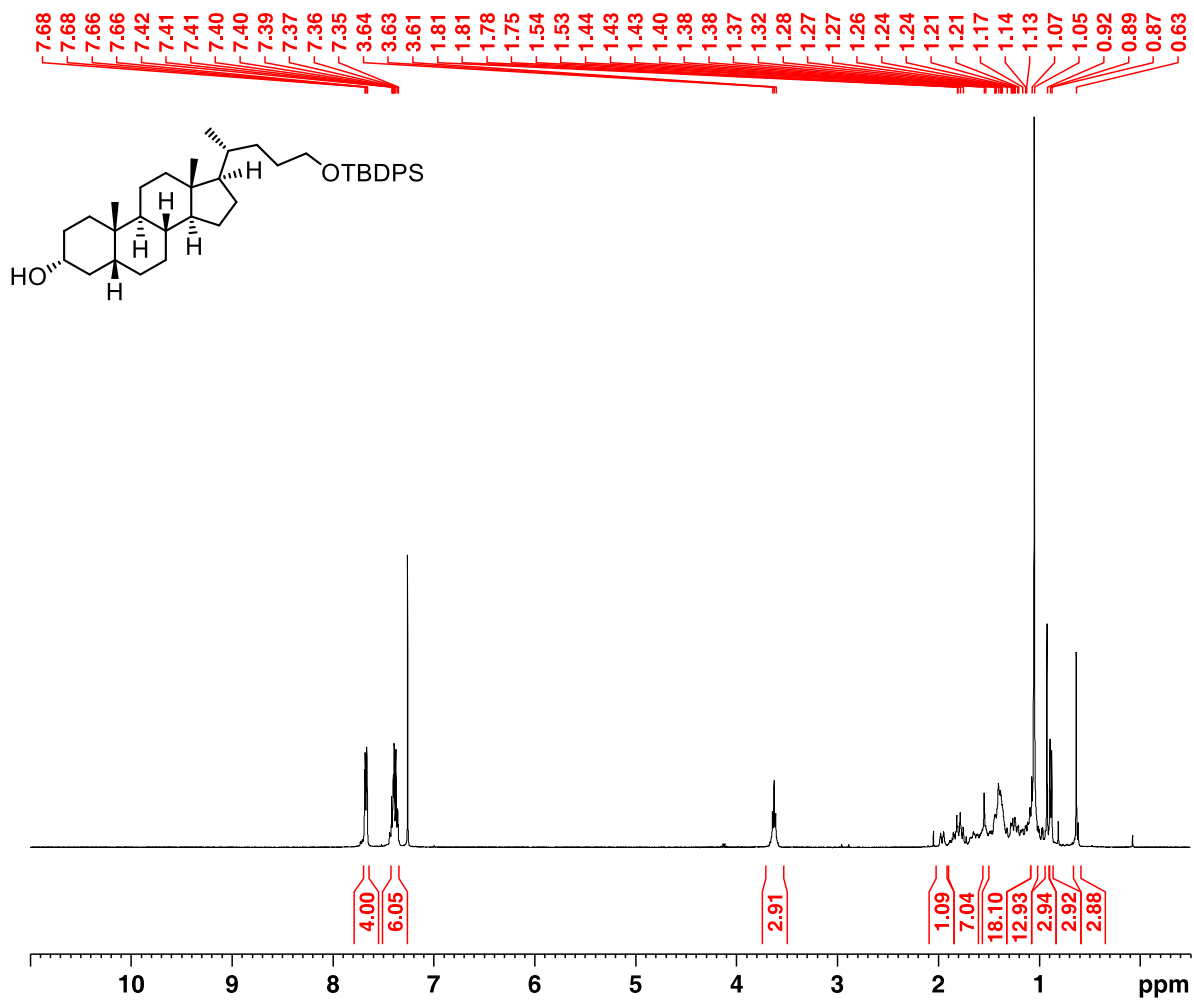


Figure S47. ¹H NMR of 24-tert-butylidiphenylsilyloxy-3α-hydroxycholeane (**16b**) (CDCl₃, 23 °C)

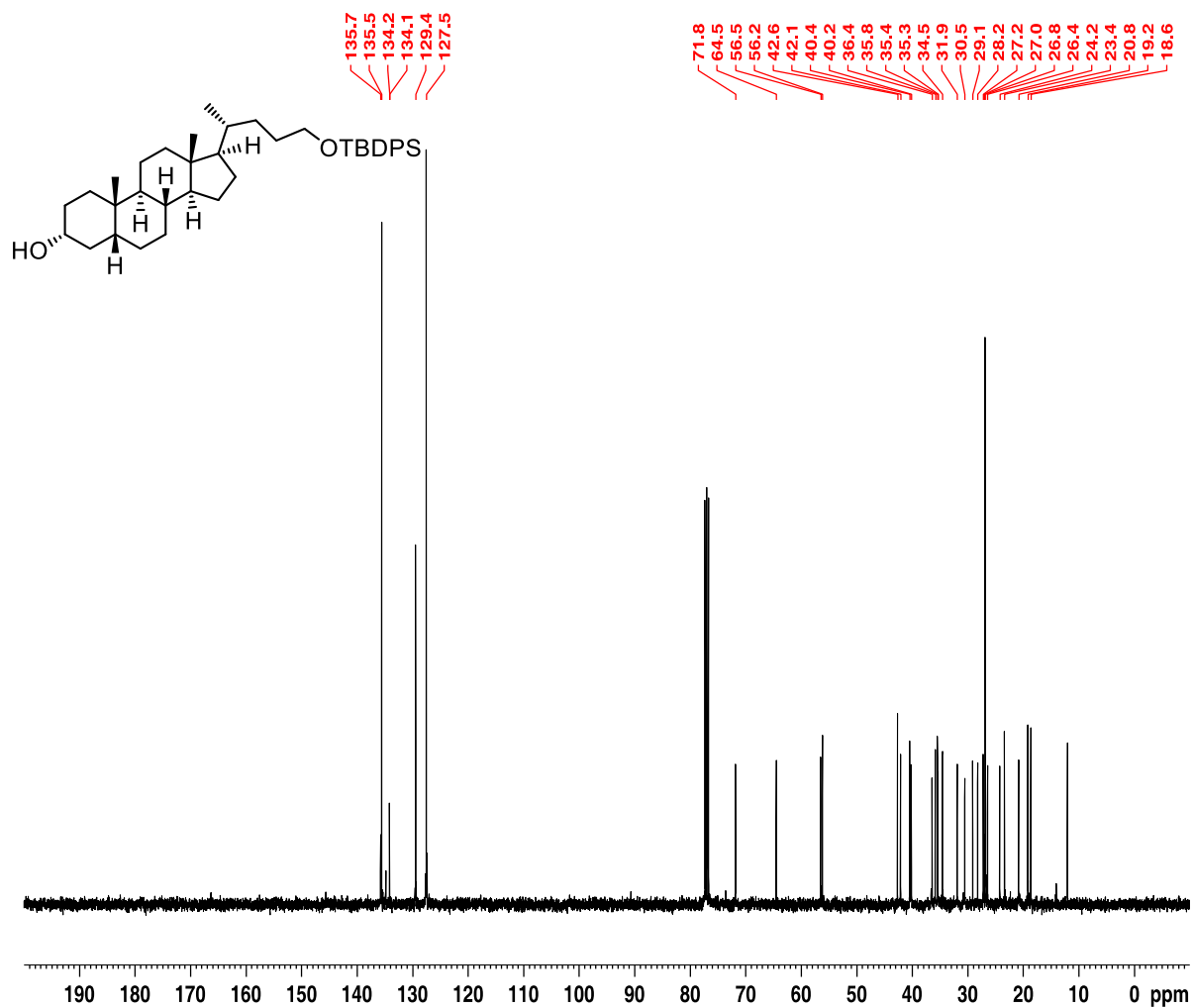


Figure S48. $^{13}\text{C}\{^1\text{H}\}$ NMR of 24-tert-butylidiphenylsilyloxy-3 α -hydroxycholeane (**16b**) (CDCl₃, 23 °C)

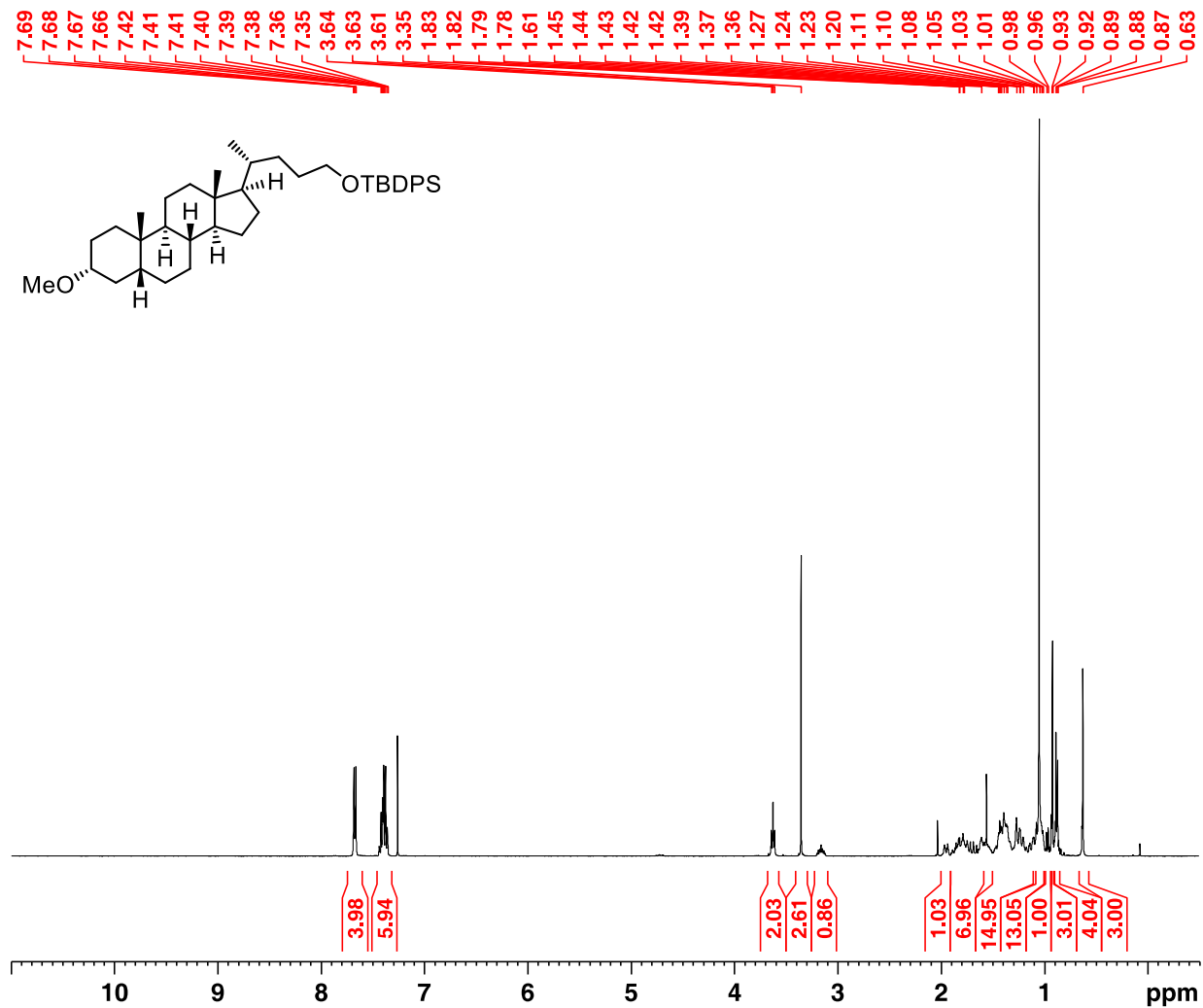


Figure S49. ^1H NMR of 3 α -methoxy-24-tert-butylidiphenylsilyloxycholeane (**16**) (CDCl₃, 23 °C)

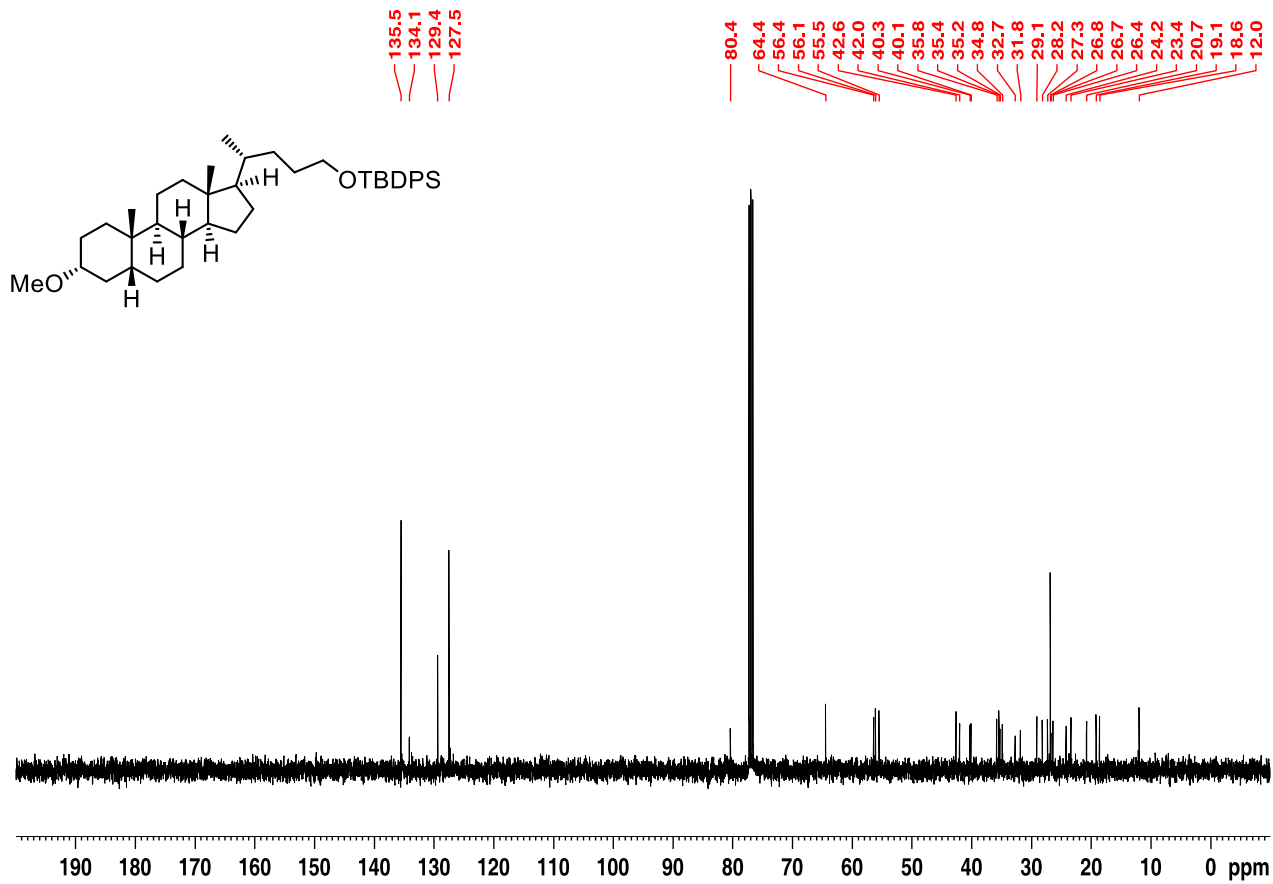


Figure S50. $^{13}\text{C}\{^1\text{H}\}$ NMR of 3 α -methoxy-24-tert-butylidiphenylsilyloxycholeane (**16**)
(CDCl_3 , 23 $^\circ\text{C}$)

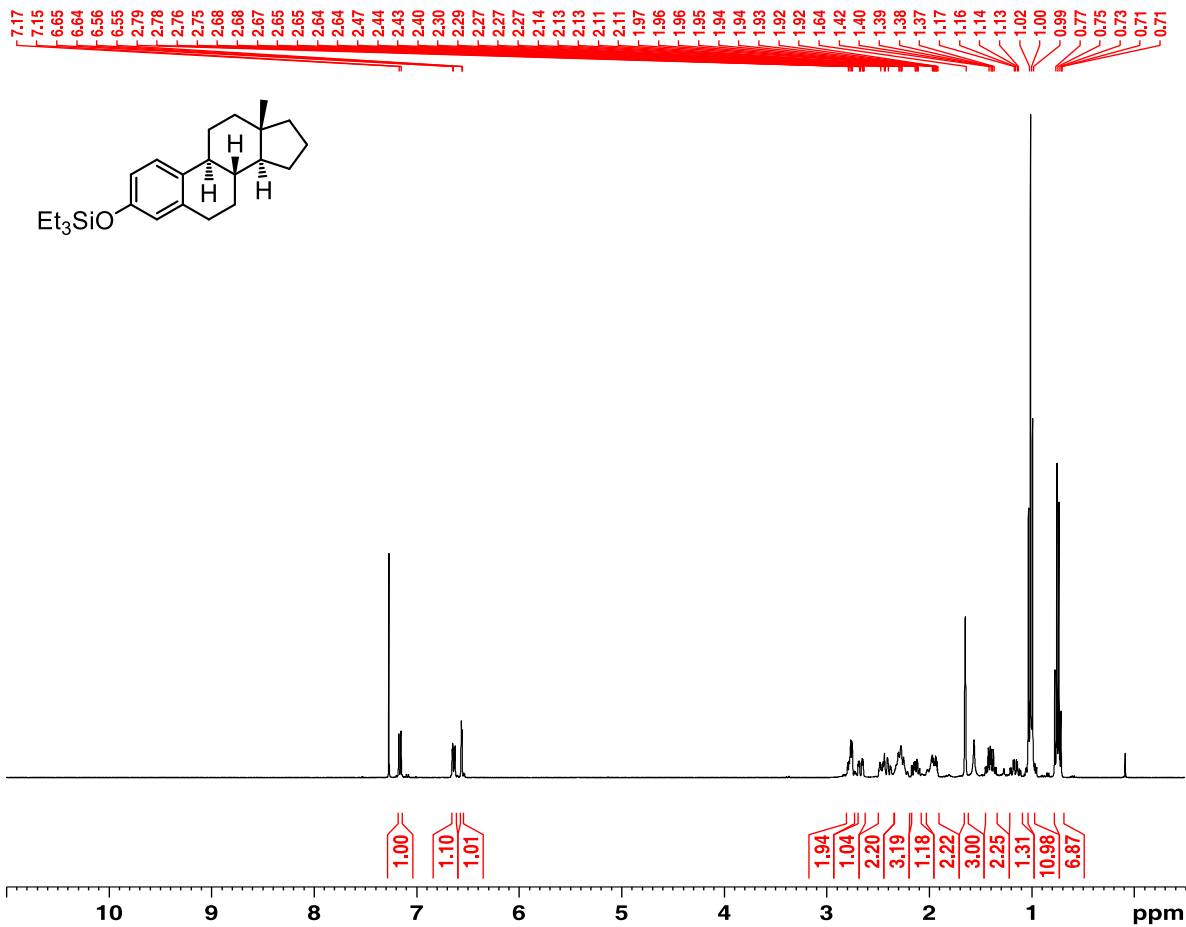


Figure S51. ¹H NMR of 3-triethylsiloxy-1,3,5(10)-estratriene (**20b**) (CDCl₃, 23 °C)

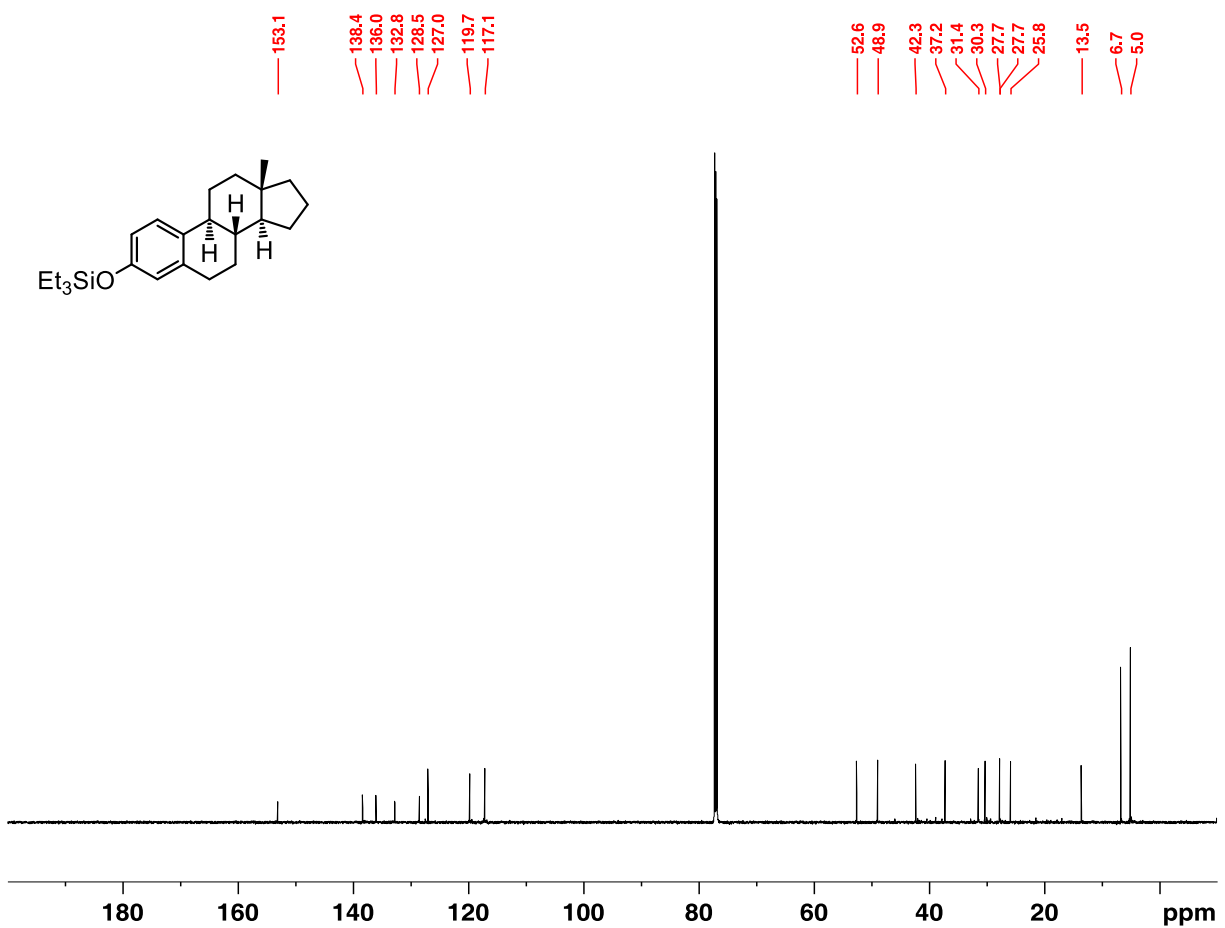


Figure S52. $^{13}\text{C}\{^1\text{H}\}$ NMR of 3-triethylsiloxy-1,3,5(10)-estratriene (**20b**) (CDCl_3 , 23 °C)

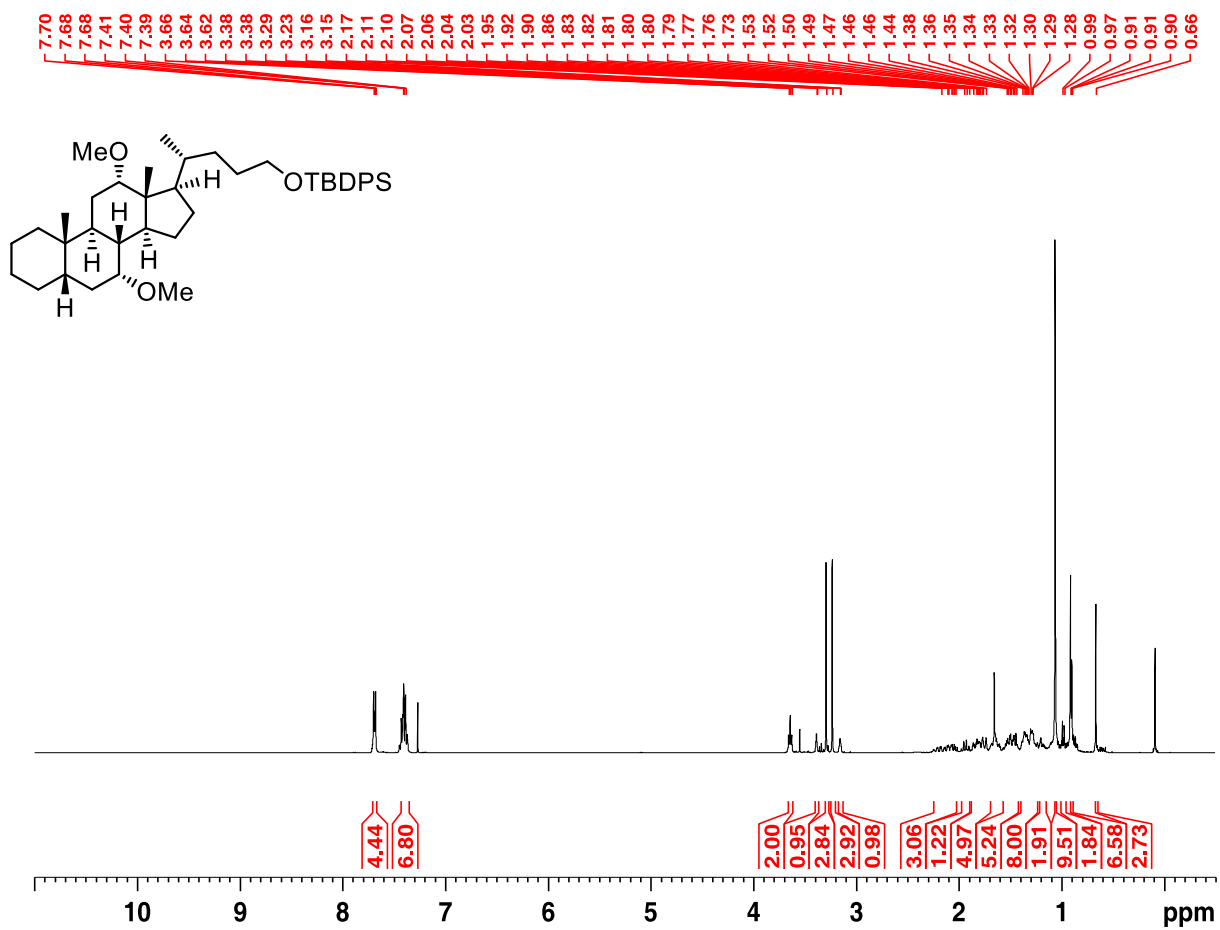


Figure S53. ¹H NMR of 7 α ,12 α , -dimethoxy-24-tert-butylidiphenylsilyloxycholeane (**19a**) (CDCl₃, 23 °C)

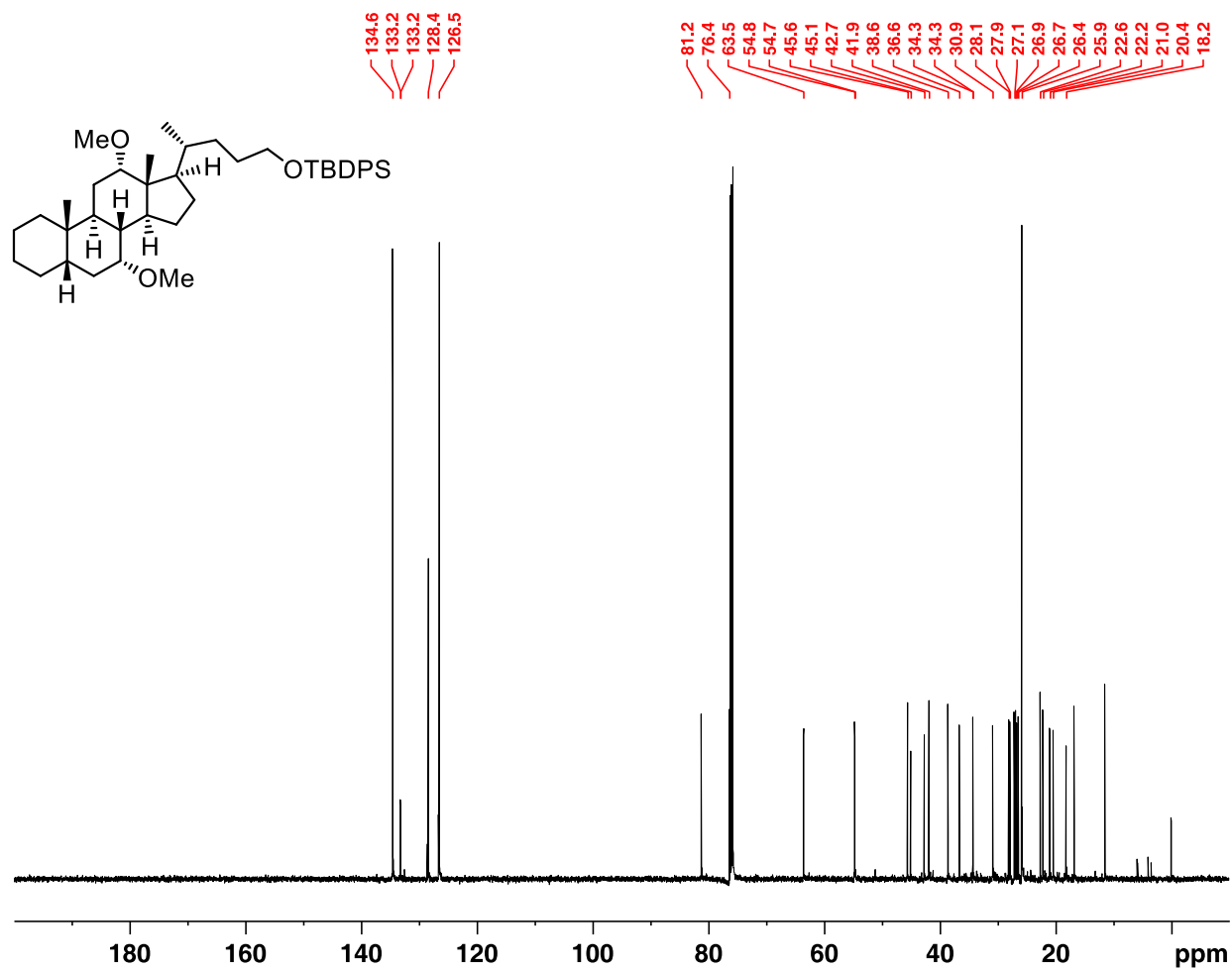


Figure S54. $^{13}\text{C}\{^1\text{H}\}$ NMR of 7 α ,12 α , -dimethoxy-24-tert-butylidiphenylsilyloxycholane (19a) (CDCl_3 , 23 $^\circ\text{C}$)

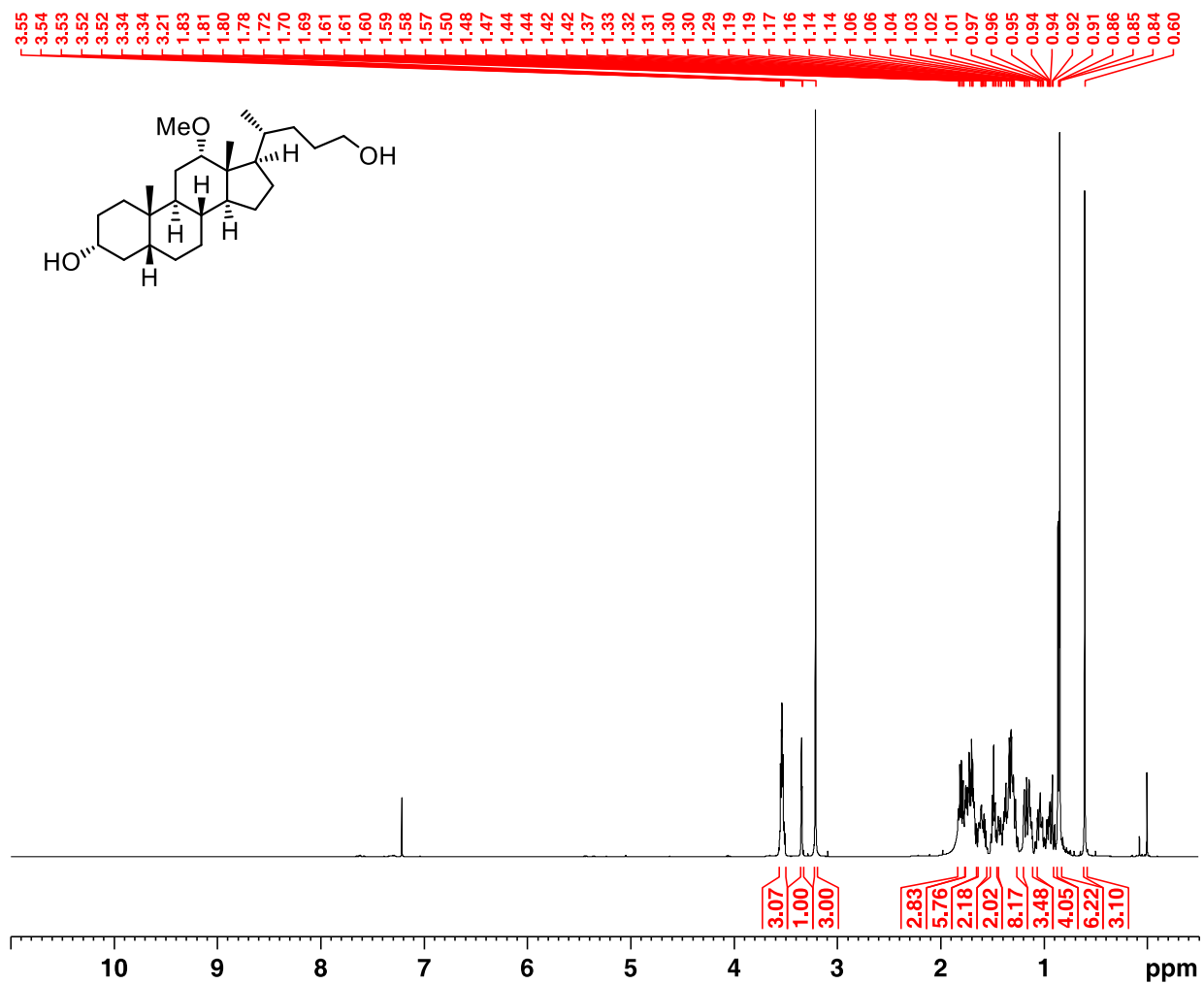


Figure S55. ¹H NMR of 3α,24-dihydroxy-12α-methoxycholane (17a) (CDCl₃, 23 °C)

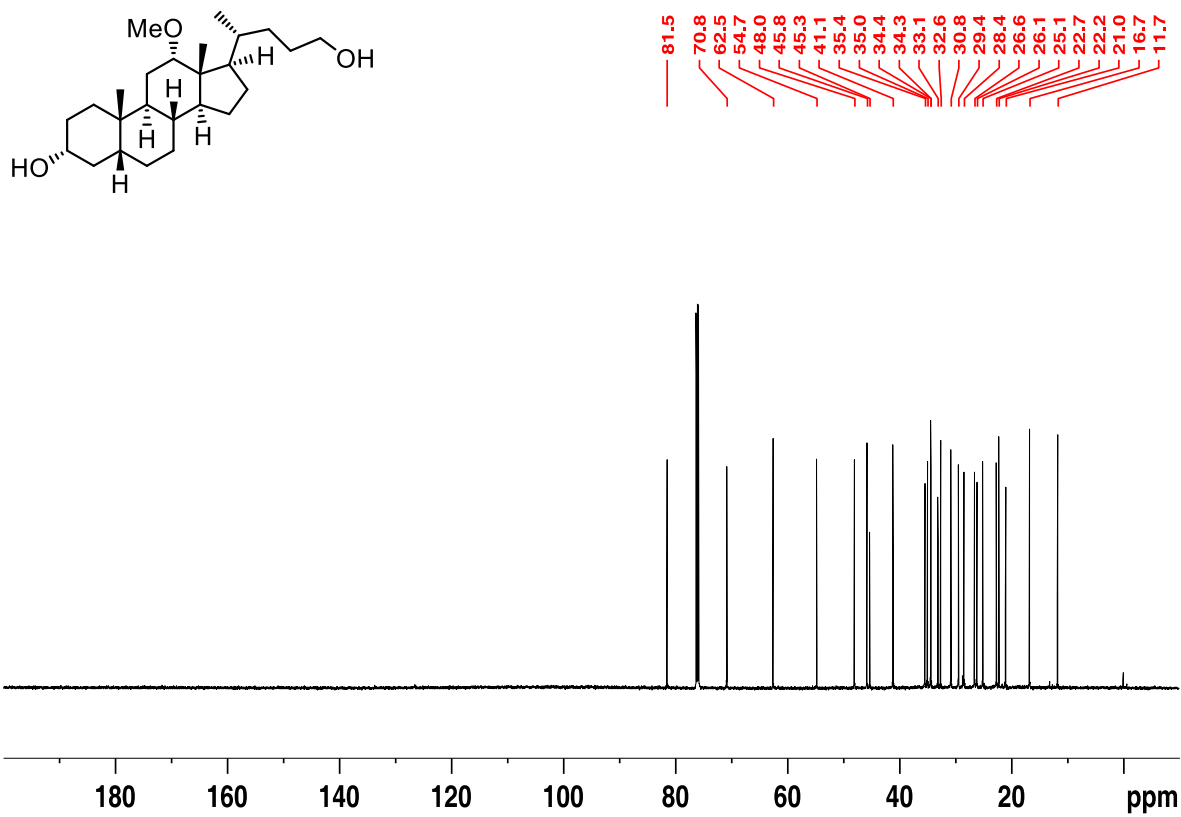


Figure S56. $^{13}\text{C}\{^1\text{H}\}$ NMR of 3 α ,24-dihydroxy-12 α -methoxycholane (**17a**) (CDCl₃, 23 °C)

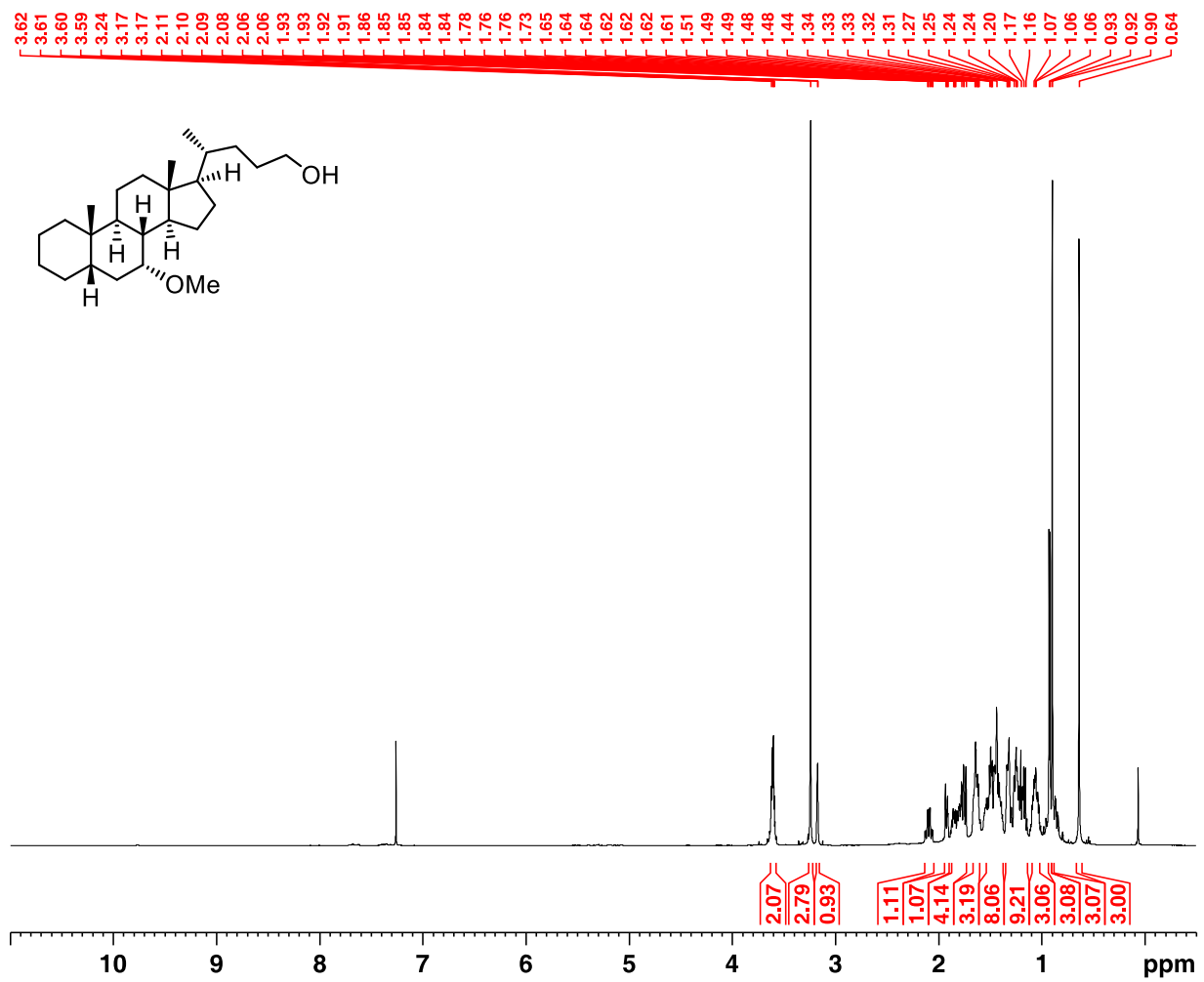


Figure S57. ¹H NMR of 24-hydroxy-7 α -methoxycholeane (**18a**) (CDCl₃, 23 °C)

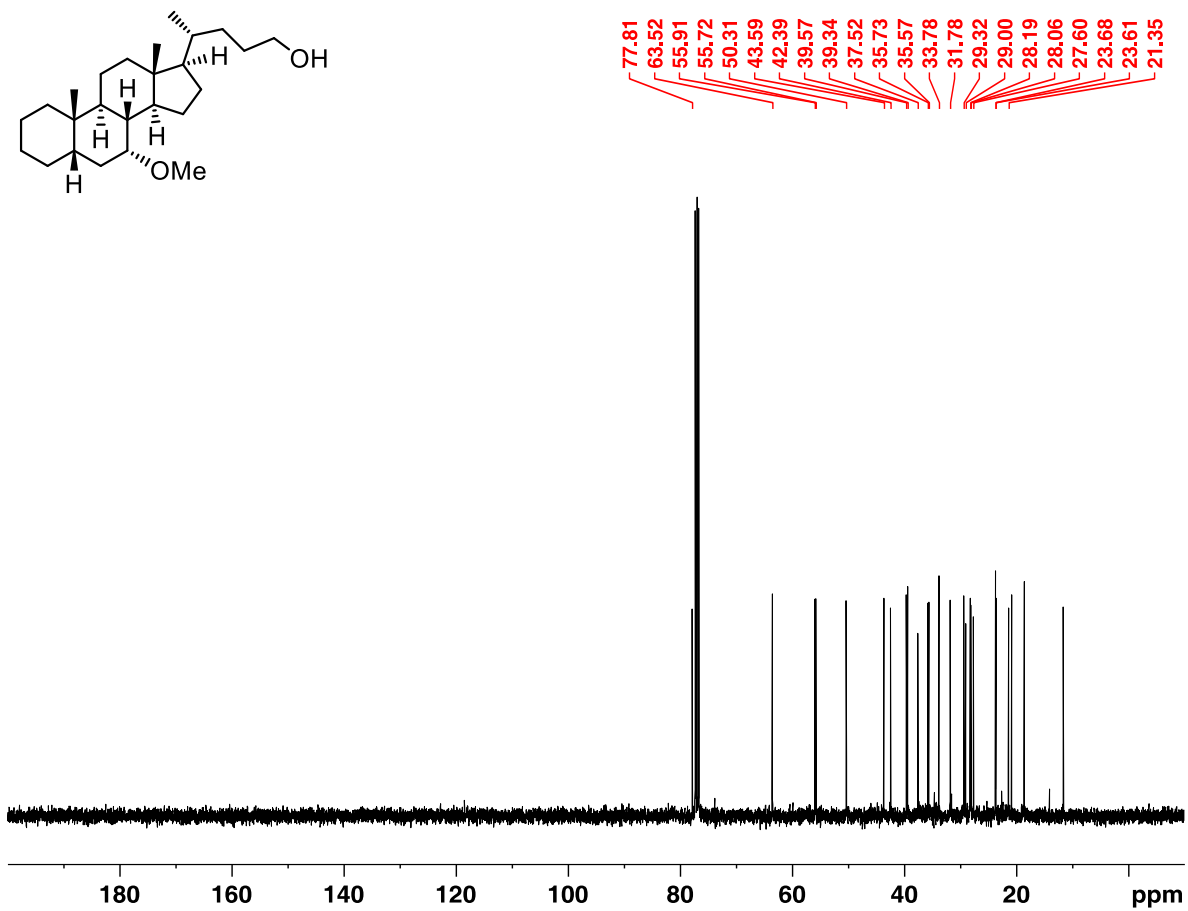


Figure S58. $^{13}\text{C}\{^1\text{H}\}$ NMR of 24-hydroxy-7 α -methoxycholeane (**18a**) (CDCl_3 , 23 $^\circ\text{C}$)

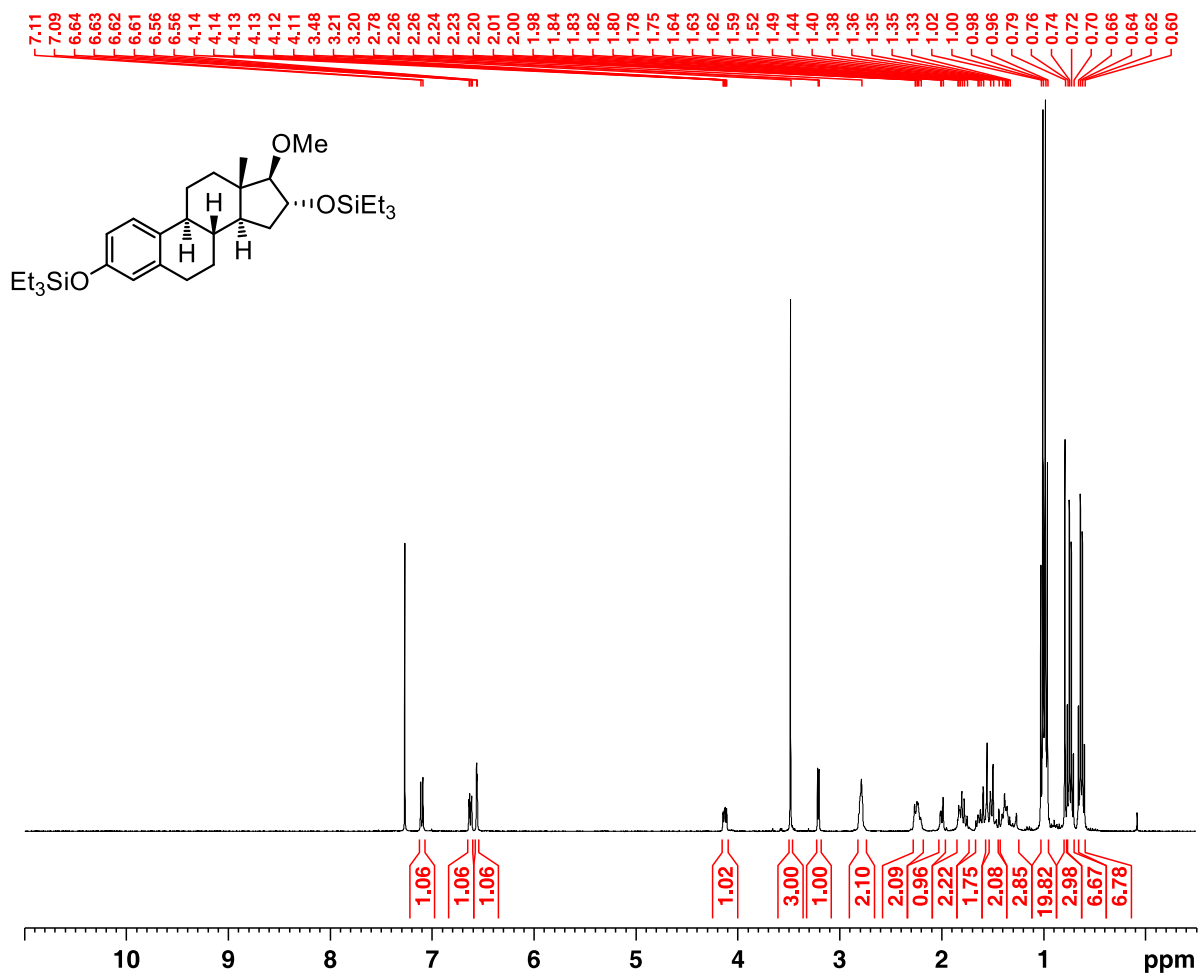


Figure S59. ¹H NMR of 3,16-bis(triethylsiloxy)-17-methoxy-1,3,5(10)-estratriene (**21a**) (CDCl₃, 23 °C)

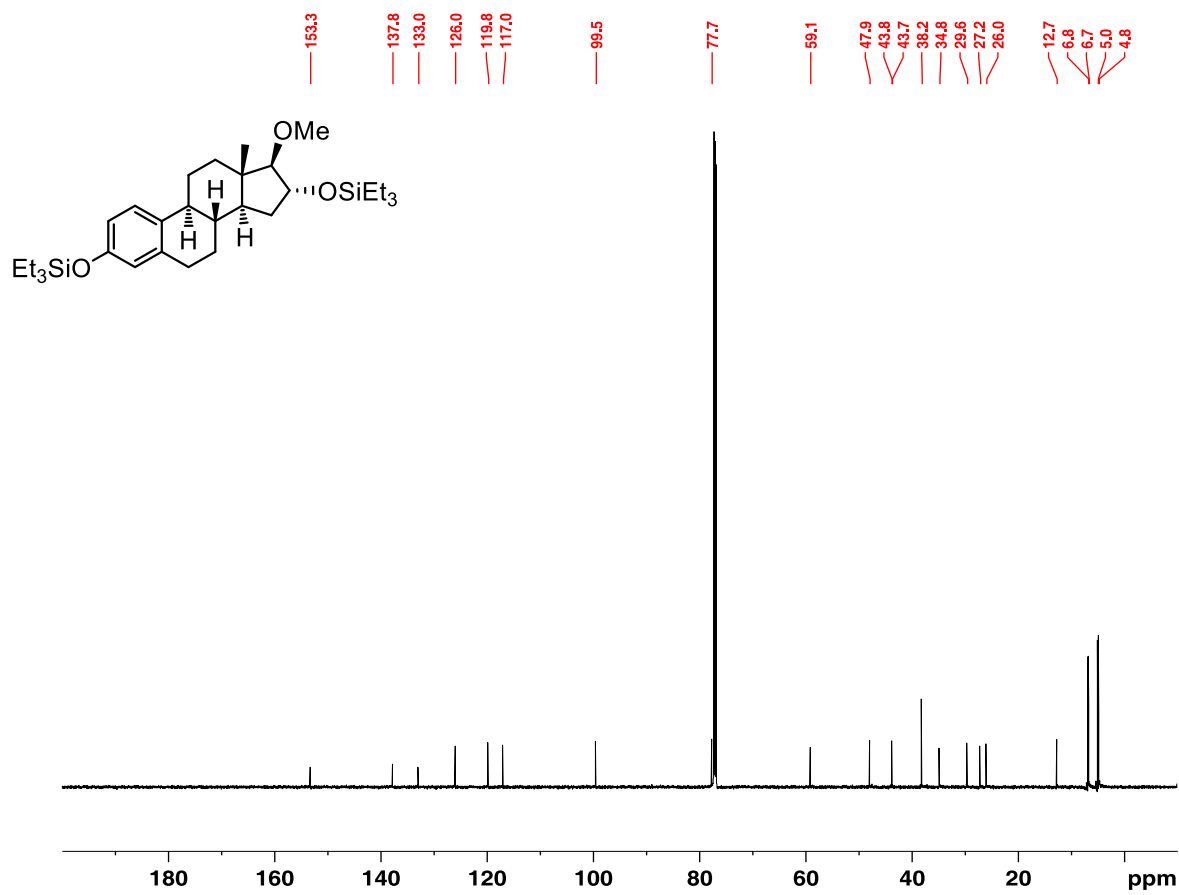


Figure S60. ¹³C{¹H} NMR of 3,16-bis(triethylsiloxy)-17-methoxy-1,3,5(10)-estratriene (21a) (CDCl₃, 23 °C)

V. Computational Methods

General Methods. Density functional theory (DFT) calculations were performed using Gaussian 09.²⁸

DFT treatment of complexes 22a and 23a. Atomic coordinates from the X-ray crystal structures of **22a** and **23a** were used as the initial conditions for their structural optimizations respectively. Initial atomic coordinates for the metal hydrides were also obtained from X-ray data according to the procedures described in the following section dealing with X-ray methods. Optimization was conducted in two steps, initially using b3lyp/lanl2dz and then a final optimization using the M06-L²⁹ functional with an expanded basis set (CHN: def2SVP, IrP: def2TZVP).³⁰ The ECP for Ir was retrieved from the EMSL basis set exchange (<http://bse.pnl.gov/>).³¹

Keyword. # opt freq m06l/gen geom=connectivity pseudo=read

The supplemental file “calc_coords.xyz” contains the computed Cartesian coordinates of all of the molecules reported in this study. The file may be opened as a text file to read the coordinates, or opened directly by a molecular modeling program such as Mercury (version 3.3 or later, <http://www.ccdc.cam.ac.uk/pages/Home.aspx>) for visualization and analysis.

Computational treatment of entries in Table 1. Initial atomic coordinates for silyloxonium ions were generated using Avogadro 1.2.0.³² A conformational search was performed for each chair conformation using molecular mechanics methods. In all cases the lowest energy places the methyl group pointed towards the ring in an eclipsing interaction with C2 (C5 when C3 is substituted). This orients the large Et₃Si group away from the ring. (Figure S61). This geometric preference was verified by DFT in two cases by conducting a scan about the Cy-O bond in 15°

increments. Results of the DFT scan for silyloxonium ions of *cis*-**3** and *trans*-**3** were consistent with the preferred geometry obtained by MM methods, thus MM-optimized geometries were used as a starting point for DFT calculations. The free energy of each chair conformer in Table 1 was then calculated after a final DFT optimization.

Keyword. # opt freq b3lyp/6-31g* geom=connectivity

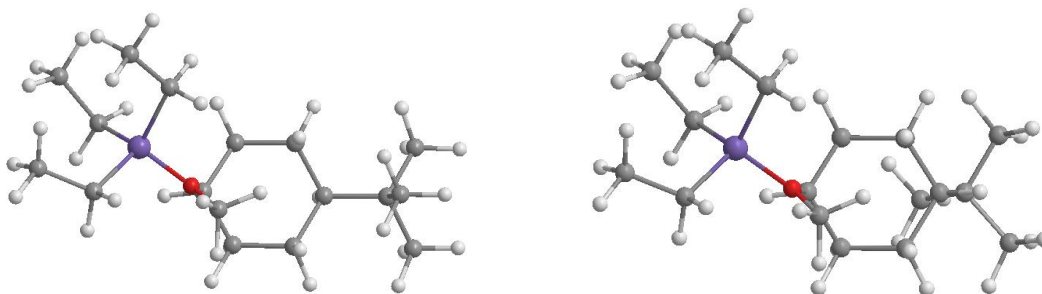


Figure S61. Representative lowest energy conformations for silyloxonium ions obtained by MM methods. *Cis-3* (left) and *trans-3* (right).

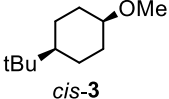
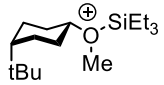
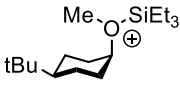
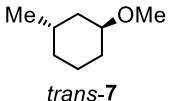
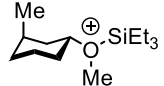
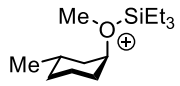
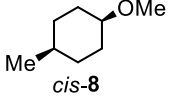
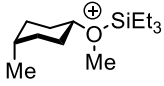
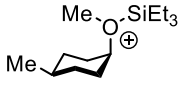
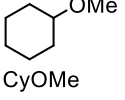
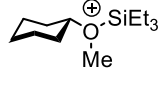
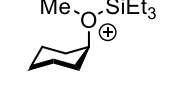
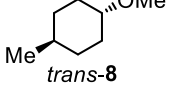
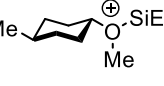
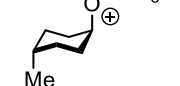
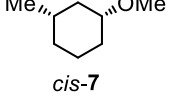
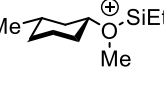
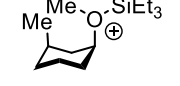
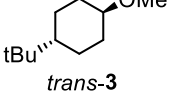

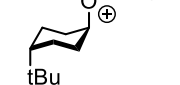
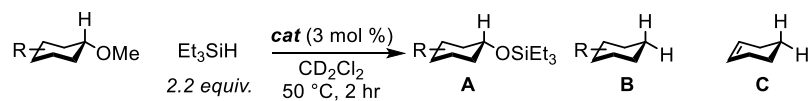
| | | Equatorial (<i>a. u.</i>) | Axial | |
|---|---|-----------------------------|--------------|---|
|  <i>cis-3</i> |  | -1034.167419 | -1034.168443 |  |
|  <i>trans-7</i> |  | -916.316654 | -916.311709 |  |
|  <i>cis-8</i> |  | -916.317871 | -916.312692 |  |
|  CyOMe |  | -877.030754 | -877.022874 |  |
|  <i>trans-8</i> |  | -916.32087 | -916.307695 |  |
|  <i>cis-7</i> |  | -916.321548 | -916.304444 |  |
|  <i>trans-3</i> |  | -1034.175577 | -1034.157607 |  |

Figure S62. Calculated energies (*a.u.*) for silyloxonium ions shown in Table 1.



| Ether | Silyloxonium | $E_{ax-E_{eq}}$ | 1a | | 1e | | |
|---------|--------------|-----------------|-----------|---------|-----------|---------|---------|
| | | | Yield A | Yield B | Yield A | Yield B | Yield C |
| cis-3 | | -0.6 | - | >95 | - | >95 | - |
| trans-7 | | 3.1 | 32 | 68 | - | 82 | 15 |
| cis-8 | | 3.2 | 31 | 69 | - | 93 | 7 |
| CyOMe | | 4.9 | 84 | 14 | - | 80 | 3 |
| trans-8 | | 8.3 | >95 | - | - | >95 | - |
| cis-7 | | 10.7 | >95 | - | - | >95 | - |
| trans-3 | | 11.3 | >95 | - | - | 95 | 4 |

Figure S63. Comparison of precatalysts **1a** and **1e** for substrates in Table 1.

VI. X-Ray Crystallographic Data

Details of crystallographic refinement for complexes 1b, 1c, 1d, 1e, 1f, 22a, 23, 23a and compounds 16a, 17, 17a, 18a, 20, and 24.

General Methods. A suitable crystal of each sample was selected for analysis and mounted in a polyimide loop. All measurements were made on a Rigaku Oxford Diffraction Supernova Eos CCD with filtered Cu-K α or Mo-K α radiation at a temperature of 100 K. Using Olex2,³³ the structure was solved with the ShelXT structure solution program using Direct Methods and refined with the ShelXL refinement package³⁴ using Least Squares minimization.

Complex 1b

Disordered trifluoromethyl groups on the anion were modeled over two sets of positions. Their thermal parameters were treated in two ways. In one case a similarity restraint was used to restrain the fluorine thermal parameters. In the second case an equivalency constraint was used to constrain the fluorine thermal parameters to be equal to the fluorine atom on the other side of the carbon position.

Complex 1c

The crystal was refined as a racemic twin with a ratio of 55:45. Disordered trifluoromethyl groups were modeled over two positions with similarity restraints placed on their thermal parameters. Unreasonable thermal parameters for two carbon atoms were restrained to be approximately isotropic.

Complex 1d

A disordered trifluoromethyl group was modeled with appropriate similarity restraints.

Complex 1e

Disorder in the trifluoromethyl groups of the anion was modeled over two sites per disordered group using similarity restraints applied to the thermal parameters of the fluorine atoms. Disorder between the methyl and trifluoromethyl groups of the phosphine was modeled over two sites without restraint.

Complex **1f**

Disorder in trifluoromethyl and aryl substituents was modeled with appropriate similarity restraints.

Compound **16a**

Disorder in the A and B rings of one of the three molecules in the asymmetric unit was modeled over two positions with similarity restraints placed on atom thermal parameters. Disorder in the side chain alcohol of one of the molecules was modeled over two positions without restraint.

Compound **17**

The model was refined without restraint.

Compound **17a**

The model was refined without restraint.

Compound **18a**

Disorder in the side chain of the two molecules was modeled over two positions without restraint.

Compound **20**

The model was refined without restraint.

Complex **22a**

The four metal hydrides were located in the difference map. The positions of the hydrides were refined with their M-H bond length restrained to be equal. Their thermal parameters were allowed to freely refine. The plausibility of these atom positions was checked by comparison to the results of DFT calculations (*vide supra*).

Complex **23**

Metal hydrides were added in idealized positions and refined with M-H, H-H and H-P distance restraints to give a flat equilateral pentagon orthogonal to the P-Ir-P axis. Their occupancy is fixed to 0.5 as the inversion center generates five additional hydride positions. Disorder in trifluoromethyl groups was modeled with appropriate similarity restraints.

Complex **23a**

Metal hydrides were located in the difference map and their positions refined with an Ir-H bond length similarity restraint. Their thermal parameters were fixed to ride on the parent iridium atom. Disordered trifluoromethyl groups and a bis(trifluoromethyl)phenyl group were modeled with appropriate similarity restraints placed on atom thermal parameters and selected C-F and C-C bonds.

Compound **24**

The model was refined without restraint.

Table S1. Crystal data and structure refinement for **1b**.

| | | |
|-----------------------------------|---|-------------------|
| Identification code | 1b | |
| Empirical formula | C ₆₆ H ₅₀ BF ₂₄ IrP ₂ | |
| Formula weight | 1564.01 | |
| Temperature | 100.0(3) K | |
| Wavelength | 1.54184 Å | |
| Crystal system | Triclinic | |
| Space group | P-1 | |
| Unit cell dimensions | a = 14.47472(15) Å | α = 107.1150(10)° |
| | b = 19.2600(2) Å | β = 90.4073(8)° |
| | c = 23.9417(3) Å | γ = 98.3956(9)° |
| Volume | 6301.76(13) Å ³ | |
| Z | 4 | |
| Density (calculated) | 1.648 Mg/m ³ | |
| Absorption coefficient | 5.593 mm ⁻¹ | |
| F(000) | 3096 | |
| Crystal size | 0.135 x 0.06 x 0.037 mm ³ | |
| Theta range for data collection | 2.430 to 66.355°. | |
| Index ranges | -15 ≤ h ≤ 17, -22 ≤ k ≤ 22, -28 ≤ l ≤ 27 | |
| Reflections collected | 84264 | |
| Independent reflections | 21638 [R(int) = 0.0373] | |
| Completeness to theta = 66.355° | 97.6 % | |
| Absorption correction | Gaussian | |
| Max. and min. transmission | 0.925 and 0.597 | |
| Refinement method | Full-matrix least-squares on F ² | |
| Data / restraints / parameters | 21638 / 72 / 1735 | |
| Goodness-of-fit on F ² | 1.018 | |
| Final R indices [I > 2σ(I)] | R1 = 0.0296, wR2 = 0.0692 | |
| R indices (all data) | R1 = 0.0331, wR2 = 0.0713 | |
| Absolute structure parameter | 0.452(4) | |
| Extinction coefficient | n/a | |
| Largest diff. peak and hole | 2.634 and -0.916 e/Å ⁻³ | |

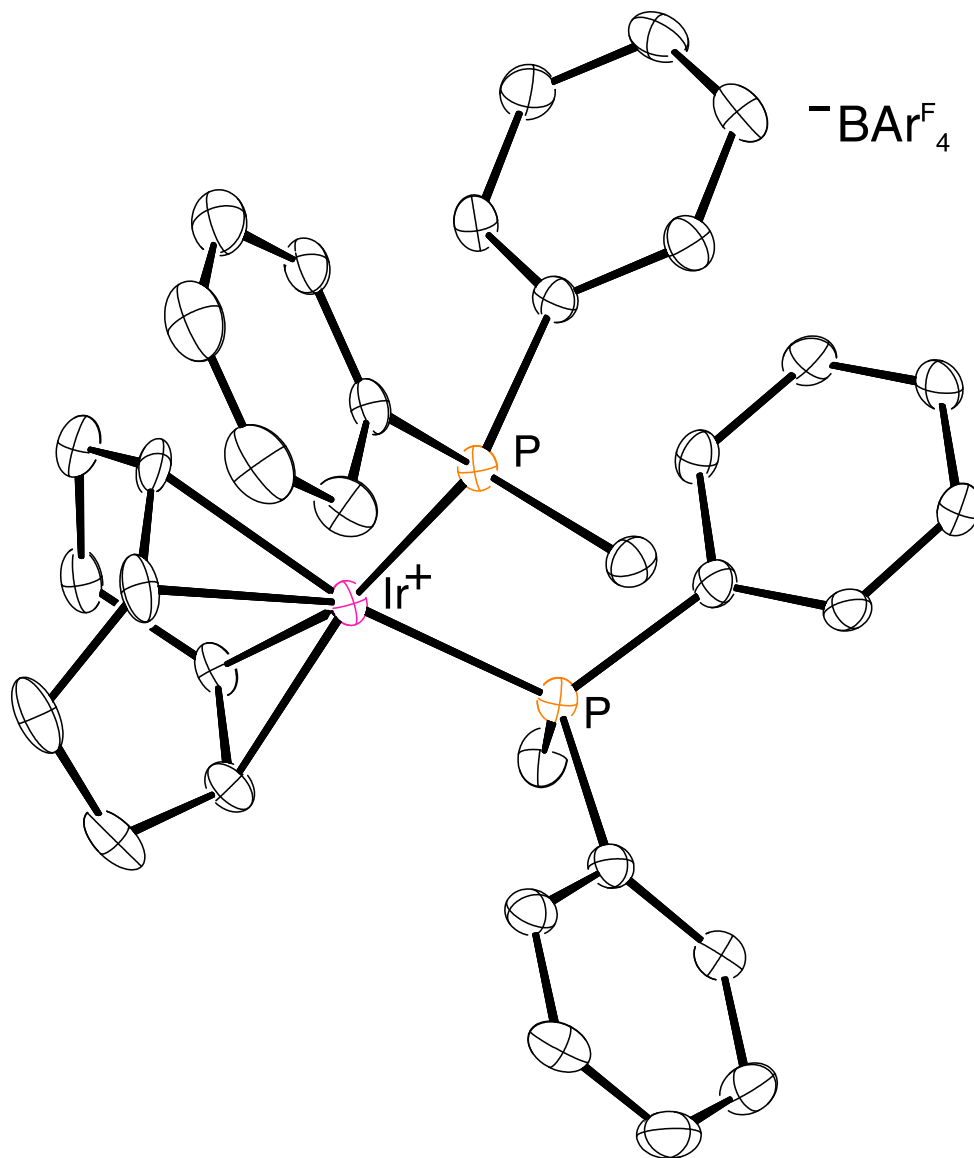


Figure S64. ORTEP diagram of **1b** shown at 50% probability. Anion and additional molecules in the asymmetric unit omitted for clarity.

Table S2. Crystal data and structure refinement for **1c**.

| | | |
|-----------------------------------|--|-------------------|
| Identification code | 1c | |
| Empirical formula | C ₅₈ H ₅₁ BF ₂₄ IrO _{0.5} P ₂ | |
| Formula weight | 1476.93 | |
| Temperature | 100.4(8) K | |
| Wavelength | 0.71073 Å | |
| Crystal system | Monoclinic | |
| Space group | P 1 21 1 | |
| Unit cell dimensions | a = 12.17636(16) Å | α = 90° |
| | b = 38.6268(5) Å | β = 100.2564(13)° |
| | c = 12.77708(18) Å | γ = 90° |
| Volume | 5913.46(15) Å ³ | |
| Z | 4 | |
| Density (calculated) | 1.659 Mg/m ³ | |
| Absorption coefficient | 2.427 mm ⁻¹ | |
| F(000) | 2924 | |
| Crystal size | 0.38 x 0.297 x 0.255 mm ³ | |
| Theta range for data collection | 2.129 to 27.485° | |
| Index ranges | -15 ≤ h ≤ 15, -50 ≤ k ≤ 50, -16 ≤ l ≤ 16 | |
| Reflections collected | 85932 | |
| Independent reflections | 27088 [R(int) = 0.0453] | |
| Completeness to theta = 25.242° | 99.9 % | |
| Absorption correction | Semi-empirical from equivalents | |
| Max. and min. transmission | 1.00000 and 0.63724 | |
| Refinement method | Full-matrix least-squares on F ² | |
| Data / restraints / parameters | 27088 / 175 / 1625 | |
| Goodness-of-fit on F ² | 1.042 | |
| Final R indices [I > 2σ(I)] | R1 = 0.0358, wR2 = 0.0689 | |
| R indices (all data) | R1 = 0.0391, wR2 = 0.0700 | |
| Absolute structure parameter | 0.452(4) | |
| Extinction coefficient | n/a | |
| Largest diff. peak and hole | 0.763 and -1.051 e/Å ⁻³ | |

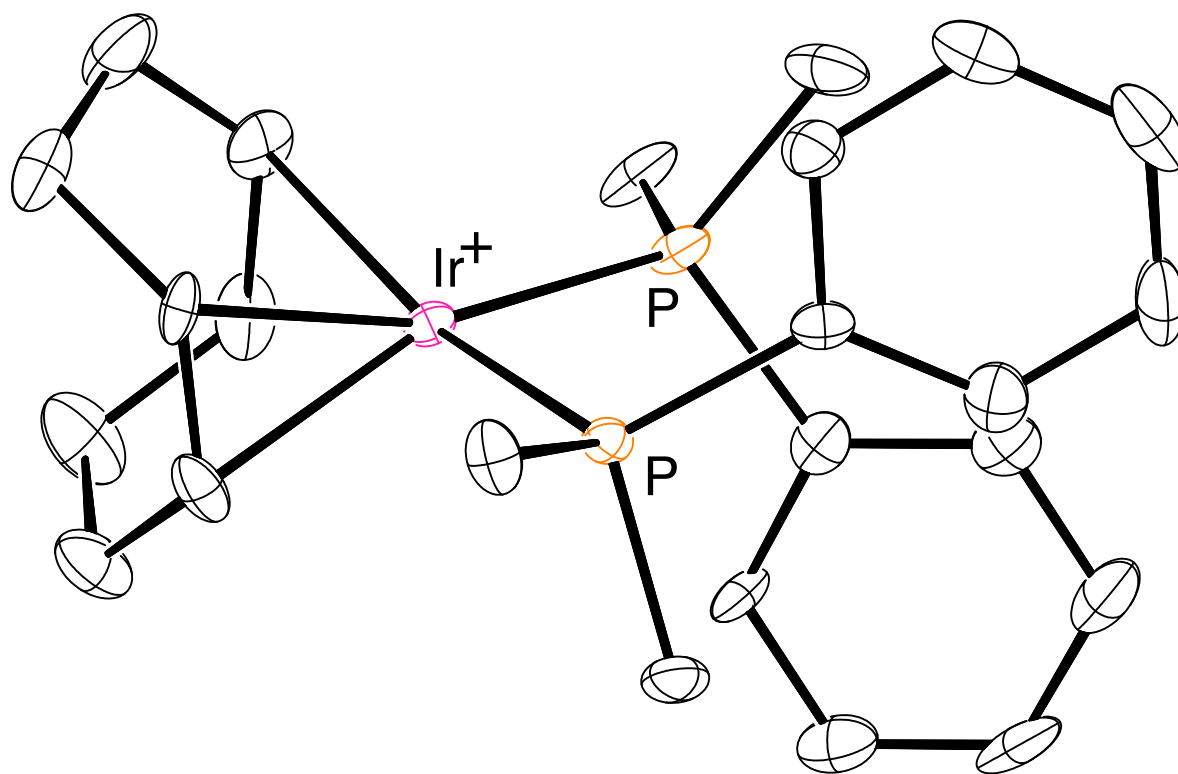


Figure S65. ORTEP diagram of **1c** shown at 50% probability. Anion and additional molecules in the asymmetric unit omitted for clarity.

Table S3. Crystal data and structure refinement for **1d**.

| | | |
|-----------------------------------|---|---|
| Identification code | 1d | |
| Empirical formula | C ₈₈ H ₇₈ BF ₂₄ IrP ₂ | |
| Formula weight | 1856.45 | |
| Temperature | 100.01(10) K | |
| Wavelength | 0.71073 Å | |
| Crystal system | Triclinic | |
| Space group | P-1 | |
| Unit cell dimensions | a = 12.9847(2) Å b = 16.3076(3) Å c = 19.9591(3) Å | α = 95.5387(14)° β = 104.5920(14)° γ = 92.1533(14)° |
| Volume | 4062.49(12) Å ³ | |
| Z | 2 | |
| Density (calculated) | 1.518 Mg/m ³ | |
| Absorption coefficient | 1.783 mm ⁻¹ | |
| F(000) | 1868 | |
| Crystal size | 0.301 x 0.246 x 0.205 mm ³ | |
| Theta range for data collection | 1.989 to 30.263°. | |
| Index ranges | -18 ≤ h ≤ 17, -21 ≤ k ≤ 23, -27 ≤ l ≤ 28 | |
| Reflections collected | 79719 | |
| Independent reflections | 21628 [R(int) = 0.0375] | |
| Completeness to theta = 25.242° | 100.0 % | |
| Absorption correction | Semi-empirical from equivalents | |
| Max. and min. transmission | 1.00000 and 0.89481 | |
| Refinement method | Full-matrix least-squares on F ² | |
| Data / restraints / parameters | 21628 / 36 / 1085 | |
| Goodness-of-fit on F ² | 1.020 | |
| Final R indices [I > 2σ(I)] | R1 = 0.0293, wR2 = 0.0606 | |
| R indices (all data) | R1 = 0.0345, wR2 = 0.0628 | |
| Absolute structure parameter | 0.03(8) | |
| Extinction coefficient | n/a | |
| Largest diff. peak and hole | 1.986 and -0.974 e/Å ⁻³ | |

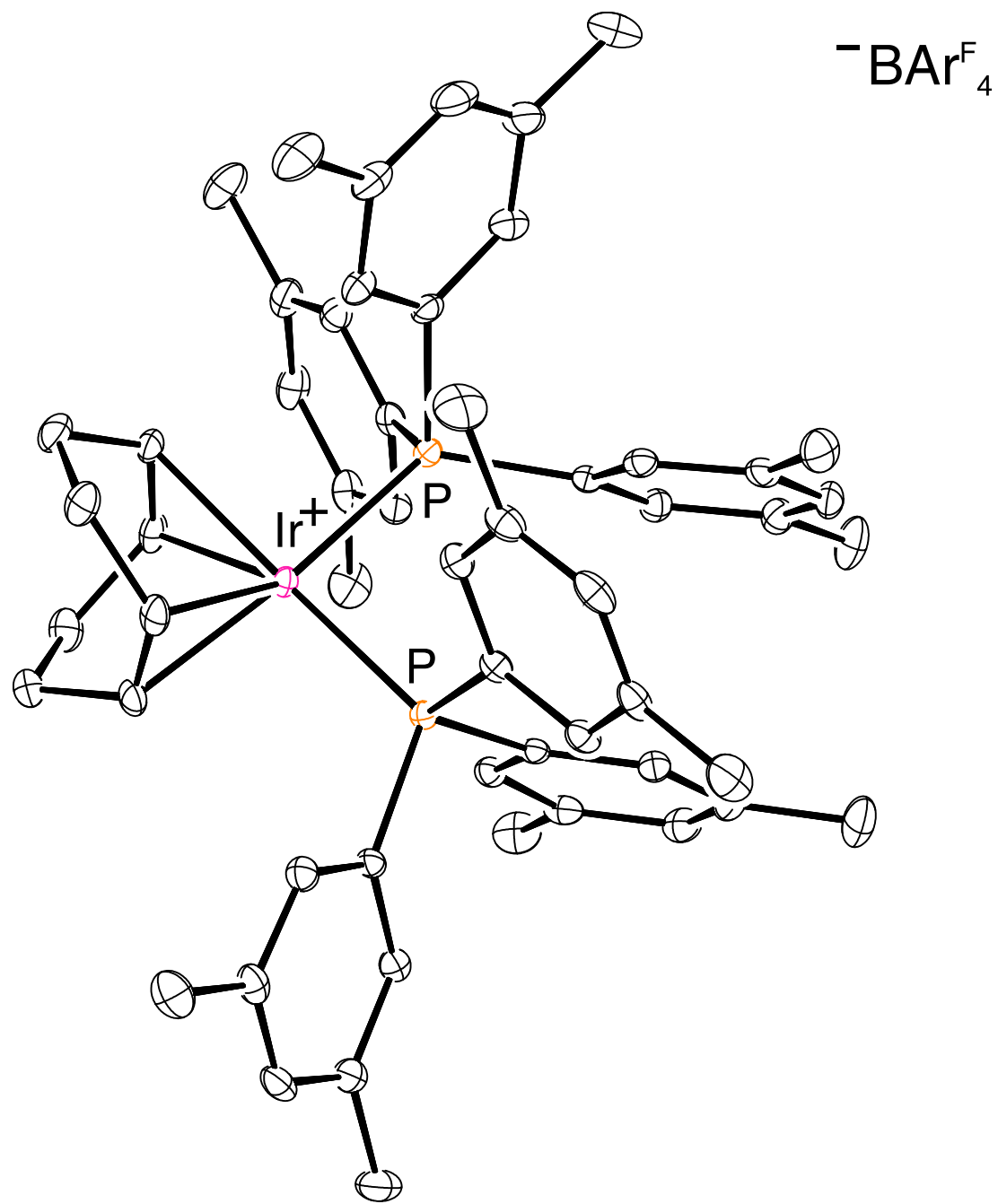


Figure S66. ORTEP diagram of **1d** shown at 50% probability. Anion and additional molecules in the asymmetric unit omitted for clarity.

Table S4. Crystal data and structure refinement for **1e**.

| | | |
|-----------------------------------|---|------------------|
| Identification code | 1e | |
| Empirical formula | C ₈₈ H ₆₀ BF ₄₂ IrP ₂ | |
| Formula weight | 2180.31 | |
| Temperature | 100.01(10) K | |
| Wavelength | 1.54184 Å | |
| Crystal system | Monoclinic | |
| Space group | P 1 21/c 1 | |
| Unit cell dimensions | a = 13.0737(2) Å | α = 90° |
| | b = 23.7759(3) Å | β = 99.7800(10)° |
| | c = 28.1916(4) Å | γ = 90° |
| Volume | 8635.7(2) Å ³ | |
| Z | 4 | |
| Density (calculated) | 1.677 Mg/m ³ | |
| Absorption coefficient | 4.589 mm ⁻¹ | |
| F(000) | 4312 | |
| Crystal size | 0.315 x 0.126 x 0.012 mm ³ | |
| Theta range for data collection | 2.446 to 73.348°. | |
| Index ranges | -16 ≤ h ≤ 15, -29 ≤ k ≤ 28, -34 ≤ l ≤ 25 | |
| Reflections collected | 65028 | |
| Independent reflections | 17098 [R(int) = 0.0450] | |
| Completeness to theta = 67.684° | 100.0 % | |
| Absorption correction | Gaussian | |
| Max. and min. transmission | 1.000 and 0.239 | |
| Refinement method | Full-matrix least-squares on F ² | |
| Data / restraints / parameters | 17098 / 72 / 1356 | |
| Goodness-of-fit on F ² | 1.136 | |
| Final R indices [I > 2σ(I)] | R1 = 0.0566, wR2 = 0.1202 | |
| R indices (all data) | R1 = 0.0653, wR2 = 0.1239 | |
| Absolute structure parameter | 0.03(8) | |
| Extinction coefficient | n/a | |
| Largest diff. peak and hole | 1.653 and -1.289 e/Å ⁻³ | |

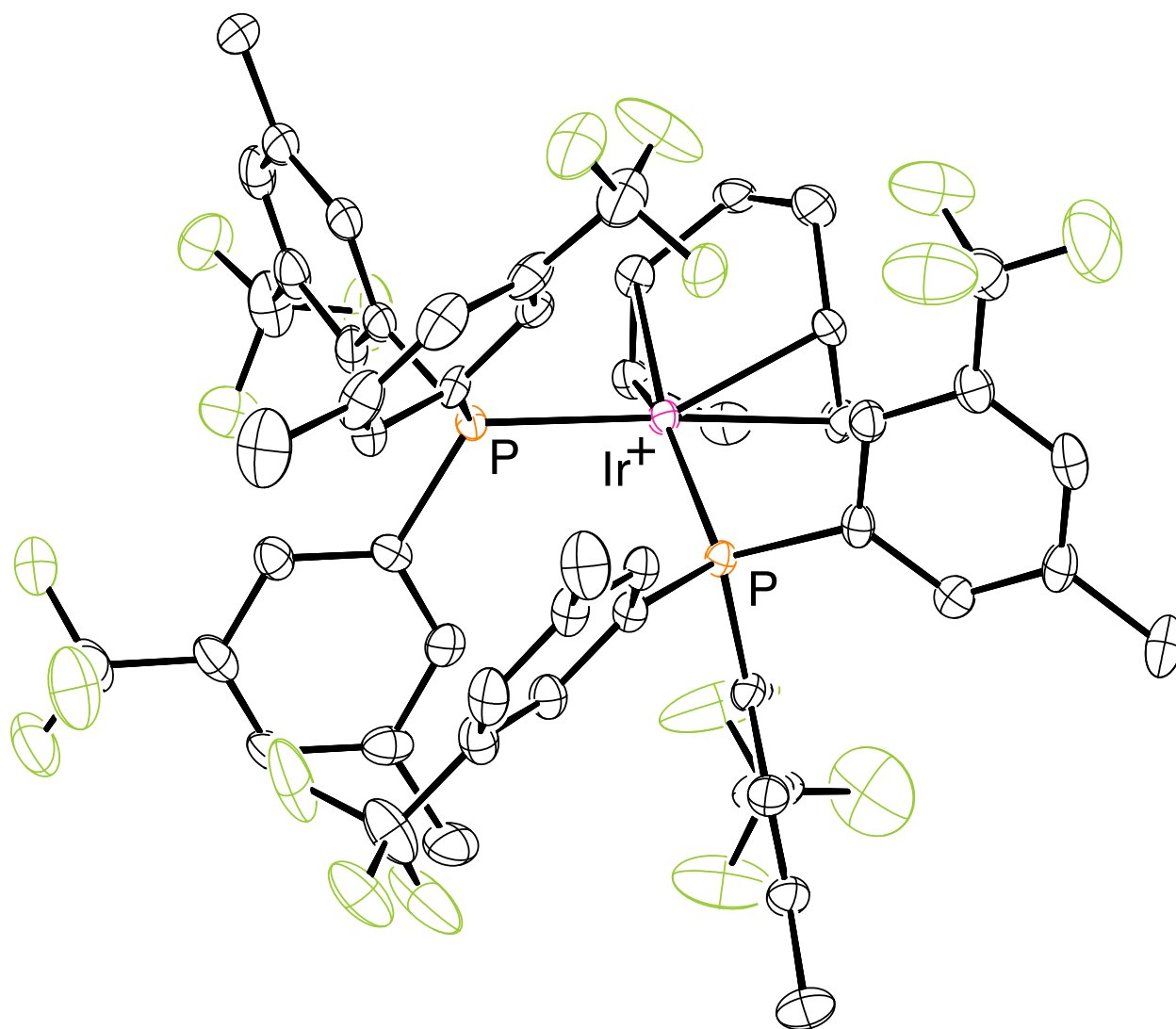


Figure S67. ORTEP diagram of **1e** shown at 50% probability. Anion and complete disorder model omitted for clarity.

Table S5. Crystal data and structure refinement for **1f**.

| | | |
|-----------------------------------|---|----------------------------|
| Identification code | 1f | |
| Empirical formula | $C_{89}H_{44}BCl_2F_{60}IrP_2$ | |
| Formula weight | 2589.09 | |
| Temperature | 100.0(3) K | |
| Wavelength | 0.71073 Å | |
| Crystal system | Monoclinic | |
| Space group | P 1 21/c 1 | |
| Unit cell dimensions | a = 18.33896(13) Å | $\alpha = 90^\circ$ |
| | b = 13.16861(12) Å | $\beta = 91.6412(6)^\circ$ |
| | c = 38.4041(3) Å | $\gamma = 90^\circ$ |
| Volume | 9270.74(12) Å ³ | |
| Z | 4 | |
| Density (calculated) | 1.855 Mg/m ³ | |
| Absorption coefficient | 1.701 mm ⁻¹ | |
| F(000) | 5056 | |
| Crystal size | 0.296 x 0.195 x 0.05 mm ³ | |
| Theta range for data collection | 2.875 to 30.419° | |
| Index ranges | -26 ≤ h ≤ 25, -18 ≤ k ≤ 17, -50 ≤ l ≤ 52 | |
| Reflections collected | 142463 | |
| Independent reflections | 25251 [R(int) = 0.0450] | |
| Completeness to theta = 25.242° | 99.8 % | |
| Absorption correction | Gaussian | |
| Max. and min. transmission | 1.000 and 0.540 | |
| Refinement method | Full-matrix least-squares on F ² | |
| Data / restraints / parameters | 25251 / 544 / 1542 | |
| Goodness-of-fit on F ² | 1.103 | |
| Final R indices [I > 2σ(I)] | R1 = 0.0409, wR2 = 0.0827 | |
| R indices (all data) | R1 = 0.0473, wR2 = 0.0852 | |
| Absolute structure parameter | 0.03(8) | |
| Extinction coefficient | n/a | |
| Largest diff. peak and hole | 1.199 and -1.525 e/Å ⁻³ | |

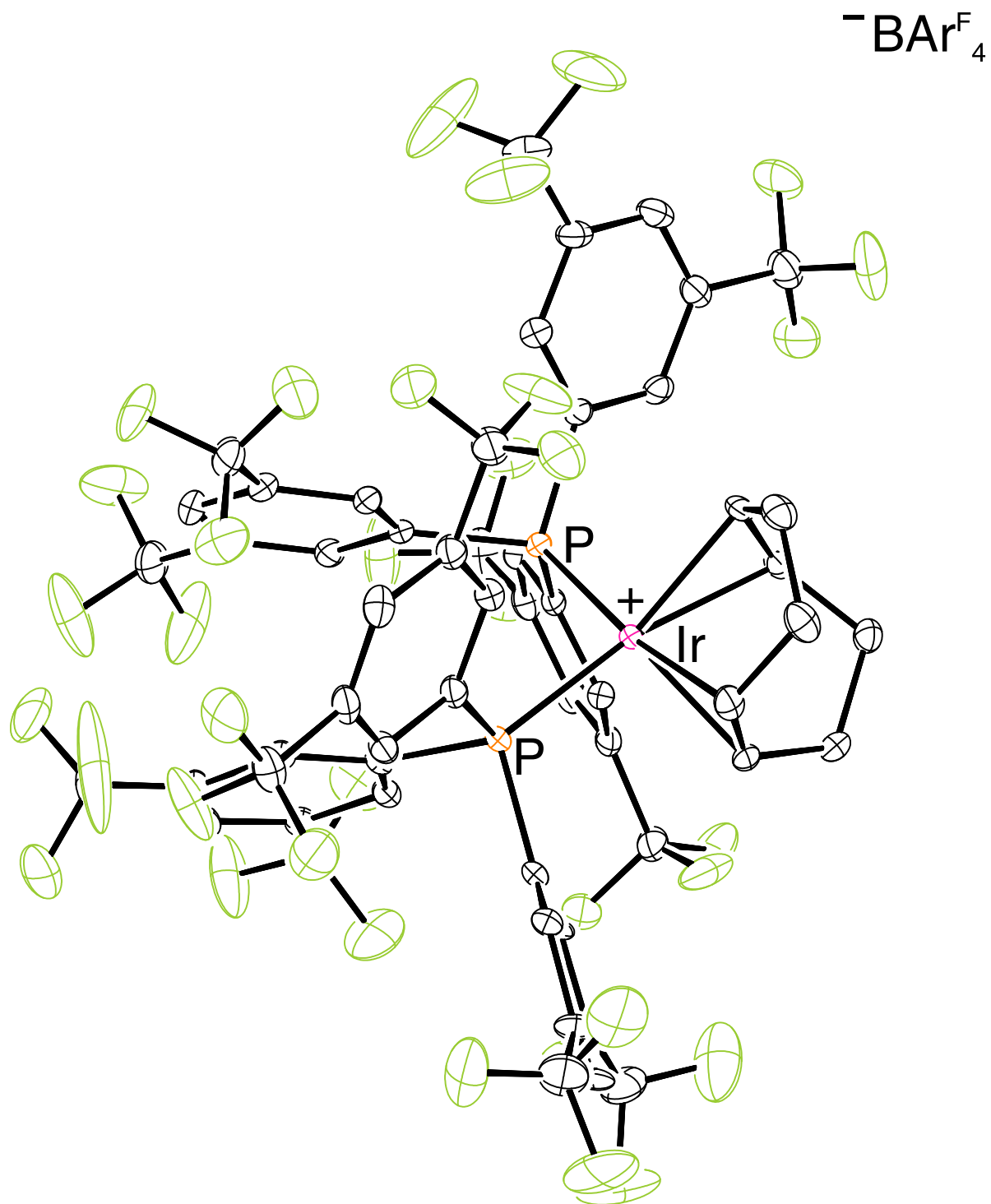


Figure S68. ORTEP diagram of **1f** shown at 50% probability. Anion, solvent and complete disorder model omitted for clarity.

Table S6. Crystal data and structure refinement for **16a**.

| | | |
|-----------------------------------|--|----------------|
| Identification code | 16a | |
| Empirical formula | C ₂₄ H ₄₂ O ₂ | |
| Formula weight | 362.57 | |
| Temperature | 100.01(10) K | |
| Wavelength | 1.54184 Å | |
| Crystal system | Monoclinic | |
| Space group | I 1 2 1 | |
| Unit cell dimensions | a = 7.6128(2) Å | α = 90° |
| | b = 9.7121(3) Å | β = 90.272(3)° |
| | c = 87.346(2) Å | γ = 90° |
| Volume | 6457.9(3) Å ³ | |
| Z | 12 | |
| Density (calculated) | 1.119 Mg/m ³ | |
| Absorption coefficient | 0.519 mm ⁻¹ | |
| F(000) | 2424 | |
| Crystal size | 0.369 x 0.054 x 0.016 mm ³ | |
| Theta range for data collection | 3.036 to 75.033°. | |
| Index ranges | -9 ≤ h ≤ 9, -12 ≤ k ≤ 12, -108 ≤ l ≤ 103 | |
| Reflections collected | 49679 | |
| Independent reflections | 12783 [R(int) = 0.0519] | |
| Completeness to theta = 67.684° | 100.0 % | |
| Absorption correction | Semi-empirical from equivalents | |
| Max. and min. transmission | 1.00000 and 0.51562 | |
| Refinement method | Full-matrix least-squares on F ² | |
| Data / restraints / parameters | 12783 / 283 / 831 | |
| Goodness-of-fit on F ² | 1.057 | |
| Final R indices [I > 2σ(I)] | R1 = 0.0476, wR2 = 0.1143 | |
| R indices (all data) | R1 = 0.0589, wR2 = 0.1275 | |
| Absolute structure parameter | 0.02(12) | |
| Extinction coefficient | n/a | |
| Largest diff. peak and hole | 0.191 and -0.205 e/Å ⁻³ | |

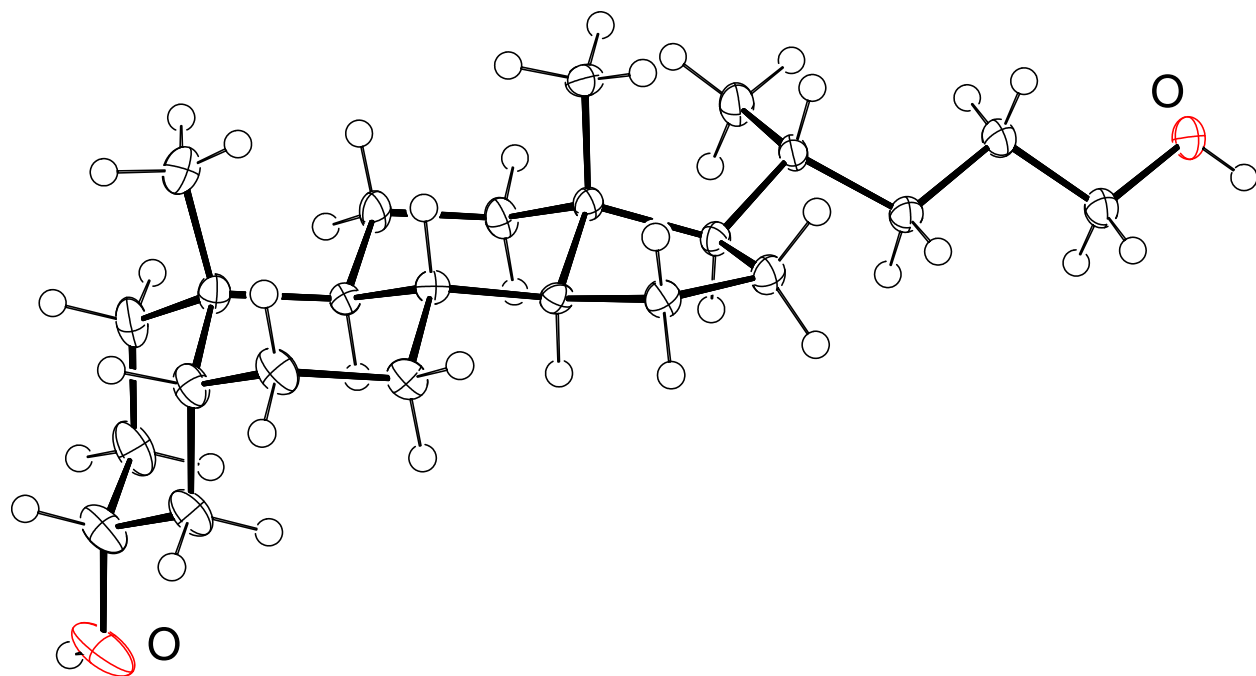


Figure S69. ORTEP diagram of **16a** shown at 50% probability. Additional molecules in the asymmetric unit omitted for clarity.

Table S7. Crystal data and structure refinement for **17**.

| | | |
|-----------------------------------|---|-------------------|
| Identification code | 17 | |
| Empirical formula | C ₄₂ H ₆₄ O ₃ Si | |
| Formula weight | 645.02 | |
| Temperature | 100.01(10) K | |
| Wavelength | 1.54184 Å | |
| Crystal system | Monoclinic | |
| Space group | P 1 21 1 | |
| Unit cell dimensions | a = 12.55791(14) Å | α = 90° |
| | b = 11.21470(10) Å | β = 107.5320(12)° |
| | c = 14.01011(16) Å | γ = 90° |
| Volume | 1881.44(4) Å ³ | |
| Z | 2 | |
| Density (calculated) | 1.139 Mg/m ³ | |
| Absorption coefficient | 0.818 mm ⁻¹ | |
| F(000) | 708 | |
| Crystal size | 0.114 x 0.058 x 0.02 mm ³ | |
| Theta range for data collection | 3.308 to 73.383°. | |
| Index ranges | -15 ≤ h ≤ 10, -13 ≤ k ≤ 13, -15 ≤ l ≤ 17 | |
| Reflections collected | 19098 | |
| Independent reflections | 7374 [R(int) = 0.0366] | |
| Completeness to theta = 67.684° | 99.9 % | |
| Absorption correction | Gaussian | |
| Max. and min. transmission | 1.000 and 0.932 | |
| Refinement method | Full-matrix least-squares on F ² | |
| Data / restraints / parameters | 7374 / 1 / 423 | |
| Goodness-of-fit on F ² | 1.057 | |
| Final R indices [I > 2σ(I)] | R1 = 0.0322, wR2 = 0.0754 | |
| R indices (all data) | R1 = 0.0353, wR2 = 0.0770 | |
| Absolute structure parameter | 0.005(14) | |
| Extinction coefficient | n/a | |
| Largest diff. peak and hole | 0.211 and -0.182 e/Å ⁻³ | |

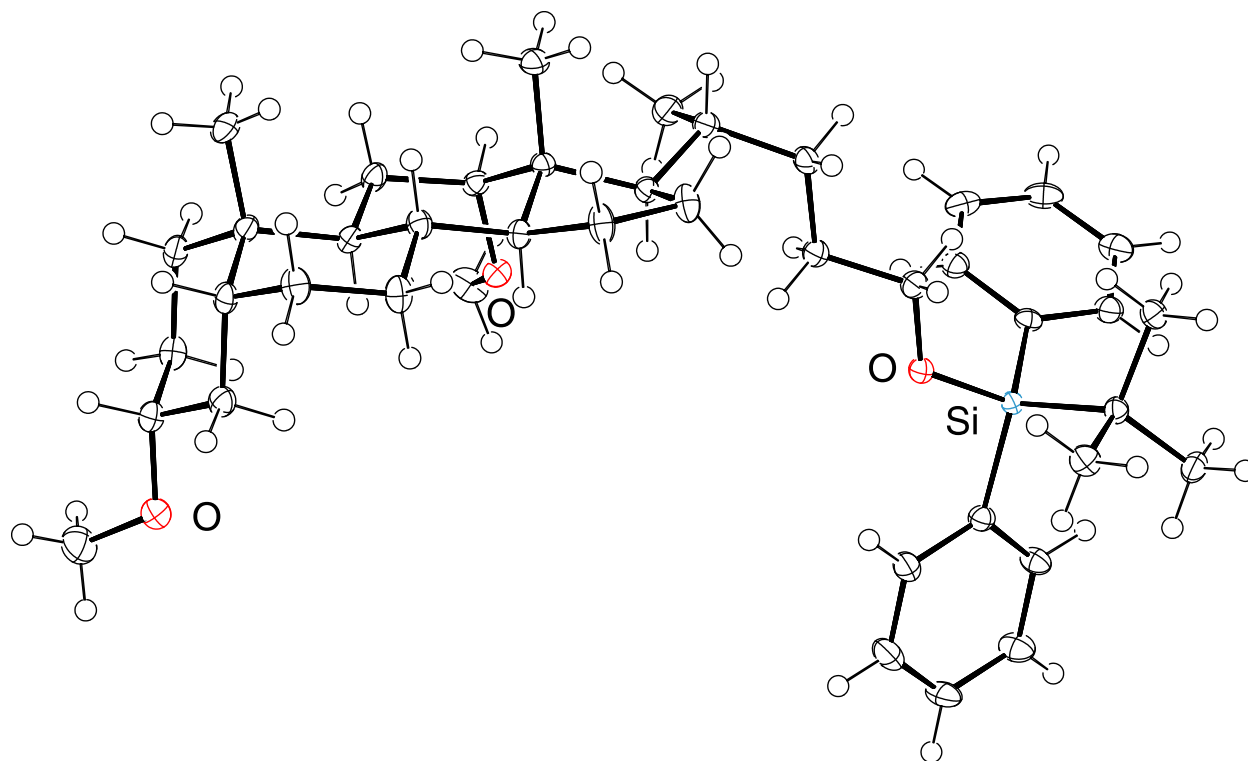


Figure S70. ORTEP diagram of **17** shown at 50% probability.

Table S8. Crystal data and structure refinement for **17a**.

| | | |
|-----------------------------------|--|-----------------|
| Identification code | 17a | |
| Empirical formula | C ₂₅ H ₄₄ O ₃ | |
| Formula weight | 392.60 | |
| Temperature | 99.98(10) K | |
| Wavelength | 1.54184 Å | |
| Crystal system | Monoclinic | |
| Space group | P 1 21 1 | |
| Unit cell dimensions | a = 12.21766(11) Å | α = 90° |
| | b = 7.39922(9) Å | β = 95.6028(9)° |
| | c = 12.74257(13) Å | γ = 90° |
| Volume | 1146.44(2) Å ³ | |
| Z | 2 | |
| Density (calculated) | 1.137 Mg/m ³ | |
| Absorption coefficient | 0.556 mm ⁻¹ | |
| F(000) | 436 | |
| Crystal size | 0.269 x 0.04 x 0.025 mm ³ | |
| Theta range for data collection | 3.485 to 73.259°. | |
| Index ranges | -15 ≤ h ≤ 15, -9 ≤ k ≤ 8, -15 ≤ l ≤ 14 | |
| Reflections collected | 15372 | |
| Independent reflections | 4287 [R(int) = 0.0298] | |
| Completeness to theta = 67.684° | 100.0 % | |
| Absorption correction | Gaussian | |
| Max. and min. transmission | 1.000 and 0.813 | |
| Refinement method | Full-matrix least-squares on F ² | |
| Data / restraints / parameters | 4287 / 1 / 259 | |
| Goodness-of-fit on F ² | 1.045 | |
| Final R indices [I > 2σ(I)] | R1 = 0.0321, wR2 = 0.0807 | |
| R indices (all data) | R1 = 0.0345, wR2 = 0.0828 | |
| Absolute structure parameter | 0.14(10) | |
| Extinction coefficient | n/a | |
| Largest diff. peak and hole | 0.218 and -0.159 e/Å ⁻³ | |

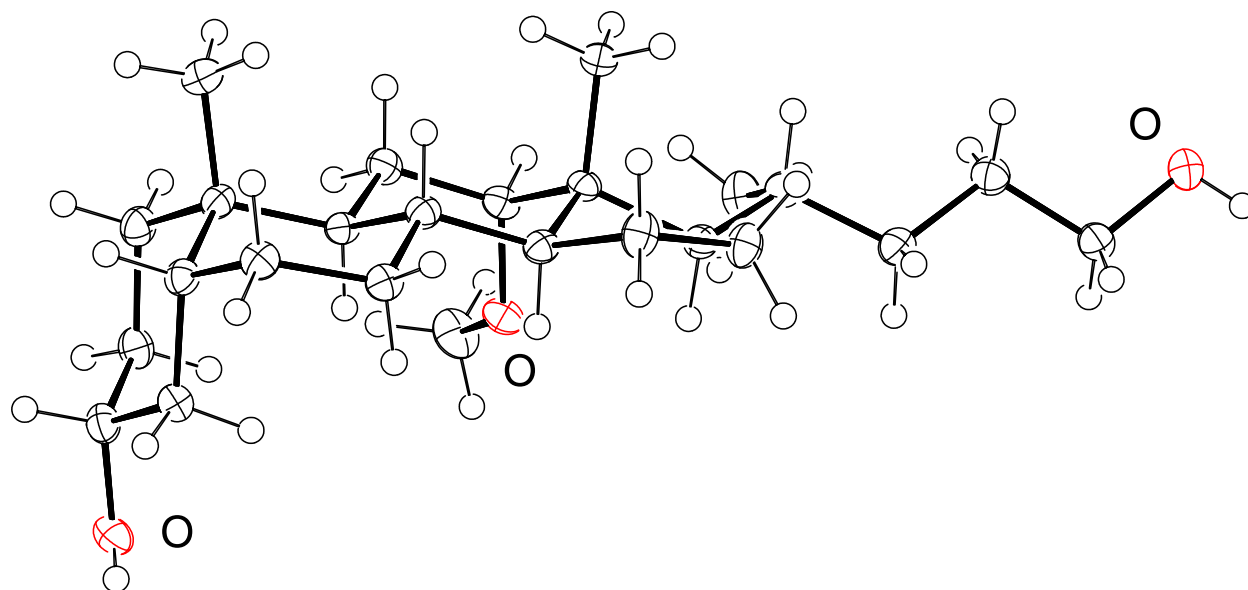


Figure S71. ORTEP diagram of **17a** shown at 50% probability.

Table S9. Crystal data and structure refinement for **18a**.

| | | |
|-----------------------------------|--|---------|
| Identification code | 18a | |
| Empirical formula | C ₂₅ H ₄₄ O ₂ | |
| Formula weight | 376.60 | |
| Temperature | 100.00(10) K | |
| Wavelength | 1.54184 Å | |
| Crystal system | Orthorhombic | |
| Space group | P2 ₁ 2 ₁ 2 | |
| Unit cell dimensions | a = 42.4084(4) Å | α = 90° |
| | b = 13.60510(10) Å | β = 90° |
| | c = 7.65680(10) Å | γ = 90° |
| Volume | 4417.75(8) Å ³ | |
| Z | 8 | |
| Density (calculated) | 1.132 Mg/m ³ | |
| Absorption coefficient | 0.522 mm ⁻¹ | |
| F(000) | 1680 | |
| Crystal size | 0.112 x 0.046 x 0.041 mm ³ | |
| Theta range for data collection | 3.412 to 73.422°. | |
| Index ranges | -47 ≤ h ≤ 51, -16 ≤ k ≤ 16, -9 ≤ l ≤ 9 | |
| Reflections collected | 42891 | |
| Independent reflections | 8833 [R(int) = 0.0344] | |
| Completeness to theta = 67.684° | 100.0 % | |
| Absorption correction | Gaussian | |
| Max. and min. transmission | 1.000 and 0.894 | |
| Refinement method | Full-matrix least-squares on F ² | |
| Data / restraints / parameters | 8833 / 0 / 555 | |
| Goodness-of-fit on F ² | 1.048 | |
| Final R indices [I > 2σ(I)] | R1 = 0.0338, wR2 = 0.0857 | |
| R indices (all data) | R1 = 0.0361, wR2 = 0.0871 | |
| Absolute structure parameter | 0.03(8) | |
| Extinction coefficient | n/a | |
| Largest diff. peak and hole | 0.187 and -0.128 e/Å ⁻³ | |

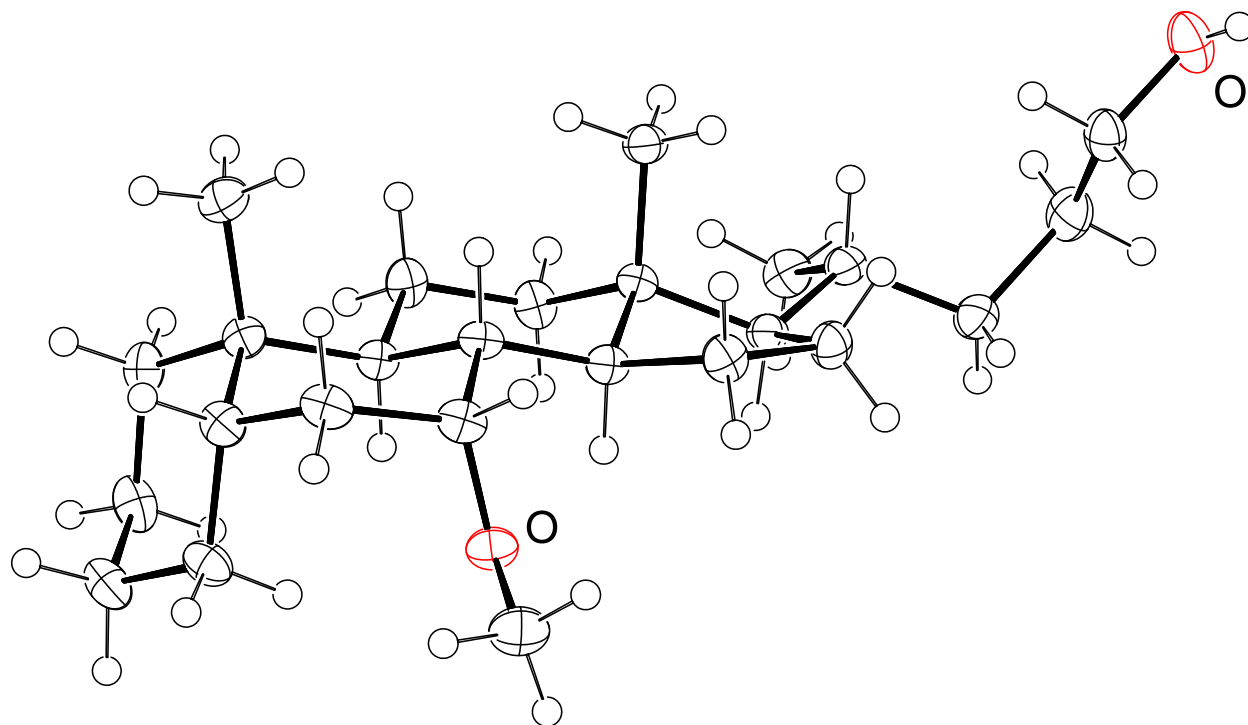


Figure S72. ORTEP diagram of **18a** shown at 50% probability. Additional molecules in the asymmetric unit and complete disorder model omitted for clarity.

Table S10. Crystal data and structure refinement for **20**.

| | | |
|-----------------------------------|--|---------|
| Identification code | 20 | |
| Empirical formula | C ₂₀ H ₂₈ O ₂ | |
| Formula weight | 300.42 | |
| Temperature | 100.01(10) K | |
| Wavelength | 1.54184 Å | |
| Crystal system | Orthorhombic | |
| Space group | P2 ₁ 2 ₁ 2 ₁ | |
| Unit cell dimensions | a = 7.77350(10) Å | α = 90° |
| | b = 12.29960(10) Å | β = 90° |
| | c = 16.91550(10) Å | γ = 90° |
| Volume | 1617.31(3) Å ³ | |
| Z | 4 | |
| Density (calculated) | 1.234 Mg/m ³ | |
| Absorption coefficient | 0.600 mm ⁻¹ | |
| F(000) | 656 | |
| Crystal size | 0.187 x 0.124 x 0.067 mm ³ | |
| Theta range for data collection | 4.445 to 73.469°. | |
| Index ranges | -9<=h<=6, -14<=k<=13, -20<=l<=20 | |
| Reflections collected | 9160 | |
| Independent reflections | 3188 [R(int) = 0.0250] | |
| Completeness to theta = 67.684° | 100.0 % | |
| Absorption correction | Gaussian | |
| Max. and min. transmission | 1.000 and 0.748 | |
| Refinement method | Full-matrix least-squares on F ² | |
| Data / restraints / parameters | 3188 / 0 / 202 | |
| Goodness-of-fit on F ² | 1.045 | |
| Final R indices [I>2sigma(I)] | R1 = 0.0307, wR2 = 0.0792 | |
| R indices (all data) | R1 = 0.0321, wR2 = 0.0804 | |
| Absolute structure parameter | 0.05(9) | |
| Extinction coefficient | n/a | |
| Largest diff. peak and hole | 0.227 and -0.173 e/Å ⁻³ | |

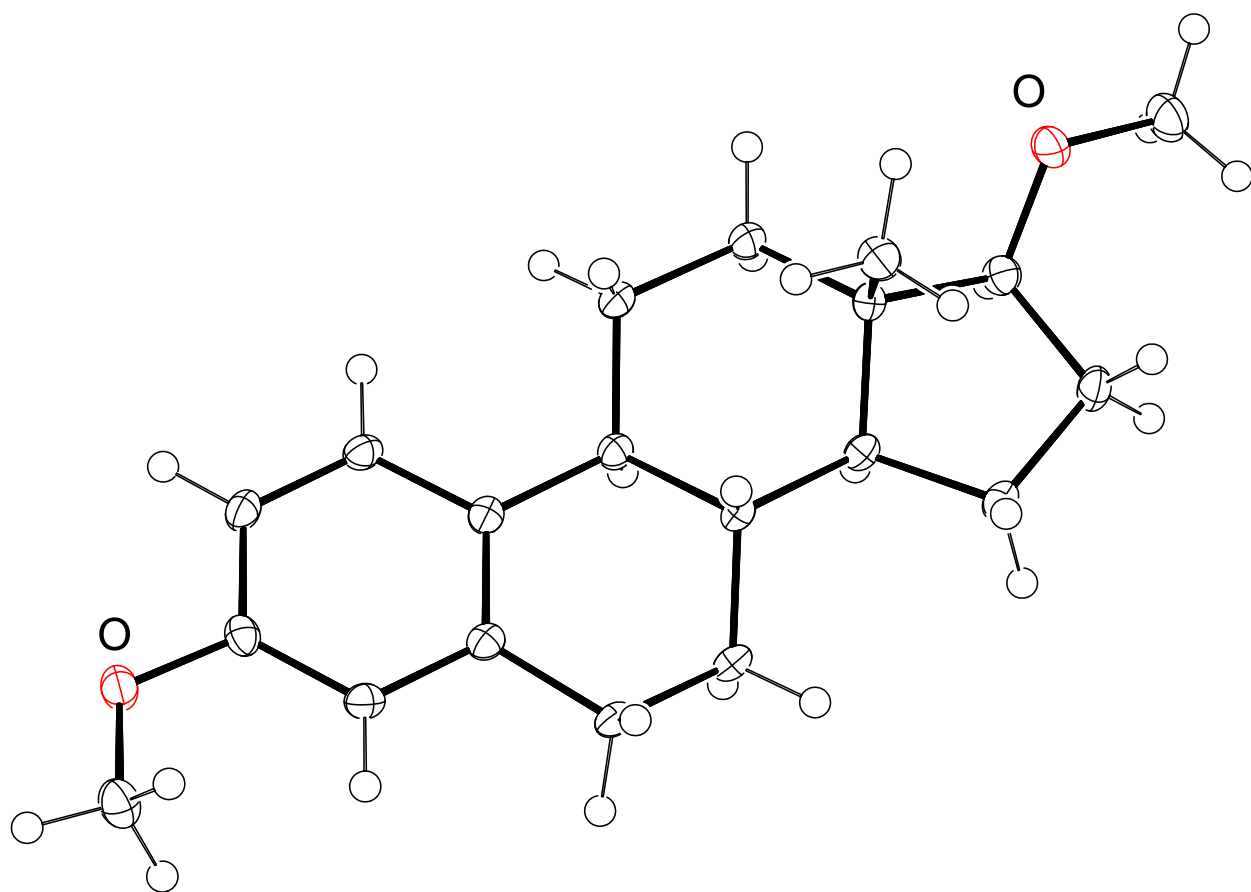


Figure S73. ORTEP diagram of **20** shown at 50% probability.

Table S11. Crystal data and structure refinement for **22a**.

| | | |
|-----------------------------------|---|-----------------|
| Identification code | 22a | |
| Empirical formula | C ₄₂ H ₄₉ IrP ₂ Si | |
| Formula weight | 836.04 | |
| Temperature | 99.97(10) K | |
| Wavelength | 1.54184 Å | |
| Crystal system | Monoclinic | |
| Space group | P 1 21/n 1 | |
| Unit cell dimensions | a = 11.88006(7) Å | α = 90° |
| | b = 21.74657(12) Å | β = 97.1277(6)° |
| | c = 14.12314(9) Å | γ = 90° |
| Volume | 3620.52(4) Å ³ | |
| Z | 4 | |
| Density (calculated) | 1.534 Mg/m ³ | |
| Absorption coefficient | 8.500 mm ⁻¹ | |
| F(000) | 1688 | |
| Crystal size | 0.131 x 0.108 x 0.023 mm ³ | |
| Theta range for data collection | 3.752 to 73.483°. | |
| Index ranges | -14 ≤ h ≤ 14, -26 ≤ k ≤ 27, -17 ≤ l ≤ 17 | |
| Reflections collected | 42723 | |
| Independent reflections | 7235 [R(int) = 0.0311] | |
| Completeness to theta = 67.684° | 100.0 % | |
| Absorption correction | Gaussian | |
| Max. and min. transmission | 0.938 and 0.397 | |
| Refinement method | Full-matrix least-squares on F ² | |
| Data / restraints / parameters | 7235 / 6 / 434 | |
| Goodness-of-fit on F ² | 1.044 | |
| Final R indices [I > 2σ(I)] | R1 = 0.0188, wR2 = 0.0462 | |
| R indices (all data) | R1 = 0.0195, wR2 = 0.0465 | |
| Extinction coefficient | n/a | |
| Largest diff. peak and hole | 0.895 and -0.823 e/Å ⁻³ | |

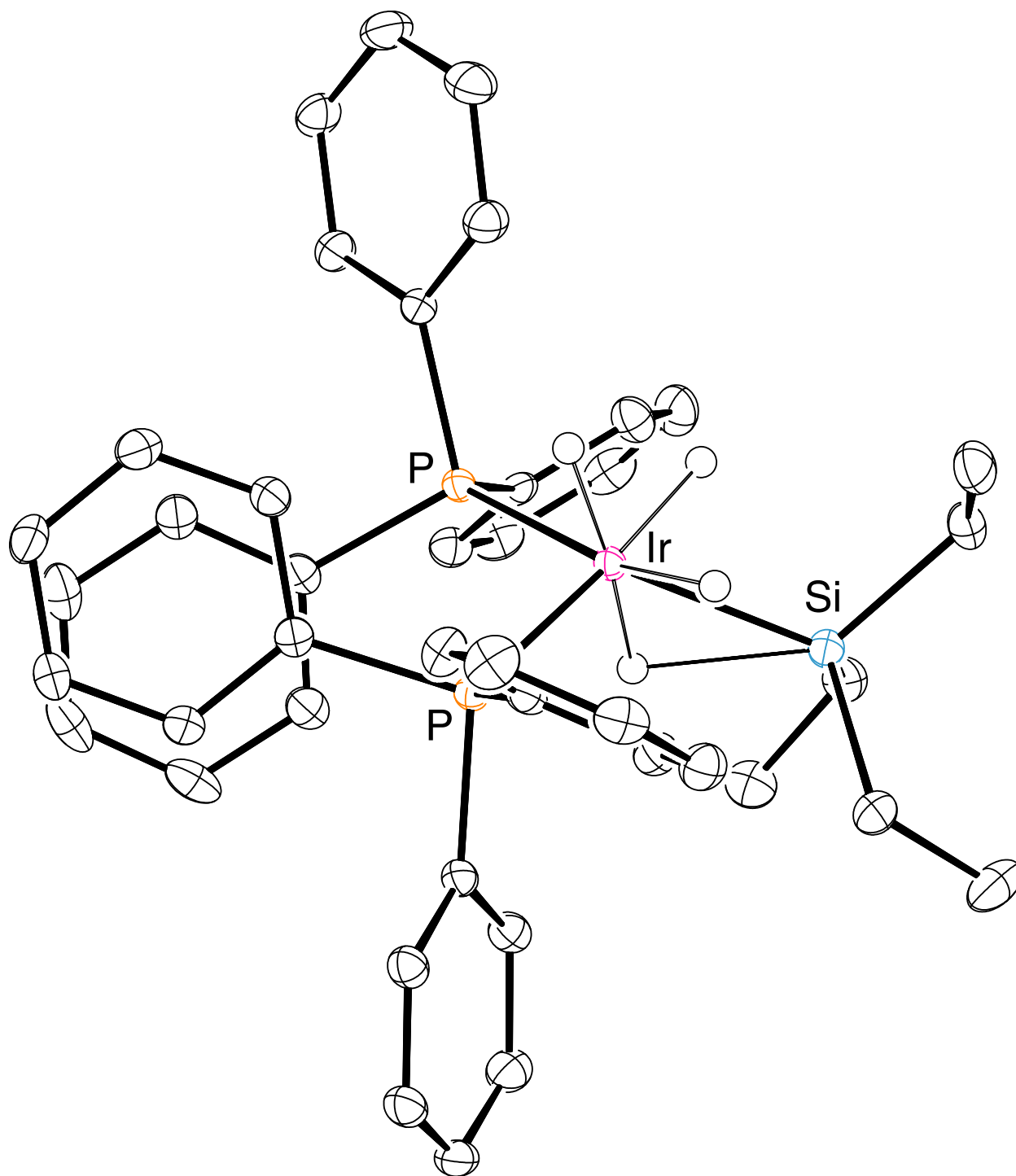


Figure S74. ORTEP diagram of **22a** shown at 50% probability.

Table S12. Crystal data and structure refinement for **23**.

| | | |
|-----------------------------------|--|----------------------------|
| Identification code | 23 | |
| Empirical formula | $C_{48}H_{23}F_{36}IrP_2$ | |
| Formula weight | 1537.80 | |
| Temperature | 100.1(6) K | |
| Wavelength | 1.54184 Å | |
| Crystal system | Triclinic | |
| Space group | P-1 | |
| Unit cell dimensions | $a = 12.3828(3)$ Å | $\alpha = 64.281(3)^\circ$ |
| | $b = 15.2107(5)$ Å | $\beta = 83.752(2)^\circ$ |
| | $c = 16.6665(5)$ Å | $\gamma = 70.114(3)^\circ$ |
| Volume | $2656.74(16)$ Å ³ | |
| Z | 2 | |
| Density (calculated) | 1.922 Mg/m ³ | |
| Absorption coefficient | 6.957 mm ⁻¹ | |
| F(000) | 1484 | |
| Crystal size | 0.058 x 0.05 x 0.006 mm ³ | |
| Theta range for data collection | 3.413 to 73.388°. | |
| Index ranges | $-15 \leq h \leq 12$, $-17 \leq k \leq 18$, $-20 \leq l \leq 20$ | |
| Reflections collected | 31423 | |
| Independent reflections | 10332 [R(int) = 0.0567] | |
| Completeness to theta = 67.684° | 98.8 % | |
| Absorption correction | Gaussian | |
| Max. and min. transmission | 0.983 and 0.706 | |
| Refinement method | Full-matrix least-squares on F ² | |
| Data / restraints / parameters | 10332 / 114 / 929 | |
| Goodness-of-fit on F ² | 1.027 | |
| Final R indices [I > 2σ(I)] | R1 = 0.0433, wR2 = 0.1008 | |
| R indices (all data) | R1 = 0.0605, wR2 = 0.1119 | |
| Extinction coefficient | n/a | |
| Largest diff. peak and hole | 1.733 and -1.212 e/Å ⁻³ | |

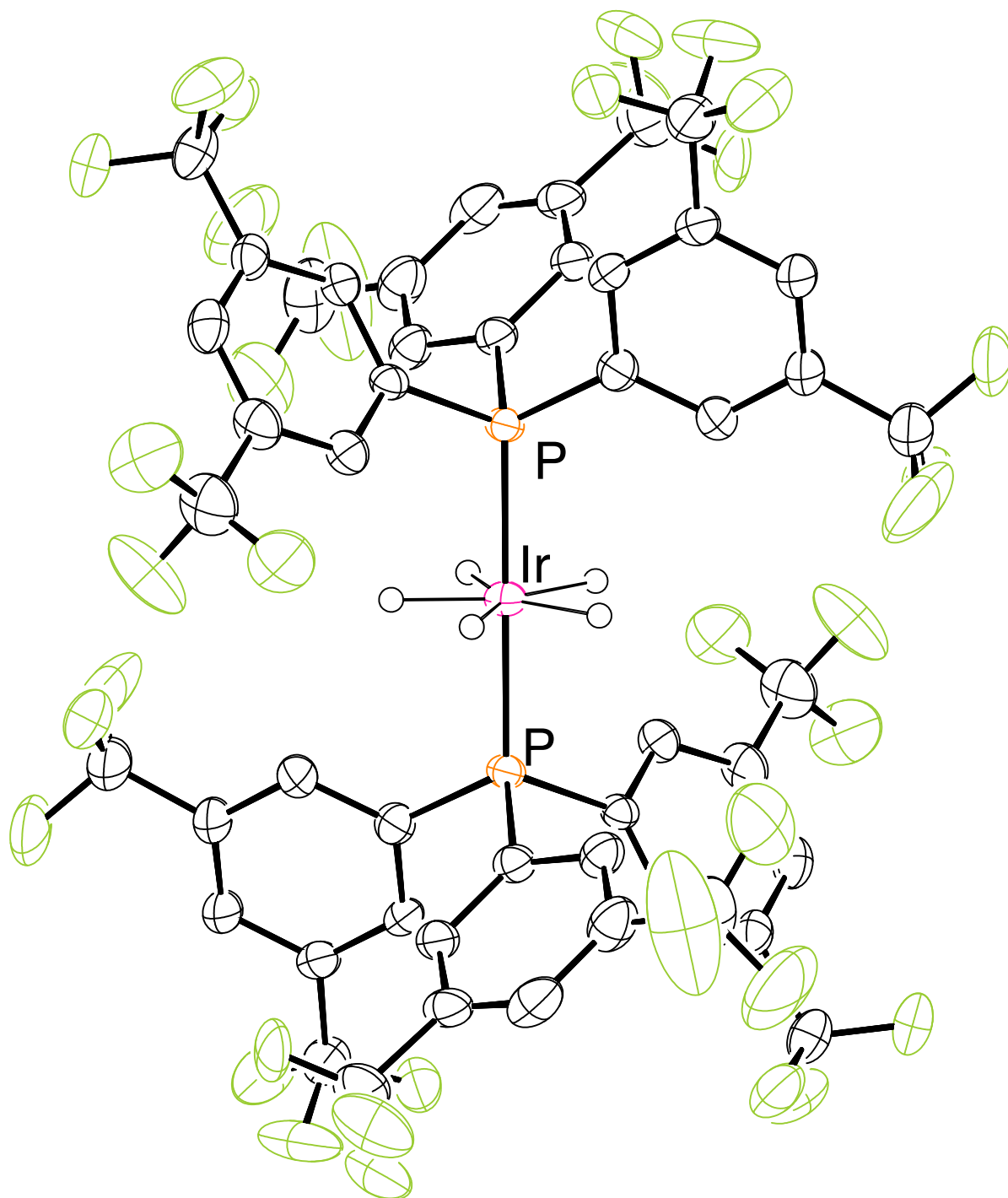


Figure S75. ORTEP diagram of **23** shown at 50% probability. Additional molecules in the asymmetric unit and complete disorder model omitted for clarity.

Table S13. Crystal data and structure refinement for **23a**.

| | | |
|-----------------------------------|---|-----------------|
| Identification code | 23a | |
| Empirical formula | C ₅₄ H ₃₇ F ₃₆ IrP ₂ Si | |
| Formula weight | 1652.06 | |
| Temperature | 100.01(10) K | |
| Wavelength | 0.71073 Å | |
| Crystal system | Triclinic | |
| Space group | P-1 | |
| Unit cell dimensions | a = 13.9408(4) Å | α = 102.527(3)° |
| | b = 14.1616(4) Å | β = 94.566(3)° |
| | c = 16.2996(5) Å | γ = 101.595(3)° |
| Volume | 3051.55(16) Å ³ | |
| Z | 2 | |
| Density (calculated) | 1.798 Mg/m ³ | |
| Absorption coefficient | 2.407 mm ⁻¹ | |
| F(000) | 1612 | |
| Crystal size | 0.255 x 0.214 x 0.184 mm ³ | |
| Theta range for data collection | 2.371 to 26.372°. | |
| Index ranges | -17 ≤ h ≤ 17, -17 ≤ k ≤ 17, -20 ≤ l ≤ 20 | |
| Reflections collected | 62109 | |
| Independent reflections | 12490 [R(int) = 0.0757] | |
| Completeness to theta = 25.242° | 99.9 % | |
| Absorption correction | Gaussian | |
| Max. and min. transmission | 1.000 and 0.599 | |
| Refinement method | Full-matrix least-squares on F ² | |
| Data / restraints / parameters | 12490 / 646 / 1054 | |
| Goodness-of-fit on F ² | 1.036 | |
| Final R indices [I > 2σ(I)] | R1 = 0.0373, wR2 = 0.0868 | |
| R indices (all data) | R1 = 0.0450, wR2 = 0.0912 | |
| Extinction coefficient | n/a | |
| Largest diff. peak and hole | 2.328 and -1.389 e/Å ⁻³ | |

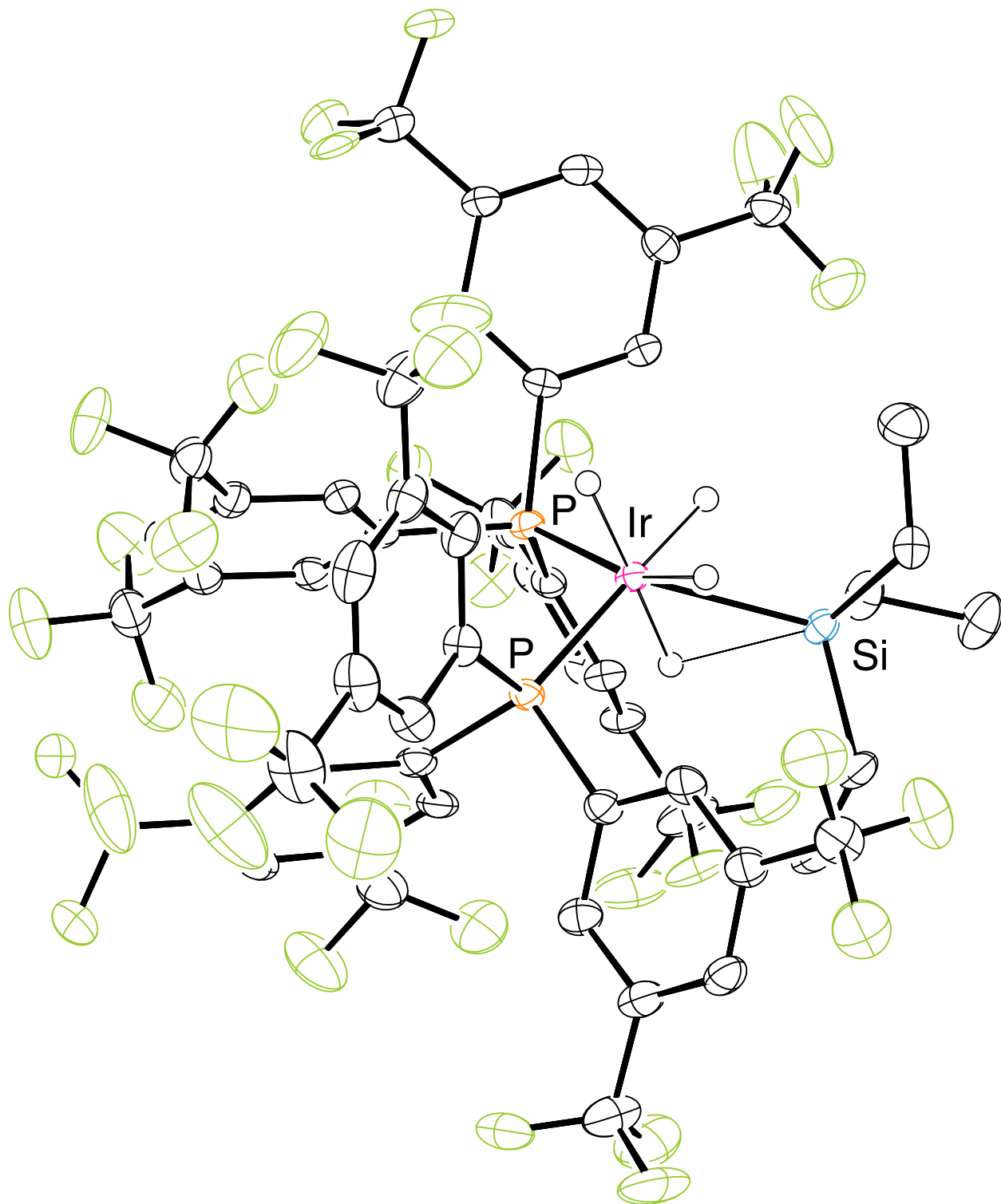


Figure S76. ORTEP diagram of **23a** shown at 50% probability. Complete disorder model omitted for clarity.

Table S14. Crystal data and structure refinement for **24**.

| | | |
|-----------------------------------|--|----------------|
| Identification code | 24 | |
| Empirical formula | C ₂₄ H ₁₈ F ₉ P | |
| Formula weight | 508.35 | |
| Temperature | 100.01(10) K | |
| Wavelength | 1.54184 Å | |
| Crystal system | Triclinic | |
| Space group | P-1 | |
| Unit cell dimensions | a = 9.2013(3) Å | α = 62.798(3)° |
| | b = 11.6473(3) Å | β = 76.382(2)° |
| | c = 12.4438(3) Å | γ = 76.134(2)° |
| Volume | 1139.23(6) Å ³ | |
| Z | 2 | |
| Density (calculated) | 1.482 Mg/m ³ | |
| Absorption coefficient | 1.849 mm ⁻¹ | |
| F(000) | 516 | |
| Crystal size | 0.209 x 0.097 x 0.059 mm ³ | |
| Theta range for data collection | 4.037 to 73.368°. | |
| Index ranges | -11 ≤ h ≤ 11, -14 ≤ k ≤ 14, -15 ≤ l ≤ 15 | |
| Reflections collected | 21511 | |
| Independent reflections | 4463 [R(int) = 0.0277] | |
| Completeness to theta = 67.684° | 98.7 % | |
| Absorption correction | Gaussian | |
| Max. and min. transmission | 1.000 and 0.782 | |
| Refinement method | Full-matrix least-squares on F ² | |
| Data / restraints / parameters | 4463 / 0 / 310 | |
| Goodness-of-fit on F ² | 1.070 | |
| Final R indices [I > 2σ(I)] | R1 = 0.0653, wR2 = 0.1666 | |
| R indices (all data) | R1 = 0.0708, wR2 = 0.1720 | |
| Extinction coefficient | n/a | |
| Largest diff. peak and hole | 1.473 and -0.879 e/Å ⁻³ | |

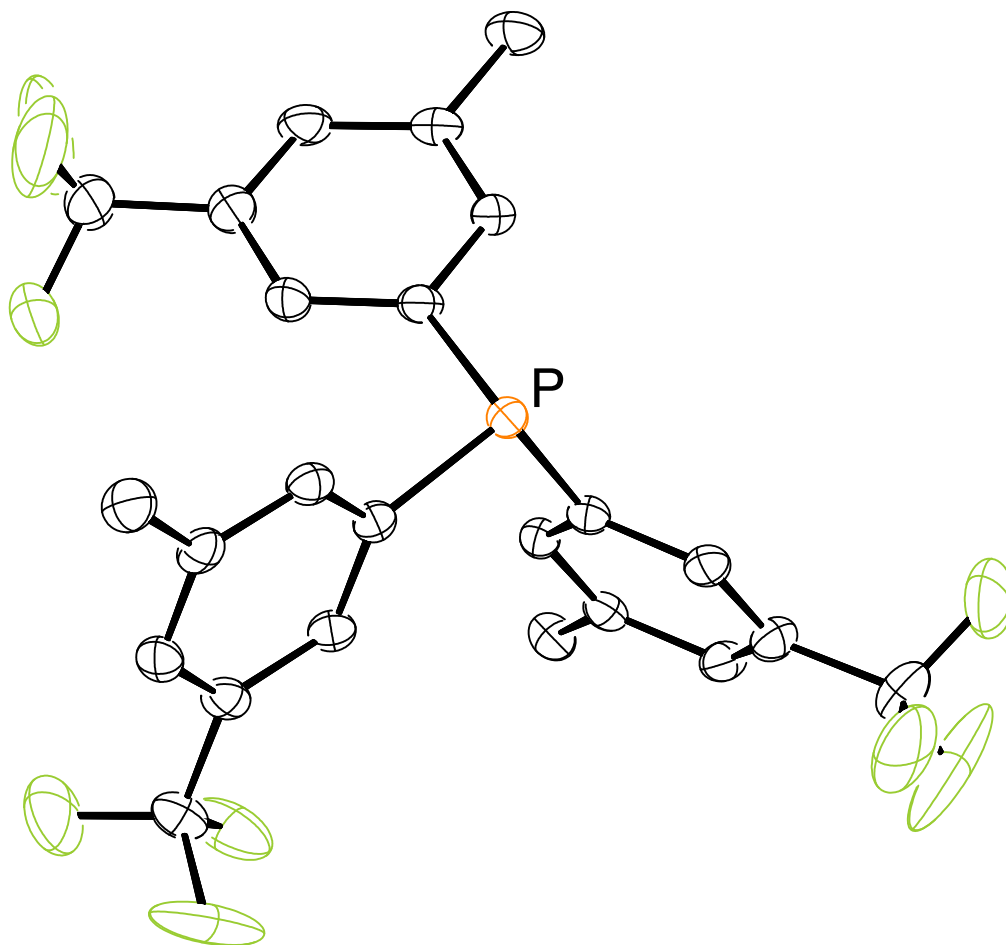


Figure S77. ORTEP diagram of **24** shown at 50% probability.

VII. References for Chapters 2 and 3 experimental

- (1) Herde, J. L.; Lambert, J. C.; Senoff, C. V.; Cushing, M. A. Cyclooctene and 1,5-Cyclooctadiene Complexes of Iridium(I). In *Inorganic Syntheses*; John Wiley & Sons, Ltd, 1974; pp 18–20.
- (2) Emerson-King, J.; Knighton, R. C.; Gyton, M. R.; Chaplin, A. B. Rotaxane Synthesis Exploiting the M(I)/M(III) Redox Couple. *Dalton Trans.* **2017**, 46 (35), 11645–11655.
- (3) Seven-Coordinate Iridium(V) Polyhydrides with Chelating Bis(silyl) Ligands | *Inorganic Chemistry*
- (4) Park, S. Un.; Chung, S. Kee.; Newcomb, Martin. Acceptor, Donor, and Captodative Stabilization in Transition States of 5-Hexen-1-Yl Radical Cyclizations. *J. Am. Chem. Soc.* **1986**, 108 (2), 240–244.
- (5) Shinohara, R.; Ogawa, N.; Kawashima, H.; Wada, K.; Saito, S.; Yamazaki, T.; Kobayashi, Y. Cover Feature: SN2 Reaction of Diarylmethyl Anions at Secondary Alkyl and Cycloalkyl Carbons (Eur. J. Org. Chem. 7/2019). *Eur. J. Org. Chem.* **2019**, 2019 (7), 1419–1419.
- (6) Booth, H.; Mark Dixon, J.; Khedhair, K. A.; Readshaw, S. A. Experimental Studies of the Anomeric Effect. Part III. Rotameric Preferences about the Exo-Cyclic C2-x Bond in Equatorial and Axial 2-Methoxy- and 2-Methylamino-Tetrahydropyrans. *Tetrahedron* **1990**, 46 (5), 1625–1652.
- (7) Sugandhi, E. W.; Slobodnick, C.; Falkinham, J. O.; Gandour, R. D. Synthesis and Antimicrobial Evaluation of Water-Soluble, Dendritic Derivatives of Epimeric 5 α -Cholestan-3-Amines and 5 α -Cholestan-3-Yl Aminoethanoates. *Steroids* **2007**, 72 (8), 615–626.

- (8) Dai, X.-J.; Li, C.-J. En Route to a Practical Primary Alcohol Deoxygenation. *J. Am. Chem. Soc.* **2016**, *138* (16), 5433–5440.
- (9) Malik, A. A.; Cormier, R. J.; Sharts, C. M. Selective Protection of the Side Chain Hydroxy Group in Bile Alcohol Derivatives. *Org. Prep. Proced. Int.* **1986**, *18* (5), 345–352.
- (10) Alexander, C.; Smith, C. R.; Whitcombe, M. J.; Vulfson, E. N. Imprinted Polymers as Protecting Groups for Regioselective Modification of Polyfunctional Substrates. *J. Am. Chem. Soc.* **1999**, *121* (28), 6640–6651.
- (11) Kim, S. J.; Bang, E.-K.; Kwon, H. J.; Shim, J. S.; Kim, B. H. Modified Oligonucleotides Containing Lithocholic Acid in Their Backbones: Their Enhanced Cellular Uptake and Their Mimicking of Hairpin Structures. *ChemBioChem* **2004**, *5* (11), 1517–1522.
- (12) Igarashi, T.; Haito, A.; Chatani, N.; Tobisu, M. Nickel-Catalyzed Reductive Cleavage of Carbon–Oxygen Bonds in Anisole Derivatives Using Diisopropylaminoborane. *ACS Catal.* **2018**, *8* (8), 7475–7483.
- (13) Lewis, J. C.; Mantovani, S. M.; Fu, Y.; Snow, C. D.; Komor, R. S.; Wong, C.-H.; Arnold, F. H. Combinatorial Alanine Substitution Enables Rapid Optimization of Cytochrome P450BM3 for Selective Hydroxylation of Large Substrates. *ChemBioChem* **2010**, *11* (18), 2502–2505.
- (14) Palladium on Carbon-Catalyzed Chemoselective Oxygen Oxidation of Aromatic Acetals | *Organic Letters*.
- (15) Kleinpeter, E.; Thielemann, J. Syntheses and Conformational Analyses of Mono- and Trans-1,4-Dialkoxy Substituted Cyclohexanes—the Steric Substituent/Skeleton Interactions. *Tetrahedron* **2007**, *63* (37), 9071–9081.

- (16) Eliel, E. L.; Krishnamurthy, S. The Products of Raney Nickel Desulfurization of Monothioketals. *J. Org. Chem.* **1965**, *30* (3), 848–854.
- (17) Ochiai, M.; Ito, T.; Takahashi, H.; Nakanishi, A.; Toyonari, M.; Sueda, T.; Goto, S.; Shiro, M. Hypervalent (Tert-Butylperoxy)Iodanes Generate Iodine-Centered Radicals at Room Temperature in Solution: Oxidation and Deprotection of Benzyl and Allyl Ethers, and Evidence for Generation of α -Oxy Carbon Radicals. *J. Am. Chem. Soc.* **1996**, *118*(33), 7716–7730.
- (18) Castelbou, J. L.; Gual, A.; Mercadé, E.; Claver, C.; Godard, C. Ligand Effect in the Rh-NP Catalysed Partial Hydrogenation of Substituted Arenes. *Catal. Sci. Technol.* **2013**, *3* (10), 2828–2833.
- (19) Gual, A.; Axet, M. R.; Philippot, K.; Chaudret, B.; Denicourt-Nowicki, A.; Roucoux, A.; Castillon, S.; Claver, C. Diphosphite Ligands Derived from Carbohydrates as Stabilizers for Ruthenium Nanoparticles: Promising Catalytic Systems in Arene Hydrogenation. *Chem. Commun.* **2008**, No. 24, 2759–2761.
- (20) de Oliveira, P. R.; Rittner, R. 1,3-Diaxial Steric Effects and Intramolecular Hydrogen Bonding in the Conformational Equilibria of New Cis-1,3-Disubstituted Cyclohexanes Using Low Temperature NMR Spectra and Theoretical Calculations. *Spectrochim. Acta. A. Mol. Biomol. Spectrosc.* **2005**, *62* (1), 30–37.
- (21) Rozen, S.; Dayan, S.; Bareket, Y. Oxidative Cleavage of Methyl Ethers Using the HOF.Cntdot.CH₃CN Complex. *J. Org. Chem.* **1995**, *60* (25), 8267–8269.
- (22) Kashman, Y. New Etherification Method. *J. Org. Chem.* **1972**, *37* (6), 912–914.
- (23) Lewis, J. R.; Shoppee, C. W. Steroids and Walden Inversion. Part XXIV. The Methylation of 3-Hydroxy-Steroids. *J. Chem. Soc. Resumed* **1955**, 1375.

- (24) Lawrence Woo, L. W.; Leblond, B.; Purohit, A.; Potter, B. V. L. Synthesis and Evaluation of Analogues of Estrone-3-O-Sulfamate as Potent Steroid Sulfatase Inhibitors. *Bioorg. Med. Chem.* **2012**, *20* (8), 2506–2519.
- (25) Seel, S.; Dagousset, G.; Thaler, T.; Frischmuth, A.; Karaghiosoff, K.; Zipse, H.; Knochel, P. Preparation of Stereodefined Secondary Alkylolithium Compounds. *Chem. – Eur. J.* **2013**, *19* (14), 4614–4622.
- (26) Jones, C. A. H.; Schley, N. D. Selective Alkyl Ether Cleavage by Cationic Bis(Phosphine)Iridium Complexes. *Org. Biomol. Chem.* **2018**.
- (27) Homogeneous catalysis of silane alcoholysis via nucleophilic attack by the alcohol on an Ir(η^2 -HSiR₃) intermediate catalyzed by [IrH₂S₂(PPh₃)₂]SbF₆ (S = solvent) | Journal of the American Chemical Society
- (28) Gaussian 09 Citation | Gaussian.com <https://gaussian.com/g09citation/>
- (29) Zhao, Y.; Truhlar, D. G. A New Local Density Functional for Main-Group Thermochemistry, Transition Metal Bonding, Thermochemical Kinetics, and Noncovalent Interactions. *J. Chem. Phys.* **2006**, *125* (19), 194101.
- (30) Weigend, F.; Ahlrichs, R. Balanced Basis Sets of Split Valence, Triple Zeta Valence and Quadruple Zeta Valence Quality for H to Rn: Design and Assessment of Accuracy. *Phys. Chem. Chem. Phys.* **2005**, *7* (18), 3297–3305.
- (31) Basis Set Exchange: A Community Database for Computational Sciences | Journal of Chemical Information and Modeling
- (32) Hanwell, M. D.; Curtis, D. E.; Lonie, D. C.; Vandermeersch, T.; Zurek, E.; Hutchison, G. R. Avogadro: An Advanced Semantic Chemical Editor, Visualization, and Analysis Platform. *J. Cheminformatics* **2012**, *4* (1), 17.

(33) Dolomanov, O. V.; Bourhis, L. J.; Gildea, R. J.; Howard, J. a. K.; Puschmann, H. OLEX2: A Complete Structure Solution, Refinement and Analysis Program. *J. Appl. Crystallogr.* **2009**, 42 (2), 339–341.

(34) (IUCr) A short history of SHELX
<https://onlinelibrary.wiley.com/iucr/doi/10.1107/S0108767307043930>

Chapter 4: Light-Promoted Transfer of an Iridium Hydride in Alkyl Ether Cleavage*

*Fast, C. D.; Jones, C. A. H.; Schley, N. D. Selectivity and Mechanism of Iridium-Catalyzed Cyclohexyl Methyl Ether Cleavage. *Organometallics*. **2021**, *40* (19), 3291-3297.

Copyright 2021 American Chemical Society

This chapter will highlight the application of illumination as an unusual alternative to synthetic modifications for tailoring selectivity in iridium-catalyzed ether silylation.

I. Introduction

Transition metal photochemistry has been a driving force behind the development of many modern photocatalytic methods for the transformation of organic substrates.¹⁻⁷ Photocatalytic transformations can be categorized based on the reactivity of the photoexcited species. In photoredox methods, the excited photocatalyst undergoes single-electron transfer (SET) with a reaction partner, with the resulting singly oxidized or reduced photocatalyst being regenerated in a subsequent SET step.⁸⁻¹² Another major class of photocatalytic processes take advantage of light-induced ligand dissociation or extrusion.¹³⁻²¹ Photoexcited transition metal complexes can also engage in two-electron bimolecular reactivity with substrates, though this class of transformations has seen very limited application to catalytic processes.

One example of bimolecular, apparently non-radical photochemistry can be found in the a class of $[\text{Cp}^*\text{IrH}(\text{bipyridine})]^+$ complexes which have been shown to undergo photoexcitation to give monohydride intermediates with significantly increased hydricity. Miller and coworkers have demonstrated a stoichiometric photo-induced hydride delivery with a nicotinamide derivative serving as the hydride acceptor in which they hypothesized that the photoexcited complex $[\text{Cp}^*\text{IrH}(\text{bipyridine})]^{+*}$ (excited state half-life $\tau = 80$ ns in MeCN)²² serves as an intermediate (Figure 4.1).²³ This system has also been applied in catalytic light-promoted H_2 evolution²⁴⁻²⁶ and in photo-induced hydrodechlorination, with a single example of catalytic hydrodechlorination

when CD_2Cl_2 solvent serves as the substrate.²⁷ Studies on H_2 evolution and hydrodechlorination by $[\text{Cp}^*\text{IrH}(\text{bipyridine})]^+$ are consistent with bimolecular self-quenching mechanisms in those cases,^{27,28} while a light-induced ligand dissociation is implicated in a related example of aqueous ketone reduction.⁷ The variety of light-promoted mechanisms apparently available to this family of complexes necessarily complicates studies of reaction mechanism, but also highlights the role that light can play in modifying catalyst reactivity.

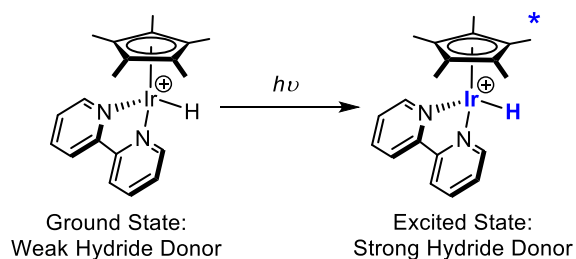


Figure 4.1. Role of light in modifying metal hydricity in $[\text{Cp}^*\text{IrH}(\text{bipyridine})]^+$ described by the Miller group.²³

The use of light to increase the hydricity of a catalytic intermediate would be an unusual strategy to modify the reactivity of existing catalyst systems. A related Cp^*Ir monohydride bearing a 2-phenylpyridine- $\kappa\text{C},\text{N}$ (ppy) ligand has been reported as a catalytic intermediate in alcohol dehydrosilylation catalysis.^{29,30} The similarity of the $[\text{Cp}^*\text{IrH}(\text{bipyridine})]^+$ photohydride system²⁷ to the light-free dehydrosilylation system reported for the phenylpyridine-derived variant²⁹ inspired an examination of the effect of light on hydrosilylative alkyl ether cleavage catalysis using the family of iridium complexes **1-3** (Figure 4.2). We now report a catalytic method for alkyl ether cleavage which appears to proceed via light-induced hydride transfer from an iridium complex to a silyloxonium ion generated in situ.

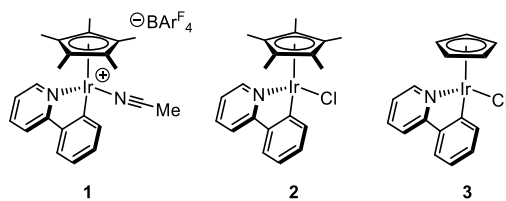
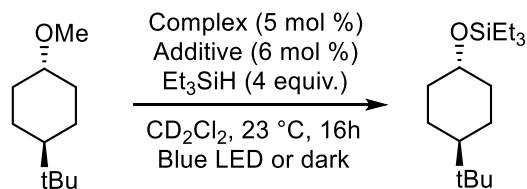


Figure 4.2. Iridium phenylpyridine complexes examined.

II. Catalytic Reaction Optimizations

Complex **1** is a reported catalyst for the dehydrosilylation of alcohols using triethylsilane in the absence of light.³⁰ The proposed mechanism for this transformation involves the intermediacy of a cationic σ silane complex that undergoes heterolytic Si-H cleavage followed by bimolecular reaction of the resulting hydride and oxonium ions in a second step.^{29,30} A closely-related mechanism is operative in hydrosilylative ether cleavage, a transformation with only a few reported catalysts comprised of either electron-deficient boranes^{31,32} or cationic iridium complexes.^{33–36} In the absence of light, **1** is a very poor catalyst for alkyl ether reduction, which we postulated might be due to the modest nucleophilicity of the hydride intermediate. Under blue-light irradiation however, **1** catalyzes the hydrosilylative demethylation of *trans*-4-(*t*-butyl)cyclohexyl methyl ether to the corresponding silyl ether in 43% yield (Table 4.1, entry 2).

Table 4.1. Identification of conditions for photochemical alkyl ether cleavage



| Entry | Complex | Additive | Light | Yield (%) |
|-------|---------|--------------------------------------|-------|-----------|
| 1 | 1 | - | - | 7 |
| 2 | 1 | - | Blue | 43 |
| 3 | 2 | - | Blue | 0 |
| 4 | 2 | NaBArF ₄ | Blue | 93 |
| 5 | 2 | [Ph ₃ C]BArF ₄ | Blue | 94 |
| 6 | 2 | NaBArF ₄ | - | 0 |
| 7 | 3 | NaBArF ₄ | Blue | 0 |

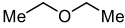
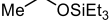
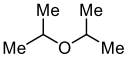
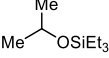
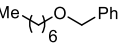
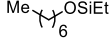

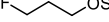
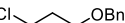
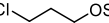

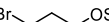

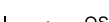
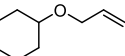
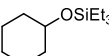
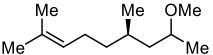
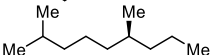
Further optimization of the reaction conditions demonstrated that the parent chloride compound **2** gives a more effective catalytic system in the presence of NaBArF₄, which presumably effects chloride abstraction to give cationic intermediates.^{37–39} These conditions allow for high yields with as little as 5 mol % **2**. Compound **2** is unreactive in the absence of NaBArF₄ (entries 3 & 4), which would be expected if the reaction proceeds via a similar cationic σ -silane intermediate to those previously reported for other ether cleavage catalysts.^{25,28,29} NaBArF₄ can be substituted by [Ph₃C][BArF₄] with similar catalytic performance (entry 5), but this reagent offers no clear benefit over the stable, commercially available sodium salt. The improved catalytic performance of the **2**/NaBArF₄ system over **1** is likely attributable to modest catalyst inhibition by the disilylamine byproduct of acetonitrile hydrosilylation reportedly formed by the reaction of **1** with triethylsilane.²⁹ The Cp* ligand is also required for activity, as compound **3** bearing the smaller

Cp ligand is inactive in hydrosilylative ether cleavage (entry 7). A more complete optimization screen can be found in the supplemental information.

III. Application of Optimized Conditions to a Broader Substrate Scope

The scope of photo-assisted hydrosilylative alkyl ether cleavage by **2**/NaBAr^F₄ was explored for a variety of symmetrical and unsymmetrical ethers (Table 4.2). Diethyl ether and diisopropyl ether show low reactivity in line with previous non light-promoted iridium catalysts.³³ A selection of alkyl benzyl ethers undergo debenzylation, with a primary alkyl chloride and bromide being tolerated. The corresponding iodide undergoes hydrodehalogenation, while the fluoride halts at partial conversion. The compatibility of primary alkyl chlorides and bromides with this hydrosilylative catalytic system contrasts the reported photochemical hydrodechlorination chemistry of [Cp*IrH(bipyridine)H]⁺, which likely occurs via a radical pathway.²⁷ The **2**/NaBAr^F₄ catalyst system also functions as a catalyst for hydrodechlorination of CD₂Cl₂ to CD₂HCl (9.3 TON), though this transformation need not involve the intermediacy of an alkyl radical under hydrosilylative conditions, as Brookhart has postulated that hydride transfer to a silyl halonium ion may be operative in a related case.⁴⁰ Cyclohexyl allyl ether undergoes selective deallylation, through the propene byproduct is not observed and is presumed to undergo hydrogenation under the reaction conditions (entry 8). As further evidence that olefins are not tolerated functionality, the reduction of a citronellol-derived secondary methyl ether gives the saturated product of demethoxylation and hydrogenation (entry 9), a limitation also observed in previous iridium systems that do not require light.^{33,36}

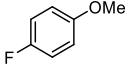
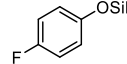
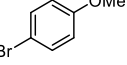
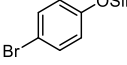
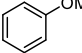
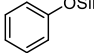
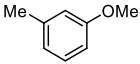
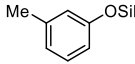
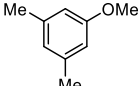
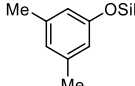
Table 4.2. Hydrosilylative alkyl ether cleavage by **2**/NaBAr^F₄

| | | | |
|--|---|--|-----|
| $ \text{R}_1\text{-O-R}_2 \xrightarrow[\text{CD}_2\text{Cl}_2, 23^\circ\text{C}, 16\text{h}, \text{Blue LED}]{\text{Complex } \mathbf{2} \text{ (5 mol \%)} \\ \text{NaBAr}^{\text{F}}_4 \text{ (6 mol \%)} \\ \text{Et}_3\text{SiH (4 equiv.)}} \text{R}_1\text{-O-SiEt}_3 \quad \text{H-R}_2 $ | | | |
| 1 |  |  | 21% |
| 2 |  |  | 9% |
| 3 |  |  | 75% |
| 4 |  |  | 25% |
| 5 |  |  | 68% |
| 6 |  |  | 88% |
| 7 |  |  | - |
| 8 |  |  | 87% |
| 9 |  |  | 58% |

In comparison to dialkyl ethers, anisole derivatives proved to be relatively challenging substrates for this system. The reactivity of the selection of anisoles shown in Table 4.3 appears to track with the electron-richness of the arene, with 4-F, 4-Br, and the parent anisole showing poor reactivity under our conditions. The more electron-rich methyl and dimethyl anisoles (Table 4.3, entries 4 and 5) do undergo demethylation to varying degrees, suggesting a role for the basicity of the ether in controlling their reactivity. A comparable trend has not been described for other anisole hydrosilylation catalysts, though both the borane catalyst $\text{B}(\text{C}_6\text{F}_5)_3$ ³¹ and Brookhart's catalyst³⁶ are effective for hydrosilylative anisole demethylation at room temperature. In all cases in Table 4.3, the balance of the reaction is the unconverted starting material.

Table 4.3. Hydrosilylative anisole demethylation by **2**/NaBAR^F₄

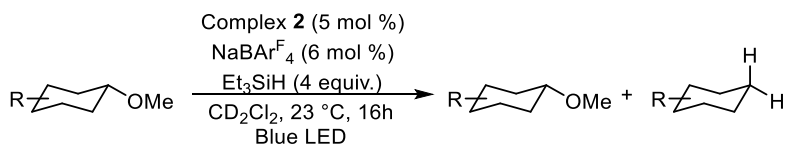
Complex **2** (5 mol %)
 NaBAR^F₄ (6 mol %)
 Et₃SiH (4 equiv.)
 Ar-OMe $\xrightarrow{\hspace{1.5cm}}$ Ar-OSiEt₃
 CD₂Cl₂, 23 °C, 16h
 Blue LED

| Entry | Substrate | Product | NMR Yield |
|-------|---|---|-----------|
| 1 |  |  | 0% |
| 2 |  |  | 8% |
| 3 |  |  | 16% |
| 4 |  |  | 50% |
| 5 |  |  | 84% |

In a previous report on iridium-catalyzed hydrosilylative ether cleavage, we interrogated the selectivity obtained for an array of cyclohexyl methyl ethers using [(cod)Ir(PPh₃)₂]BAR^F₄ as a precatalyst.³⁴ In that case, we observed that the selectivity for demethylation versus 2° C-O cleavage depended on conformational factors, and showed that selectivity was correlated with the computationally predicted conformational preferences of the substrate triethylsilyloxonium ions. Substrates with strong preferences for the silyloxonium group in the equatorial conformation ($E_{ax}-E_{eq} > 4$ kcal·mol⁻¹) underwent preferential demethylation, while substrates predicted to have greater populations in the axial conformation underwent selective demethoxylation, with the switch in reactivity being ascribed to the relative rates of S_N2 demethylation versus S_N1 demethoxylation. A similar trend is observed here using the light-assisted **2**/NaBAR^F₄ system (Table 4.4). Substrates previously predicted³⁴ to have highly positive $E_{ax}-E_{eq}$ values undergo

selective demethylation (entries 1 and 2), while *cis*-4-(*t*-butyl)cyclohexyl methyl ether undergoes preferential cleavage at the secondary position. (entry 4)

Table 4.4. Cyclohexyl methyl ether cleavage by **2**/NaBAr^F₄

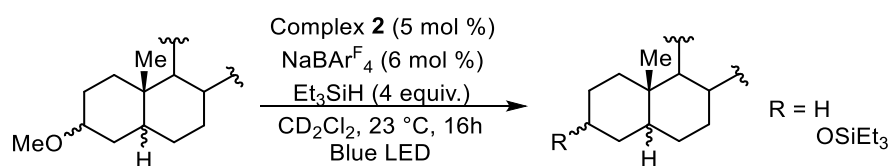


| Entry | Substrate | Product(s) | E_{ax-} E_{eq}^a | Yield ^c |
|----------------|-----------|------------|-------------------------|--------------------|
| 1 | | | 11.3 | 93% |
| 2 | | | 10.7 | 58% |
| 3 | | | 4.9 | 74%:10% |
| 4 ^b | | | -0.6 | 74% |

Further similarities between this system and the previously reported bis(phosphine)iridium system can be found by examination of hydrosilylative ether cleavage in sterol-derived substrates. The A-ring methyl ethers in β - and α -methyl cholestanol are conformationally fixed in equatorial and axial dispositions respectively (Table 4.5, entries 1 and 2). The equatorial substrate (entry 1) undergoes catalytic demethylation with **2**/NaBAr^F₄, while the axial substrate undergoes demethoxylation. The cholic acid derivative in entries 3 and 4 undergo selective demethylation and demethoxylation of the A-ring methoxy groups respectively with **2**/NaBAr^F₄. This same selectivity was previously observed for the hydrosilylative ether cleavage catalyst

$[(\text{cod})\text{Ir}(\text{PPh}_3)_2]\text{BAr}^{\text{F}_4}$ and was ascribed to conformation effects resulting from substitution of the B ring.³⁴ In total, the conformational factors that influence selectivity in cyclohexyl ether cleavage using **2**/ $\text{NaBAr}^{\text{F}_4}$ are essentially identical to those observed for $[(\text{cod})\text{Ir}(\text{PPh}_3)_2]\text{BAr}^{\text{F}_4}$.³⁴ The principal factors distinguishing **2**/ $\text{NaBAr}^{\text{F}_4}$ from $[(\text{cod})\text{Ir}(\text{PPh}_3)_2]\text{BAr}^{\text{F}_4}$ are therefore the necessity of light and the requirement for somewhat higher catalyst loading of **2** versus $[(\text{cod})\text{Ir}(\text{PPh}_3)_2]\text{BAr}^{\text{F}_4}$.^{33,34}

Table 4.5. Sterol methyl ether cleavage by **2**/ $\text{NaBAr}^{\text{F}_4}$



| Entry | Substrate | Product | Yield |
|----------------|-----------|---------|-------|
| 1 | | | 79% |
| 2 ^a | | | 54% |
| 3 | | | 39% |
| 4 | | | 80% |

IV. Reaction Mechanism Studies

The similar conformational influences on selectivity observed for light-promoted hydrosilylative alkyl ether cleavage with **2**/ $\text{NaBAr}^{\text{F}_4}$ and the thermal bis(phosphine)iridium systems strongly imply mechanistic similarities between the two systems. A proposed mechanism

for the light-promoted hydrosilylative cleavage of alkyl ethers by **2**/NaBAR^F₄, is given in Figure 4.3.

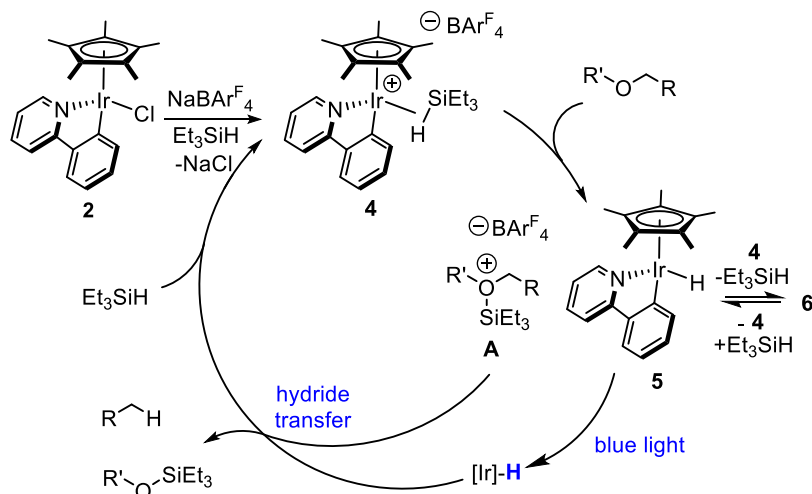
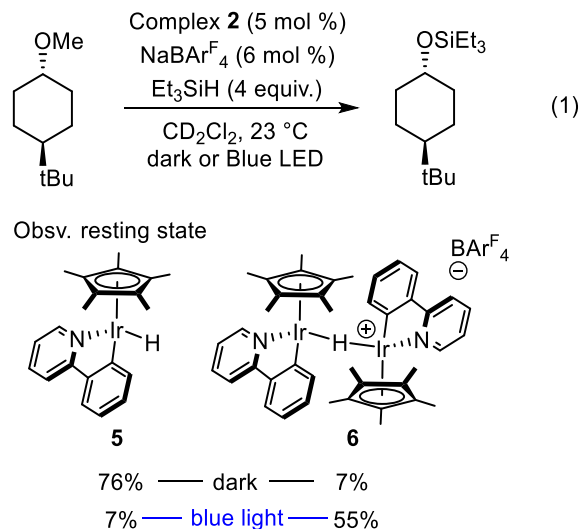


Figure 4.3. Proposed mechanism for catalytic ether cleavage via photochemical hydride transfer to silyloxonium ions.

This proposal is inspired by work on related systems which operate without light,^{23,30,33–36,41} as well as the reported photochemical behavior of the bipyridine-supported iridium hydride reported by Miller. Complex **2** likely reacts with NaBAR^F₂₄ and triethylsilane to form an electrophilic σ-silane complex **4** that has been previously characterized by Djukic and coworkers under relevant alcohol dehydrosilylation conditions.²⁹ **4** transfers an equivalent of triethylsilylium ion to substrate ether to give the neutral monohydride complex Cp*Ir(ppy)H (**5**) and an equivalent of silyloxonium ion (**A**). Since visible light absorption is necessary for efficient catalytic turnover, we hypothesize photoexcitation of complex **5** give a more nucleophilic hydride complex which reacts with silyloxonium ion **A** by delivery of the hydride.



Scheme 4.1: Resting state analysis of 2/NaBARF₄ under catalytic conditions.

Aspects of the proposal in Figure 4.3 can be tested experimentally. First, we examined the metal complexes which are formed under catalytic conditions in the absence of illumination (eqn. 1). Under these conditions no catalytic turnover is observed and **5** is detected as the major Ir-containing product by ¹H NMR. The same species is observed after illumination for 20 minutes (*ca.* 1.4 TON), though a second complex **6** represents the major metal-containing species at this point. The identity of **5** was confirmed by comparison of the upfield region of the ¹H NMR spectrum of the dark reaction to the hydride resonance of independently synthesized **5**. The second, major species is the known monocationic dimer **6** formed by capture of **5** by an equivalent of [Cp*Ir(ppy)]BARF₄. Complexes **5** and **6** have been reported to exist in equilibrium during catalytic dehydrosilylation of alcohols,^{29,30} and so their observation here is consistent with the operation of a related mechanism. The visible absorbance spectrum of **5** overlaps well with the 34W H150 Blue LED Lamp used under catalytic conditions. (Figure 4).

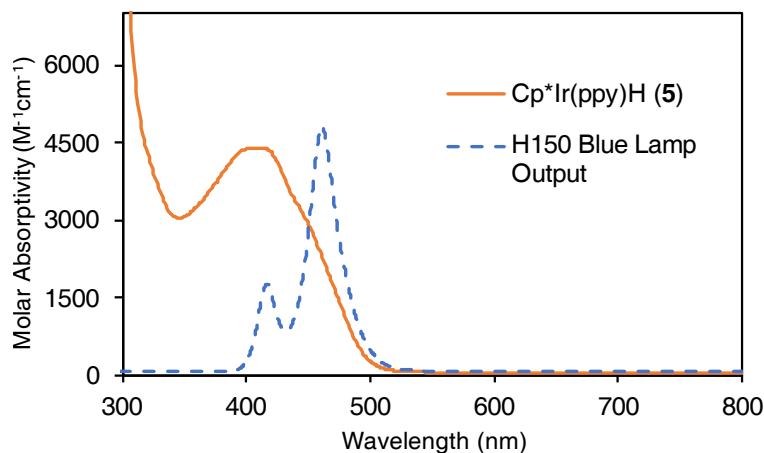
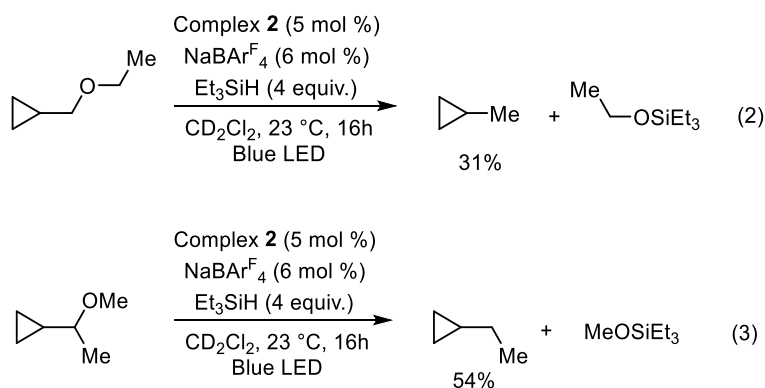


Figure 4.4. Comparison of absorbance spectrum of **5** with the output of the commercial 34W H150 Blue LED Lamp used in this study.

Evidence that C-O bond scission occurs via a non-radical mechanism can be obtained through the analysis of the fate of substrates containing fast radical clocks. The cyclopropyl alkyl ether substrates cyclopropylmethyl ethyl ether and (1-methoxyethyl)cyclopropane were selected to examine the mechanism for primary and secondary alkyl ether cleavage respectively.



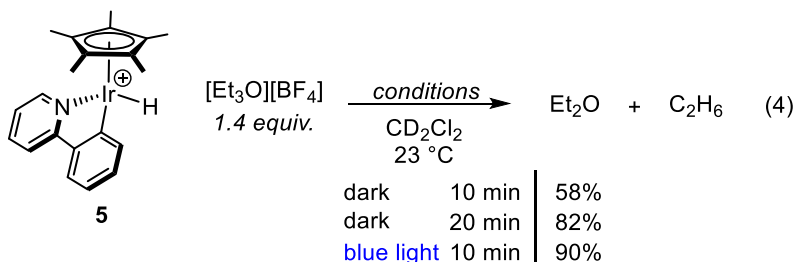
Scheme 4.2: Cleavage of cyclopropyl-type substrates under catalytic conditions.

Light-promoted hydrosilylative ether cleavage of cyclopropylmethyl ethyl ether produces methylcyclopropane in 31% yield with the cyclopropyl ring intact (eqn. 2). The balance of the substrate is converted to (cyclopropylmethoxy)triethylsilane via cleavage of the unsymmetrical ether at the ethyl group. As the cyclopropylmethyl radical has a reported rate of ring opening of 1

* 10^8 s^{-1} , the lack of observed products of ring opening is inconsistent with a long-lived alkyl radical intermediate.⁴² Reduction of (1-methoxyethyl)cyclopropane gives cyclopropyl ethane as the only observed product of secondary C-O cleavage in 54% yield (eqn. 3). The reported rate for ring opening of the 1-cyclopropylethyl radical is $4 * 10^7 \text{ s}^{-1}$.⁴² Together, these observations argue for a non-radical mechanism for light-promoted hydrosilylative ether cleavage in this case, an outcome consistent with the 2-electron proposal in Figure 3. That said, the fast radical clocks selected for this analysis only allow us to rule out the intermediacy of cyclopropylmethyl radicals with lifetimes on the order of their intramolecular ring-opening rates, and not, for instance, the intermediacy of odd-electron metal-containing species. This limitation is potentially significant since Miller has found that light-promoted hydrodehalogenation of chloroalkanes by $[\text{Cp}^*\text{Ir}(\text{bipyridine})\text{H}]^+$ likely proceeds via bimolecular quenching of the photoexcited catalyst and the involvement of short-lived alkyl radical intermediates.²⁷ In the case of catalysis by **2**/ $\text{NaBAr}^{\text{F}_4}$, SET reduction of silyloxonium ion intermediates is very unlikely to give the selectivity observed for substrates in Tables 4.4 and 4.5, which has been previously rationalized in the context of competitive $\text{S}_{\text{N}}1$ and $\text{S}_{\text{N}}2$ processes.³⁴

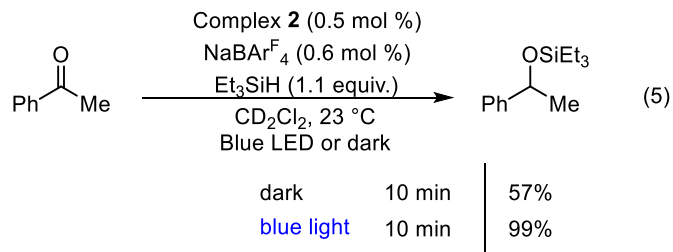
The observation that **2**/ $\text{NaBAr}^{\text{F}_4}$ catalyzes the hydrosilylation of carbonyl derivatives^{38,39} and dehydrosilylation of alcohols²⁹ in the dark, but does not catalyze hydrosilylative ether cleavage in the absence of light can be interpreted in the context of the relative reactivity of the plausible reaction intermediates. These three transformations share similar mechanisms, with heterolytic Si-H cleavage giving silyloxycarbenium,^{37,38} and mono-²⁹ and dialkyl silyloxonium^{33,34,40} ions respectively. Our observation that the catalyst resting state after illumination is a mixture of the neutral monohydride complex **5** and the dimeric monohydride **6** is consistent with a catalytic cycle resting at the silyloxonium/**5** reactant pair (with **5** in equilibrium with **6**). Absorption of a blue

photon is presumably required to enable C-O bond cleavage via nucleophilic attack on the silyloxonium ion, and thus catalyst turnover. This hypothesis can be tested in stoichiometric fashion by examining the reaction of Cp*Ir(ppy)H (**5**) with the closely-related triethyloxonium electrophile. In the dark, Cp*Ir(ppy)H reacts at a moderate rate with [Et₃O][BF₄] to produce ethane and diethyl ether, achieving 58% conversion with respect to Et₂O formation after 10 minutes, and reaching 82% after 20 minutes. In contrast, the same transformation proceeds more-rapidly under irradiation with blue light, leading to near-quantitative (90%) ethane formation in just 10 minutes.



Scheme 4.3: Reduction of a triethyloxonium ion by **5**.

A final piece of evidence in support of the photohydride hypothesis for **5** can be obtained by examining the role of light in related catalytic transformations where **5** serves as an intermediate. When acetophenone is subjected to hydrosilylation by **2**/NaBAR^F₄ in the dark, complex **5** is observed as the catalyst resting state by ¹H NMR spectroscopy. Although the reaction is relatively fast in the absence of light, a significant rate enhancement is observed under illumination. Catalytic acetophenone hydrosilylation subjected to blue light is complete within 10 minutes, while at the same point the corresponding dark reaction has only reached 57% yield (eqn. 5).⁴⁸ Although both 1-⁴³ and 2-electron light-induced reactivity is known for Cp*Ir monohydride complexes, the balance of our catalytic and stoichiometric observations argue for the role of light in modulating the nucleophilicity of iridium hydride complex **5** or a closely-related species.



Scheme 4.4: Reduction of acetophenone under dark and illuminated condition.

V. Conclusions

In summary, the hydrosilylative cleavage of alkyl ethers by **2**/NaBAR^F₄ has been demonstrated to occur via a light-promoted path. Experiments support a mechanism where the iridium complex [Cp*Ir(ppy)H] (**5**) or a related complex serves as a hydride source for the C-O cleavage of an alkyl ether-derived silyloxonium ion after light absorption. Selectivity trends in the cleavage of unsymmetrical alkyl ethers align with a previous non-photochemical system shown to result from competitive S_N1 and S_N2 reduction of silyloxonium ion intermediates. The identity of the two species observed as the catalyst resting state have been confirmed by NMR experiments. Lack of ring-opening observed for a pair of cyclopropyl substrates argue against a 1 e⁻ pathway for C-O bond scission involving alkyl radical intermediates, providing further evidence for a polar, 2 e⁻ mechanism involving heterolytic Si-H cleavage followed by hydride delivery in a subsequent step. Apparently increased hydride nucleophilicity under illumination also manifests in stoichiometric oxonium ion reduction and in acetophenone hydrosilylation, a related catalytic transformation that shares the same catalyst resting state. This system is a rare example of photohydride transfer chemistry in a catalytic application to organic synthesis.

VI. References

- (1) Prier, C. K.; Rankic, D. A.; MacMillan, D. W. C., Visible Light Photoredox Catalysis with Transition Metal Complexes: Applications in Organic Synthesis. *Chem. Rev.* **2013**, *113*, 5322-5363.
- (2) Narayanam, J. M. R.; Stephenson, C. R. J. Visible Light Photoredox Catalysis: Applications in Organic Synthesis. *Chem. Soc. Rev.* **2010**, *40* (1), 102–113.
- (3) Crisenza, G. E. M.; Melchiorre, P. Chemistry Glows Green with Photoredox Catalysis. *Nat. Commun.* **2020**, *11* (1), 803.
- (4) Twilton, J.; Le, C. (Chip); Zhang, P.; Shaw, M. H.; Evans, R. W.; MacMillan, D. W. C. The Merger of Transition Metal and Photocatalysis. *Nat. Rev. Chem.* **2017**, *1* (7), 1–19.
- (5) Romero, N. A.; Nicewicz, D. A., Organic Photoredox Catalysis. *Chem. Rev.* **2016**, *116*, 10075-10166.
- (6) Cheng, W.-M.; Shang, R. Transition Metal-Catalyzed Organic Reactions under Visible Light: Recent Developments and Future Perspectives. *ACS Catal.* **2020**, *10* (16), 9170–9196.
- (7) Kaphan, D. M.; Brereton, K. R.; Klet, R. C.; Witzke, R. J.; Miller, A. J. M.; Mulfort, K. L.; Delferro, M.; Tiede, D. M. Photocatalytic Transfer Hydrogenation in Water: Insight into Mechanism and Catalyst Speciation. *Organometallics* **2021**, *40* (10), 1482–1491.
- (8) Kalyanasundaram, K. Photophysics, Photochemistry and Solar Energy Conversion with Tris(Bipyridyl)Ruthenium(II) and Its Analogues. *Coord. Chem. Rev.* **1982**, *46*, 159–244.
- (9) Wagenknecht, P. S.; Ford, P. C. Metal Centered Ligand Field Excited States: Their Roles in the Design and Performance of Transition Metal Based Photochemical Molecular Devices. *Coord. Chem. Rev.* **2011**, *255* (5), 591–616.

- (10) Scaltrito, D. V.; Thompson, D. W.; O'Callaghan, J. A.; Meyer, G. J. MLCT Excited States of Cuprous Bis-Phenanthroline Coordination Compounds. *Coord. Chem. Rev.* **2000**, *208* (1), 243–266.
- (11) Arias-Rotondo, D. M.; McCusker, J. K. The Photophysics of Photoredox Catalysis: A Roadmap for Catalyst Design. *Chem. Soc. Rev.* **2016**, *45* (21), 5803–5820.
- (12) Eum, M.-S.; Chin, C. S.; Kim, S. yi; Kim, C.; Kang, S. K.; Hur, N. H.; Seo, J. H.; Kim, G. Y.; Kim, Y. K. Ligand Effects on Luminescence of New Type Blue Light-Emitting Mono(2-Phenylpyridinato)Iridium(III) Complexes. *Inorg. Chem.* **2008**, *47* (14), 6289–6295.
- (13) Johnson, C. E.; Fisher, B. J.; Eisenberg, R. Stereoselectivity and Kinetic Control of Hydrogen Oxidative Addition to Iridium(I) Complexes. *J. Am. Chem. Soc.* **1983**, *105* (26), 7772–7774.
- (14) Kunin, A. J.; Eisenberg, Richard. Photochemical Carbonylation of Benzene by Iridium(I) and Rhodium(I) Square-Planar Complexes. *J. Am. Chem. Soc.* **1986**, *108* (3), 535–536.
- (15) Maguire, J. A.; Boese, W. T.; Goldman, A. S., Photochemical dehydrogenation of alkanes catalyzed by trans-carbonylchlorobis(trimethylphosphine)rhodium: aspects of selectivity and mechanism. *J. Am. Chem. Soc.* **2002**, *111*, 7088-7093.
- (16) Choi, J.-C.; Sakakura, T. Oxidative Addition of C–H Bonds to RhCl(PMe₃)₃: Relevant to the Catalytic Transformation of Hydrocarbons. *J. Am. Chem. Soc.* **2003**, *125* (26), 7762–7763.
- (17) Rosini, G. P.; Boese, W. T.; Goldman, A. S. Study of the Mechanism of Photochemical Carbonylation of Benzene Catalyzed by Rh(PMe₃)₂(CO)Cl. *J. Am. Chem. Soc.* **1994**, *116* (21), 9498–9505.

- (18) Chen, H.; Hartwig, J. F., Catalytic, Regiospecific End-Functionalization of Alkanes: Rhenium-Catalyzed Borylation under Photochemical Conditions. *Angew. Chem. Int. Ed.* **1999**, *38*, 3391-3393.
- (19) Chapp, S. M.; Schley, N. D. Group-Transfer Reactions of a Cationic Iridium Alkoxycarbene Generated by Ether Dehydrogenation. *Inorg. Chem.* **2020**, *59* (10), 7143–7149.
- (20) Whited, M. T.; Grubbs, R. H. Late Metal Carbene Complexes Generated by Multiple C–H Activations: Examining the Continuum of M=C Bond Reactivity. *Acc. Chem. Res.* **2009**, *42* (10), 1607–1616.
- (21) Burk, M. J.; Crabtree, R. H.; McGrath, D. V. Thermal and Photochemical Catalytic Dehydrogenation of Alkanes with $[\text{IrH}_2(\text{CF}_3\text{CO}_2)(\text{PR}_3)_2]$ (R = C₆H₄F-p and Cyclohexyl). *J. Chem. Soc. Chem. Commun.* **1985**, No. 24, 1829–1830.
- (22) Ziesel, R. Photocatalysis. Mechanistic Studies of Homogeneous Photochemical Water Gas Shift Reaction Catalyzed under Mild Conditions by Novel Cationic Iridium(III) Complexes. *J. Am. Chem. Soc.* **1993**, *115* (1), 118–127.
- (23) Barrett, S. M.; Pitman, C. L.; Walden, A. G.; Miller, A. J. M. Photoswitchable Hydride Transfer from Iridium to 1-Methylnicotinamide Rationalized by Thermochemical Cycles. *J. Am. Chem. Soc.* **2014**, *136* (42), 14718–14721.
- (24) Pitman, C. L.; Miller, A. J. M., Molecular Photoelectrocatalysts for Visible Light-Driven Hydrogen Evolution from Neutral Water. *ACS Catalysis* **2014**, *4*, 2727-2733.
- (25) Barrett, S. M.; Slattery, S. A.; Miller, A. J. M. Photochemical Formic Acid Dehydrogenation by Iridium Complexes: Understanding Mechanism and Overcoming Deactivation. *ACS Catal.* **2015**, *5* (11), 6320–6327.

- (26) Brereton, K. R.; Bonn, A. G.; Miller, A. J. M. Molecular Photoelectrocatalysts for Light-Driven Hydrogen Production. *ACS Energy Lett.* **2018**, *3* (5), 1128–1136.
- (27) Barrett, S. M.; Stratakes, B. M.; Chambers, M. B.; Kurtz, D. A.; Pitman, C. L.; Dempsey, J. L.; Miller, A. J. M. Mechanistic Basis for Tuning Iridium Hydride Photochemistry from H₂ Evolution to Hydride Transfer Hydrodechlorination. *Chem. Sci.* **2020**, *11* (25), 6442–6449.
- (28) Chambers, M. B.; Kurtz, D. A.; Pitman, C. L.; Brennaman, M. K.; Miller, A. J. M. Efficient Photochemical Dihydrogen Generation Initiated by a Bimetallic Self-Quenching Mechanism. *J. Am. Chem. Soc.* **2016**, *138* (41), 13509–13512.
- (29) Hamdaoui, M.; Ney, M.; Sarda, V.; Karmazin, L.; Bailly, C.; Sieffert, N.; Dohm, S.; Hansen, A.; Grimme, S.; Djukic, J.-P., Evidence of a Donor–Acceptor (Ir–H)→SiR₃ Interaction in a Trapped Ir(III) Silane Catalytic Intermediate. *Organometallics* **2016**, *35*, 2207–2223.
- (30) Hamdaoui, M.; Desrousseaux, C.; Habbita, H.; Djukic, J.-P. Iridacycles as Catalysts for the Autotandem Conversion of Nitriles into Amines by Hydrosilylation: Experimental Investigation and Scope. *Organometallics* **2017**, *36* (24), 4864–4882.
- (31) Gevorgyan, V.; Liu, J.-X.; Rubin, M.; Benson, S.; Yamamoto, Y. A Novel Reduction of Alcohols and Ethers with a HSiEt₃catalytic B(C₆F₅)₃ System. *Tetrahedron Lett.* **1999**, *40* (50), 8919–8922.
- (32) Gevorgyan, V.; Rubin, M.; Benson, S.; Liu, J.-X.; Yamamoto, Y. A Novel B(C₆F₅)₃-Catalyzed Reduction of Alcohols and Cleavage of Aryl and Alkyl Ethers with Hydrosilanes. *J. Org. Chem.* **2000**, *65* (19), 6179–6186.
- (33) Jones, C. A. H.; Schley, N. D., Selective alkyl ether cleavage by cationic bis(phosphine)iridium complexes. *Organic & Biomolecular Chemistry* **2019**, *17*, 1744–1748.

- (34) Fast, C. D.; Jones, C. A. H.; Schley, N. D. Selectivity and Mechanism of Iridium-Catalyzed Cyclohexyl Methyl Ether Cleavage. *ACS Catal.* **2020**, *10* (11), 6450–6456.
- (35) Jones, C. A. H.; Schley, N. D., Selective demethylation of O-aryl glycosides by iridium-catalyzed hydrosilylation. *Chem. Commun.* **2021**, *57*, 5953-5956.
- (36) Yang, J.; White, P. S.; Brookhart, M. Scope and Mechanism of the Iridium-Catalyzed Cleavage of Alkyl Ethers with Triethylsilane. *J. Am. Chem. Soc.* **2008**, *130* (51), 17509–17518.
- (37) Corre, Y.; Rysak, V.; Trivelli, X.; Agbossou-Niedercorn, F.; Michon, C. A Versatile Iridium(III) Metallacycle Catalyst for the Effective Hydrosilylation of Carbonyl and Carboxylic Acid Derivatives. *Eur. J. Org. Chem.* **2017**, *2017* (32), 4820–4826.
- (38) Corre, Y.; Rysak, V.; Capet, F.; Djukic, J.-P.; Agbossou-Niedercorn, F.; Michon, C., Selective Hydrosilylation of Esters to Aldehydes Catalysed by Iridium(III) Metallacycles through Trapping of Transient Silyl Cations. *Chemistry - A European Journal* **2016**, *22*, 14036-14041.
- (39) Corre, Y.; Iali, W.; Hamdaoui, M.; Trivelli, X.; Djukic, J.-P.; Agbossou-Niedercorn, F.; Michon, C. Efficient Hydrosilylation of Imines Using Catalysts Based on Iridium(III) Metallacycles. *Catal. Sci. Technol.* **2015**, *5* (3), 1452–1458.
- (40) Yang, J.; Brookhart, M. Iridium-Catalyzed Reduction of Alkyl Halides by Triethylsilane. *J. Am. Chem. Soc.* **2007**, *129* (42), 12656–12657.
- (41) Robert, T.; Oestreich, M. Si-H Bond Activation: Bridging Lewis Acid Catalysis with Brookhart's Iridium(III) Pincer Complex and B(C₆F₅)₃. *Angew. Chem. Int. Ed.* **2013**, *52* (20), 5216–5218.

- (42) Newcomb, M. Competition Methods and Scales for Alkyl Radical Reaction Kinetics. *Tetrahedron* **1993**, *49* (6), 1151–1176.
- (43) Schreier, M. R.; Pfund, B.; Guo, X.; Wenger, O. S. Photo-Triggered Hydrogen Atom Transfer from an Iridium Hydride Complex to Unactivated Olefins. *Chem. Sci.* **2020**.

VII. Appendix for Chapter 4

I. General Information

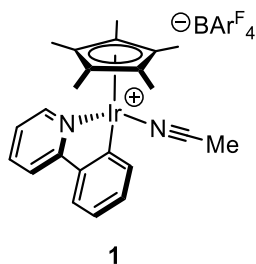
General Considerations. Syntheses, manipulations, and catalytic reactions with organometallic reagents were carried out using standard vacuum, Schlenk, cannula, or glovebox techniques under N₂ unless otherwise specified. Tetrahydrofuran, dichloromethane, toluene, pentane, and diethyl ether were degassed with argon and dried over activated alumina using a solvent purification system. The following chemicals were purchased from chemical vendors and used as received: IrCl₃·H₂O, 1,2,3,4,5-pentamethylcyclopenta-1,3-diene, 2-phenylpyridine, 2,2'-bipyridine, sodium-cyclopentadienide (2.0 M in THF), NaOAc·3H₂O, and Red-Al®.

Spectroscopy. ¹H and ¹³C{¹H} NMR spectra were recorded on Bruker NMR spectrometers at ambient temperatures unless otherwise noted. ¹H and ¹³C{¹H} chemical shifts are referenced to residual solvent signals. UV-Vis spectra were collected using a JASCO V-670 Spectrophotometer.

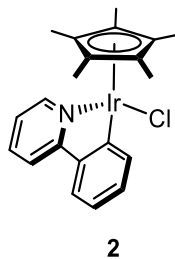
Elemental Analysis. Elemental analyses are of bulk samples for which yields are reported. No additional purification operations are carried out prior to packaging for analysis, but samples are dried under vacuum for *ca.* 2 days to remove residual or co-crystallized solvent. Elemental analyses were performed Atlantic Microlab.

II. Synthesis and Characterization

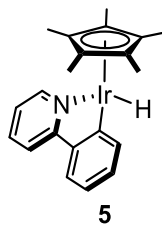
$[(\eta^2\text{-cyclooctene})_2\text{IrCl}]_2$,¹ $[\text{Cp}^*\text{IrCl}_2]_2$,² sodium tetrakis[3,5-bis(trifluoromethyl)phenyl]borate ($\text{NaBAr}^{\text{F}_4}$),³ and $[\text{Ph}_3\text{C}][\text{BAr}^{\text{F}_4}]$ ⁴ were prepared by published procedures.



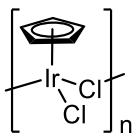
$[\text{Cp}^*\text{Ir}(\text{ppy})(\text{MeCN})]\text{BAr}^{\text{F}_4}$ (**1**). This compound was prepared by a reported method.⁵



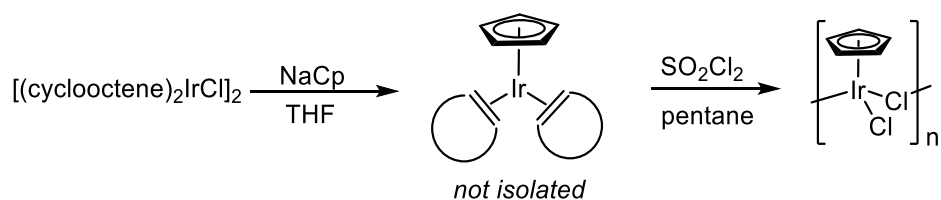
$\text{Cp}^*\text{Ir}(\text{ppy})\text{Cl}$ (**2**). This compound was prepared by a reported method.⁶



$\text{Cp}^*\text{Ir}(\text{ppy})\text{H}$ (**5**). This compound was prepared by a reported method.⁷



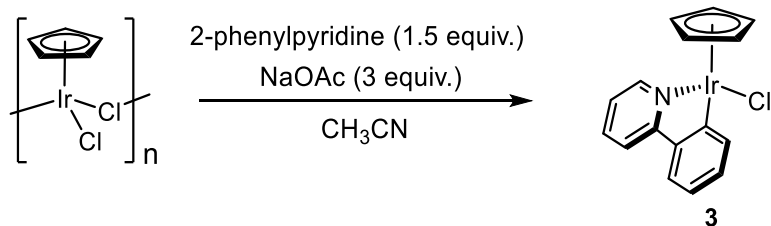
[CpIrCl₂]_n. This compound has been previously reported via oxidation of CpIr(C₂H₄)₂ with anhydrous HCl⁸ or Cl₂.⁹ We have developed a simplified procedure given below. This variation has been employed prior to its publication here.¹⁰



[CpIrCl₂]_n. A flame-dried 100 mL Schlenk flask was charged with [(η^2 -cyclooctene)₂IrCl]₂ (0.911 g, 1.02 mmol) and 40 mL dry, degassed THF under nitrogen. A solution of NaCp in THF (2.0 M, 1.1 mL) was then added dropwise over two minutes at room temperature. The reaction flask was heated to 45 °C for one hour, cooled to room temperature, and evaporated to dryness under vacuum. 90 mL degassed pentane was added and the resulting suspension was stirred 30 minutes. The supernatant was transferred to a round bottom flask under nitrogen by means of a filter cannula, and neat sulfonyl chloride (0.67 mL, 8.3 mmol) was then added dropwise over five minutes. After an additional five minutes the solution was allowed to settle and the product was collected by vacuum filtration in air. Yield: 0.514 g (77%). The product is insoluble in most solvents, but dissolves slowly in acetonitrile to form the adduct CpIrCl₂(MeCN). Crystal samples of CpIrCl₂(MeCN) were obtained by cooling a warm MeCN solution.

¹H NMR (400 MHz, CD₃CN) δ 5.74 (s).

¹³C{¹H} NMR (126 MHz, CD₃CN) δ 76.95.



CpIrCl(2-phenylpyridine- κ C,N) (3) – A 10 mL Schlenk flask was charged with NaOAc·3H₂O (0.0482 g, 0.354 mmol), and [CpIrCl₂]_n (0.0582 g, 0.117 mmol) in 5 mL degassed MeCN, and neat 2-phenylpyridine (0.026 mL, 0.18 mmol) was then added. The flask was heated to 70 °C under nitrogen for 5 h, then the flask was cooled and the solvent removed *in-vacuo*. The residue was extracted with 12 mL CH₂Cl₂ and then filtered through a pad of anhydrous Na₂SO₄ in air. The filtrate was reduced to 3 mL on a rotary evaporator and then treated with 20 mL heptane. The suspension was chilled in an ice bath and then filtered to afford an orange microcrystalline solid which was washed with heptane and dried *in-vacuo*. Yield: 0.0549 g (69%). Crystal samples of **3** were grown by layering a saturated dichloromethane solution with diethyl ether at -10 °C.

¹H NMR (400 MHz, CD₂Cl₂) δ 9.16 (m, 1H), 7.96 (m, 1H), 7.87 (d, *J* = 8.1 Hz, 1H), 7.75 (td, *J* = 7.6, 1.6 Hz, 2H), 7.15 – 7.02 (m, 3H), 5.48 (s, 5H).

¹³C NMR (126 MHz, CD₂Cl₂) δ 167.29, 156.93, 156.73, 145.12, 138.69, 138.19, 130.65, 125.19, 123.00, 122.92, 119.73, 79.88.

Calcd for C₁₆H₁₃ClIrN: C, 43.00; H, 2.93; N, 3.13. Found: C, 42.90; H, 2.82; N, 3.17.

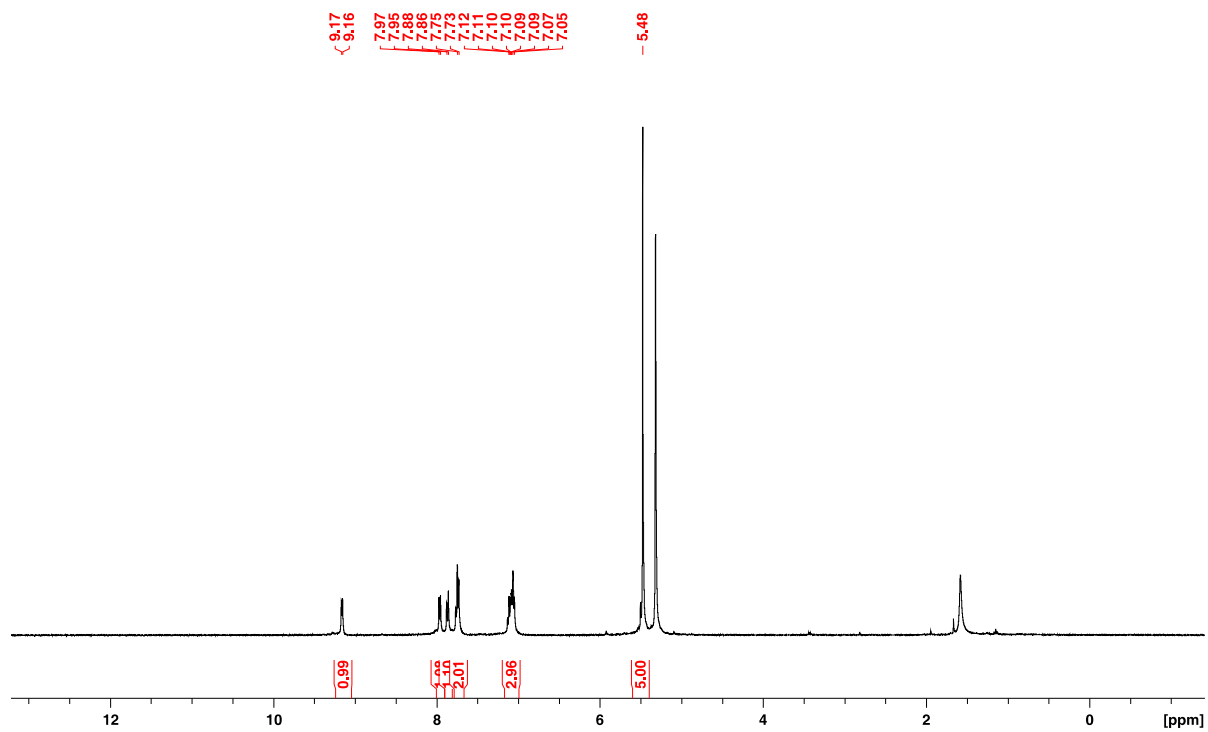


Figure S1. ^1H NMR of $\text{CpIrCl}(2\text{-phenylpyridine-}\kappa\text{C},\text{N})$ (**3**) in CD_2Cl_2 at $23\text{ }^\circ\text{C}$

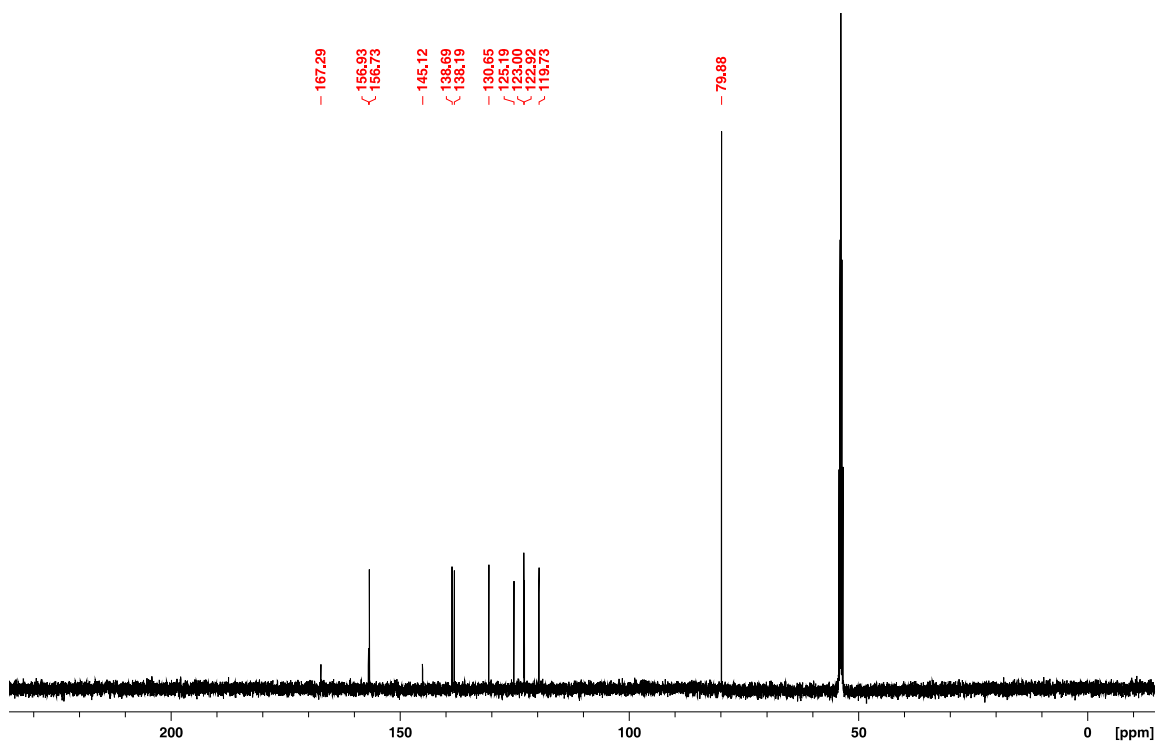
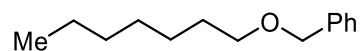
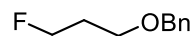


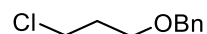
Figure S2. $^{13}\text{C}\{^1\text{H}\}$ NMR of $\text{CpIrCl}(2\text{-phenylpyridine-}\kappa\text{C},\text{N})$ (**3**) in CD_2Cl_2 at $23\text{ }^\circ\text{C}$



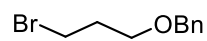
Benzyl 7-oxoheptanoate (*Table 2, Entry 3*): This compound was synthesized by a reported method.¹¹



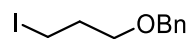
3-Benzyl 3-fluoropropanoate (*Table 2, Entry 4*): This compound was synthesized by a reported method.¹²



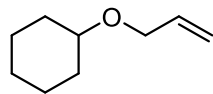
3-Benzyl 3-chloropropanoate (*Table 2, Entry 5*): This known compound was prepared according to a reported method.¹²



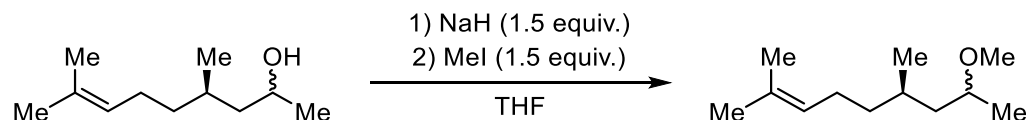
3-Benzyl 3-bromopropanoate (*Table 2, Entry 6*): This known compound was prepared according to a reported method.¹²



3-Benzyl 3-iodopropanoate (*Table 2, Entry 7*): This known compound was prepared according to a reported method.¹²



(allyloxy)cyclohexane (*Table 2, Entry 8*): This known compound was prepared according to a reported method.¹³



(6R)-8-methoxy-2,6-dimethylnon-2-ene (Table 2, Entry 9): A flame-dried 150 mL Schlenk flask was charged with NaH (0.3010g, 12.54 mmol, 1.5 equiv.) in an inert atmosphere glove box. The vessel was then brought outside of the box and attached to a nitrogen Schlenk line. Dry THF (30 mL) was added to give a suspension which was cooled to 0 °C. (4R)-4,8-dimethylnon-7-en-2-ol¹⁴ (1.424 g, 8.36 mmol) in a solution in dry THF (20 mL) was added dropwise over the course of 1 hour and allowed to stir at 0 °C for an additional hour. Maintaining a 0 °C reaction temperature, MeI (1.7784 g, 12.54 mmol, 0.78 mL, 1.5 equiv.) was added dropwise over the course of 1 hour. The reaction was slowly quenched with saturated aqueous NH₄Cl and was diluted with water until all solid is dissolved (*ca.* 50 mL). The aqueous solution was extracted with three, 150 mL portions of EtOAc and washed with two, 100 mL portions of water followed by three, 100 mL portions of brine. The resulting organic layer was dried over Na₂SO₄ and filtered. The solution was concentrated under vacuum and the residue was purified on silica gel using 40% EtOAc/Hexanes as eluent to the product as a colorless oil. Yield: 1.1429 g (74%).

¹H NMR (400 MHz, CDCl₃) δ 5.10 (tt, *J* = 7.1, 1.3 Hz, 1H), 3.36 (sext, *J* = 5.9 Hz, 1H), 3.31 (s, 3H), 1.98 (m, 2H), 1.68 (s, 3H), 1.60 (s, 3H), 1.52, (sep, *J* = 6.7, 1H), 1.46 – 1.38 (m, 1H), 1.38 – 1.24 (m, 2H), 1.21 – 1.12 (m, 1H), 1.11 (d, *J* = 5.9 Hz, 3H), 0.88 (d, *J* = 6.5 Hz, 3H).

¹³C NMR (101 MHz, CDCl₃) δ 131.29, 124.99, 75.37, 56.00, 44.13, 37.47, 29.48, 25.85, 25.55, 20.02, 19.28, 17.78.

EI-MS calculated for C₁₂H₂₄O: 184.1827, Measured: 184.2.

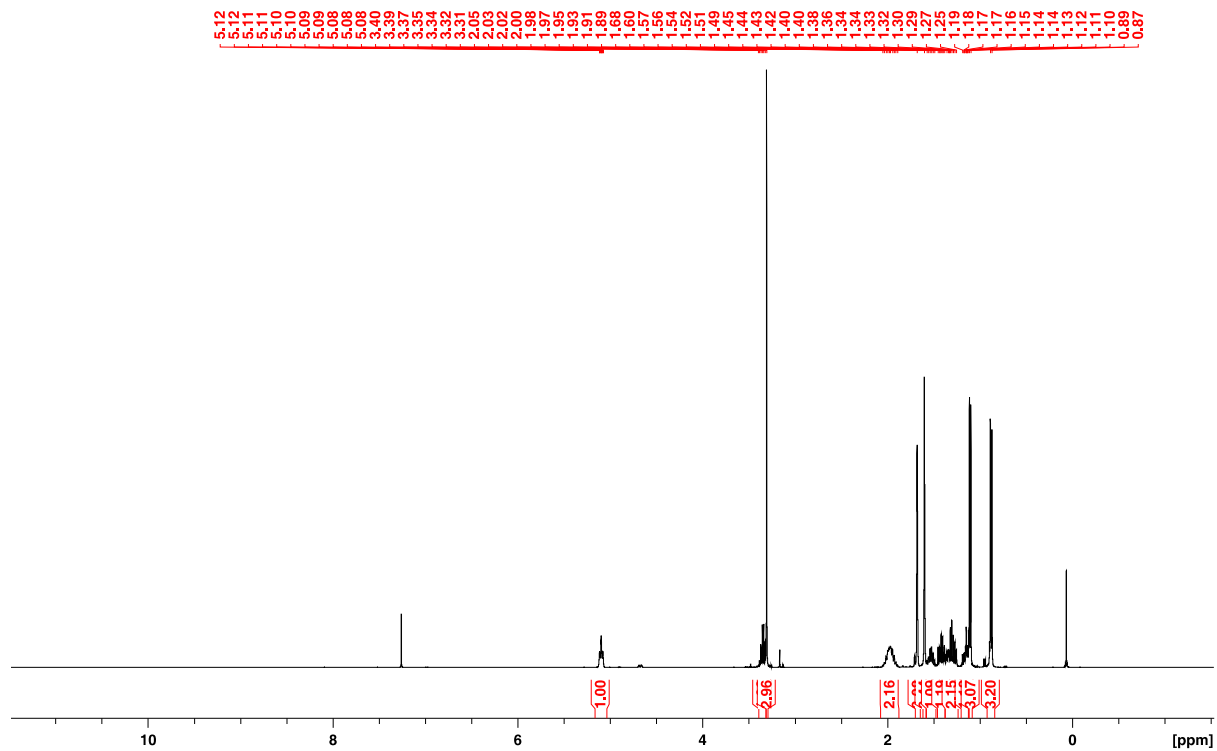


Figure S3. ^1H NMR of (6R)-8-methoxy-2,6-dimethylnon-2-ene in CDCl_3 at $23\text{ }^\circ\text{C}$

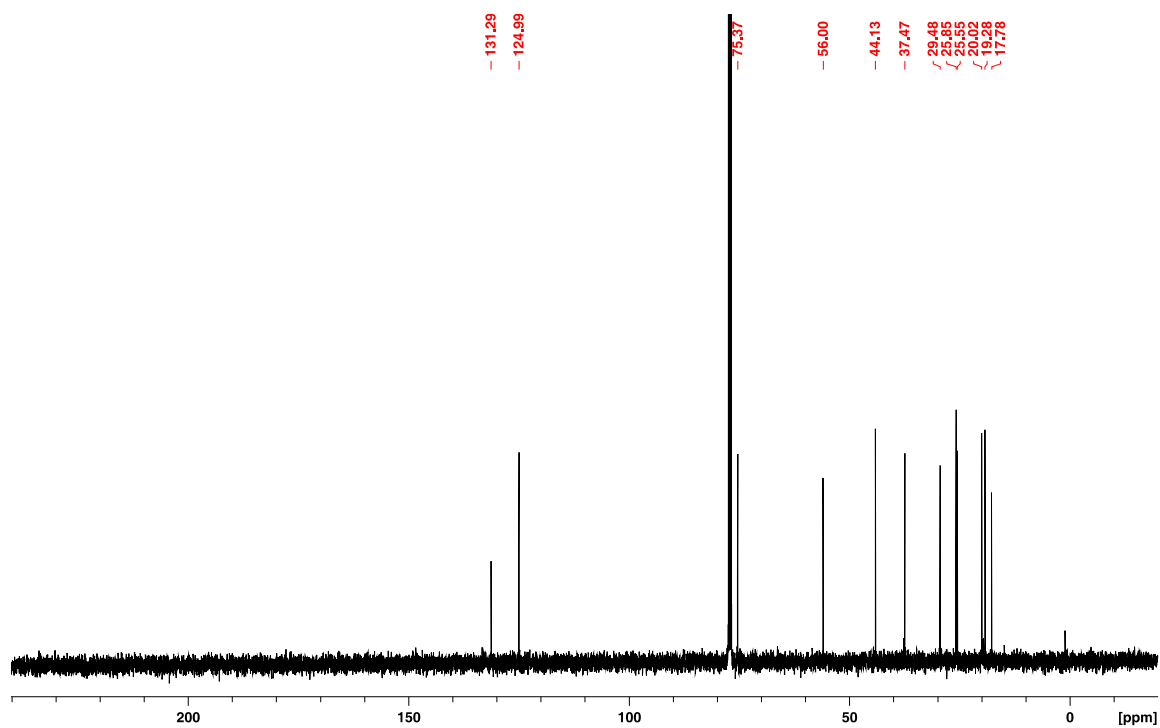
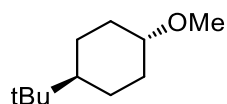
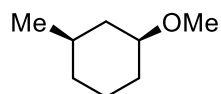


Figure S4. $^{13}\text{C}\{^1\text{H}\}$ NMR of (6R)-8-methoxy-2,6-dimethylnon-2-ene in CDCl_3 at $23\text{ }^\circ\text{C}$

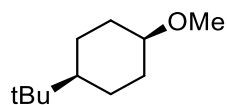
Assorted anisole derivatives (Table 3, Entries 1-5): These known compounds were obtained from commercial sources.



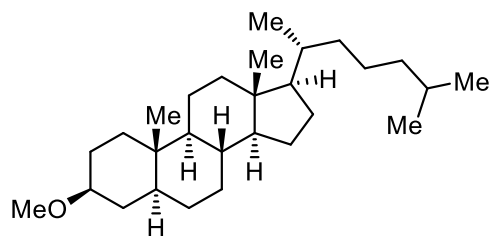
Trans-1-(tert-butyl)-4-methoxycyclohexane (Table 4, Entry 1): This compound was prepared by a reported method.¹⁵



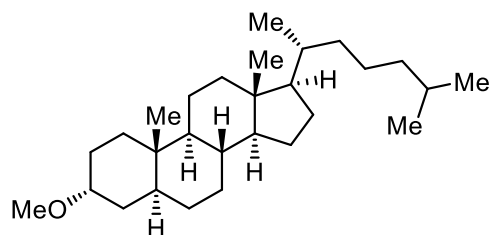
cis-1-methoxy-3-methylcyclohexane (Table 4, Entry 2): This known compound⁹ was prepared using a variation of the reported method for *trans*-1-(tert-butyl)-4-methoxycyclohexane.¹⁵



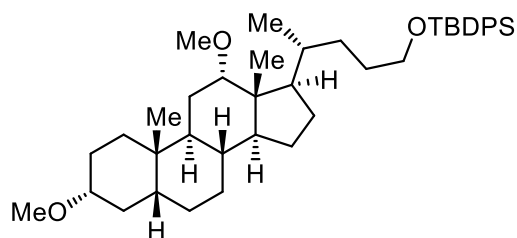
Cis-1-(tert-butyl)-4-methoxycyclohexane (Table 4, Entry 4): This compound was prepared by a reported method.¹⁵



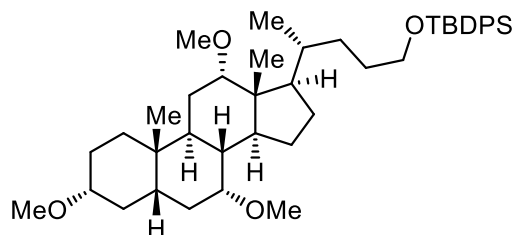
3 β -methoxy-5 α -cholestane (*Table 5, Entry 1*): This known compound was prepared according to a reported method.¹⁶



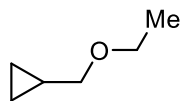
3 α -methoxy-5 α -cholestane (*Table 5, Entry 2*): This compound was prepared according to a reported method.¹⁶



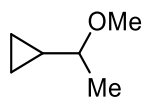
3 α ,12 α -dimethoxy-24-tert-butyl diphenylsilyloxycholane (*Table 5, Entry 3*): This compound was prepared according to a reported method.¹⁶



3 α ,7 α ,12 α -trimethoxy-24-tert-butyl diphenylsilyloxycholane (*Table 5, Entry 4*): This compound was prepared according to a reported method.¹⁶



(ethoxymethyl)cyclopropane (*Eqn 2*): This known compound¹⁷ was prepared according to a variation of the reported method for *trans*-1-(tert-butyl)-4-methoxycyclohexane.⁸ No purification was required after extraction.



(1-methoxyethyl)cyclopropane (*Eqn 3*): This known compound¹⁸ was prepared according to a variation of the reported method for *trans*-1-(tert-butyl)-4-methoxycyclohexane.⁸ No purification was required after extraction.

III. Procedures for Catalytic Reactions

General Procedure for Catalytic C-O Cleavage via Ether Silylation. In an inert glovebox atmosphere, a 4 mL vial was charged with NaBARF₄ (0.0020g, 0.0023 mmol), triethylsilane (0.0179 g, 0.155 mmol, 24.7 μ L), ether substrate (0.039 mmol) [e.g. *Trans*-1-(tert-butyl)-4-methoxycyclohexane (0.0065 g, 0.0387 mmol, 7.9 μ L)], and 0.10 mL of a 19.3 mM (0.010 g/mL) stock solution of Cp*Ir(ppy)Cl (**2**) (0.00193 mmol) in CD₂Cl₂. The sealed 4 mL vial was illuminated with a 34W Kessil™ H150 blue LED lamp for 16 h in a EvoluChem-style photoreactor at room temperature.¹⁹ After illumination, the solution was diluted with 0.30 mL CD₂Cl₂ and transferred to an NMR tube; yields were calculated using an internal standard of mesitylene (0.0065 g, 0.036 mmol, 5.0 μ L). 0.10 mL of a 38.6 mM (0.020 g/mL) stock solution of Cp*Ir(ppy)Cl (**2**) (0.00193 mmol) in CD₂Cl₂ was used for substrates requiring 10 mol % catalyst loading.

Representative crude NMR spectra of catalytic reactions.

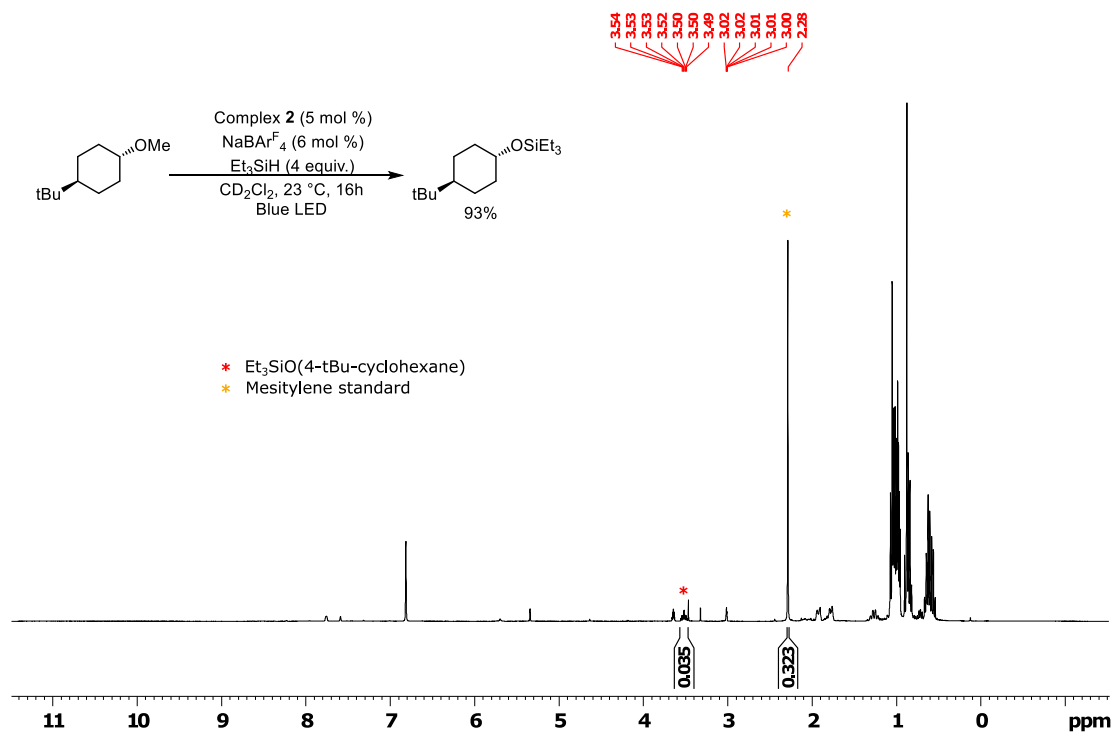


Figure S5. ^1H NMR of catalytic demethylation of *Trans*-1-(tert-butyl)-4-methoxycyclohexane.

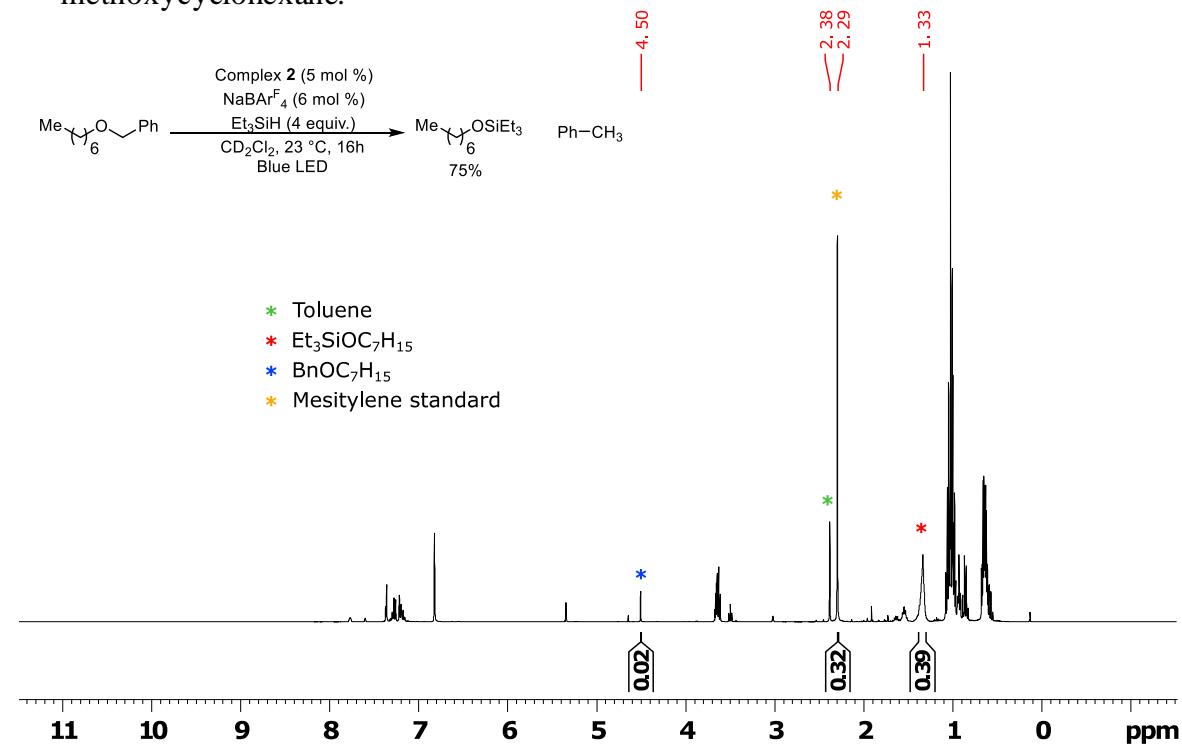


Figure S6. ^1H NMR of catalytic debenylation of (heptyloxy)methylbenzene.

General Procedure for Catalytic C-O Cleavage of Cyclopropyl alkyl ethers. In an inert glovebox atmosphere, a septum-capped NMR tube was charged with NaBAR^F₄ (0.0020 g, 0.0023 mmol), triethylsilane (0.0179 g, 0.155 mmol, 24.7 μ L), ether substrate (0.039 mmol) [e.g. 4.5 μ L (ethoxymethyl)cyclopropane or 4.7 μ L (1-methoxyethyl)cyclopropane] and 0.10 mL of 19.3 mM (0.010 g/mL) stock solution of Cp*Ir(ppy)Cl (**2**) (0.00193 mmol) in CD₂Cl₂. The sealed tube was illuminated with a 34W Kessil™ H150 blue LED lamp for 16 h in a repurposed gas chromatograph oven regulated at 23° C. The NMR sample was then diluted with 0.3 mL of CD₂Cl₂. Yields were calculated using an internal standard of tetrachloroethane (0.0079 g, 0.0472 mmol, 5.0 μ L).

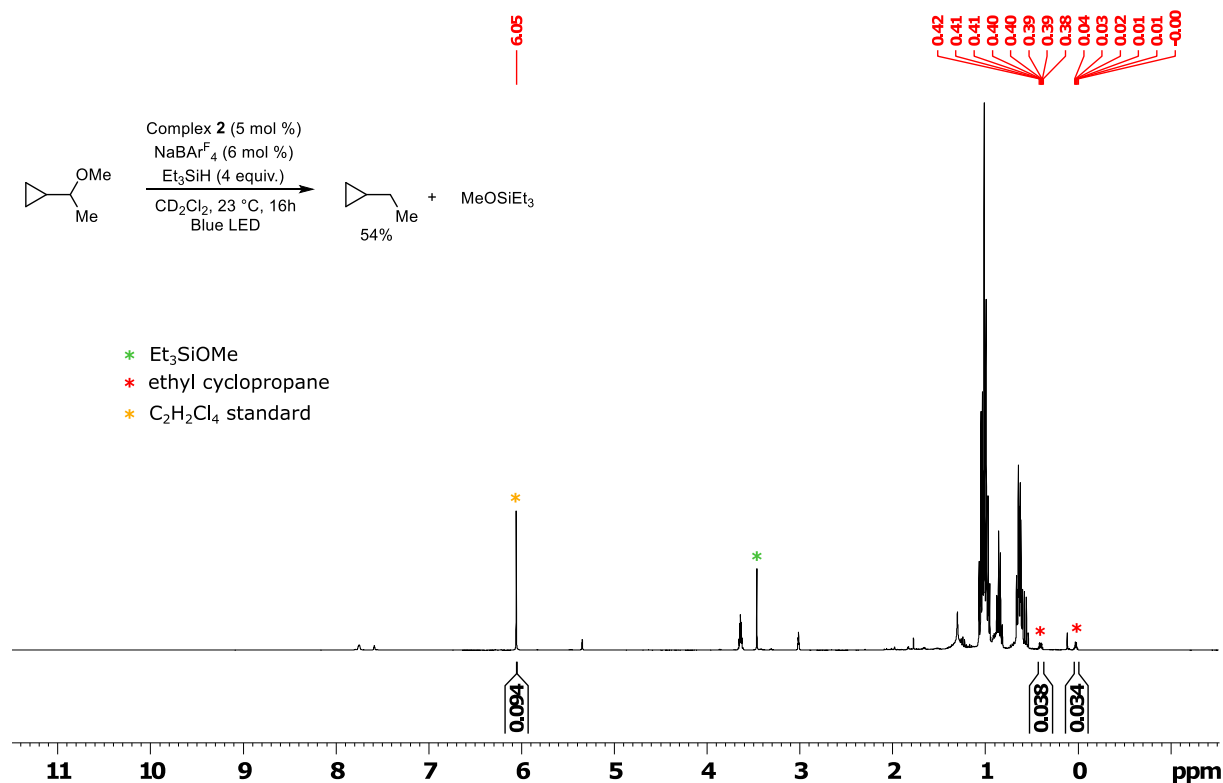
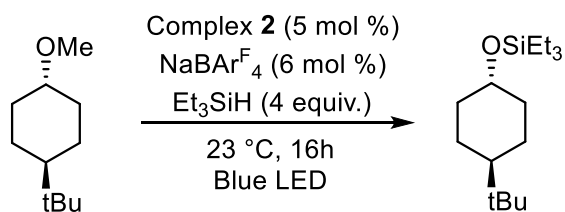
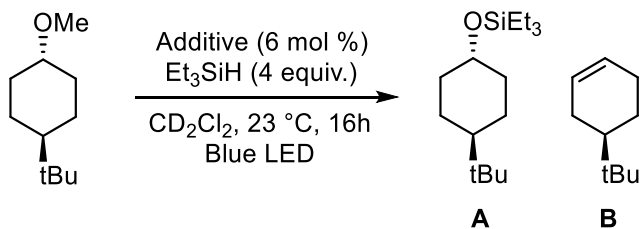


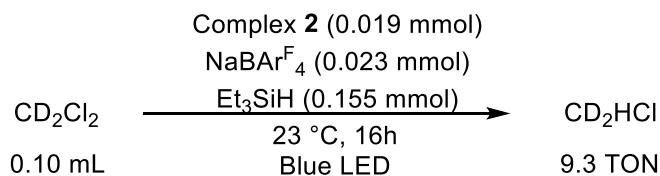
Figure S7. ¹H NMR of catalytic demethoxylation of (1-methoxyethyl)cyclopropane.

Table S1. Comparison of solvents for C-O cleavage.

| Entry | Solvent | Yield (%) |
|-------|---------------------------------|-----------|
| 1 | CD ₂ Cl ₂ | 93 |
| 2 | Toluene | 0 |
| 3 | C ₆ H ₅ F | 0 |
| 4 | MeCN | 0 |
| 5 | Pentane | 0 |

Table S2. Iridium-free control reactions.

| Entry | Complex | Additive | Yield A (%) | Yield B (%) |
|-------|---------|--|--------------------|--------------------|
| 1 | None | NaBAR ^F ₄ | 0 | 0 |
| 2 | None | [Ph ₃ C]BAR ^F ₄ | 0 | 58 |



Procedure for Catalytic Hydrodechlorination of CD_2Cl_2 . In an inert glovebox atmosphere, a septum-capped NMR tube was charged with $\text{NaBAR}_4^{\text{F}}$ (0.0020 g, 0.023 mmol), triethylsilane (0.0179 g, 0.155 mmol, 24.7 μL) and 0.10 mL of a 19.3 mM (0.010 g/mL) stock solution of $\text{Cp}^*\text{Ir}(\text{ppy})\text{Cl}$ (**2**) (0.0019 mmol) in CD_2Cl_2 . The sealed tube was illuminated with a 34W Kessi™ blue LED lamp for 16 h in a repurposed gas chromatograph oven regulated at 23° C. The sample was then diluted with an additional 0.30 mL of CD_2Cl_2 and analyzed by ^1H NMR spectroscopy. CD_2HCl production was calculated using an internal standard of 1,1,2,2-tetrachloroethane (0.0079g, 0.0472 mmol, 5.0 μL).

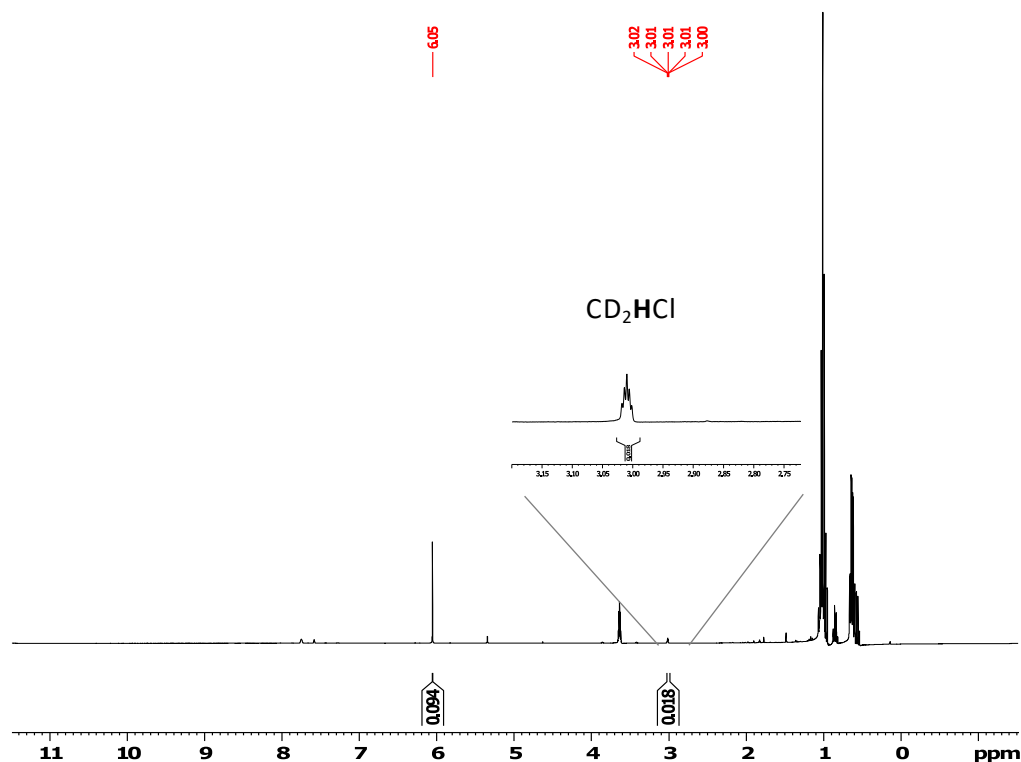


Figure S8. ^1H NMR of Catalytic Hydrodechlorination of CD_2Cl_2 .

Procedure for the Hydrosilylation of Acetophenone using 2/NaBAr^F₄. In an inert glovebox atmosphere, a septum-capped NMR tube was charged with NaBAr^F₄ (0.0020 g, 0.0023 mmol), triethylsilane (0.0494 g, 0.425 mmol, 67.9 μ L), acetophenone (0.0465 g, 0.387 mmol, 45.1 μ L), and 0.40 mL of a 4.82 mM (0.0025 g/mL) stock solution of Cp*Ir(ppy)Cl (**2**) (0.00193 mmol) in CD₂Cl₂. The sealed tube was illuminated* with a 34W Kessil™ blue LED lamp in a repurposed gas chromatograph oven regulated at 23° C for 10 minutes prior to being analyzed by ¹H NMR. Yields were calculated using an internal standard of mesitylene (0.0065 g, 0.036 mmol, 5.0 μ L).

*The dark variant was performed with the lamp switched off.

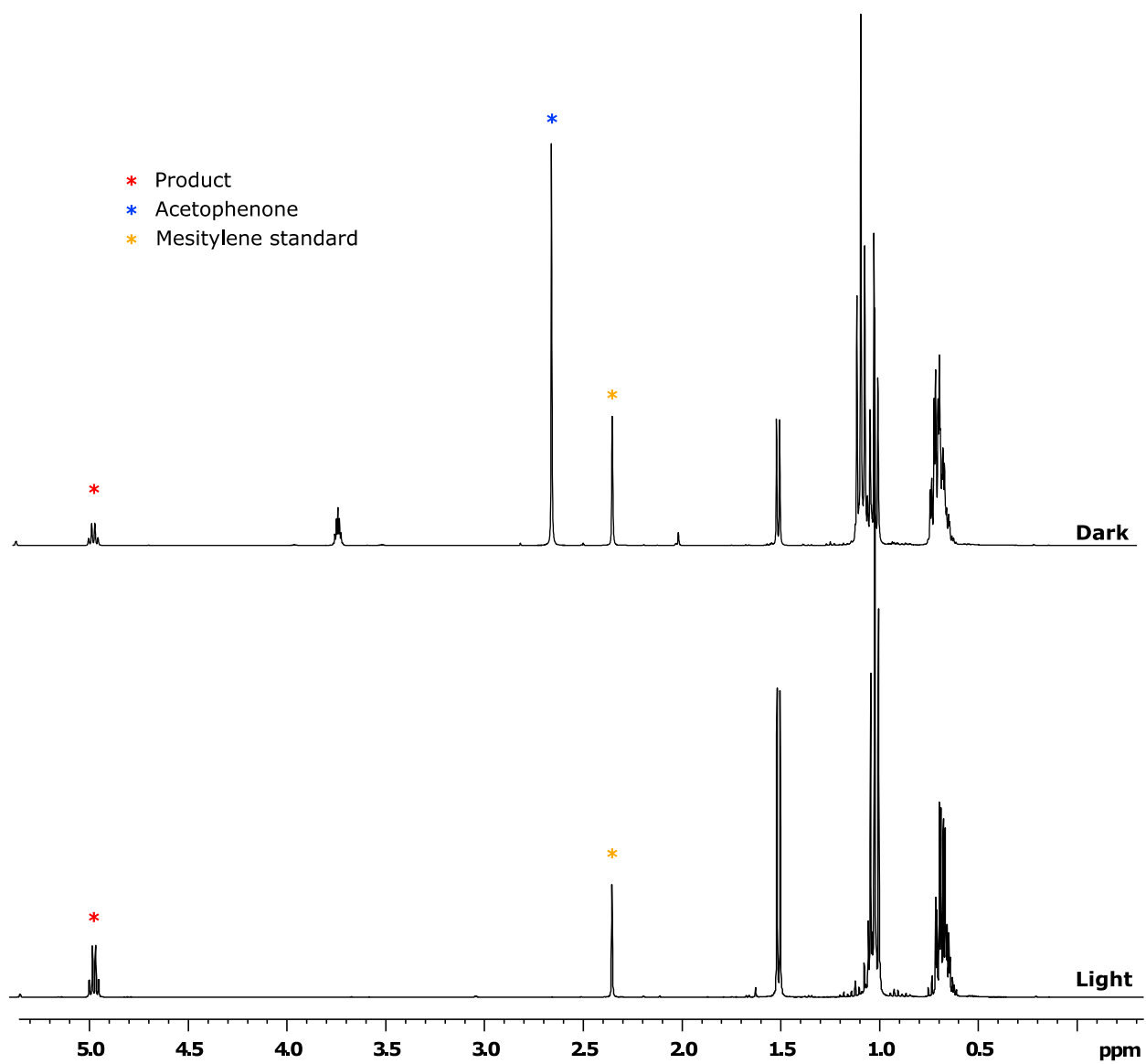


Figure S9. ¹H NMR of Catalytic Hydrosilylation of acetophenone.

IV. Mechanistic Studies

Analysis of Cp*Ir(ppy)H (5) by UV-Vis. In an inert glovebox atmosphere, a screw-cap 1.0 cm cuvette was charged with 2.0 mL of a 0.41 mM stock solution of Cp*Ir(ppy)H (**5**) (0.00083 mmol) in dichloromethane. The cuvette was analyzed in a Jasco V-670 UV-Vis in absorbance mode and an absorbance spectrum of **5** was collected.

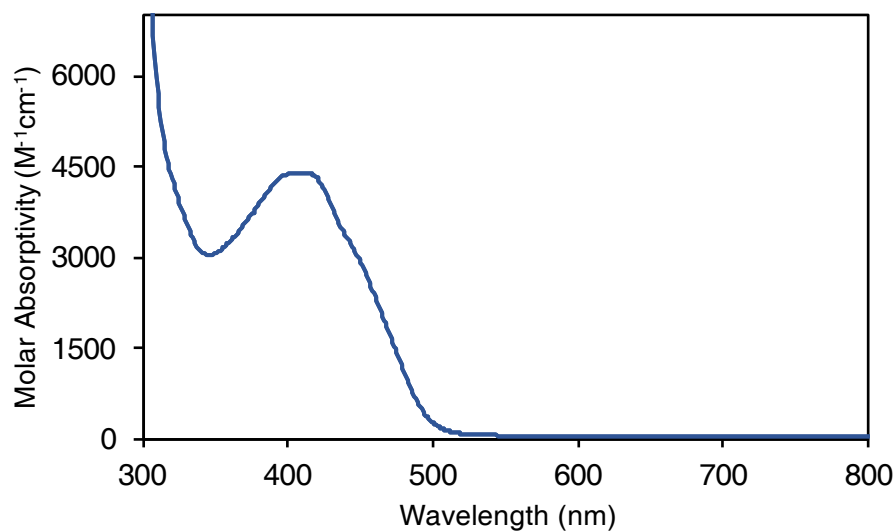


Figure S10. UV-Vis spectrum of Cp*Ir(ppy)H (**5**) in CH₂Cl₂.

Analysis of the Resting State by ^1H NMR Spectroscopy.

Dark variant. In an inert glovebox atmosphere, a septum-capped NMR tube was charged with $\text{NaBAR}^{\text{F}}_4$ (0.0020 g, 0.0023 mmol), triethylsilane (0.0179 g, 0.155 mmol, 24.7 μL), *Trans*-1-(tert-butyl)-4-methoxycyclohexane (0.0065 g, 0.0387 mmol, 7.9 μL), and 0.10 mL of a 19.3 mM (0.010 g/mL) stock solution of $\text{Cp}^*\text{Ir}(\text{ppy})\text{Cl}$ (**2**) (0.00193 mmol) in CD_2Cl_2 . The sample was allowed to stand for 5 minutes, at which point it was diluted with 0.3 mL of CD_2Cl_2 and analyzed by ^1H NMR spectroscopy. A hydride signal at -15.2 ppm matches that of independently synthesized **5**. Integration of the signals corresponding to **5** and **6** relative to the BAR^{F}_4 anion signals is consistent with the following speciation under illuminated conditions: **5** (76%), **6** (7%).

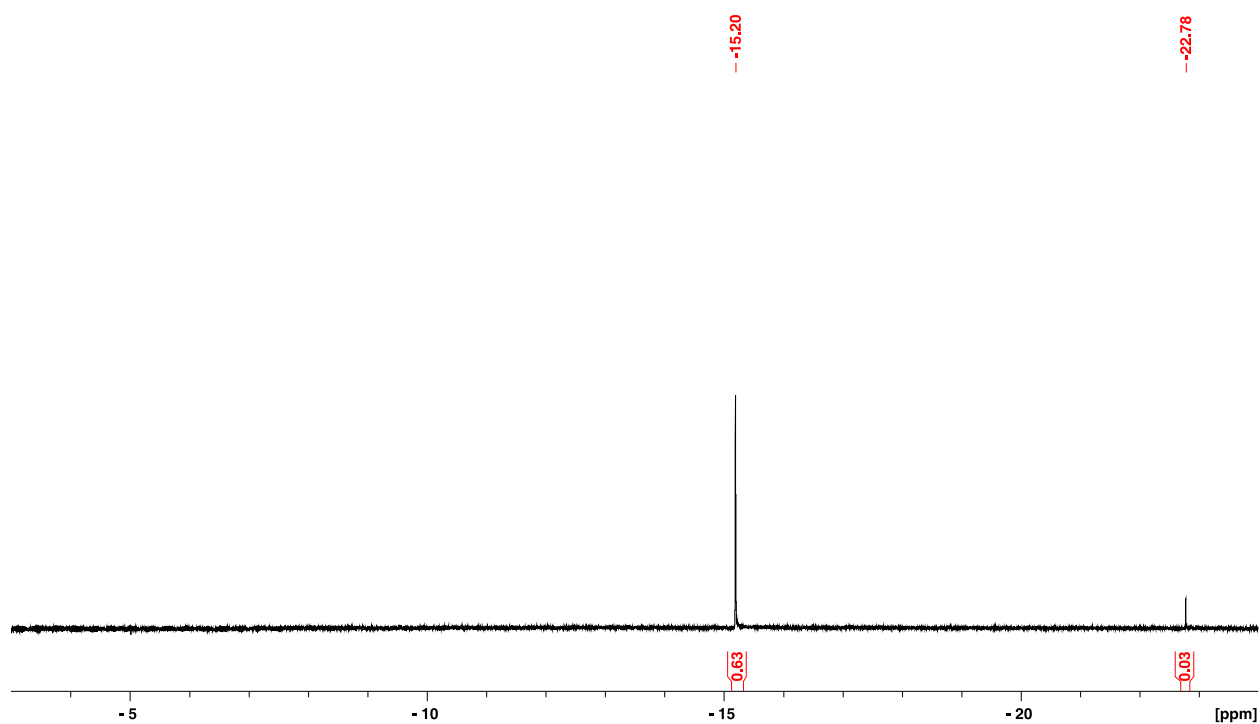


Figure S11. ^1H NMR analysis of catalytic reaction mixture without illumination.

Illuminated variant. In an inert glovebox atmosphere, a septum-capped NMR tube was charged with NaBAr^F₄ (0.0020g, 0.0023 mmol), triethylsilane (0.0179 g, 0.155 mmol, 24.7 μL), *Trans*-1-(tert-butyl)-4-methoxycyclohexane (0.0065g, 0.0387 mmol, 7.9 μL), and 0.10 mL of a 19.3 mM (0.010 g/mL) stock solution of Cp*Ir(ppy)Cl (**2**) (0.00193 mmol) in CD₂Cl₂. The sealed tube was illuminated with a 34W Kessil™ blue LED lamp in a repurposed gas chromatograph oven regulated at 23° C for 10 minutes prior to being diluted with 0.3 mL of CD₂Cl₂ and analyzed by ¹H NMR spectroscopy. Integration of the signals corresponding to **5** and **6** relative to the BAr^F₄ anion signals is consistent with the following speciation under illuminated conditions: **5** (7%), **6** (55%).

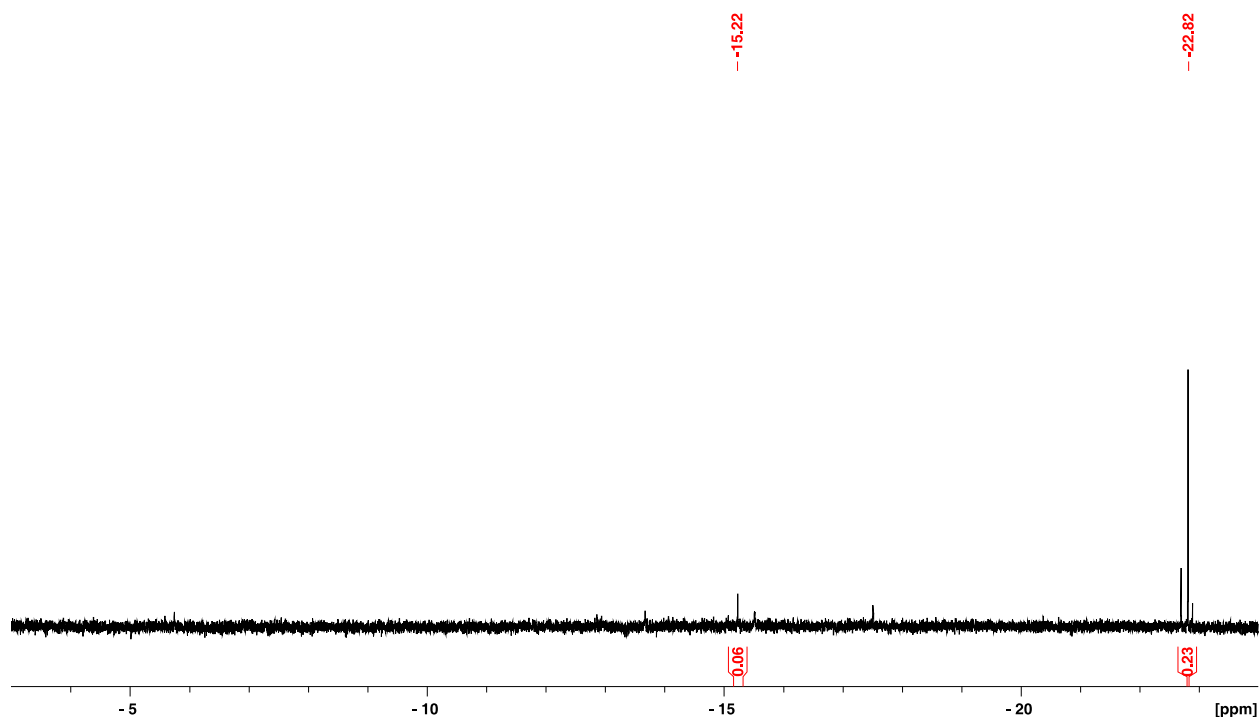


Figure S12. ¹H NMR analysis of catalytic reaction mixture after illumination.

Procedure for the Stoichiometric Reduction of [OEt]₃[BF₄] using Cp*Ir(ppy)H (5). In an inert glovebox atmosphere, a septum-capped NMR tube was charged with [OEt]₃[BF₄] (0.0022 g, 0.0116 mmol) and 0.4 mL of 20.7 mM stock solution (0.010 g/mL) of Cp*Ir(ppy)H (5) (0.00828 mmol). The sealed tube was illuminated* with a 34W Kessil™ blue LED lamp in a repurposed gas chromatograph oven regulated at 23° C for 10 minutes prior to being analyzed by ¹H NMR spectroscopy. Yields of diethyl ether were calculated using an internal standard of mesitylene (0.0065 g, 0.036 mmol, 5.0 μL). The ethane byproduct is observed as well, but was not quantified owing to its volatility.

*The dark variants were performed with the lamp switched off.

V. X-Ray Crystallographic Data

Details of crystallographic refinement.

General Methods. A suitable crystal of each sample was selected for analysis and mounted in a polyimide loop. All measurements were made on a Rigaku SCX-Mini CCD with filtered Mo-K α radiation at a temperature of 223 K. Using Olex2,²⁰ the structure was solved with the ShelXS structure solution program using Direct Methods and refined with the ShelXL refinement package²¹ using Least Squares minimization.

CpIrCl₂(MeCN)

This structure was modeled without restraint.

Complex 3

Disorder in the phenylpyridine group was modeled over two positions by refinement of the partially occupied C and N atoms with constraints placed on their positions and atomic thermal parameters.

Table S3. Crystal data and structure refinement for CpIrCl₂(MeCN).

| | | |
|-----------------------------------|---|----------------------------|
| Empirical formula | C7 H8 Cl2 Ir N | |
| Formula weight | 369.24 | |
| Temperature | 223(2) K | |
| Wavelength | 0.71075 Å | |
| Crystal system | Monoclinic | |
| Space group | P 1 21/c 1 | |
| Unit cell dimensions | a = 11.349(3) Å | $\alpha = 90^\circ$ |
| | b = 7.3426(17) Å | $\beta = 103.680(7)^\circ$ |
| | c = 11.662(3) Å | $\gamma = 90^\circ$ |
| Volume | 944.3(4) Å ³ | |
| Z | 4 | |
| Density (calculated) | 2.597 Mg/m ³ | |
| Absorption coefficient | 14.640 mm ⁻¹ | |
| F(000) | 672 | |
| Crystal size | 0.2 x 0.2 x 0.1 mm ³ | |
| Theta range for data collection | 3.306 to 27.389°. | |
| Index ranges | -14 ≤ h ≤ 14, -9 ≤ k ≤ 9, -15 ≤ l ≤ 15 | |
| Reflections collected | 8850 | |
| Independent reflections | 2138 [R(int) = 0.0620] | |
| Completeness to theta = 25.242° | 99.8 % | |
| Absorption correction | Semi-empirical from equivalents | |
| Max. and min. transmission | 0.3222 and 0.1578 | |
| Refinement method | Full-matrix least-squares on F ² | |
| Data / restraints / parameters | 2138 / 0 / 101 | |
| Goodness-of-fit on F ² | 1.040 | |
| Final R indices [I > 2σ(I)] | R1 = 0.0353, wR2 = 0.0432 | |
| R indices (all data) | R1 = 0.0517, wR2 = 0.0462 | |
| Largest diff. peak and hole | 0.956 and -1.133 e/Å ⁻³ | |

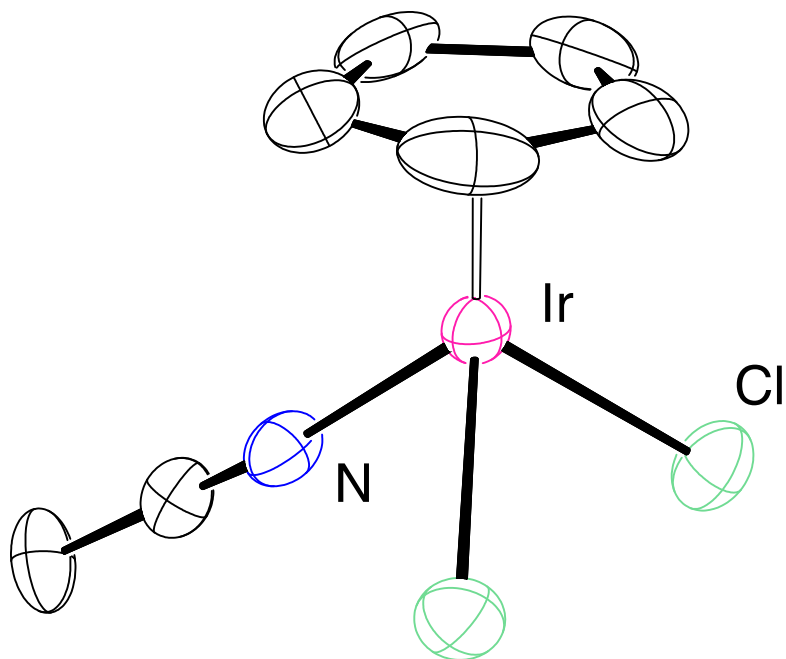


Figure S13. ORTEP of CpIrCl₂(MeCN) drawn at 50% probability level.

Table S4. Crystal data and structure refinement for CpIr(ppy)Cl.

| | | |
|-----------------------------------|---|----------------|
| Empirical formula | C ₁₆ H ₁₃ ClIrN | |
| Formula weight | 446.92 | |
| Temperature | 223.15 K | |
| Wavelength | 0.71075 Å | |
| Crystal system | Monoclinic | |
| Space group | P 1 21/c 1 | |
| Unit cell dimensions | a = 10.605(12) Å | α = 90° |
| | b = 8.189(9) Å | β = 101.17(2)° |
| | c = 15.347(17) Å | γ = 90° |
| Volume | 1308(3) Å ³ | |
| Z | 4 | |
| Density (calculated) | 2.270 Mg/m ³ | |
| Absorption coefficient | 10.398 mm ⁻¹ | |
| F(000) | 840 | |
| Crystal size | 0.1 x 0.1 x 0.1 mm ³ | |
| Theta range for data collection | 3.166 to 26.728°. | |
| Index ranges | -13 ≤ h ≤ 13, -10 ≤ k ≤ 10, -19 ≤ l ≤ 19 | |
| Reflections collected | 12094 | |
| Independent reflections | 2765 [R(int) = 0.0647] | |
| Completeness to theta = 25.242° | 99.8 % | |
| Absorption correction | Semi-empirical from equivalents | |
| Max. and min. transmission | 0.4228 and 0.4228 | |
| Refinement method | Full-matrix least-squares on F ² | |
| Data / restraints / parameters | 2765 / 0 / 173 | |
| Goodness-of-fit on F ² | 1.129 | |
| Final R indices [I > 2σ(I)] | R1 = 0.0389, wR2 = 0.0503 | |
| R indices (all data) | R1 = 0.0567, wR2 = 0.0534 | |
| Largest diff. peak and hole | 0.772 and -0.873 e/Å ⁻³ | |

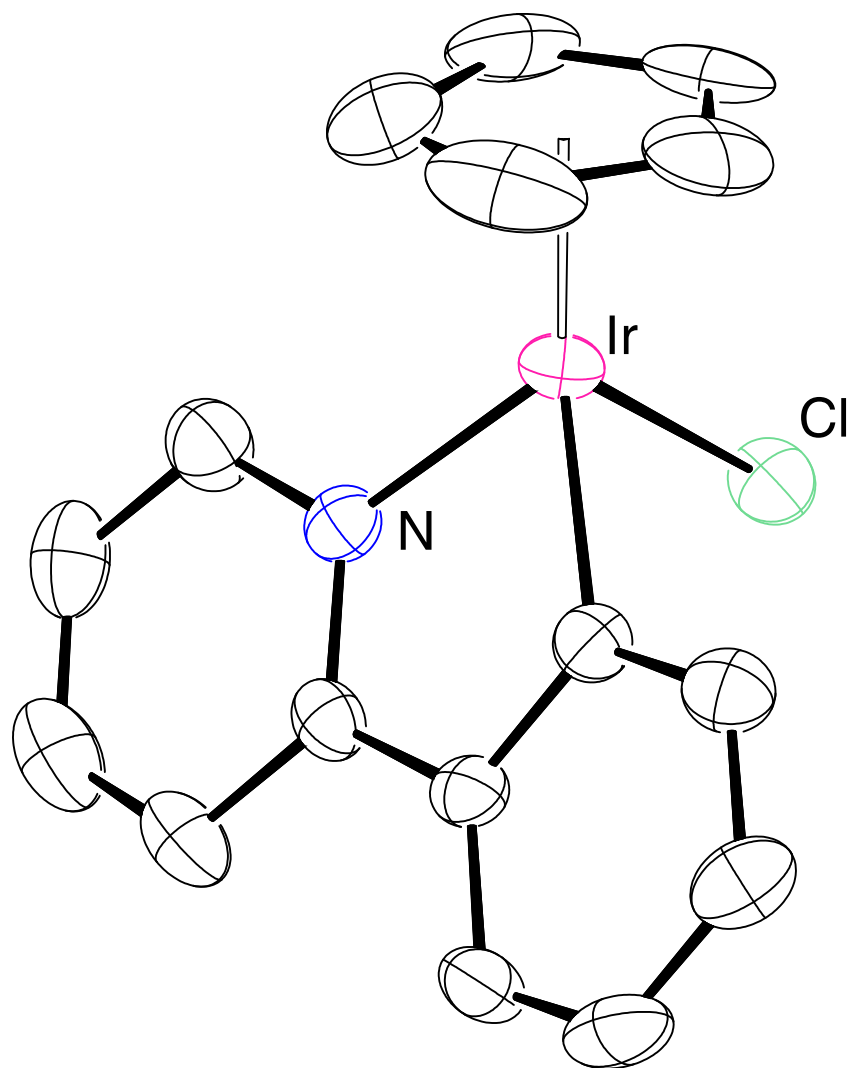


Figure S14. ORTEP of CpIr(ppy)Cl drawn at 50% probability level. Disorder in the phenylpyridine moiety is omitted for clarity.

VI. References

- (1) Herde, J. L.; Lambert, J. C.; Senoff, C. V.; Cushing, M. A., "Cyclooctene and 1,5-Cyclooctadiene Complexes of Iridium(I)." *Inorg. Synth.* **1974**, 18-20.
- (2) White, C.; Yates, A.; Maitlis, P. M.; Heinekey, D. M., " $(\eta^5$ -Pentamethylcyclopentadienyl)Rhodium and -Iridium Compounds." *Inorg. Synth.* **1992**, 228-234.
- (3) Lesley, M. J. G.; Norman, N. C.; Rice, C. R.; Reger, D. L.; Little, C. A.; Lamba, J. J. S.; Brown, K. J.; Peters, J. C.; Thomas, J. C.; Sahasrabudhe, S.; Yearwood, B. C.; Atwood, D. A.; Hill, R. F.; Wood, G. L.; Danzer, R.; Paine, R. T.; Wagner, N. L.; Murphy, K. L.; Haworth, D. T.; Bennett, D. W.; Byers, P. K.; Canty, A. J.; Honeyman, R. T.; Arnáiz, F. J.; Miranda, M. J.; Bohle, D. S.; Sagan, E. S.; Chivers, T.; Sandblom, N.; Schatte, G., "Main Group Compounds." In *Inorg. Synth.*, 2004; pp 1-48.
- (4) Straus, D. A.; Zhang, C.; Tilley, T. D., "Trityl tetraphenylborate as a reagent in organometallic chemistry." *Journal of Organometallic Chemistry* **1989**, 369 (2), C13-C17.
- (5) Hamdaoui, M.; Ney, M.; Sarda, V.; Karmazin, L.; Bailly, C.; Sieffert, N.; Dohm, S.; Hansen, A.; Grimme, S.; Djukic, J.-P., "Evidence of a Donor–Acceptor (Ir–H)→SiR₃ Interaction in a Trapped Ir(III) Silane Catalytic Intermediate." *Organometallics* **2016**, 35 (13), 2207-2223.
- (6) Li, L.; Brennessel, W. W.; Jones, W. D., "An Efficient Low-Temperature Route to Polycyclic Isoquinoline Salt Synthesis via C–H Activation with [Cp**M*Cl₂]₂ (M = Rh, Ir)." *J. Am. Chem. Soc.* **2008**, 130 (37), 12414-12419.
- (7) Hu, Y.; Li, L.; Shaw, A. P.; Norton, J. R.; Sattler, W.; Rong, Y., "Synthesis, Electrochemistry, and Reactivity of New Iridium(III) and Rhodium(III) Hydrides." *Organometallics* **2012**, 31 (14), 5058-5064.

- (8) Bell, T. W.; Brough, S. A.; Partridge, M. G.; Perutz, R. N.; Rooney, A. D., "Competition between intramolecular and intermolecular carbon-hydrogen bond activation in iridium ethene complexes." *Organometallics* **1993**, *12* (8), 2933-2941.
- (9) Werner, H.; Wolf, J.; Nessel, A.; Fries, A.; Stempfle, B.; Nürnberg, O., "Novel binuclear doubly vinyl-bridged iridium complexes formed by olefinic C—H activation." *Can. J. Chem.* **1995**, *73* (7), 1050-1057.
- (10) Brewster, T. P.; Miller, A. J. M.; Heinekey, D. M.; Goldberg, K. I., "Hydrogenation of Carboxylic Acids Catalyzed by Half-Sandwich Complexes of Iridium and Rhodium." *J. Am. Chem. Soc.* **2013**, *135* (43), 16022-16025.
- (11) Urgoitia, G.; SanMartin, R.; Herrero, M. T.; Domínguez, E., "Vanadium-Catalyzed Oxidative Debenzylation of O-Benzyl Ethers at ppm Level." *Adv. Synth. Catal.* **2016**, *358* (20), 3307-3312.
- (12) Jones, C. A. H.; Schley, N. D., "Selective alkyl ether cleavage by cationic bis(phosphine)iridium complexes." *Organic & Biomolecular Chemistry* **2019**, *17* (7), 1744-1748.
- (13) Huo, X.; Quan, M.; Yang, G.; Zhao, X.; Liu, D.; Liu, Y.; Zhang, W., "Hydrogen-Bond-Activated Palladium-Catalyzed Allylic Alkylation via Allylic Alkyl Ethers: Challenging Leaving Groups." *Org. Lett.* **2014**, *16* (6), 1570-1573.
- (14) Tietze, L. F.; Weigand, B.; Völkel, L.; Wulff, C.; Bittner, C., "Synthesis of Enantiopure Homoallylic Ethers by Reagent Controlled Facial Selective Allylation of Chiral Ketones." *Chemistry – A European Journal* **2001**, *7* (1), 161-168.
- (15) Booth, H.; Mark Dixon, J.; Khedhair, K. A.; Readshaw, S. A., "Experimental studies of the anomeric effect. part III. Rotameric preferences about the exo-cyclic c2-x bond in equatorial and axial 2-methoxy- and 2-methylamino-tetrahydropyrans." *Tetrahedron* **1990**, *46* (5), 1625-1652.

- (16) Fast, C. D.; Jones, C. A. H.; Schley, N. D., "Selectivity and Mechanism of Iridium-Catalyzed Cyclohexyl Methyl Ether Cleavage." *ACS Catalysis* **2020**, *10* (11), 6450-6456.
- (17) Bart, S. C.; Chirik, P. J., "Selective, Catalytic Carbon–Carbon Bond Activation and Functionalization Promoted by Late Transition Metal Catalysts." *J. Am. Chem. Soc.* **2003**, *125* (4), 886-887.
- (18) Smith, M. B.; Hrubiec, R. T.; Zezza, C. A., "Reaction of amines with cyclopropylcarbonyl halides: SN2' or solvolysis?" *J. Org. Chem.* **1985**, *50* (24), 4815-4821.
- (19) Bazin, M. J.; Buzdygon, R. S. Photochemistry device. WO2018098189A1, 2018.
- (20) Dolomanov, O. V.; Bourhis, L. J.; Gildea, R. J.; Howard, J. A. K.; Puschmann, H., "OLEX2: a complete structure solution, refinement and analysis program." *J. Appl. Crystallogr.* **2009**, *42* (2), 339-341.
- (21) Sheldrick, G., "A short history of SHELX." *Acta Crystallographica Section A* **2008**, *64* (1), 112-122.